Solid-state NMR study of polymorphism in pharmaceuticals

Elizabeth Anne Christopher

Solid-State NMR Study of Polymorphism in Pharmaceuticals

by

Elizabeth Anne Christopher, B.Sc.

A Thesis submitted in partial fulfilment of the requirements for the degree of Doctor of Philosophy.

Department of Chemistry
University of Durham
1993

Solid-State NMR Study of Polymorphism in Pharmaceuticals

Elizabeth Anne Christopher

Abstract

This thesis is concerned with attempts to establish solid-state NMR as a complementary technique to X-ray crystallography for providing information on crystal structure, i.e. information regarding conformation, packing and inter- or intra-molecular interactions.

Methods of assigning the solid-state NMR spectrum have been used which rely upon ^{1}H-^{13}C dipolar interactions and upon the shielding anisotropy experienced by the nuclei. Single pulse experiments have also been used to identify solvate molecules. Of particular importance, the anisotropy and asymmetry have been found for a number of steroids, and the values used to assign the high frequency region of the spectrum. This has enabled chemical shifts to be linked to the hydrogen bonds that are present. Thus, the mode of hydrogen bonding can be predicted in forms of cortisone acetate for which the crystal structure is not available. Chemical shifts have also been linked with the conformation of the D ring. In this way, important crystallographic information has been gleaned from the solid-state NMR spectrum.

The effect of the formation of hydrogen bonds upon the shielding tensor components of carbonyl and ester carbons has been studied, and found to cause a high frequency shift in δ_{22}, which is probably oriented along the C=O bonds. This leads to a high frequency shift in the isotropic chemical shift.

The effect of the spinning speed upon the centreband intensity of a peak as the anisotropy and asymmetry are varied has been investigated. It has been found that at low spinning speeds, the centreband intensity does not vary in a simple fashion. Thus it is recommended that full shielding tensor analysis is performed.

The effect of the spinning speed on the sample temperature has also been studied. Results show that at low spinning speeds (up to 2 kHz) there is sample cooling as the spinning speed increases (attributed to the Joule -Thompson effect). But at higher spinning speeds (above 2 kHz) then there is sample heating as the spinning speed increases. The importance of this result is discussed.

The effect of quadrupolar nuclei (^{35}Cl and ^{14}N) upon the spectrum of a spin-$\frac{1}{2}$ nucleus (^{13}C) has been studied. In favourable cases, the anisotropy in the spin-spin coupling constant has been found, whilst in other cases, the sign and magnitude of the quadrupolar coupling constant have been obtained. The broadening of resonances of carbon atoms adjacent to quadrupolar nuclei has been valuable in assigning the solid-state NMR spectra. The broadening effect has also been observed at more distant sites. It has not been possible to distinguish the effects of ^{37}Cl and ^{35}Cl on the carbon spectra of chlorine containing steroids.

Memorandum

The research presented in this thesis has been carried out at the Department of Chemistry, University of Durham, between October 1989 and September 1992. It is the original work of the author unless stated otherwise. None of this work has been submitted for any other degree.

Acknowledgements

I would like to thank my supervisors Prof. R. K. Harris at the University of Durham, and Dr. R. A. Fletton at Glaxo Group Research Ltd., Greenford for their help and advice during the course of study. I should also like to thank Mr. B. J. Say and Dr. R. R. Yeung for their assistance, and my fellow research students for providing a friendly atmosphere in which to work. I would also like to thank Dr. R. W. Lancaster at Glaxo Group Research Ltd. for his assistance and all in the Structural Chemistry group at Glaxo for their help.

I would also like to acknowledge the financial support of the Science and Engineering Research Council, and of Glaxo Group Research Ltd.

Publication

E.A. Christopher, R.K. Harris, R.A. Fletton.
Assignments of solid-state ^{13}C Resonances for Polymorphs of Cortisone Acetate using Shielding Tensor Components.
Solid-State Nuclear Magnetic Resonance 1, 93-101 (1992)

Conferences Attended

British Radiofrequency Spectroscopy Group and NMR Discussion Group Meeting: Solid-State NMR, New materials and new techniques.
University of Warwick. England.
5-7th September 1990

Posters presented at :

Tenth International Meeting on NMR Spectroscopy
University of St. Andrews, Scotland.
8-12th July 1991

Eleventh European Experimental NMR Conference
Lisbon, Portugal.
14-19th June 1992

Table of Contents

List of Figures

Chapter 6 Cortisone Acetate

Chapter 9 Beclomethasone Dipropionate

Chapter 10 Cefuroxime Axetil

List Of Tables

Chapter 4

Chapter 5

Chapter 1

Introduction

Chapter 1 Introduction

1.1. Polymorphism

Polymorphism is the existence of more than one crystal form of a compound[1]. Mitscherlich has been credited with being the first to recognise this phenomenon[2]. However, the polymorphism of tin (more correctly termed allotropy when referring to elements) is reputed to have played an important role in history. The buttons of Napoleon's soldiers uniforms were made from the white, metallic form of tin. In the cold Moscow winter of 1812, the extreme cold is said to have lead to the transformation of the tin into the grey form. The buttons crumbled and Napoleon's army was defeated by the effects of the cold weather.

The occurrence of polymorphism is due to different molecular conformations and packing arrangements in the solid-state. Each crystal structure corresponds to a free energy minimum, but is not necessarily the global minimum. The free energy is affected by intermolecular interactions that can be thought of in three categories[1,3]:

i) non-bonded, non-electrostatic (e.g. Van der Waals and London) interactions
ii) electrostatic (coulombic) interactions
iii) hydrogen bonding

However, these interactions are of quite low energy and tend to be sufficient to cause only changes in torsion angles, which require less energy than do changes in bond lengths or bond angles. Thus often the differences in conformation are restricted to differences in the torsion angles. Certain packing arrangements may be particularly favourable (e.g. planar molecules can pack together very efficiently), in which case there may be a predominance of certain conformations of the molecule.

1.2. The Importance Of Polymorphism

Polymorphism has significant industrial importance in the manufacture of pharmaceuticals, dyes and explosives. In the case of pharmaceuticals, strict regulatory requirements mean that polymorphism is very important. This is as it should be, as the different polymorphs of a drug can have very different biological activities. The rate at which the polymorphs can be absorbed by the body vary from one form to another, and this will affect the dosage[4].

1.3. Solid-State NMR And The Study Of Polymorphism

Perhaps the most obvious tool to use in the study of polymorphism is X-ray crystallography. This provides information on the molecular conformation (bond angles, lengths and torsional angles) as well as the packing arrangement. Also, the presence of intermolecular interactions such as hydrogen bonds can be inferred by the close proximity of atoms. However, the main disadvantage of X-ray crystallography is that single crystals or crystalline powders are required, whilst for other physical techniques, the range of suitable sample types is much greater[5].

In recent years there have been a number of reports of studies of polymorphism by various physical techniques. Certain drugs and especially steroids exist in a number of polymorphic or pseudopolymorphic structures that have formerly been characterized by infrared spectroscopy and differential scanning calorimetry (DSC). But as pharmaceutical manufacturers have an interest in finding fast analytical methods of identifying the polymorphic forms that exist in a sample, the value of solid-state NMR is becoming evident.

Solid-state NMR is perhaps one of the best techniques for studying polymorphism in the pharmaceutical field. High-resolution spectra are obtainable in most cases and can provide much information. The chemical shifts are affected by the environment of the nucleus, so this reflects the

bonding, conformation and packing. Of course the difficulty remains in separating these effects so that 'crystallographic' information (such as bond lengths and angles) can be obtained from the spectrum. The study of these effects is presented in this thesis.

1.4. Definitions Of Polymorphic Types

Some of the terms connected with this work are defined as follows[6]:

i) polymorphs - these are different forms of the same compound. The forms may be crystalline, disordered or amorphous.

ii) conformational polymorphism - the polymorphs have significantly different conformations of the molecules (i.e. dihedral angles and bond lengths).

iii) configurational polymorphism - the polymorphs have different configurations e.g. cis and trans isomers.

With respect to conformational polymorphs:

iv) anhydrate - crystals that contain no water or other solvent of crystallization.

v) solvates - this term is used to refer to the molecules of the solvent of crystallization that may be present in the crystal structure. If the crystals contain water as the solvate molecule then they would be called hydrates. However, the term "solvate" is also used rather loosely to describe any crystal form that contains solvate molecules. More correctly, one of the following, more specific terms should be used.

vi) polymorphic solvates - the solvate molecules interact with the host molecules to hold the crystal together. Desolvation causes the collapse of the crystal, which then recrystallises into another form.

vii) pseudopolymorphic solvates - the solvate molecule plays no part in holding the host molecules together, i.e. it acts solely as a filler in the structure. Desolvation does not destroy the crystal structure.

1.5. Definitions Of Crystallographic Nomenclature

The following terms will be used in this work:

i) The unit cell. Crystals are built up by the repetition of a three dimensional structural unit[6]. This structural unit is the unit cell. Continuous replication of the unit cell generates the entire lattice.

ii) The unit cell dimensions are lengths a, b and c (usually in Å), and angles α, β and γ (in degrees).

iii) The space group defines the translational symmetry of the unit cells.

iv) Z is the number of molecules in the unit cell.

v) The asymmetric unit is the smallest possible repeating unit. The unit cell may comprise several asymmetric units.

vi) N is the number of molecules in the asymmetric unit

1.6. Definitions Of Steroid Nomenclature

Steroids consist of four fused rings that have a fixed stereochemistry[7]. Three of the rings contain six atoms each, whilst the other ring has only five atoms. The rings are lettered A, B, C and D. The A ring is the furthest from the five-membered ring, and is usually shown on the left of the structure. The other rings are lettered sequentially from here. The numbering of atoms starts in the A ring and works around the structure[8] as shown in figure 1.1:

Figure 1.1 - Showing the numbering scheme adopted for steroids

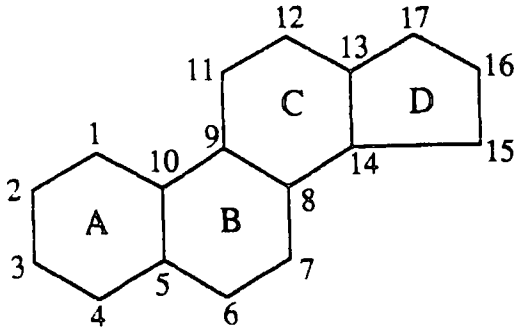

In steroids the conformation of the rings is fixed. The A and B rings may be joined in either a cis or a trans fashion. The other ring junctions are usually trans-fused. Now if the A and B rings are trans-fused then

substituents at the ring junctions (i.e. carbon atoms numbered 5 and 10) will be pointing in opposite directions, see figure 1.2. Often there is a methyl group attached at C10 (and numbered 19). The molecule is oriented so that C19 is above the plane of the steroid backbone. This is known as the β-face of the steroid. This means that any substituent at C5 will necessarily point down, i.e. it is below the plane of the steroid backbone, on the α–face of the molecule. If the A and B rings are cis-fused, then substituents at both C5 and C10 will point in the same direction, i.e. they are above the plane of the steroid backbone, on the β-face of the molecule. This is shown in figure 1.2.

Figure 1.2 - Showing the α and β faces of the steroid.

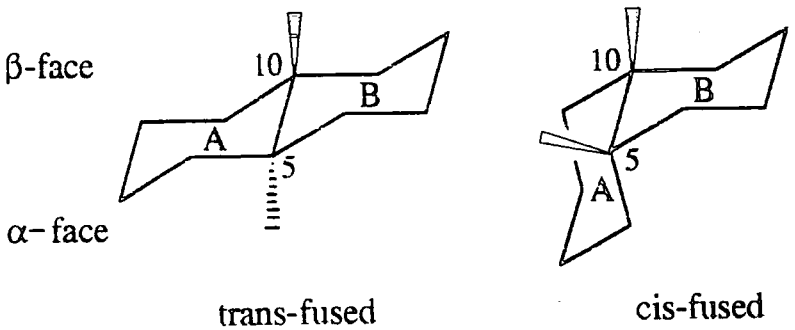

trans-fused cis-fused

1.7. References

(1) Bernstein, J. In *Organic Solid State Chemistry*; Eds. Desiraju, G.; Elsevier: New York, (1987); Vol. 32; chap. 13; pp 471.

(2) Mitscherlisch, E. *Ann. Chim. Phys.* **19**, 350 (1822).

(3) Bernstein, J., Hagler A.T. *J. Am. Chem. Soc.* **100**, 673 (1978).

(4) Otsuka, M., Kaniniwa N. *Proc. 2nd Japan-Soviet Symp. Mechanochemistry* 209 (1988).

(5) Etter, M.C., Hoye R.C., Vojta G.M. *Cryst. Reviews* **1**, 281 (1988).

(6) Byrn, S.R. *Solid-State Chemistry Of Drugs*; Academic Press: London, (1982).

(7) McMurray, J. *Organic Chemistry*; Brooks/Cole Publishing Co.: Monterey, (1984);pp 1090.

(8) IUPAC In *Pure and Applied Chemistry*, Butterworth: London, (1972); Vol. 31; pp 285.

Chapter 2

Literature Review

Chapter 2 Literature Review

2.1. Introduction

An excellent review of the use of solid-state NMR and X-ray crystallography as complementary tools for studying molecular structure has appeared in the literature[1]. In recent years there have been many advances in solid-state NMR techniques, so that now high-resolution spectra may be obtained routinely. One of the main advantages of solid-state NMR over crystallography is that a wide range of samples are suitable for study - crystalline materials (as powders or single crystals), amorphous samples, mixtures and even living tissue. Also, crystals that decompose when exposed to X-rays may be studied by solid-state NMR. The NMR technique is very versatile as one may detect polymorphism, multiple molecules in the asymmetric unit, disorder[2-4] and solvation by solid-state NMR. Phase transformations[5] may also be studied. Clathrates and complexes have also been examined by NMR[6]. Perhaps the main disadvantage of solid-state NMR is that whilst connectivity patterns and local electronic environments may be studied, the techniques cannot provide information directly on precise bond lengths, angles and packing arrangements. Another disadvantage of NMR is that usually peaks must be assigned in order to extract structural information and this is not always a simple task. In the solution-state, many techniques are available for assignment (see chapter 5) but fewer are feasible in the solid-state, and so assignments are transferred from solution to solid spectra. The differences in chemical shift between solution and solid-state arise from the differential effects of solution and solid-state media on the molecular structure[7,8]. In solids, if the intermolecular interactions are primarily of the Van der Waals type (i.e. quite weak interactions) then the chemical shifts are usually similar to those in the solution-state[1]. If the interactions are stronger (e.g. as for dipolar, ionic, charge-transfer or hydrogen-bonding interactions) then the differences in shift between solid and solution may be significant. Another complication is that in the solution-state there is

usually an equilibrium mixture of conformers, whilst in the solid usually only one conformer is present.

Generally there will be one set of NMR peaks that represents all the molecules in the unit cell (i.e. a one-to-one correspondence between the number of peaks in the spectrum and the number of chemically inequivalent sites in the molecule). However, sometimes more peaks are present. The causes may be the presence of a quadrupolar nucleus, non-congruent molecules or a loss of symmetry. When there is more than one conformer present in a crystal, then the spectrum will appear as the composite of the spectra of the two isolated conformers.

The information most readily available from the NMR spectrum is the chemical shift. The chemical shift reflects the environment of the nucleus. This is affected by the nearest neighbouring atoms, and also the bonding, as the electrons shield the nucleus from the magnetic field. However, the shielding effect is orientation dependent. The anisotropy is greatest for nuclei with electrons that are highly directional, e.g. for a carbonyl group. In the case of a carbonyl carbon atom, the shielding is greatest in a direction that is perpendicular to the sp^2 plane[9].

The anisotropy can be represented by tensor components[10] and it is often useful to study these tensors. The tensors can be found from single-crystal NMR but the experiment is very time consuming[1] and requires a large crystal (1-100 cm^3). Methods have been developed to find the shielding tensors components from powdered samples, and these are described in chapter 7.

Two of the most frequently asked questions in solid-state NMR are firstly, can the mode of hydrogen bonding be established from the spectrum, and secondly, in the case where splittings have been observed, what is the cause of the splittings? These questions will be addressed in the following sections.

2.2. Hydrogen Bonding

The formation of hydrogen bonds has been observed to cause a deshielding effect on the carbon chemical shift of carbonyls[1]. The deshielding effect originates in the displacement of electron density away from the carbon atom, and towards the electrophilic hydrogen nucleus. The magnitude of the shift depends upon the bond strength and upon the nature of the groups involved in the hydrogen bond. Indeed, studies of the effect of hydrogen bonding on the shielding tensors[11-16] have revealed that there is a significant increase (of 10-50 ppm) in the value of σ_{22}. This alone would lead to high frequency shifts in the chemical shift (δ) of one third of this amount (about 3-15 ppm)[17-19], and also an increase in the asymmetry, if both other tensor components remained the same. Studies have also been made that correlate the length of the hydrogen bond with the chemical shift[18]. The difference in chemical shift between solid and solution (which is assumed to be non hydrogen bonded) shows an inverse relationship with the hydrogen bond length. These matters will be discussed again in chapters 7 and 8.

In homopolypeptide chains a relationship has been seen between the chemical shift for the glycine carbonyl carbon and its conformation[20]. The conformation is strongly influenced by the hydrogen bonds that are formed, so a relationship between chemical shift and hydrogen bond length might be expected. It is not possible to study such effects in solution as only an average chemical shift (over all rotational isomers) is observed. A study was undertaken by using X-ray analysis to determine hydrogen bond length and conformation, and solid-state NMR to measure the chemical shift of the carbonyl carbon. It was found that there are two types of bond: (i) amide C=O...H-N and (ii) amide C=O...H_3N^+. Type (i) shows that as the hydrogen bond length R_{NO} decreases there is a high frequency shift. There is a linear relationship which holds for dimers, trimers and also for polypeptides. A similar effect has been seen in hydroxybenzaldehydes[18] for the formation of inter- and intra-molecular

C=O...H-O type bonds. Type (ii) shows the opposite relationship i.e. that there is a low frequency shift with a decrease in hydrogen bond length. This result indicates that there is considerable difference in electronic environment between the types of hydrogen bond. Shielding constant calculations have shown that the strength of the hydrogen bond has little effect on the chemical shift if the bond is longer than 2.6Å. At longer bond lengths the chemical shift dependence is dominated by the conformation[20]. Both types of bond show only small directional effects when the hydrogen bond is strong, but the shift is affected considerably by conformation if the bond is only weak.

2.3. The Origin Of Splittings

A spectrum may contain more peaks than there are chemically different atoms in the molecule. When this occurs, there are several possible causes of these splittings.

The first case to consider is the situation when there are quadrupolar nuclei present in the sample e.g. ^{14}N or ^{35}Cl. The presence of these nuclei can have a range of effects from broadening of signals to the extreme case of splitting resonances[21-40]. Examples of this phenomenon have been observed in this work and are discussed in chapters 9 and 10. The effect is usually limited to causing splitting of adjacent nuclei only, although sometimes the effect can be seen at more distant sites. The broadening or splitting effect of the quadrupolar nucleus on the spectrum is often helpful in assigning the spectrum.

Molecules that possess symmetry often have solution-state NMR spectra that contain fewer peaks than the molecular formula suggests, each chemically different atom having a unique chemical shift. In the solid-state however, the symmetry is often reduced. This may occur due to the way the molecules pack together[41,42]. An example of this phenomenon was seen in the study of polymorphs of the anti-bacterial compounds sulphathiazole[43] and sulphanilamide[44]. However, in the solid-state molecular motion is much slower compared to solution, and this may be the cause of reduced symmetry. The

solution-state spectrum of 1,3,5-trimethoxy-benzene[45] shows three peaks from the three different carbon atoms in the molecule. Molecular motion means that the symmetry is high. In the solid-state however, the three protonated ring carbon atoms have different chemical shifts. The reduced symmetry occurs because the rapid motion of the methoxy groups is no longer possible, and only one asymmetric conformation of the molecule is found. This gives rise to the three different peaks for the protonated ring atoms. The symmetry of a molecule may be lowered by the formation of tautomers. Keto-enol tautomerism of 1,3-diketones often occurs and so the molecule has a lower symmetry than might be first expected. This too can lead to the presence of extra peaks in the spectrum[14,15].

An interesting effect is sometimes seen when a polymorph exists in a form that has two or more molecules in the crystallographic asymmetric unit[46-49]. Then the molecules in the asymmetric unit may have different conformations and hydrogen bond lengths and also experience different packing forces. Then atoms in the asymmetric unit are in different environments and will give peaks at different frequencies in the NMR spectrum. One peak is seen from each atom in the asymmetric unit. There have been several observations of this effect in steroids[48-50] and in other compounds e.g. 4'-methyl-2'-nitro-acetanilide[51] (where the distribution of electrons in the molecule has also been studied) and methadone hydrochloride[52].

It is sometimes possible to infer from the solid-state NMR spectra crystallographic information - for example the number of molecules in the asymmetric unit or, if spectra of polymorphs are very similar, possession of a similar crystal structure that is different in some minor detail. This information may be particularly valuable when the crystal structure cannot be elucidated by the more conventional techniques using X-rays.

2.4. Polymorphs Of Pharmaceuticals - Effects On Bio-Availability.

The unambiguous determination of the polymorph present in a sample is of particular importance to the manufacturers of pharmaceutical preparations. It is known that for some drugs only particular polymorphs are biologically active[53]. A recent study[53] has shown that particle size and physico-chemical properties of drug powders affect the bio-availability through polymorphic transitions, as the polymorphs may have different dissolution rates. Three drugs were studied, chloroamphenicol palmitate, indomethacin and cephalexin.

Chloroamphenicol palmitate has three polymorphs A, B and C, of which only B and C are suitable for clinical use. Grinding causes the transitions represented in figure 2.1.

Figure 2.1 - Showing the grinding induced transformations undergone by chloroamphenicol palmitate

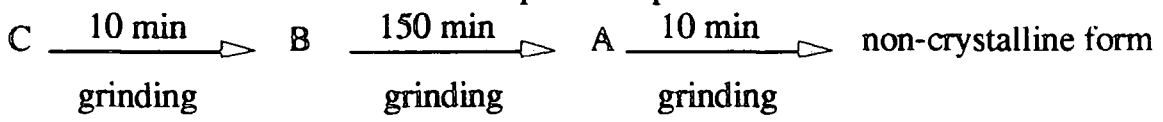

Polymorph C is the most soluble and A the least. This suggests that C is the most suitable form for clinical use, as it has a higher bio-availability. However smaller particles are more bio-available than large particles, so there is a conflict between particle size and solubility.

Indomethacin[53] also undergoes transitions upon grinding from the stable (c) form via the meta-stable (a) form, to an unstable non-crystalline state 60% more soluble than the c form. Also cephalexin[53] became increasingly non-crystalline with increased grinding time. The non-crystalline form has a higher hygroscopicity and a solubility twice that of the crystalline form - thereby affecting bio-availability with increased grinding time.

The pathways for crystalline transformation may be represented schematically as in figure 2.2. If crystal growth is slow, then a non-crystalline solid is formed upon grinding.

Figure 2.2 - Schematic diagram showing the transformations that may accompany the grinding process

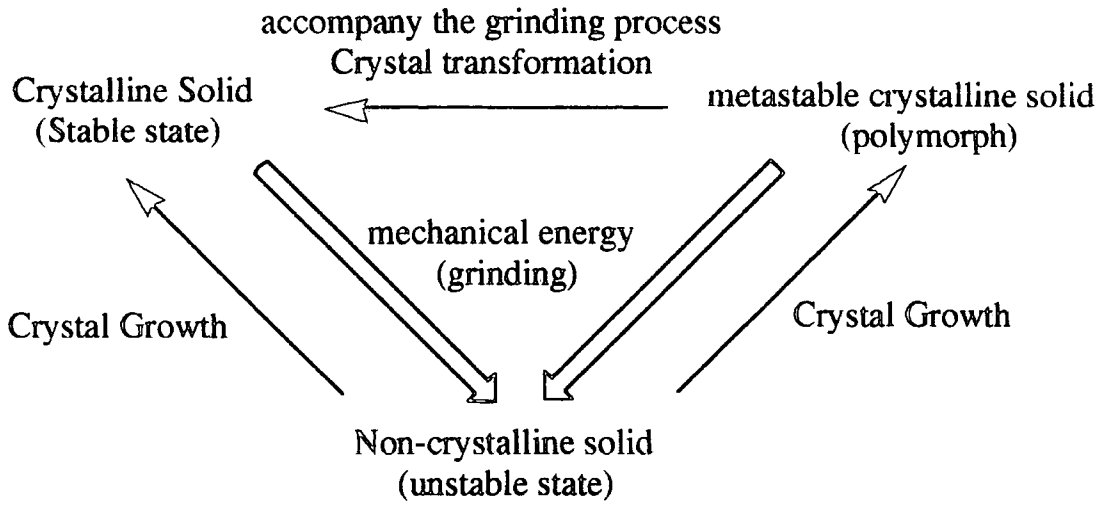

Solid-state NMR has also been used in the study of the pharmaceuticals carbamazepine[54], cefazolin, benoxaprofen and nabilone[55] to quantify the relative proportions of each component in a mixture of polymorphic forms. In the cases of the latter three compounds the work is particularly interesting because the samples used were of the prescribed drugs (which contain bulking agents).

2.5. Studies Of Pharmaceutical Compounds

2.5.1. Testosterone

Testosterone is known to exist in three crystal forms[56-58], and solid-state NMR spectra of each form have been reported[49,59]. The two molecules in the asymmetric unit of the α form are linked by head to tail hydrogen bonds C(3)=O...HO-C(17). Conformational differences between the molecules lead to two hydrogen bond lengths, which increases the differences in environment of the two molecules. These combined effects have lead to substantial crystallographic splittings at C3 (1.5 ppm), C5 (1.4 ppm) and C17 (2.3 ppm) and also to smaller splittings notably at C9 and C11. The splittings are shown in figure 2.3.

Figure 2.3 - Showing the crystallographic splittings (in ppm) of α-testosterone

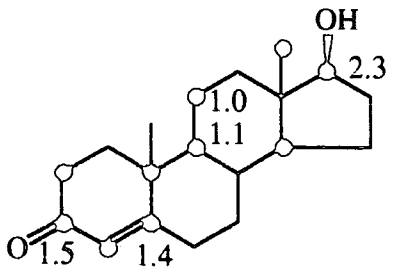

The splittings at C3, C5 and C17 may be attributed mostly to the different hydrogen bond lengths. C3 and C17 are directly linked by the hydrogen bond and C5 is conjugated to C3. This shows, as might be intuitively expected, that the degree of conjugation is affected by the strength of any hydrogen bond that is formed. It is not possible to assign the peaks to a particular molecule as many factors may affect the chemical shifts of the peaks from atoms in different environments.

The β and γ forms contain only one molecule in the asymmetric unit each, so no splittings are expected, and none are found in pure samples. However the three forms show different chemical shifts for all atoms and so mixtures of polymorphic forms may be identified by comparison with spectra from pure samples. The largest differences in peak positions between the three forms are at C3, C5, C11, C12 and C17. The differences at C3, C5 and C17 may be explained as before by various hydrogen bond lengths and the associated degree of conjugation. Indeed, the β form is known to be more planar than the δ form around C3, C4 and C5 and this could explain why C5 is shifted to high frequency from that in the δ form, as increased planarity will increase the level of conjugation. The differences at C11 and C12 seem to indicate a change in conformation in the C ring between the forms.

2.5.2. Androstanolone

Figure 2.4 - Showing the structure of androstanolone

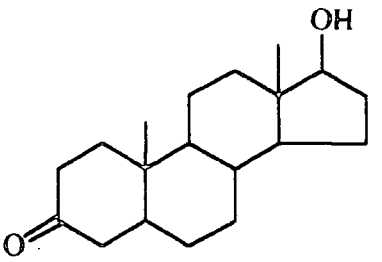

Androstanolone is another steroid (shown in figure 2.4) that has been studied by solid-state NMR with respect to polymorphism[50]. There are two forms known, one form (the anhydrate) with two molecules in the asymmetric unit. The molecules are involved in intermolecular hydrogen bonding (OH...O=C) in a head-to-tail fashion, which creates two different hydrogen bond lengths of 2.75Å and 2.82Å. Crystallographic splittings appear at most atoms on the molecule, which suggests that the two molecules are in rather different environments. The C17 resonance at the hydroxyl group is split, which can be explained by the presence of the two different hydrogen bond lengths. However, the differences are surprisingly not seen at C3 (the carbonyl). The reason is unclear but it could be that the effect is masked by conformational differences at nearby atoms. There is also splitting at C18 (the methyl group attached at the C/D ring junction), which can be explained by different van der Waals distances.

The hydrate has only one molecule in the asymmetric unit. As in the anhydrate there is intermolecular hydrogen bonding forming a head-to-tail chain of molecules, but with water molecules intervening (O-O bond lengths of 2.67 Å and 2.83Å). Comparison of the monohydrate form with the anhydrate shows there are differences in chemical shift at C18 and C19 (the methyl group attached at the A/B ring junction), associated with different Van der Waals interactions. The large shift of the C3 resonance from that in the solution can be attributed to hydrogen bonding, but the position of the C17 resonance does not seem to be affected in the same way.

2.5.3. Prednisolone Tertiarybutyl Acetate

Figure 2.5 - Showing the numbering of prednisolone tert-butyl acetate

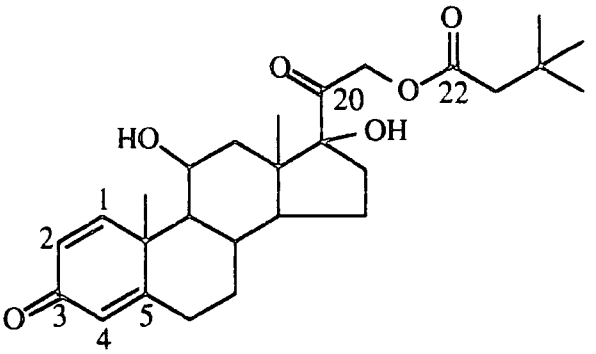

The steroid prednisolone tert-butyl acetate has a structure (shown in figure 2.5) that is very similar to those of testosterone and cortisone acetate. There are five polymorphs[60,61]. There is rather fewer detailed chemical shift data available for this steroid but it seems that the largest variations in chemical shift between the forms are at the carbonyl carbons C3, C20 and C22 and at unsaturated carbons C1, C2, C4 and C5. The largest difference occurs at C1 (up to 8 ppm between forms).

Attempts have been made to correlate the hydrogen bond lengths with the chemical shift. The chemical shifts of C1, C3, C5 and C22 increase as the strength of the hydrogen bonding increases. In particular, a graph[60] of the difference in chemical shift (between solid and solution) of C3 against the hydrogen bond length shows an inverse relationship. A similar graph of data for C1 also shows a similar relationship.

2.5.4. Cortisone Acetate

Figure 2.6 - Showing the structure of cortisone acetate

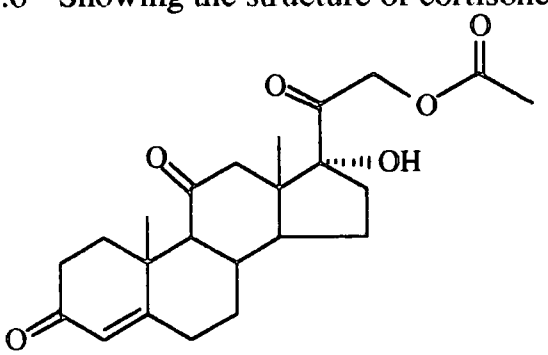

At least five polymorphs of cortisone acetate (shown in figure 2.6) have been reported[62-67], three of which could be described as true polymorphs, being anhydrous, and the others are hydrates. There have also been reports of solvates of some forms. There are a number of papers describing the preparation of the polymorphs, many using different nomenclature and so the situation is not immediately clear. However, by comparison of the preparative methods, the situation can be untangled. The nomenclature used in this thesis will be that of Carless et al.[63]. Full crystal structure determinations of four polymorphs have been performed, and the unit cell dimensions of another two forms are available from powder diffraction studies[68-71]. Full details of the preparative methods are given in chapter 4 and crystal structure information is presented in chapter 6.

High resolution solid-state NMR spectra of six forms have been published[48] and show significant differences, so that identification of the form present in the sample is easy, and impurities of other forms can be detected and identified. The complete assignment of the spectra was not possible and so the differences in the spectra could not be easily attributed to specific differences in the conformation, packing or intermolecular interactions.

The work of Harris et al[48] has shown that cortisone acetate is a steroid worthy of further study, particularly as it is uncommon to find a compound with so many polymorphs (and with the crystal structures determined). There is also one form that appears to have three molecules in the asymmetric unit, which allows other aspects of polymorphism to be studied.

2.5.5. Penicillins

A number of penicillins have been studied in order to obtain conformational information[32]. Many of the atoms around the rigid four- and five-membered (see figure 2.7) rings have chemical shifts that remain almost constant between forms. However, it has been found that the chemical shift of the methyl group (marked β) is sensitive to the conformation of that ring. If the sulphur atom is out of the plane of the other four atoms in that ring, then the methyl resonance shifts to low frequency, but if C3 is the atom that is out of the plane of

the other four atoms in the ring, then the methyl resonance will shift to high frequency. The effect of the quadrupolar ^{14}N nucleus on the resonances of adjacent carbon atoms has also been observed by the appearance of a pair of peaks with intensities in a 2:1 ratio.

Figure 2.7 - Showing the basic penicillin structure

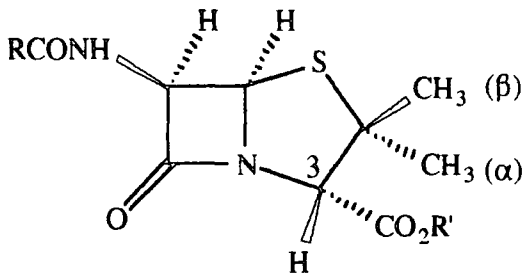

2.5.6. Other Drugs

The anti-bacterial compounds trimethoprim (TMP)(i) and sulphamethoxazole (SMZ)(ii) are often used in a 1:5 mixture as a pharmaceutical preparation. The structures are shown in figure 2.8. A recent study has shown the existence of a 1:1 molecular complex which is insoluble in aqueous media. As it is known that the nature of the interaction may affect the bioavailability of the complex, an investigation of the nature of the interaction was carried out [72].

Figure 2.8 - Showing the structures of trimethoprim (TMP) and sulphamethoxazole (SMZ).

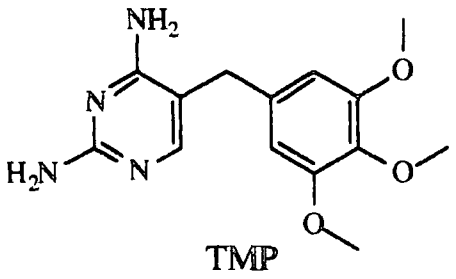

TMP

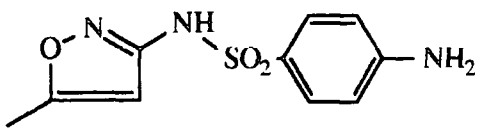

SMZ

The chemical shifts are consistent with one proposed mode of hydrogen bonding, but also the chemical shifts suggest that the formation of the complex causes a change in the conformation of the two component molecules. A similar study of 2-aminobenzoic acid also addresses the question of the mode of hydrogen bonding via the chemical shifts[73] as these are dependent upon the

charge distribution in the molecule, and it is therefore possible to find out if the molecule is neutral or zwitterionic.

2.6. Conclusions

Solid-state NMR has been used widely to study many aspects of solid-state molecular and crystal structure. The main areas of use of solid-state NMR may be summarised briefly as follows:

i) to confirm the existence of new polymorphs

ii) to identify the components of a mixture

iii) to find the relative proportions of the components of a mixture

iv) to identify the presence of hydrogen bonds via the effect on the chemical shifts

v) to find the number of molecules in the crystallographic asymmetric unit

vi) to study conformational analysis

vii) to find the electron distribution in a molecule (i.e. to find out if molecules are neutral or zwitterionic or to find out if a 1,3 -diketone is present in the enol form)

This very brief list of uses is intended to demonstrate the great potential of the solid-state NMR technique to provide information in a way that is complementary to crystal structure determination. In certain cases, where X-ray diffraction is not feasible, solid-state NMR is one of the few tools that is capable of providing what could be regarded as 'crystallography information'.

2.7. References

(1) Etter, M.C., Hoye R.C., Vojta G.M. *Cryst. Reviews* 1, 281 (1988).

(2) Horii, F., Yamamoto H., Hirai A., Kitamaru R. *Carbohydrate Research* **160**, 29 (1987).

(3) Isogai, A., Usuda M., Kato T., Uryu T., Atalla R. *Macromolecules* 22, 3168 (1989).

(4) Atalla, R.H., Gast J.C., Sindorf P.W., Bartuska V.J., Maciel G.E. *J. Am. Chem. Soc.* 102, 3249 (1980).

(5) Lifshitz, E., Goldfarb D., Yega S., Luz Z., Zimmermann H. *J. Am. Chem. Soc.* **109**, 7280 (1987).

(6) Ripmeester, J.A. *Chem. Phys. Lett* 74, (1980).

(7) Lippmaa, E.T., Alla M.A., Pehk T.J., Engelhardt G. *J. Am. Chem. Soc.* **100**, 1929 (1978).

(8) Etter, M., Reutzel S., Vojta G. *J. Molec. Struct.* 237, 165 (1990).

(9) Mehring, M. *C-13 shielding tensors*; Springer-Verlag: Heidelburg, (1976); NMR Basic Principles and Progress; Vol. 11, pp 183.

(10) Harris, R.K. *Nuclear magnetic resonance spectroscopy*; Pitman: London, (1983).

(11) Griffin, R., Pines A., Pausak S., Waugh J. *J. Chem. Phys.* **63**, 1267 (1975).

(12) Torman, J.v.D., Veeman W., Boer E.d. *J. Magn. Reson.* 32, 49 (1978).

(13) Veeman, W. *Phil. Trans. R. Soc. Lond.* A299, 629 (1981).

(14) Imashiro, F., Maeda S., Takegoshi K., Terao T., Saika A. *Chem. Phys. Lett* **92**, 642 (1982).

(15) Takegoshi, K., Naito A., McDowell C. *J. Magn. Reson.* **65**, 34 (1985).

(16) Takegoshi, K., McDowell C.A. *J. Am. Chem. Soc.* **108**, 6852 (1986).

(17) Nagaoka, S., Terao T., Imashiro F., Saika A., Hirota N., Hayashi S. *Chem. Phys. Lett* **80**, 580 (1981).

(18) Imashiro, F., Maeda S., Takegoshi K., Terao T., Saika A. *Chem. Phys. Lett* **99**, 189 (1983).

(19) Imashiro, F., Maeda S., Takegoshi K., Terao T., Saika A. *J. Am. Chem. Soc.* **109**, 5213 (1987).

(20) Ando, S., Ando I., Shoji A., Ozaki T. *J. Am. Chem. Soc.* **110**, 3380 (1988).

(21) Lindman, B., S.Forsen In *NMR Basic Principles and Progress*; Eds. Diehl, P., Fluck, E. and Kosfeld, R.; Springer-Verlag: Berlin, (1976); Vol. 12.

(22) Opella, S.J., Frey M.H., Cross T.A. *J. Am. Chem. Soc.* **101**, 5856 (1979).

(23) Groombridge, C.J., Harris R.K., Packer K.J., Say B.J., Tanner S.F. *J. Chem. Soc. Chem. Commun.* 174 (1980).

(24) Frey, M.H., Opella S.J. *J. Chem. Soc. Chem. Commun.* 474 (1980).

(25) Fleming, W.W., Fyfe C.A., Lyerla J.R., Vanni H., Yannoni C.S. *Macromol.* 13, 460 (1980).

(26) Naito, A., Ganapathy S., McDowell C.A. *J. Chem. Phys.* 74, 5393 (1981).

(27) Zumbulyadis, N., Henrichs P.M., Young R.H. *J. Chem. Phys.* 75, 1603 (1981).

(28) Hexem, J.G., Frey M.H., Opella S.J. *J. Chem. Phys.* 77, 3847 (1982).

(29) Naito, A., Ganapathy S., McDowell C.A. *J. Magn. Reson.* 48, 367 (1982).

(30) Menger, E.M., Veeman W.S. *J. Magn. Reson.* 46, 257 (1982).

(31) Bohm, J., Fenzke D., Pfeifer H. *J. Magn. Reson.* 55, 197 (1983).

(32) Clayden, N.J., Dobson C.M., Lian L.Y., Twynman J.M. *J. Chem. Soc. Perkin II* 1933 (1986).

(33) Olivieri, A.C., Frydman L., Diaz L.E. *J. Magn. Reson.* 75, 50 (1987).

(34) Komoroski, R.A., Parker R.G., Mazany A.M. *J. Magn. Reson.* 73, 389 (1987).

(35) Harris, R.K. *J. Magn. Reson.* 78, 389 (1988).

(36) Olivieri, A., Frydman L., Grasselli M., Diaz L. *Magn. Reson. Chem.* 26, 615 (1988).

(37) Apperley, D.C., Bai H., Harris R.K. *Molec. Phys.* 68, 1277 (1989).

(38) Olivieri, A.C. *J. Magn. Reson.* 81, 201 (1989).

(39) Martinez, H., Byrn S.R., Pfieffer R.R. *Pharmaceutical Research* 7, 147 (1990).

(40) Gobetto, R., Harris R.K., Apperley D.C. *J. Magn. Reson.* 96, 119 (1992).

(41) Hays, G. *Analyst* 107, 241 (1982).

(42) Hays, G.R. *J. Chem. Soc. Perkin II* 1049 (1983).

(43) Anwar, J., Tarling S.E., Barnes P. *J. Pharm. Sci.* 78, 337 (1989).

(44) Frydman, L., Olivieri A.C., Diaz L.E., Frydman B., Schmidt A., Vega S. *Molec. Phys.* 70, 563 (1990).

(45) Steger, T.R., Stejskal E.O., McKay R.A., Stults B.R., Schaefer J. *Tetrahedron Lett.* 4, 295 (1979).

(46) Balimann, G., Groombrigde C., Harris R., Packer K., Say B., Tanner S. *Philos. Trans. R. Soc. Lond.* A299, 643 (1981).

(47) Jeffrey, G., Wood R., Pfeffer P., Hicks K. *J. Am. Chem. Soc.* 105, 2128 (1983).

(48) Harris, R.K., Kenwright A.M., Say B.J., Yeung R.R., Fletton R.A., Lancaster R.W., Hardgrove G.L. Jnr. *Spectrochim. Acta* 46A, 927 (1990).

(49) Fletton, R.A., Harris R.K., Kenwright A.M., Lancaster R.W., Packer K.J., Sheppard N. *Spectrochim. Acta* 43A, 1111 (1987).

(50) Harris, R.K., Say B.J., Yeung R.R., Fletton R.A., Lancaster R.W. *Spectrochim. Acta* 45A, 465 (1989).

(51) Fletton, R., Lancaster R., Harris R., Kenwright A., Packer K., Waters D., Yeadon A. *J. Chem. Soc. Perkin II* 1705 (1986).

(52) Sumner, S., Moreland C., Carrol F., Brine G., Boldt K. *Magn. Reson. Chem.* 27, 311 (1989).

(53) Otsuka, M., Kaniniwa N. *Proc. 2nd Japan-Soviet Symp. Mechanochemistry* 209 (1988).

(54) Suryanarayanan, R., Wiedmann T.S. *Pharmaceutical Research* 7, 184 (1990).

(55) Byrn, S.R., Gray G., Pfeiffer R.R., Frye J. *J. Pharm. Sci.* 74, 565 (1985).

(56) Roberts, P.J., Pettersen R.C., Sheldrick G.M., Isaacs N.W., Kennard O. *J. Chem. Soc. Perkin II* 1978 (1973).

(57) Busetta, P.B., Courseille C., Leroy F., Hospital M. *Acta Cryst.* B28, 3293 (1972).

(58) Isaacs, N.W., Motherwell W.D.S., Coppola J.C., Kennard O. *J. Chem. Soc. Perkin II* 2335 (1972).

(59) Hayamizu, K., Ishii T., Yangisawa M., Kamo O. *Magn. Reson. Chem.* 28, 250 (1990).

(60) Byrn, S.R., Sutton P.A., Tobias B., Frye J., Main P. *J. Am. Chem. Soc.* 110, 1609 (1988).

(61) Byrn, S.R., Tobias B., Kessler D., Frye J., Sutton P., Saindon P., Kozlowski J. *Am. Crystallographic Assoc. Trans.* 24, 41 (1988).

(62) Callow, R.K., Kennard O. *J. Pharm. Pharmacol.* 13, 723 (1961).

(63) Carless, J.E., Moustafa M.A., Rapson H.D.C. *J. Pharm. Pharmacol.* 18, 190 (1966).

(64) Mesley, R.J. *J. Pharm. Pharmacol.* 20, 877 (1968).

(65) Kuhnert-Brandstatter, M., Gasser P. *Microchem. J.* 16, 590 (1971).

(66) Mesley, R.J., Johnson C.A. *J. Pharm. Pharmacol.* 17, 329 (1965).

(67) Mesley, R.J. *Spectrochim. Acta* 22, 889 (1966).

(68) Kanters, J.A., de Koster A., van Geerestein V.J., van Dijck L.V. *Acta Cryst.* C41, 760 (1985).

(69) Declercq, J.P., Germain G., van Meerssche M. *Cryst. Struct. Commun.* 1, 59 (1972).

(70) van Geerestein, V.J., Kanters J.A. *Acta Cryst.* C43, 136 (1987).

(71) van Geerestein, V.J., Kanters J.A. *Acta Cryst.* C43, 936 (1987).

(72) Fruttero, R., Hawkes G.E., Randall E.W., Gasco A., Groombridge C.J. *J. Chem. Soc. Perkin II* 1863 (1988).

(73) Harris, R.K., Jackson P. *J. Phys. Chem. Solids* 48, 813 (1987).

Chapter 3

Solid-State NMR Theory

Chapter 3 Solid-State NMR Theory

The NMR techniques that have been used in the work presented in this thesis are well established. Detailed theoretical approaches may be found in many texts, and experimental considerations are also well understood[1-6]. Therefore the aim of this chapter is to provide a brief outline of the theory of solid-state NMR, as it has been applied to the study of polymorphism. Where it has been necessary to consider the theory in more detail for specific experiments, the discussion is presented in the relevant chapter. The main nucleus that has been studied in this thesis is ^{13}C, with spin-$\frac{1}{2}$. Therefore the theory described here will be that relating particularly to the spectra of spin-$\frac{1}{2}$ nuclei and any related factors.

3.1. Introduction

Nuclei possess a property known as spin (I) that is quantized and may take any positive integral, half-integral, or zero value. Nuclear magnetic resonance is an effect that is based upon nuclei with non-zero nuclear spin[1,3,4]. Motion of the nucleus induces a magnetic moment (μ) that is dependent upon the value of I. The possible orientations of μ are defined by the azimuthal quantum number (m_I), which takes values of -I, -I+1 ... +I (i.e. 2I+1 values of m_I exist). When magnetic moments are placed in a static magnetic field of flux density $\mathbb{B}_0$, the degeneracy of the energies of the magnetic moments is lifted. The magnetic moment precesses about $\mathbb{B}_0$, describing a cone. The population of each energy level is given by the Boltzmann distribution, and as these are unequal for the different energy levels (i.e. different orientations of μ), transitions may occur if radiation of the appropriate frequency is applied. The lifting of degeneracy of the energy levels is called Zeeman splitting. In NMR spectroscopy transition frequencies are usually tens or hundreds of MHz, in the radio-frequency range of the electromagnetic spectrum[7]. The transition frequency (ν) is known as the Larmor frequency and is given by equation (1).

$$\nu = \frac{\gamma}{2\pi} B \quad \ldots\ldots (1)$$

where γ is the magnetogyric ratio for the nucleus and B is the magnitude of $\mathbb{B}_0$.

Figure 3.1 - Showing the two orientations of the magnetic moments

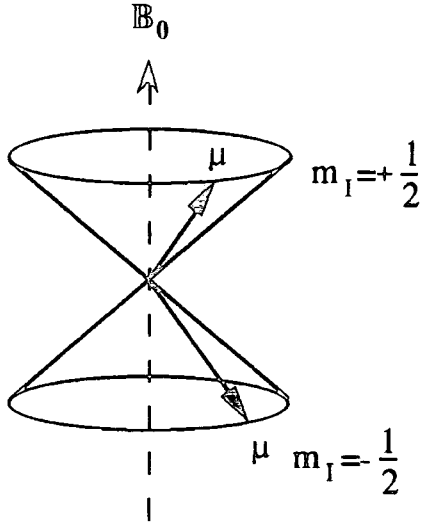

In a macroscopic sample the magnetic moments are distributed at random around a cone and precess at the Larmor frequency. If one views this from a frame of reference that is rotating about $\mathbb{B}_0$ at the Larmor frequency, then the magnetic moments appear static. It is usually more convenient to consider the total or resultant magnetic moment. This is referred to as the magnetization. When the system is in equilibrium, the magnetization vector ($\mathbb{M}$) is aligned with the magnetic field $\mathbb{B}_0$. The direction of the magnetic field usually defines the z-axis of a co-ordinate system. If radio frequency radiation is applied in the form of a second magnetic field $\mathbb{B}_1$ that is perpendicular to $\mathbb{B}_0$, then the magnetization will precess about $\mathbb{B}_1$, tipping towards the x-y plane. So if then a 90° pulse along x is applied, the magnetization will be brought into the y direction. If $\mathbb{B}_1$ is then switched to be along y, then the spins are said to be spin locked.

Figure 3.2 - Showing the effect of a second magnetic field $\mathbb{B}_1$ on the magnetisation vector $\mathbb{M}$

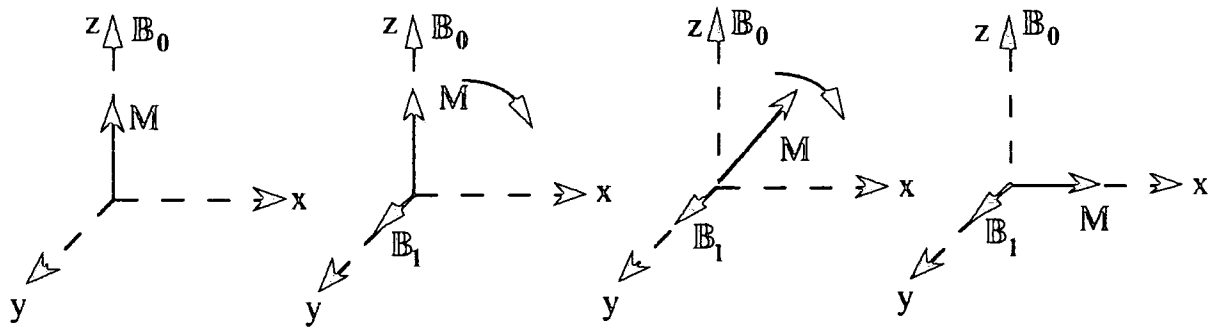

When B_1 is switched off, M slowly returns to the equilibrium position. The moving magnetization in the x-y plane induces a current in the receiver coils. This process is known as free induction decay (FID). The signal contains information about the transition frequencies, and Fourier transform of the FID gives the spectrum.

3.2. Relaxation

It is the decay or relaxation of the magnetization that gives rise to the NMR signal. There are several important mechanisms by which relaxation can occur[1,3,7,8]:

Spin-lattice (longitudinal) relaxation. The energy is transferred to the surroundings of the nucleus so that the Boltzmann populations of each energy level can be re-established. Spin-lattice relaxation requires that there is a fluctuating magnetic field at the Larmor frequency so that energy transfer can occur. This refers to the growth of M_z and is characterised by the time constant T_1.

Spin-spin (transverse) relaxation. This refers to the decay of M_x and M_y. Direct interactions of the spin states means that energy can be transferred in a flip-flop process called spin diffusion. Spin-spin relaxation causes dephasing of the magnetization vectors thus reducing the magnetization in the x-y plane. Spin-spin relaxation may be aided by field inhomogeneities and is characterised by time constant T_2.

Spin-lattice relaxation in the rotating frame. This refers to the relaxation of magnetisation whilst it is spin-locked. $T_{1\rho}$ is the time constant that characterises this type of relaxation.

In the solution-state where motion is rapid $T_1=T_2=T_{1\rho}$. But in solids, T_1 is much greater than $T_{1\rho}$, which is in turn greater than T_2, since spin diffusion is much faster in solids due to the spins being in much closer proximity, and because motion is much slower. In solids generally T_2 is of the order of microseconds, $T_{1\rho}$ is usually milliseconds, whilst T_1 may be seconds or minutes.

3.3. Line broadening mechanisms

A spectrum may contain resonances at many frequencies, i.e. resonances with different chemical shifts. As $\nu = \gamma B$ and γ is a constant, the frequency is dependent upon the actual magnetic field experienced at the nucleus. So the chemical shift is influenced by shielding. However, the resonances have a significant width. The main causes of line broadening are outlined as follows:

3.3.1. Shielding anisotropy

In an isolated atom the electrons might be spherically arranged around the nucleus. In molecules, this is not the case, and the shielding effect of the electrons is orientation dependent. In powdered solids, the orientation in each particle will be different and so a range of shielding effects are felt[9,10]. This gives rise to a range of frequencies and hence broad lines called powder patterns. The shielding anisotropy gives frequency shifts that can be as large as those arising from purely chemical differences in shielding. In solutions molecular tumbling averages the orientation dependence so only narrow lines are observed. In solids lines may be very broad.

3.3.2. Spin-spin coupling

A nucleus that is coupled to others will experience a varying field as each nucleus has a magnetic moment. The interaction is mediated by bonds and is dependent upon distance and upon orientation. As these can vary so will the

frequency, again leading to broadening of the signal. In solids, the spin-spin coupling is usually weak and obscured by other interactions.

3.3.3. Dipolar coupling

A nucleus is affected by the presence of nearby nuclei that possess magnetic moments. Dipolar coupling has distance dependence but is a direct through-space effect, and is again dependent upon orientation. The average (isotropic) value of the interaction, as for the solution-state, is zero, but powder patterns for solids may be many kHz wide.

3.3.4. Quadrupolar coupling

Nuclei with spin > $\frac{1}{2}$ possess a nuclear quadrupole moment. The electric field gradient that is caused by a non-spherical distribution of electrons around the nucleus will interact with the quadrupole moment[11]. This has the effect of perturbing the Zeeman splitting of the nuclear energy levels and so the transition frequencies are affected.

3.3.5. Chemical Shift Dispersion

In amorphous samples a continuous range of molecular environments may exist. These can each resonate at slightly different frequencies. This give rise to broad lines.

3.4. Enhancement Techniques

High quality solid-state NMR spectra may be obtained with the use of certain enhancement techniques. In order to obtain spectra with a high signal-to-noise (S/N) ratio several FIDs are acquired and added together in order to improve the signal level. Between each acquisition, the nuclei must be allowed to relax. To obtain a high quality spectrum quickly the time left for relaxation should be as short as possible, whilst still allowing complete relaxation to occur. This period for relaxation is known as the recycle delay. Generally the recycle delay should be five times T_1. It is also necessary to remove (or at least reduce) the amount of line broadening in order to obtain high-resolution spectra.

The effects of line broadening mechanisms and the problem of long relaxation times and low natural abundance of rare nuclei have been addressed by the following techniques.

3.4.1. Shielding Anisotropy and Magic Angle Spinning.

Shielding anisotropy arises from a non-spherical distribution of electrons around the nucleus. The shielding[1,9,12] has an orientation dependence of $(3\cos^2\theta-1)$, and so when $\theta= 54.7^\circ$ the orientation dependence is removed. This can be achieved by spinning the sample at 54.7° (the magic angle) to $\mathbb{B}_0$[13]. However, the broadening effect of shielding anisotropy can only be completely removed if the spinning speed is greater than the static linewidth. The practical details of setting the magic angle are given elsewhere[14]. A more detailed discussion is presented in chapter 7.

3.4.2. Dipolar interactions and High Power Decoupling

Dipolar coupling is heavily dependent upon internuclear distances. For rare spins (of low natural abundance) homonuclear coupling is weak as the spins are well separated. Heteronuclear coupling (to protons) however is important and can be eliminated by irradiating one type of nucleus (the protons), whilst performing a normal pulse sequence on the other nucleus[15]. This is termed decoupling. Heteronuclear interactions in solids may be strong, and so high power decoupling is required.

3.4.3. Low Sensitivity and Cross Polarisation

The problem with many rare nuclei is that in order to a obtain high S/N ratio, many FIDs must be acquired. The rate of repetition of a pulse sequence is limited by the relaxation time T_1, which is often long. The relaxation times of abundant nuclei are usually much shorter as spin-diffusion is possible. Therefore the method of cross polarisation has been developed[16-19].

The process of spin locking has already been described, but briefly this means that the magnetization and B_1 are in the same direction. Therefore M will precess about B_1 at the frequency γB_1. The cross-polarisation technique involves

spin-locking an abundant and a rare nucleus with different B_1 fields so that the frequency of each is the same.

For example $\gamma_I B_{1I} = \gamma_S B_{1S}$ ..... (2)

where γ_I and γ_S are the magnetogyric ratios of the rare and abundant nuclei, and B_{1I} and B_{1S} are the spin-locking fields of each nucleus. This is called the Hartmann-Hahn matching condition and allows magnetization to be transferred efficiently from the abundant nuclei to the rare nuclei. The magnetisation of the rare nucleus can be observed as usual when B_{1I} is switched off.

There are several advantages to the cross polarization experiment over the single pulse experiment. Firstly that the signal intensities are increased by a factor of $\frac{\gamma_S}{\gamma_I}$, improving the signal to noise. For cross polarisation from protons to carbon, the enhancement in intensity is about four times. Secondly, relaxation depends on the relaxation of the abundant spin which is much faster. However, a third point for consideration is that the rate of magnetization transfer depends on the number and distance of the coupled nuclei. This means that signal intensities are no longer proportional only to the number of nuclei present in the sample with a particular chemical shift. But this can provide additional information[20-22]. It is necessary to optimise the contact time (i.e. the time during which both are nuclei are spin locked) to obtain the maximum signal intensity. The rate at which magnetization is transferred must be balanced against the relaxation of the abundant nuclei ($T_{1\rho}$).

The magnetization (M(t)) at any given time (t) is described for the proton-carbon system by equation (3)[23].

$$M(t) = M_0 \lambda^{-1} \left(1-\exp\left(\frac{-\lambda t}{T_{CH}}\right)\exp\left(\frac{-t}{T^H_{1\rho}}\right)\right) \quad \text{..... (3)}$$

where

$$\lambda = 1+ \frac{T_{CH}}{T^C_{1\rho}} - \frac{T_{CH}}{T^H_{1\rho}}$$

T_{CH} = time constant for the rate of cross-polarisation

$T_{1\rho}^{H}$ = time constant for the rate of spin lattice relaxation in the rotating frame for protons

$T_{1\rho}^{C}$ = time constant for the rate of spin lattice relaxation in the rotating frame for ^{13}C

Usually $T_{1\rho}^{H}$ and $T_{1\rho}^{C}$ are long compared with T_{CH} therefore $\lambda \approx 1$.

Therefore,

$$M(t) = M_0 \left(1-\exp\left(\frac{-t}{T_{CH}}\right)\exp\left(\frac{-t}{T_{1\rho}^{H}}\right)\right) \quad \text{.....(4)}$$

This gives the signal intensity, which is proportional to M(t), and is characterized in the rising part by T_{CH}, and then decreases as characterized by $T_{1\rho}^{H}$. The contact time should be chosen so that the maximum signal intensity is obtained. Clearly this depends on T_{CH}, which varies from carbon to carbon. Recent work has suggested that relaxation may in fact be a two stage process[24].

Figure 3.3 -Showing the intensity vs. contact time as described by equation 4. The vertical line shows that the optimum contact time occurs, in this example, at about 2 ms.

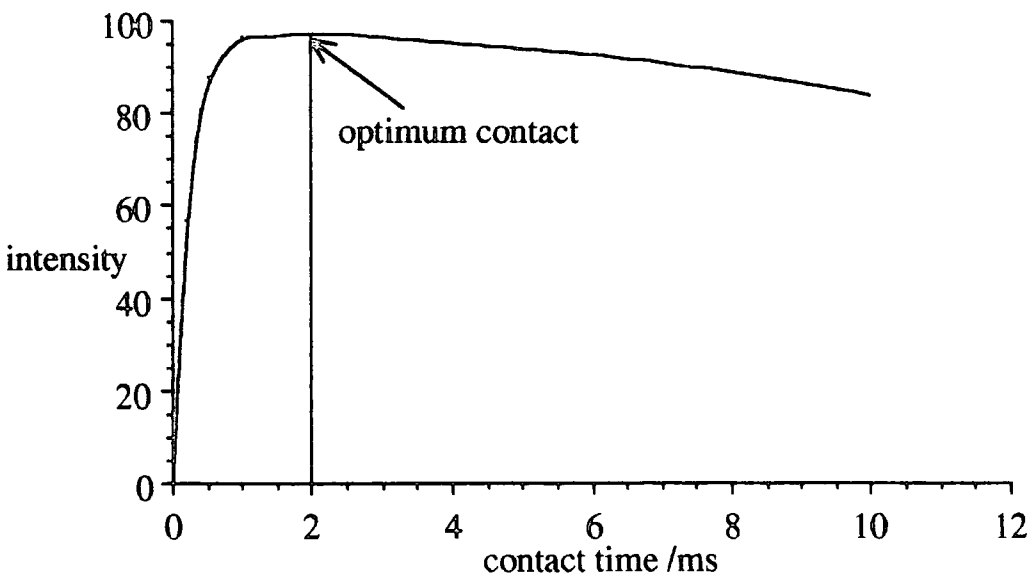

3.5. Summary

The enhancement techniques described have been combined into one experiment: cross-polarization and magic angle spinning with high-power

decoupling (often referred to as CPMAS). The effect of each part is summarised as follows:

CP - signal intensities increased and recycle delay is shortened.

MAS - removal of shielding anisotropy.

HP decoupling - removal of heteronuclear dipolar interactions.

Together, these techniques are widely used and are the basis for high resolution solid-state NMR spectra.

3.6. References

(1) Harris, R.K. *Nuclear magnetic resonance spectroscopy*; Pitman: London, (1983).

(2) Haeberlen, U. *High Resolution NMR in Solids: Selective Averaging*; Academic Press: New York, (1976); Advances in Magnetic Resonance; Vol. Supplement 1.

(3) Shaw, D. *Fourier Transform NMR Spectroscopy;* 2nd ed.; Elsevier: Amsterdam, (1984); Studies in Physical and TheoreticalChemistry; Vol. 30.

(4) Derome, A.E. *Modern NMR Techniques For Chemistry Research*; Pergamon Press: Oxford, (1987); Organic Chemistry Series; Vol. 6.

(5) Balimann, G., Groombrigde C., Harris R., Packer K., Say B., Tanner S. *Philos. Trans. R. Soc. Lond.* A299, 643 (1981).

(6) Harris, R.K. *Analyst* 110, 649 (1985).

(7) Fukushima, E., Roeder S.B.W. *Experimental Pulse NMR*; Addison-Wesley: London, (1981).

(8) Fyfe, C.A. *Solid-State NMR for Chemists*; CFC Press: Guelph, (1983).

(9) Mehring, M. *C-13 shielding tensors*; Springer-Verlag: Heidelburg, (1976); NMR Basic Principles and Progress; Vol. 11, pp 183.

(10) Maricq, M.M., Waugh J.S. *J. Chem. Phys.* 70, 3300 (1979).

(11) Naito, A., Ganapathy S., McDowell C.A. *J. Chem. Phys.* 74, 5393 (1981).

(12) Veeman, W.S. *Prog. NMR Spectr.* 16, 193 (1984).

(13) Andrew, E.R. *Phil. Trans. R. Soc. Lond.* A299, 505 (1981).

(14) Frye, J.S., Maciel G.E. *J. Magn. Reson.* 48, 125 (1982).

(15) Ernst, R.R. *J. Chem. Phys.* 45, 3845 (1966).

(16) Hartmann, S.R., Hahn E.L. *Physical review* 128, 2042 (1962).

(17) Demco, D.E., Tegenfeldt J., Waugh J.S. *Phys. Rev. B* 11, 4133 (1975).

(18) Jakobsen, H.J., Daugaard P., Langer V. *J. Magn. Reson.* 76, 1620168 (1988).

(19) Pines, A., Gibby M.G., Waugh J.S. *J. Chem. Phys.* 59, 569 (1973).

(20) Alemany, L.B., Grant D.M., Pugmuire R.J., Alger T.D., Zilm K.W. *J. Am. Chem. Soc.* 105, 2133 (1983).

(21) Alemany, L.B., Grant D.M., Pugmuire R.J., Alger T.D., Zilm K.W. *J. Am. Chem. Soc.* 105, 2142 (1983).

(22) Alemany, L.B., Grant D.M., Alger T.D., Pugmuire R.J. *J. Am. Chem. Soc.* 105, 6697 (1983).

(23) *High-resolution NMR spectroscopy of synthetic plymers in bulk*; Komoroski, R.A., Ed.; VCH Publishers: Florida, (1986); Vol. 7, pp 42.

(24) Wu, X., Zhang S., Wu X. *Phys. Rev. B* 37, 9827 (1988).

Chapter 4

Experimental

Chapter 4 Experimental

4.1. Spectrometer Details

All the solid-state spectra were acquired using a Bruker CXP-200 spectrometer at the Chemistry Department, University of Durham unless noted otherwise. The spectrometer is equipped with a 4.7 T, wide bore (89.5 mm) superconducting magnet operating at 50.323 MHz for carbon-13 and 200.130 MHz for protons. Carbon-13 spectra were obtained using a Bruker broad band probe. The rotors are 7 mm in diameter and are made of zirconia with Kel-F end-caps. Magic angle spinning is employed, with the "magic angle" set using the ^{79}Br resonance of KBr to give the maximum number of sharp spinning sidebands[1]. The spinning system uses compressed air, and speeds of 3-4 kHz are routinely achieved. The tuning procedure of the proton amplifier makes use of a sample of silicone rubber, and the 90° proton pulse is set to 4 μs. The width at half height of the proton resonance of the tuning sample is generally 16-20 Hz. Setting the cross polarisation condition is done on a sample of adamantane. This is also used to reference the spectrum. The peaks are set to 38.5 ppm and 29.5 ppm, so that the chemical shifts are effectively quoted with respect to tetramethyl silane. This method of referencing should allow chemical shifts to be reported to within ±0.1 ppm. A dead time of 50 μs is used unless stated otherwise to allow for ring-down before the acquisition is begun.

Some work at higher field has been carried out on a Bruker AMX-500 spectrometer at the University of Durham Industrial Research Laboratories, operating at 500.130 MHz for protons and 125.773 MHz for carbon.

All solution-state spectra were acquired using a Varian VXR-400 spectrometer at Glaxo Group Research, Greenford. The spectrometer is equipped with a 9.4 T, 54 mm bore superconducting magnet operating at 100.577 MHz for C-13 and 399.952 MHz for protons, using a 5 mm Varian switchable dual channel probe. The field is locked onto the deuterium signal of the solvent, and coarse shimming is done automatically, with fine shimming completed manually.

4.2. Solid State Pulse Sequences

The solid state pulse sequences used in this work are described below and in figure 4.1.

i Single pulse with no decoupling

There is a four phase cycling of pulses and receiver. This pulse sequence is used to tune the proton and carbon amplifiers, using samples of silicone rubber and adamantane respectively.

ii Single pulse with decoupling

iii Cross polarisation (CP) - this is the pulse sequence usually used for carbon-13 spectra. The contact time is the length of time for which the proton and carbon nuclei are both being simultaneously excited. This sequence may be used with a variable contact time in order to find the optimum conditions.

iv Non quaternary suppression (NQS) - this sequence is designed to give a carbon spectrum from non-protonated atoms only. In practice methyl carbons are also present in the spectrum.

v Single pulse determination of T_1 values - measurement of the T_1 relaxation time by the inversion-recovery method. It may be used (a) with proton decoupling to study dilute nuclei (e.g. ^{13}C), or (b) to study abundant nuclei (e.g. ^{1}H).

Figure 4.1 - The solid-state NMR pulse sequences

i single pulse without decoupling

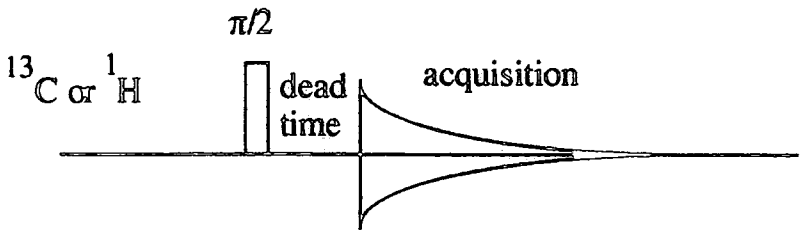

ii single pulse with decoupling

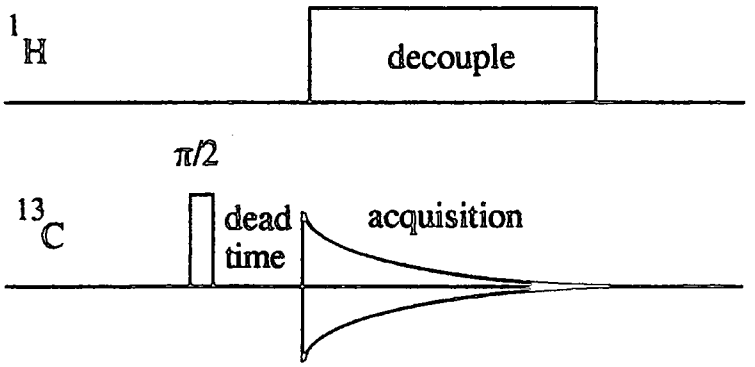

iii cross polarisation

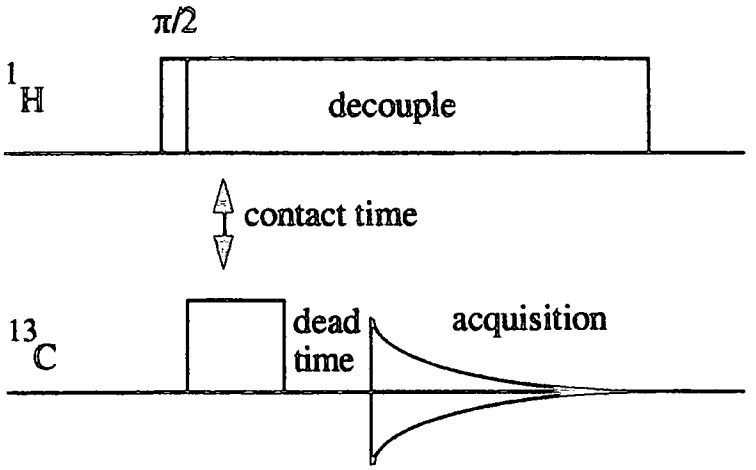

Figure 4.1 continued - The solid-state NMR pulse sequences

iv non quaternary suppression

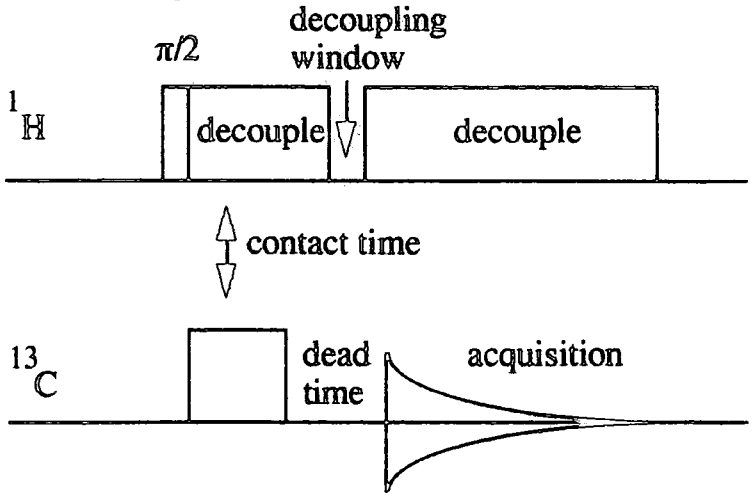

v (a) for dilute nuclei with decoupling

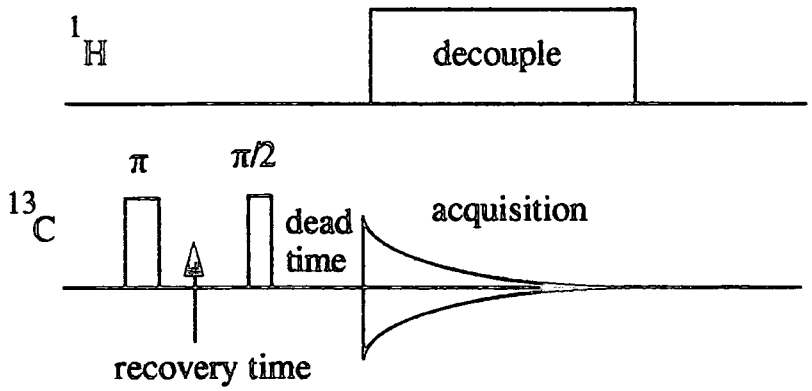

v (b) for abundant nuclei without decoupling

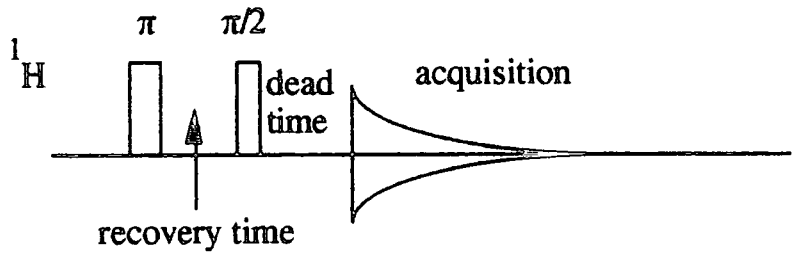

4.3. Assignment Of Solution State Spectra - Techniques Available

The primary method of assigning solution-state spectra is by comparison of the chemical shifts with those of other known compounds that contain similar structural groups. Certain reference texts are particularly useful for this purpose: general assignment[2,3], steroids[4] and cephalosporins[5]. These texts may help with the first stage of assignment, but experiments have been developed to provide unambiguous assignment for complex molecules. These experiments will not be discussed in detail here as they are described fully in many texts and may now be considered to be routine experiments. However, briefly they are described as follows:

i Carbon spectrum (proton decoupled). The high resolution spectra give the isotropic chemical shifts.

ii Proton spectrum. The coupling patterns of protons are quite well understood and so the line multiplicities may help the assignment process.

iii Proton-coupled carbon spectrum. This gives a complex spectrum with each carbon resonance split by attached and adjacent protons. Carbon-carbon coupling is not observed for this dilute nucleus. This method has largely been superseded by other methods (e.g. APT, DEPT) that do not suffer from low intensity signals.

iv Attached proton test (APT)[6].This experiment gives a proton-decoupled carbon spectrum with CH_3 and CH resonances as negative signals, whilst CH_2 and quaternary carbons have positive signals. The pulse sequence is as follows:

^1H decouple .....
^{13}C $\pi/2$- τ - π - τ - acquisition

v Distortionless enhancement by polarisation transfer (DEPT)[7]. This experiment allows the editing of the spectrum into subspectra for each carbon type.

^1H $\pi/2$- τ - π - τ - ϕ - τ - decouple
^{13}C $\pi/2$- τ - π - τ - acquisition

τ is set to 1/2J (where J is the one bond ^{13}C-^{1}H coupling constant) and ϕ is cycled 90°, 45°, 135°.

subspectrum obtained when ϕ is:	
45°	all protonated carbons
90°	CH carbons only
135°	CH_2 down and CH/CH_3 up

vi Homonuclear correlated spectra (COSY)[7]. This two-dimensional technique correlates chemical shifts of coupled protons. The two axes are both proton chemical shifts and the one-dimensional proton spectrum is seen along the diagonal. Cross peaks are seen for each coupling. The pulse sequence is:

COSY-90	^{1}H	$\pi/2$ -	τ -	$\pi/2$ -	acquisition
COSY-45	^{1}H	$\pi/2$ -	τ -	$\pi/4$ -	acquisition

The problems associated with the COSY-90 experiment, i.e. the large number of cross peaks that crowd the very intense diagonal, are largely overcome in the COSY-45 experiment as the mixing of unconnected transitions is reduced by the shorter second pulse. As a result there are fewer cross peaks, and it may be possible to determine the relative sign of the coupling constant to distinguish geminal and vicinal couplings.

vii Heteronuclear correlated spectra (HETCOR)[7]. Another two dimensional technique, but this time the correlation is of carbon-13 chemical shifts with proton chemical shifts. Carbon assignments may be made from a characteristic proton shift or vice versa. The sequence is:

^{1}H	$\pi/2$ -	$\tau/2$ -	$\tau/2$ -	Δ_1 -	$\pi/2$ -	Δ_2 -	decouple
^{13}C	$\tau/2$ -	π -	$\tau/2$ -	Δ_1 -	$\pi/2$ -	Δ_2 -	acquisition

Δ_1 is set to $(2J)^{-1}$ and Δ_2 to $\approx(3J)^{-1}$. For one-bond couplings ^{1}J = 100-200 Hz, therefore Δ_1 is usually 2.5-5 ms whilst Δ_2 is about 2 ms.

viii Relayed heteronuclear correlated spectra. This experiment is very similar to the HETCOR experiment described above. The difference is that the cross peaks correspond to the carbon - proton two and three bond correlations (and not one bond correlations as in HETCOR). The aim is to establish the carbon skeleton of the molecule. The experiment works by

transfering magnetisation (by coupling) from one proton to another, and then to the heteronucleus. The problem with such experiments is that it is difficult to optimise the delays for a diverse spin system with a wide range of coupling constants. Typically both ^2J and ^3J are in the range 5-10 Hz. This is why both two and three bond correlations may be observed.

ix Nuclear Overhauser effect difference spectroscopy (NOE diff)[7]. The experiment involves saturating one resonance, and then comparing the intensities of the other peaks with their equilibrium value. This is easily accomplished by subtracting the equilibrium spectrum from the NOE spectrum. The intensities of peaks from nuclei that are coupled to the irradiated peak will be perturbed.

x Partial deuteration. This has been used successfully to distinguish carbon atoms that are adjacent to NH groups. The deuteration is easily accomplished by adding one drop of a mixture of H_2O and D_2O to the NMR solution. Deuteration of an adjacent site causes a small change in the chemical shift and so a pair of peaks is seen where originally there was only one. One peak arises from the deuterated molecules whilst the other is from the protonated molecules.

4.4. Chemical Shift Databases.

The use of chemical shift databases as an aid to spectral assignment is now a commonplace occurrence. The solution-state chemical shifts of many compounds are collected together along with structural information. The use of the database known as STN has been available to me whilst at Glaxo. Prediction of chemical shifts is quite straightforward and involves entering the structure of the compound in question, and then the database finds the nearest matches to the structure from those contained in the program, and then outputs the predicted chemical shifts.

4.5. Infrared Spectroscopy

The infrared spectra of polymorphs are distinctive and may be helpful in finding the composition of a sample once a standard spectrum is available. In many cases it is the differences in the IR spectra that have led to the discovery of polymorphic forms of a compound.

Practically, sample preparation is simple. A small amount of the material (a few milligrams) is ground, and a drop of the mulling agent Nujol is added and then ground again. Samples may also be studied as salt discs, but the great pressures that are applied to form the discs, may cause polymorphic transformations. Such transformations do not generally occur in mulls.

Two IR spectrometers have been used in this work. A Nicolet 20SXB FT-IR spectrometer at Glaxo Group Research, Greenford, operating under a continuous nitrogen purge at 1 cm^{-1} resolution has been used for the majority of the IR work. On occasions a Mattson Sirius FT-IR spectrometer at Durham has been used operating at 2 cm^{-1} resolution.

4.6. Preparation Of Samples.

Pharmaceutical compounds have been provided by Glaxo Group Research Ltd. and Glaxo Manufacturing Services (Barnard Castle). The samples provided were chemically pure, and could be used without further purification. However in many cases the polymorphs are not stable over a long period of time, undergoing polymorphic transformations. It has been necessary therefore to prepare the specific polymorphs required by the methods set out in table 4.1.

4.6.1. General Method Of Recrystallisation

Dissolve the sample in the minimum volume of boiling solvent, heated in a water bath. Cool to room temperature without stirring, with just the bottom of the flask in the hot water. Then cool in a refrigerator. Filter and wash with cold solvent. Dry under vacuum for one hour at room temperature unless otherwise stated.

4.6.2. Preparation Of Cortisone Acetate Polymorphs

This was provided as form II and was used in each case as the starting material. Solvents were reagent grade and supplied in each case by May and Baker, except in the following cases: ethanol from James Burrough (F.A.D.) Ltd., and benzene from Hopkin and Williams.

Table 4.1 - showing methods of preparation of cortisone acetate polymorphs

Form	Method	Volume of solvent per 1g of cortisone acetate
I	Heating to 200°C for one hour	-
II	Recrystallised from ethyl acetate or chloroform or benzene.	$C_4H_8O_2$ 39 ml $CHCl_3$ < 5 ml C_6H_6 125 ml
III	Recrystallised from 7:3 v/v acetone/water, then heating under vacuum to 60°C for one hour.	12 ml
IV_{aq}	Recrystallised from 7:3 v/v acetone/water	12 ml
IV_{et}	Recrystallised from 95:5 v/v ethanol/water	26 ml
IV_{ac}	Recrystallised from acetone	29 ml
V_{aq}	Recrystallised from 3:1 v/v carbon tetrachloride/methanol	12 ml

These methods (reported in the literature[8-14]) are reliable for all forms except form III. This method of producing form III gives a poor quality sample. I have found that a better method is to make form IV_{aq} and then to leave the sample in a closed bottle in a drawer for several (about 6) months.

Also the literature suggests that to produce form V_{aq} , dried distilled methanol must be used. I have not found it necessary to take such precautions against excluding water.

4.6.3. Preparation Of Carbon-13 Labelled Cortisone Acetate

It has been necessary to prepare samples of cortisone acetate that have been enriched with ^{13}C at certain positions in the molecule.

Sources of chemicals were as follows: 99% ^{13}C-labelled acetic anhydride, labelled at both the carbonyl carbons purchased from ISOTEC inc.; 99% ^{13}C-

labelled acetic anhydride, labelled at all carbon atoms from ISOTEC inc.; 99% ^{13}C-labelled ethanol, labelled at both carbon atoms from ISOTEC inc.; unlabelled acetic anhydride form Fluka-Chemie; pyridine from Aldrich Chemical Company; cortisone supplied by courtesy of Glaxo Group Research.

The preparations were performed as follows:

i) Esterification of cortisone with acetic anhydride to prepare cortisone acetate enriched at C22 (the ester carbon). 0.5 g of 99% ^{13}C-labelled acetic anhydride, labelled at both the carbonyl carbons, was mixed with 2.1 g of unlabelled acetic anhydride (to give acetic anhydride enriched to about 20%). 0.5 g of cortisone were dissolved in 3.5 ml of pyridine. To this was added slowly, 2.6 g of enriched acetic anhydride. The mixture was left overnight to allow the reaction to proceed to completion. Later, 10 ml of distilled water was added, followed by about 25 ml of dilute (approx. 5 M) hydrochloric acid. The product precipitated from the solution, was filtered off, washed with more distilled water, and put to dry on a vacuum line (about 8 mbar pressure) for one hour.

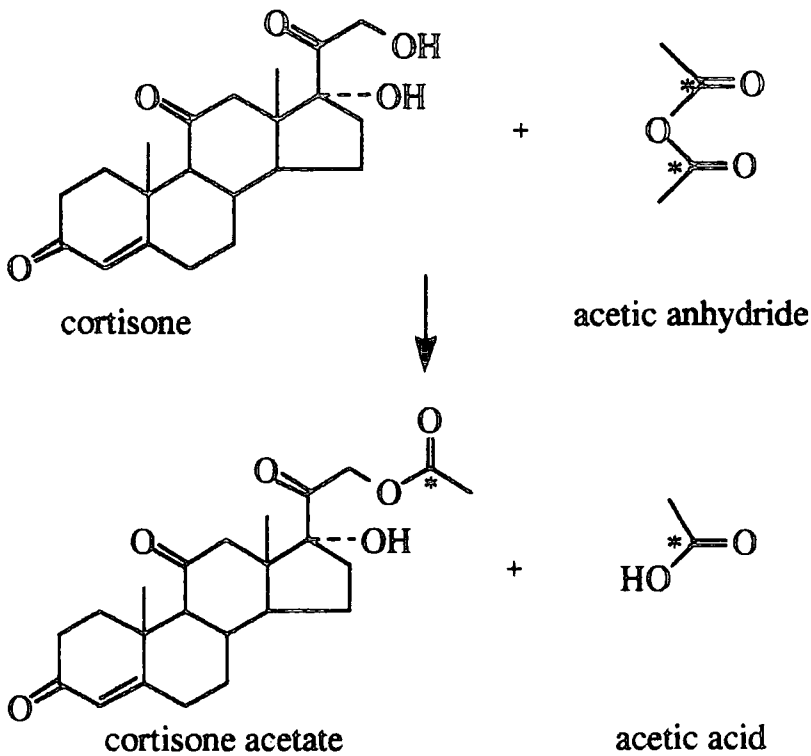

cortisone + acetic anhydride → cortisone acetate + acetic acid

^{13}C-labelled atoms have been marked with an asterisk in the above reaction scheme. The yield was 0.52 g (about 92%). Generally, this method of

preparation gives cortisone acetate as form III. The product could then be recrystallised in the normal manner to produce other polymorphs.

ii) Esterification of cortisone with acetic anhydride to prepare cortisone acetate enriched at C22 and C23 (the ester carbon and adjacent methyl). 1.0 g of 99% ^{13}C-labelled acetic anhydride (purchased from ISOTEC inc.), labelled at all positions, was mixed with 4.2 g of unlabelled acetic anhydride (to give acetic anhydride enriched to about 20%). 1.0 g of cortisone were dissolved in 5.0 ml of pyridine. To this was added slowly, 5.2 g of enriched acetic anhydride. The mixture was left overnight to allow the reaction to proceed to completion. Later, 20 ml of distilled water was added, followed by about 50 ml of dilute hydrochloric acid. The product precipitated from the solution, was filtered off, washed with more distilled water, and put to dry on a vacuum line for one hour. The yield was 1.0 g (about 90%).

iii) Preparation of the enriched ethanol solvate. 0.5 g of 99% ^{13}C-labelled ethanol, labelled at both carbon atoms, was mixed with 7.7 g of a solution of (47.5 ml unlabelled ethanol and 2.5 ml distilled water). This gave an ethanol solution enriched to about 6%. This was then used to recrystallise 0.3 g of unlabelled cortisone acetate to give form IV_{et} with ^{13}C-enriched ethanol.

4.6.4. Stability Of Cortisone Acetate Polymorphs

This is the approximate length of time for which the samples stay pure (i.e. impurities of other polymorphs are not detectable by solid-state NMR) when stored in air at room temperature. The stabilities are given in table 4.2.

Table 4.2 - approximate stabilities of cortisone acetate polymorphs

Form	Stability	Notes
I	>2 years	
II	>2 years	
III	6 months	transforms to form II
IV_{aq}	2 months	transforms to forms II and III
IV_{et}	2 days	transforms to form III
IV_{ac}	2 days	transforms to forms II and III
V_{aq}	>2 years	

4.6.5. Preparation Of Beclomethasone Dipropionate Polymorphs

Beclomethasone dipropionate (BDP) was supplied by Glaxo Group Research Ltd. in the form of anhydrate and monohydrate samples. Solvates can be prepared by recrystallising from the appropriate solvent using the anhydrate as the starting material. Only the ethyl acetate solvate was prepared for this work as follows:

1 g of BDP anhydrate in about 7 ml of hot, reagent grade, ethyl acetate (supplied by May and Baker). This is then cooled, filtered and washed with cold solvent. The samples were dried using only a water vacuum pump in an attempt to dry only the surface of the crystals, and not to take the solvent out of the channels in the crystal structure.

4.6.6. Preparation Of Cefuroxime Axetil Polymorphs

Cefuroxime axetil was supplied by Glaxo Group Research Ltd. as separate samples of the AI and BI diastereoisomers. Preparation of other forms was carried out as follows:

i) form AII from 0.5 g of AI dissolved in 12.5 ml of warm acetone (warmed with hot tap water). This solution is then added slowly (over about one to two minutes) to 62.5 ml of cold and stirred distilled water. The precipitate is then filtered and washed with water and then dried under vacuum for about an hour.

ii) form BII from 0.5 g of BI dissolved as before in 12.5 ml warm acetone, then added to distilled water, filtered, washed and dried.

iii) a pure sample of form I of each diastereoisomer can be prepared by dissolving the appropriate isomer in a equal volumed mixture of ethyl acetate and ether.

4.7. Measuring The Probe Temperature

The Bruker CXP200 is not usually operated in the variable-temperature mode. Therefore the probe temperature is often assumed to be the same as the

'ambient' temperature. However this is a very vague claim, so the 'ambient' probe temperature has been measured.

The use of samarium acetate (see figure 4.2) as a chemical shift thermometer has been demonstrated[15,16]. Each of the three peaks exhibit Curie law behaviour in that the chemical shift varies as a function of inverse temperature. Chemical shifts of each peak have been measured at several temperatures, and a least-squares fit of the data has yielded calibration equations, where δ is the chemical shift in ppm relative to TMS, and T_S is the sample temperature:

chelating-only carbonyl	$\delta = (-4867/T_S) + 209$
chelating and bridging carbonyl	$\delta = (-2670/T_S) + 195$
methyl	$\delta = (+2672/T_S) + 14$

The chelating-only carbonyl signal (the more intense of the high-frequency pair), having the largest gradient, is the most sensitive to temperature changes. These results have been used in the present work to calculate the temperature given the chemical shift, using the equation:

$$T_S = 4867/(209 - \delta)$$

4.7.1. Experimental

Samarium acetate was kindly given by Dr. R.R. Yeung of the University of Durham Industrial Research Laboratory, and used without further purification. The sample was allowed to spin in the MAS rotor for 10 minutes before acquisition was begun, so that the sample temperature could equilibrate with its surroundings. The spectrum was acquired using the standard cross-polarisation pulse sequence: proton 90° pulse = 4 μs, contact time = 2 ms, recycle delay = 4 s, number of transients = 1000, number of dummy pulses applied prior to acquisition = 500. Phasing of the spectra at high spinning speeds is straightforward, but at low speeds the large number of spinning sidebands makes phasing difficult. Therefore the spectra were processed by phasing a high-speed spectrum and then applying the same phasing to all the other spectra in the series.

Figure 4.2 - The solid-state NMR spectrum of samarium acetate

operating conditions	^{1}H 90° pulse	contact time	acquisition time	recycle delay	number of transients	spin rate
50 MHz	4 μs	2 ms	0.16 s	4 s	1000	3.1 kHz

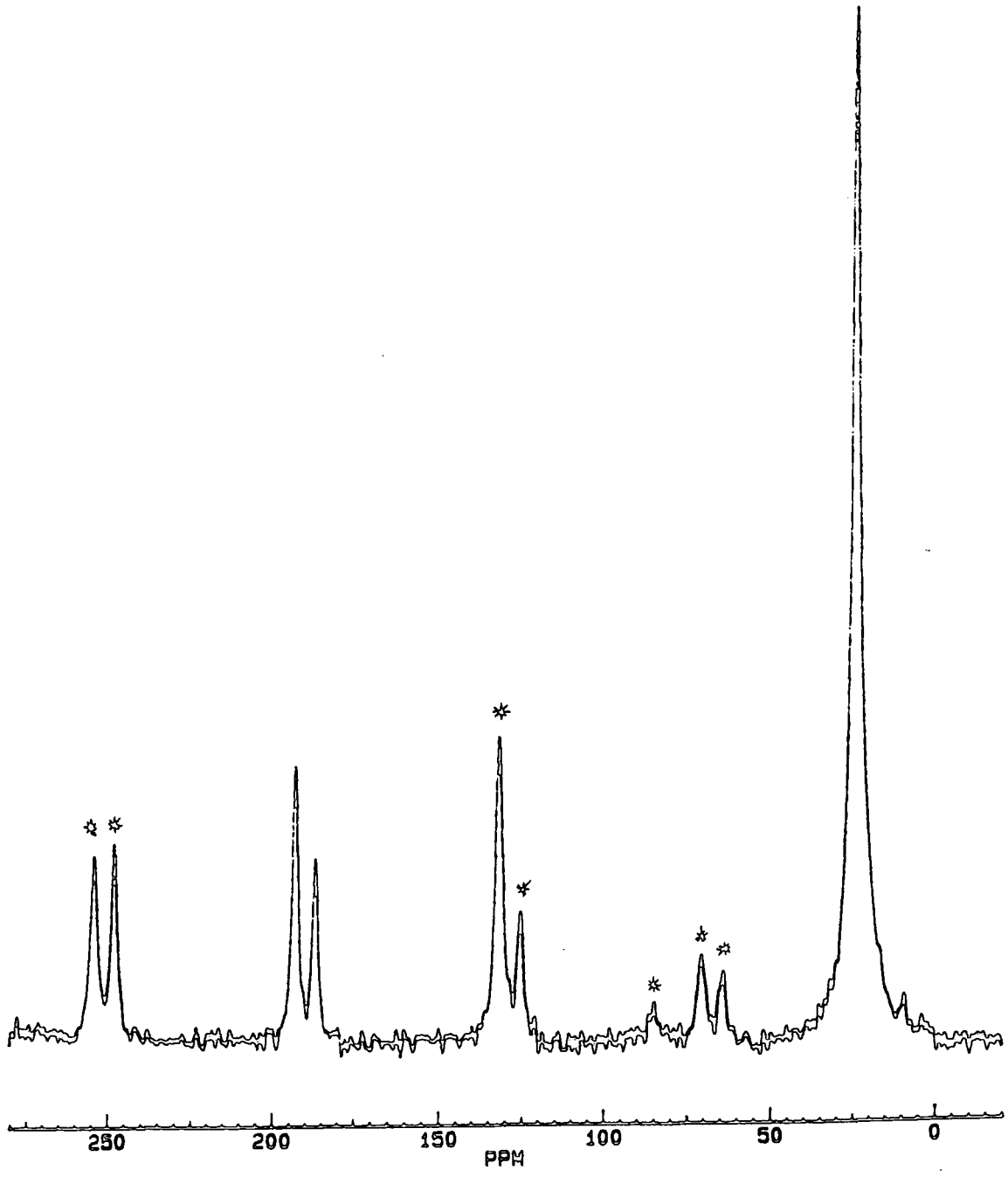

4.7.2. Results

The first experiment was simply intended to establish the exact value of the 'ambient' temperature in the probe. This was done at 3 kHz (a typical moderate spinning speed) and then checked at 1 kHz (a typical slow-spinning speed). RO is the spinning speed used in each case, and the calculated temperatures are given in table 4.3.

Table 4.3 - Results of experiment 1.

RO/kHz	δ/ppm	T_s/K
3.07	192.5	295
1.00	192.3	291

As the difference in temperature was unexpected, three further investigations were carried out over a wider range of spinning speeds. The results are presented in tables 4.4 - 4.6 and in figures 4.3-6.

Table 4.4 - Results of experiment 2.

RO/kHz	δ/ppm	T_s/K
1.10	192.82	300.8
1.55	192.18	289.4
2.00	192.42	293.5
2.50	192.52	295.3
3.03	192.48	294.6
3.50	192.56	296.0
4.01	192.67	298.0
4.50	192.69	298.4
5.00	192.72	299.0

Figure 4.3 - Graph of data from experiment 2

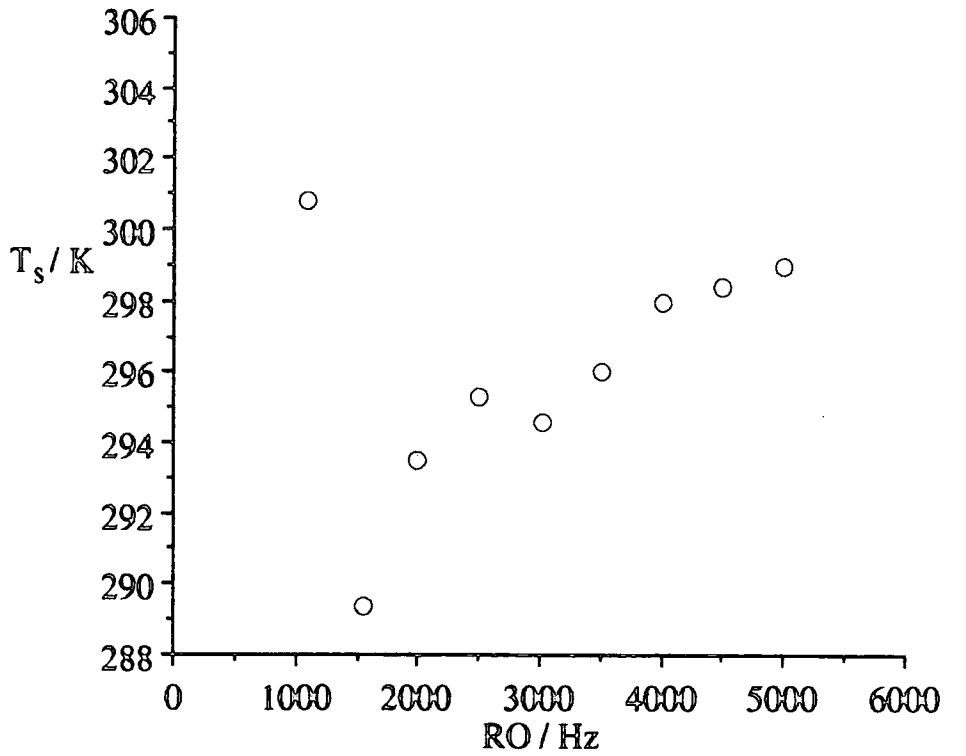

Table 4.5 - Results of experiment 3.

RO / kHz	δ / ppm	T_S / K
1.01	192.65	297.7
1.26	192.37	292.7
1.41	192.44	293.9
1.60	192.42	293.5
1.82	192.40	293.2
2.00	192.39	293.0
2.41	192.34	292.1
2.82	192.49	294.8
3.25	192.53	295.5
3.60	192.58	296.4
4.02	192.73	299.1
4.40	192.74	299.3
4.72	192.83	301.0
5.02	192.85	301.4

Figure 4.4 - Graph of data from experiment 3

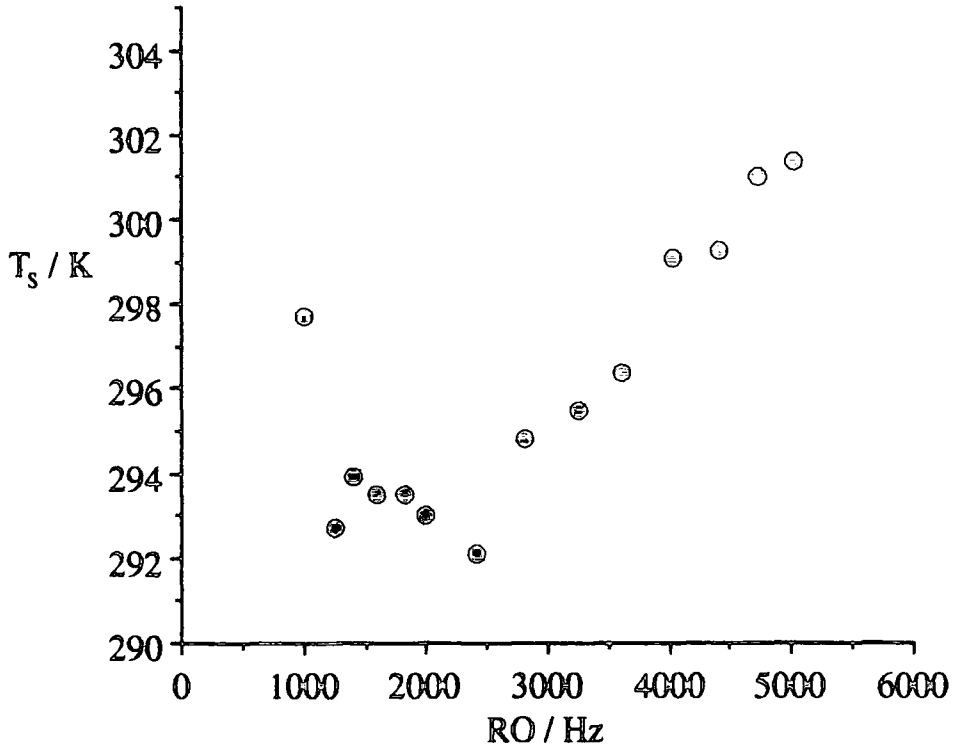

Table 4.6 - Results of experiment 4.

RO/kHz	δ/ppm	T_S/K
0.50	193.77	319.6
0.75	193.11	306.3
1.00	192.56	296.0
1.25	192.38	292.8

Figure 4.5 - Graph of data from experiment 4

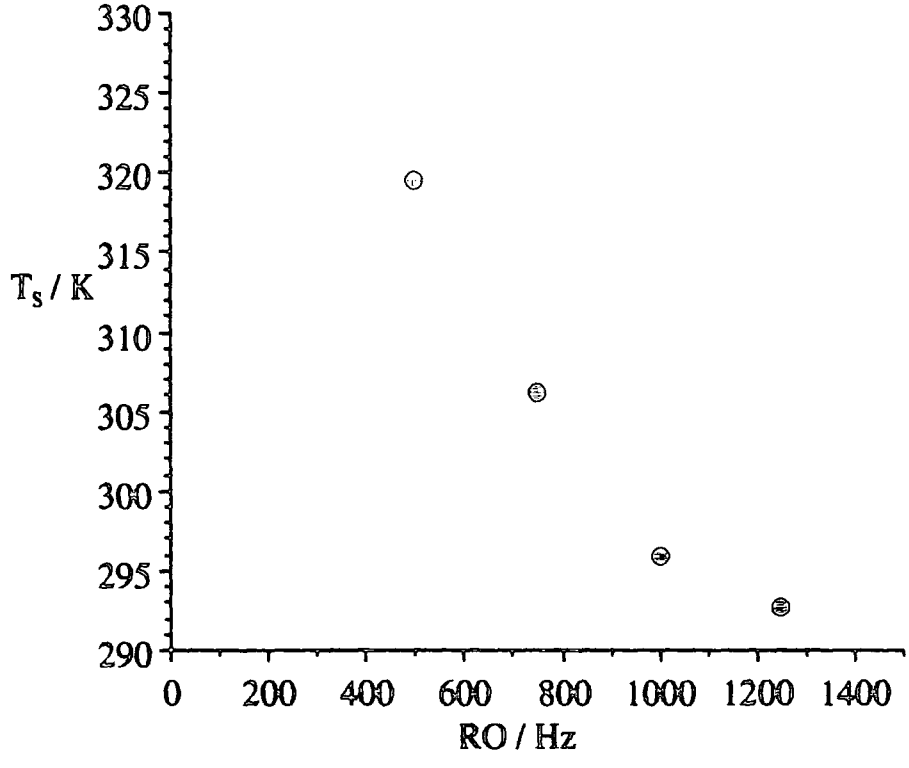

Figure 4.6 - Graph of combined data from all four experiments

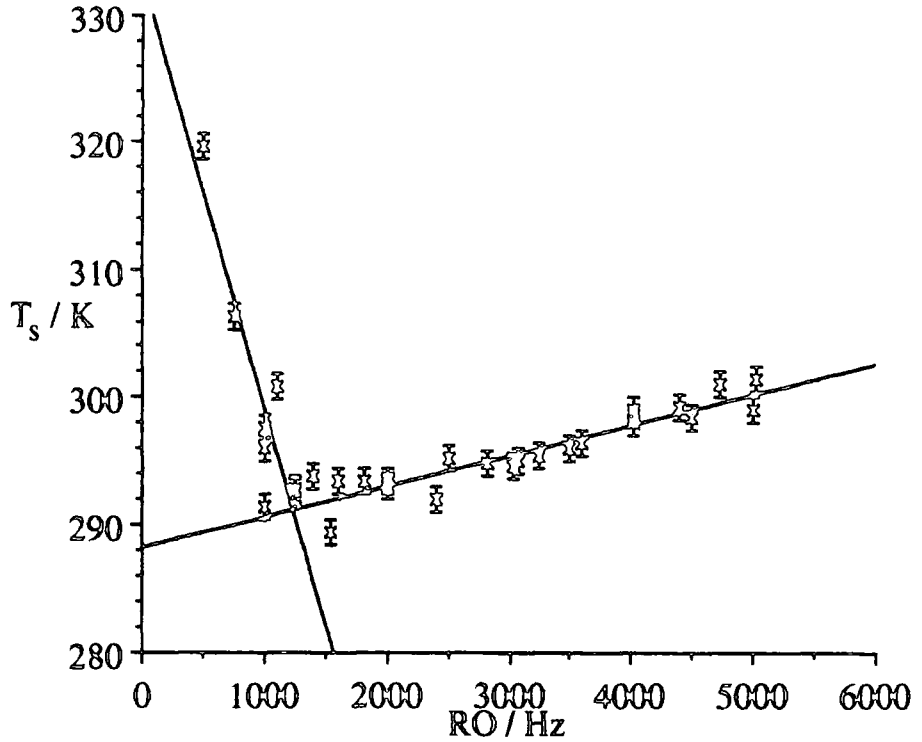

At low speeds (below 1.2 kHz)	$y=332.54 - 3.34e^{-2}x$	$R^2 = 0.81$
and at higher speeds	$y=288.31 + 2.39e^{-3}x$	$R^2 = 0.85$

The error bars are based upon on estimated error in the spinning speed of ±5 Hz, and an error of ±1 K in the temperature (arising from an error of ±0.05 ppm in the chemical shift).

4.7.3. Discussion and Conclusions.

Each data set clearly shows that at low spinning speeds (0-2 kHz), as the spinning speed increases the temperature drops, whilst at high spinning speeds (2-5 kHz) the temperature increases as the spinning speed increases. The minimum temperature (ca. 294 K) corresponds approximately to room temperature and a spinning speed of about 2 kHz.

There are several possible causes of the temperature changes: insufficient temperature equilibration times, frictional heating, rf heating and Joule-Thompson cooling or heating. Problems caused by insufficient equilibration times should have been eliminated by waiting 10 minutes before acquisition is

begun, and possible variations in rf heating was overcome by using dummy pulses and a long recycle delay.

The spinning system uses bearing and drive gases (both are air) that are expelled through small openings. These openings may act as Joule-Thompson expansion valves. As air has a maximum inversion temperature of 603 K, one might expect cooling on expansion. The cause of heating at higher spinning speed is more difficult to explain, but may be due to friction.

These experiments have shown that there could be significant heating of samples at high spinning speeds (ca. 3 K for each additional 1 kHz in spinning speed). This is very important for fast spinning probes where speeds of over 10 kHz are used. Thus it seems that if the sample temperature is important, then the experiment should be run as a variable temperature experiment even if the required temperature is about room temperature.

4.8. The Effect Of Decoupler Power On Solid-State Spectra

It has been noticed that in many steroids, e.g. cortisone acetate, testosterone, androstanolone, cortisone etc., that solid-state NMR spectra show that many of the CH_2 resonances are rather broader than most of other peaks in the spectrum. A number of causes have been proposed, including molecular motion and incomplete decoupling of the protons.

Experiments at temperatures lower than the 'ambient' temperature have failed to reduce the linewidth[17], although further investigation would be required to rule out this possibility completely. However, the effect of varying the decoupler power has been investigated.

Spectra of the α-form of testosterone were acquired using the CMX-200 (operating at a proton frequency of 200 MHz) Chemagnetics spectrometer at the University of Leeds Interdisciplinary Research Centre in Polymer Science and Technology. The results are given in table 4.7 and two specimen spectra are presented in figure 4.7.

Figure 4.7 - The solid-state ^{13}C NMR spectrum of α-testosterone. Decoupler power: (a) 698 mV (i.e. 72 kHz) and (b) 571 mV (i.e. 62.5 kHz)

operating conditions	^{1}H 90° pulse	contact time	recycle delay	number of transients
50 MHz	4 μs	1.5 ms	3 s	480

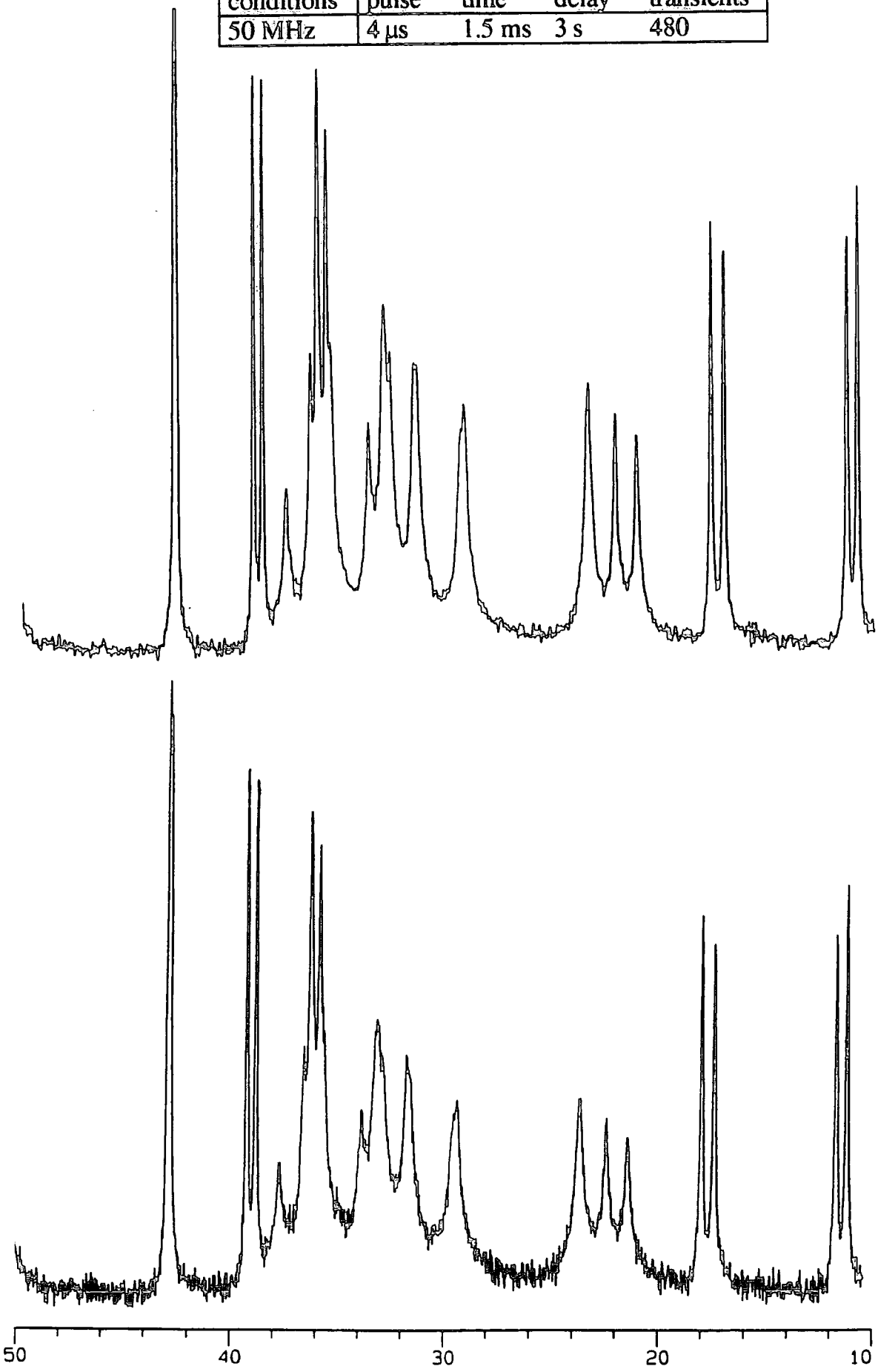

Figure 4.8 - The solid-state ^{13}C NMR spectrum of α-testosterone. Decoupler offset from ^{1}H frequency: (a) +0.002 MHz and (b) -0.001 MHz. The decoupler power is 86 kHz.

operating conditions	^{1}H 90° pulse	contact time	recycle delay	number of transients
75 MHz	2.9 μs	1 ms	20 s	72

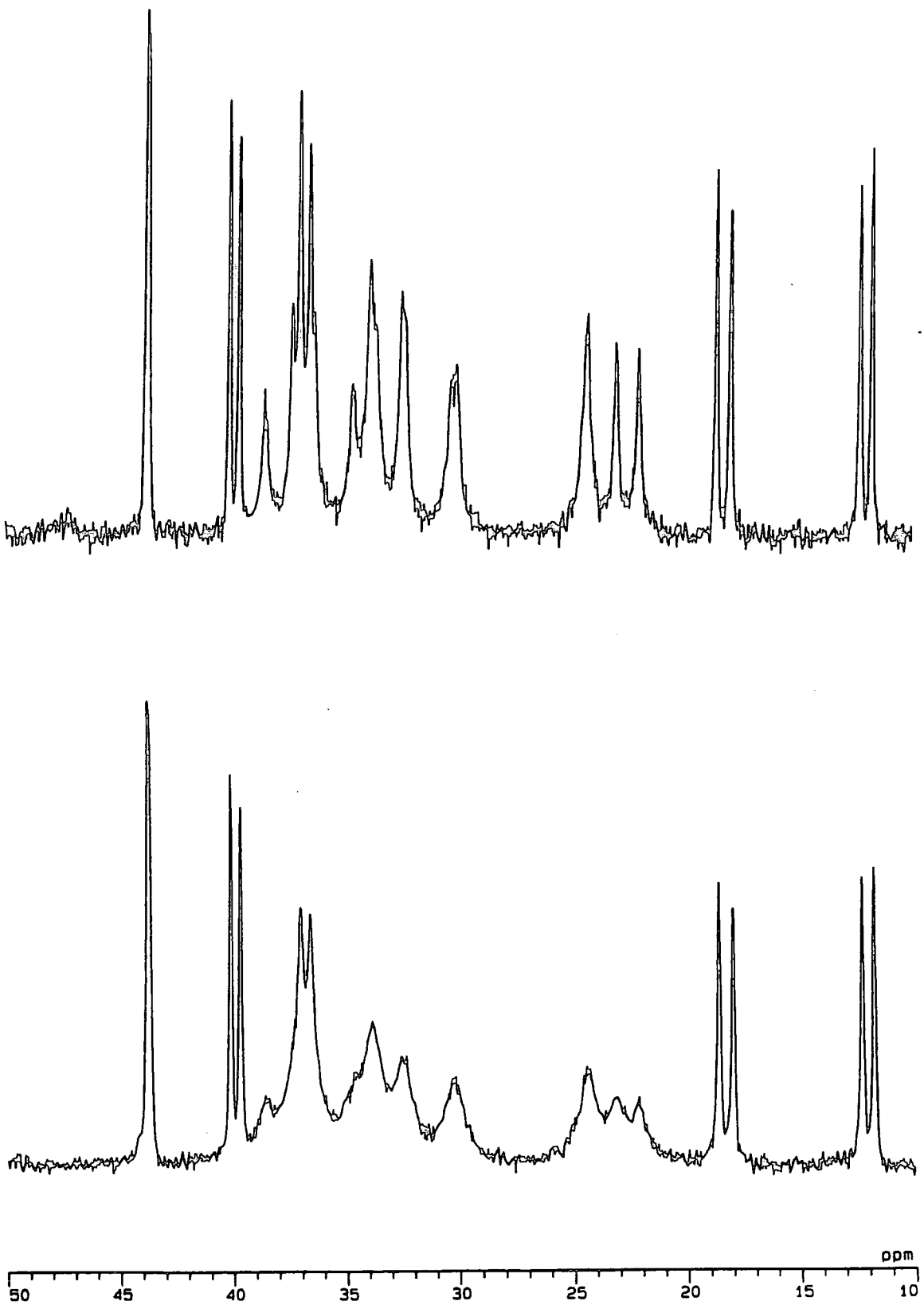

Table 4.7 - The linewidths of testosterone resonances as the decoupler power is varied

decoupler power	width at half height (in Hz) of certain peaks:		
	21 ppm	22 ppm	23 ppm
62.5 kHz	26	20	19
72.0 kHz	21	12	14

These show improvements of 20-40 % in the linewidth for a 22 % increase in the decoupler power. These results provide confirmation that it is insufficient decoupler power that is causing the line broadening of the CH_2 groups as this is where the strongest dipolar ^{13}C-^{1}H interactions are felt. A similar effect of the decoupling power on the linewidth of 4-n-butoxybenzoic acid has been reported[18].

Spectra have also been run in the United States on a Chemagnetics CMX-300 (operating at a proton frequency of 300 MHz) spectrometer using various decoupler offsets. The results are summarised in table 4.8 and two specimen spectra are presented in figure 4.8.

Table 4.8 - The linewidths of testosterone resonances as the decoupler offset is varied. The decoupler power is 86 kHz.

offset / MHz	width at half height of certain peaks	
	24 ppm	32.5 ppm
-0.001	70	*
0	46	58
+0.001	32	37
+0.002	23	35

* The width could not be measured for this resonance as there was overlap with an adjacent peak.

The varying linewidth with decoupler offset also confirms the conclusions drawn from the first experiment. If the decoupler power is too low to completely decouple all the protons, then the degree to which decoupling will occur is dependent upon the frequency of the decoupler (i.e. the linewidth will vary with decoupler offset).

The incomplete decoupling of CH_2 groups in steroids is not necessarily a disadvantage. As the cause of the broadness is known, then this may even be used to identify resonances in a spectrum from CH_2 groups.

4.9. Reference Deconvolution

This is a method of data processing designed to correct lineshapes to that of an ideal shape[19-21]. Imperfect lineshapes may arise from many sources, in particular instrumental instabilities in field homogeneity and drifting, and errors in pulse phases and amplitudes. The method is based upon a comparison of a reference line and its known ideal shape, in order to produce a correction function that may then be applied to the whole spectrum

	deconvolve		reconvolve	
experimental reference line	⇨	infinitely sharp line	⇨	ideal reference line

4.9.1. Experimental

Practically, the method involves selecting the region of the spectrum that contains the reference line and then the rest of the spectrum may be set to zero. Care must be taken to include all the reference signal intensity, but in some cases truncation of the line is unavoidable and may cause artefacts. The program then calculates the correction function and applies it to the whole experimental spectrum.

The method is usually used in solution state studies to improve the lineshape. However in this work the method has been used to try to improve the resolution of the lines in a solid state spectrum. The procedure followed was to choose a well resolved line as the reference, and then to artificially narrow it. The correction function has the purpose therefore of line narrowing with the aim of enhancing resolution.

4.9.2. Results

i Cortisone Acetate Form IV_{ac}

The acetone solvate is known from the crystal structure to occupy two different sites in the crystal. It is hoped therefore to resolve the acetone peaks to

reveal two distinct chemical shifts for each of the two molecules. The reference peak is chosen to be the one at 205.6 ppm and a line broadening factor of 3 Hz is used. See figure 4.9. The spectra show that although the enhanced resolution has not distinguished the two acetone sites, the resolution of those peaks at ca. 50 ppm (C12,13,14) has been improved upon.

ii Cortisone Acetate Form IV_{aq}

Two of the high frequency peaks are coincident at 204.2 ppm. It is hoped to resolve these peaks and find the chemical shifts. See figure 4.10. This was more successful as a peak to lower frequency (at 203.9 ppm) could be resolved. Also, as with form IV_{ac}, the resolution of the 50 ppm region is improved. In this case the reference peak was chosen to be at 63.0 ppm and the line broadening set to 1 Hz.

iii Cortisone Acetate Form III

This is a very interesting polymorph in that there are three molecules in the asymmetric unit, each giving a unique spectrum. In parts of the spectrum the lines overlap and it is hoped to resolve these. See figure 4.11. The results are summarised in table 4.9.

Table 4.9 - Results of reference deconvolution of spectra of cortisone acetate polymorphs

δ_C / ppm	Comments
209.7	unresolved
203.7	resolved - 203.8 and 203.6 ppm
203.0	resolved - 203.1 and 202.9 ppm
173.7	resolved - 173.75 and 173.6 ppm
89.1	resolved - 89.4, 89.2 and 89.0 ppm
64.2	resolved - 64.5 and 64.3 ppm
ca. 50	resolved - 52.5, 51.3, 51.2, 51.1, 50.9, 50.7, 50.6, 50.3 and 48.3 ppm
15.5	resolved - 15.8 and 15.7 ppm

Note that the splitting of the peak at 14.5 ppm is not expected and is just noise, as it is not present when other reference peaks are used.

To conclude, this method does have some interesting applications and may be used successfully in certain cases to enhance resolution. However care must be taken as different reference peaks and line broadening factors can affect the spectrum.

Figure 4.9 - The solid-state ^{13}C spectrum of cortisone acetate form IV_{ac}.
(a) standard spectrum and (b) resolution enhanced spectrum

operating conditions	^{1}H 90° pulse	contact time	recycle delay	number of transients
50 MHz	4 μs	2 ms	5 s	3500

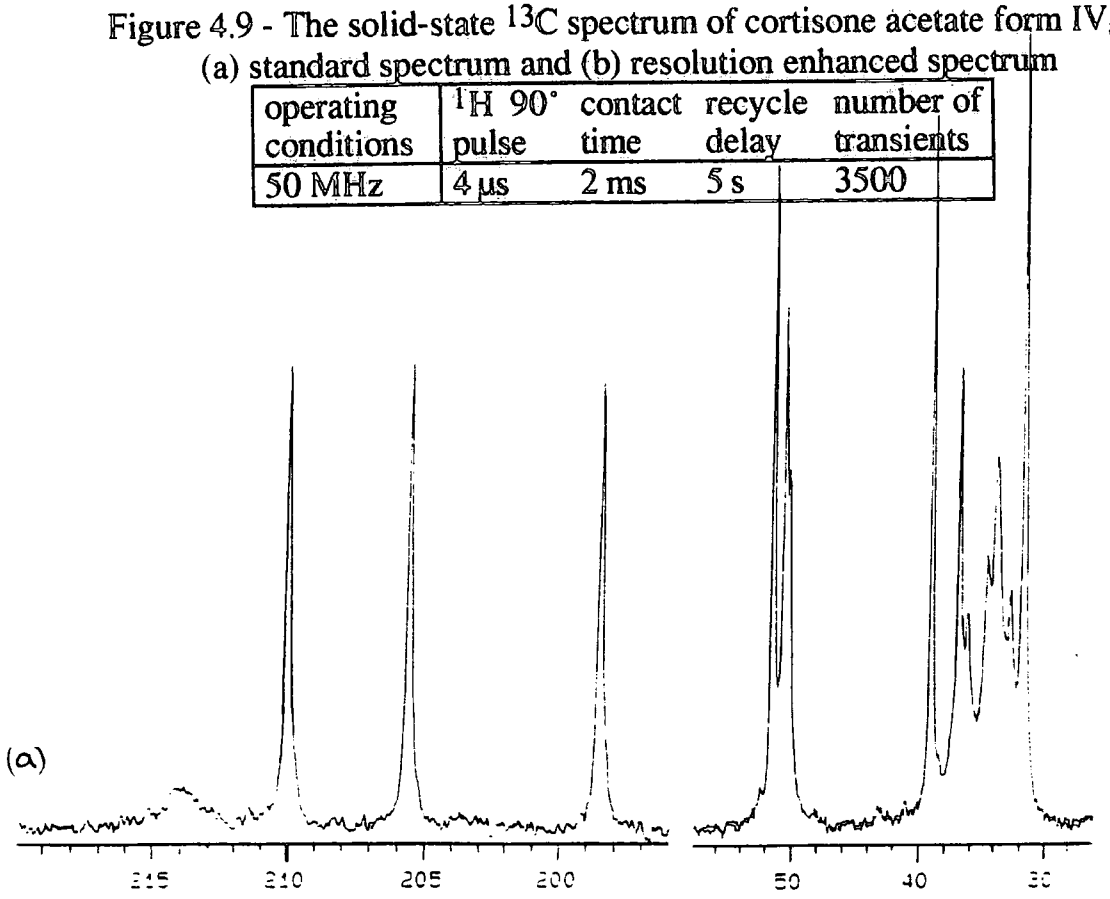

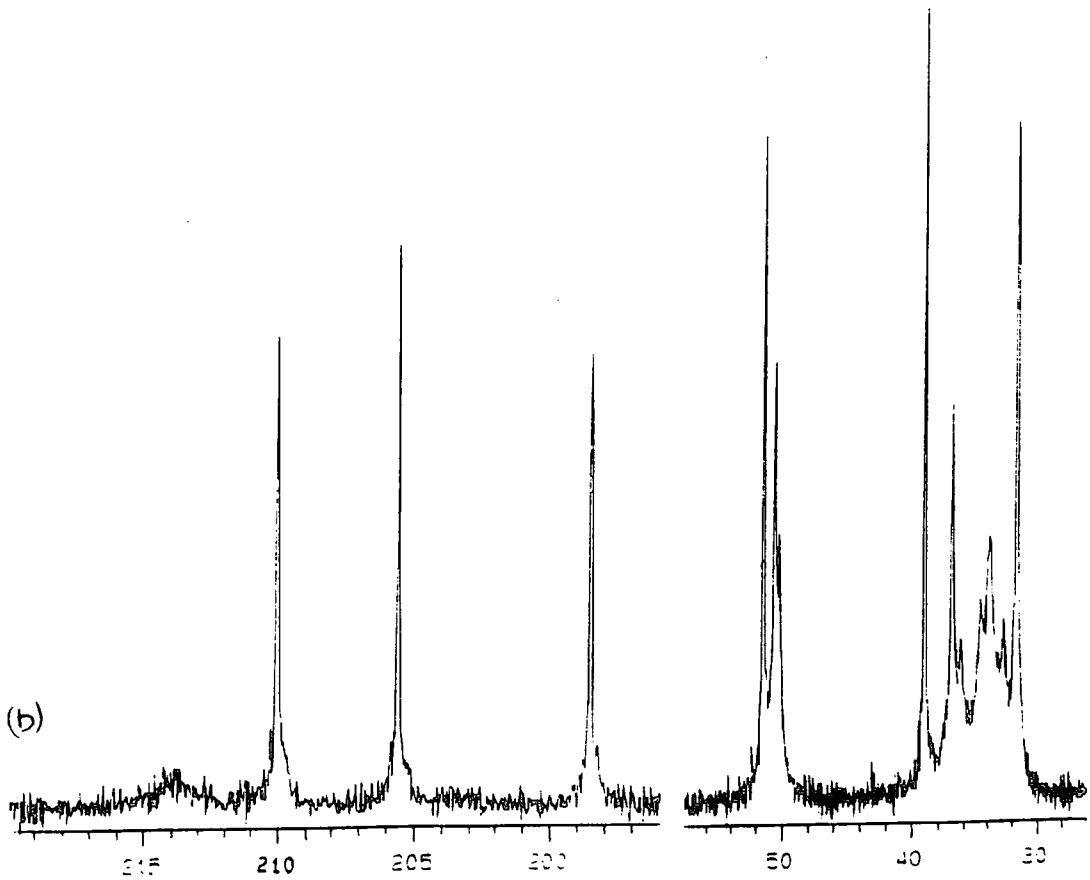

Figure 4.10 - The solid-state ^{13}C spectrum of cortisone acetate form IV_{aq}.
(a) standard spectrum and (b) resolution enhanced spectrum

operating conditions	^{1}H 90° pulse	contact time	recycle delay	number of transients
50 MHz	4 µs	2 ms	5 s	3620

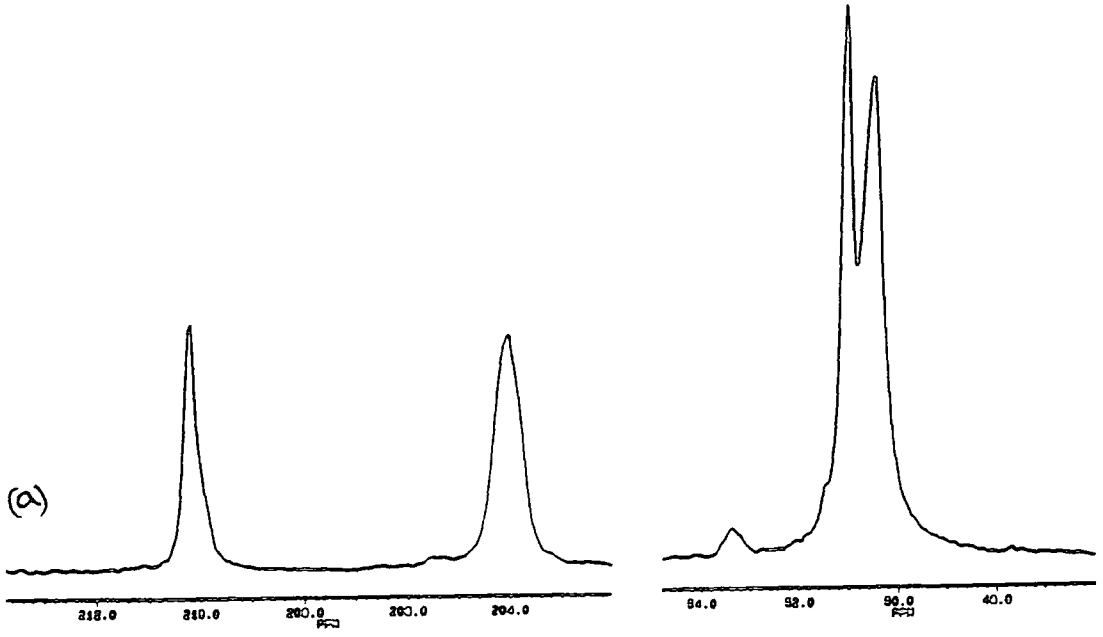

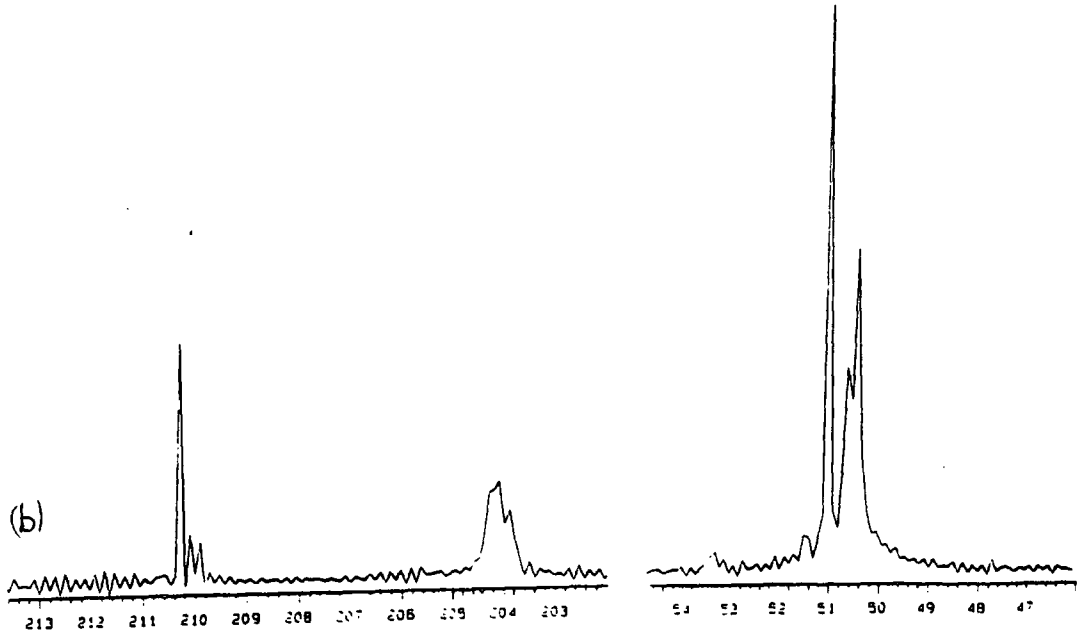

Figure 4.11 - The solid-state ^{13}C resolution enhanced spectrum of cortisone acetate form III.

operating conditions	^{1}H 90° pulse	contact time	recycle delay	number of transients
50 MHz	4 µs	2 ms	5 s	18550

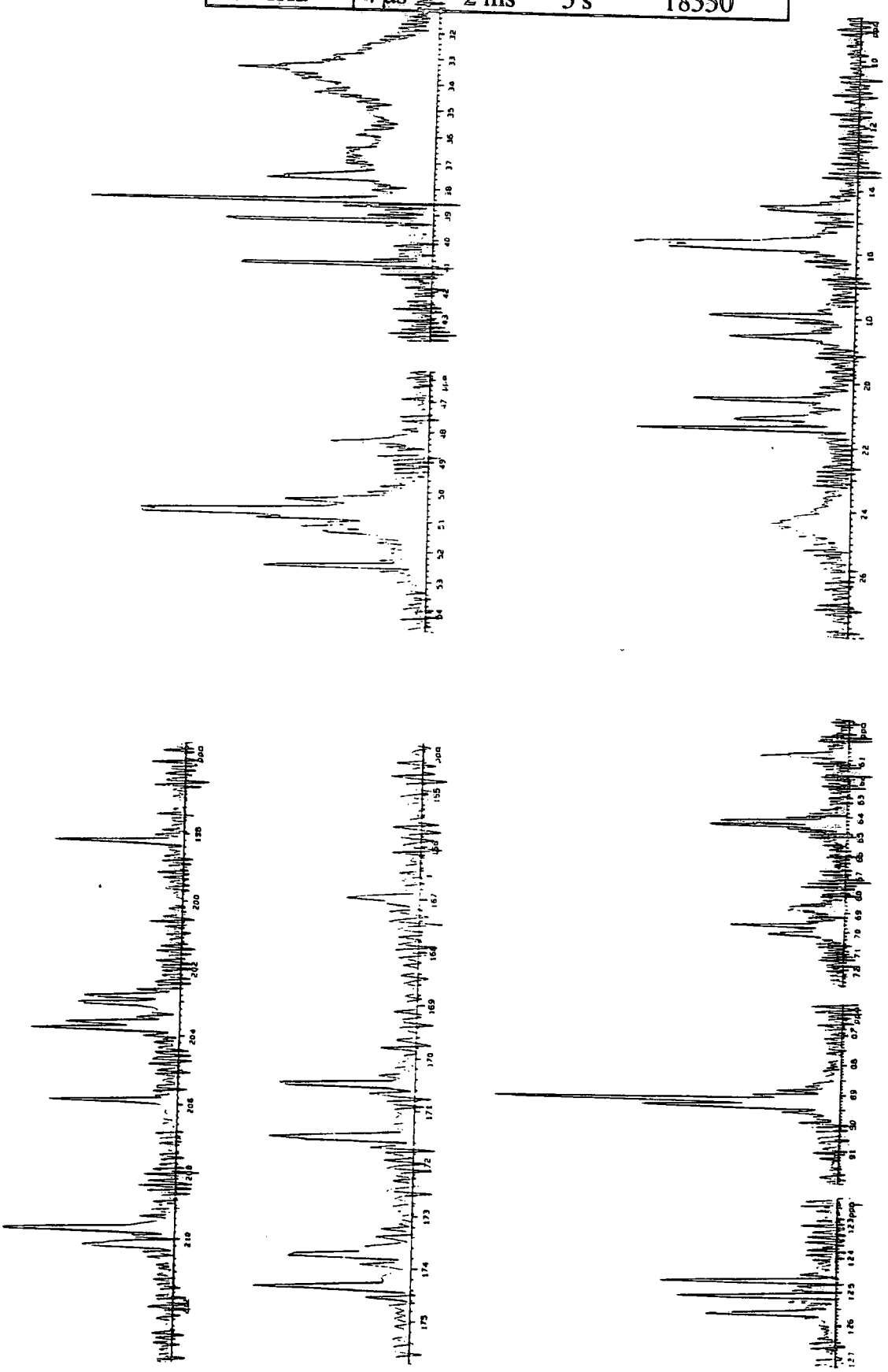

4.10. Rates Of Cross Polarisation

Cross polarisation[22] relies upon the strong ^{13}C-^{1}H dipolar interactions in the solid to transfer the large proton magnetisation to the carbons in order to enhance the signal from a dilute nucleus[23-25]. The rate of cross-polarisation depends upon several factors - the strength of the dipolar interactions, the degree to which the Hartmann-Hahn condition is fulfilled (i.e. $\gamma_C B_{1C}=\gamma_H B_{1H}$), the initial polarisation of the proton reservoir, molecular motion and possibly the spinning speed of the sample. The dipolar interactions have a very strong distance dependence of r^{-6} (where r is the internuclear distance):

for protonated carbons	r = 1.1 Å
for non-protonated carbons	r > 2.0 Å

Large differences in the strength of the dipolar interactions occur for the different carbon types. In practice CH and CH_2 groups have very strong interactions, CH_3 groups have moderate strength interactions (due to internal rotation modulating both the ^{13}C-^{1}H and ^{1}H-^{1}H dipolar interactions) and quaternary carbons have only weak interactions. The interactions are in the following order in terms of the strength of the interactions: $CH_2 > CH > CH_3 \geq Q$. It is desirable to maximize the carbon magnetisation for all carbon atoms in a molecule in order to get the maximum signal intensity. However, if the contact time (when cross polarisation occurs) is too long then intensity is lost due to the relaxation of the protons (the rate of relaxation important in this case is characterized by $T_{1\rho}(H)$). Thus it should be expected from the variations in strength of interaction that the contact times that give the maximum intensity would vary as follows: $CH_2 < CH < CH_3 \leq Q$. An experiment can be done that allows the best signal intensity to be obtained for the whole spectrum by varying the contact time. The contact times used in such an investigation vary from 0.05 ms to 10 ms and the results for Reichsteins d-diacetate are given in Table 4.10. Figure 4.12 shows the spectrum of Reichsteins d-diacetate with a contact time of 2 ms that gives the optimum intensity for the whole spectrum.

Figure 4.12 - The solid-state ^{13}C spectrum of Reichsteins d-diacetate

operating conditions	^{1}H 90° pulse	contact time	recycle delay	number of transients
50 MHz	4 μs	2 ms	5 s	1800

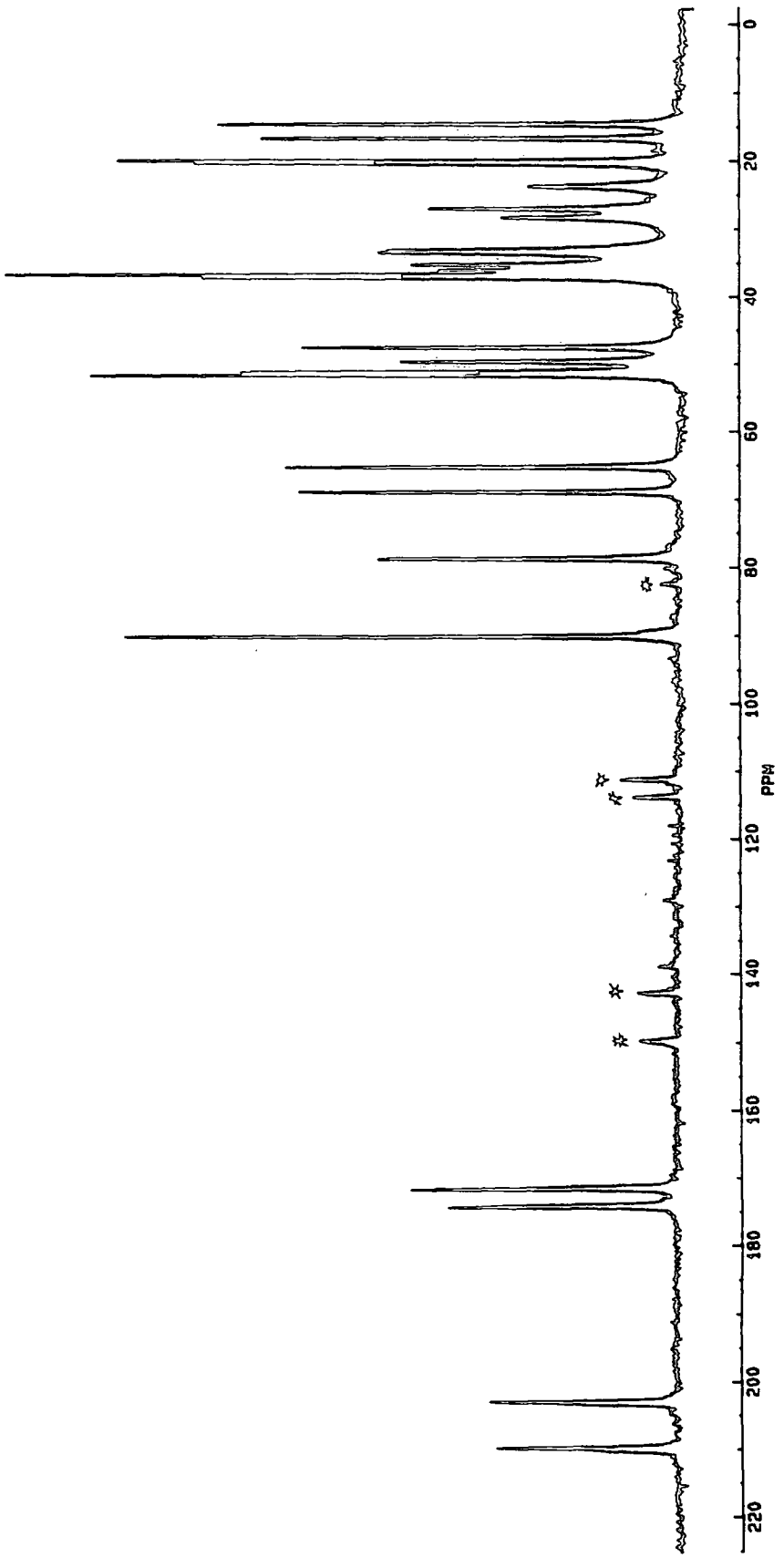

Table 4.10 - Summary of optimum contact times for Reichsteins d-diacetate

shift	time	shift	time	shift	time	shift	time	shift	time
209.5	1-2	78.6	1-4	49.6	1-2	35.1	1-2	23.6	1-2
202.7	2	68.7	2-3	47.4	1	33.4	2-3	20.3	2-4
174.1	3-4	65.0	1	37.0	1-2	33.0	1-2	19.8	2-4
171.4	3-4	51.6	2-3	36.6	1-2	28.3	*	16.6	2-4
89.9	2-3	51.1	1-3	35.9	1-2	26.9	1-3	14.5	2-3

where "shift" is the chemical shift in ppm, and "time" is the contact time (in milliseconds) for which that peak has maximum intensity. A selection of graphs representing the fitting of this data are shown in figure 4.13. The asterisk indicates that the data for this peak was too poor to give a reasonable estimate of the optimum contact time. The fully assigned solution state spectrum is presented in chapter 5.

The variable contact time experiment shows clearly that the different carbon types cross polarise at different rates and that the maximum signal intensity cannot be obtained for all peaks in the spectrum simultaneously. Reasonable intensities may be obtained across the whole spectrum if a contact time of 2 ms is used. These results may be used as an aid to assignment and are summarised as follows:

Atom type	Optimum contact time / ms
CH_2	0.5-1.5
CH	2-3
CH_3	2-4
Q	1-3
C=O	1-2
CO_2C	3-4

These results agree quite well with the order in which the optimum time would have been predicted based on a knowledge of the relative strengths of the dipolar interactions.

The intensities of the peaks can be fitted[23,26] by computer program to a theoretical relationship (equation 4.1) that links the rate of cross polarisation T_{CH} with the rate of proton spin-lattice relaxation in the rotating frame $T_{1\rho}$.

$$I = I_0 \frac{T_{1\rho}}{T_{1\rho} - T_{CH}} \left[1 - exp\left(\tau \left(\frac{T_{1\rho} - T_{CH}}{T_{CH} T_{1\rho}} \right) \right) \right] exp\left(- \frac{\tau}{T_{1\rho}} \right)$$ ..... equation 4.1

where I=intensity at time τ and I_0=magnitude factor. This equation is only valid when $T_{1\rho}(C) > T_{1\rho}(H) \gg T_{CH}$.

Three forms of cortisone acetate have also been studied by this method and the results are presented in table 4.11.

Table 4.11 - Results of the fitting of contact time data with the rate of cross polarisation for cortisone acetate polymorphs.

no. of attached protons	no. of near protons	T_{CH} /ms			Carbon number
		II	IV_{et}	IV_{ac}	
0	2	0.40	0.51	0.34	20
0	3*	0.61	0.67	0.52	22
0	3	0.30	0.33	0.27	17,3,11,5
0	6*	0.29	0.35	0.23	10,13
3*	0	0.18	0.23	0.13	18,19,23
1	0	0.09	0.14	0.04	4
1	1	0.07	0.12	0.04	9
1	3	0.07	0.08	0.05	14
1	4	0.07	0.11	0.20	8
2	0	0.07	0.10	0.05	12,21
2	2	0.05	0.08	0.04	1,2,6, 16
2	3	0.05	0.08	0.04	7,15

Note: the error in the values of T_{CH} is estimated to be ±0.05 ms

Figure 4.13 - Graphs showing the peak intensity vs. contact time

Carbonyl carbon at 202.67 ppm

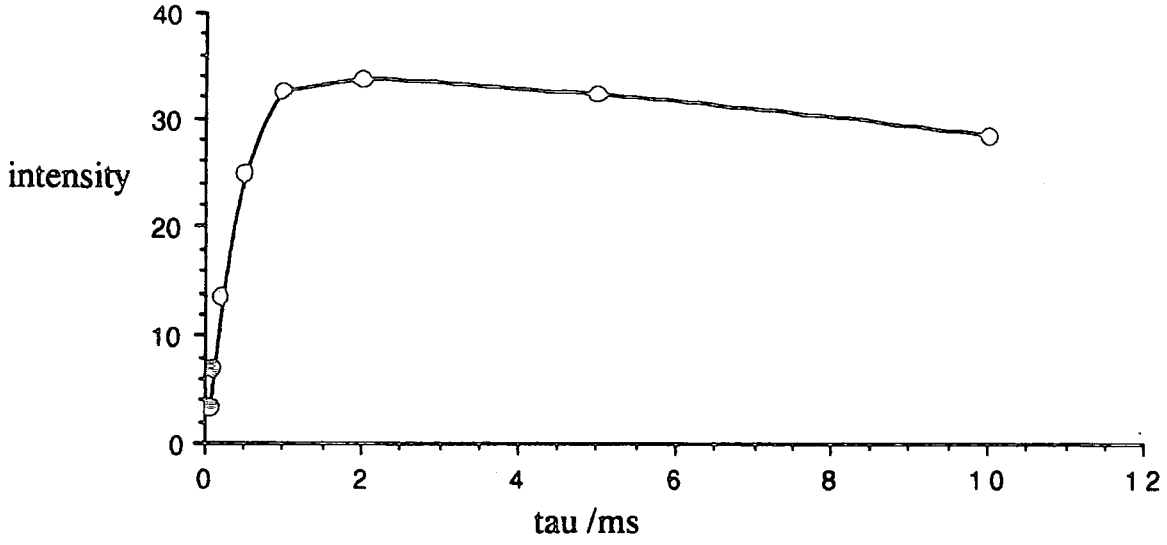

Ester carbon at 174.04 ppm

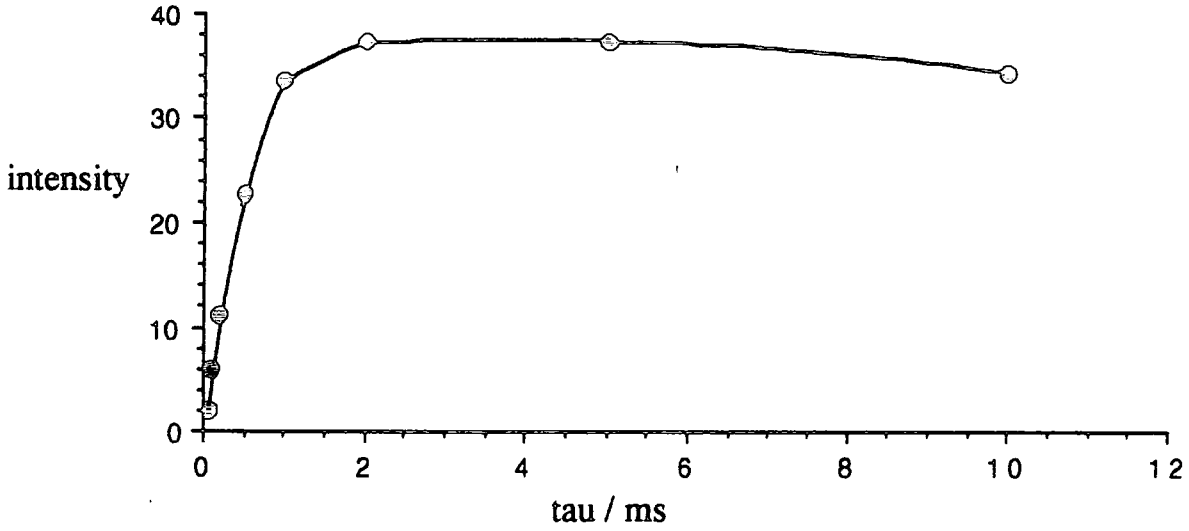

Quaternary carbon at 89.97 ppm

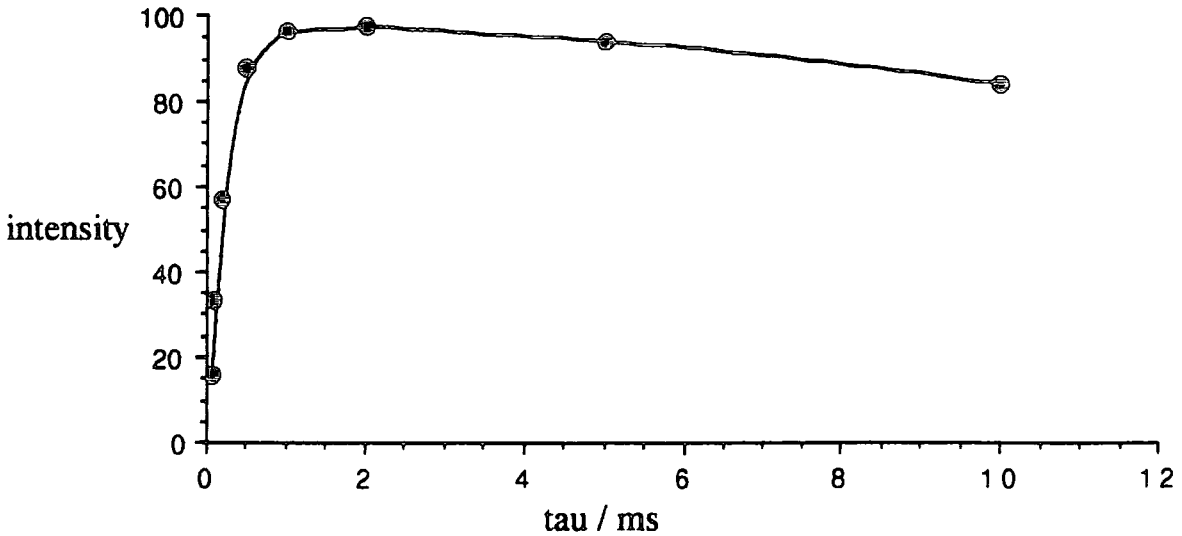

Figure 4.13 continued - Graphs showing the peak intensity vs. contact time

Methine carbon at 68.72 ppm

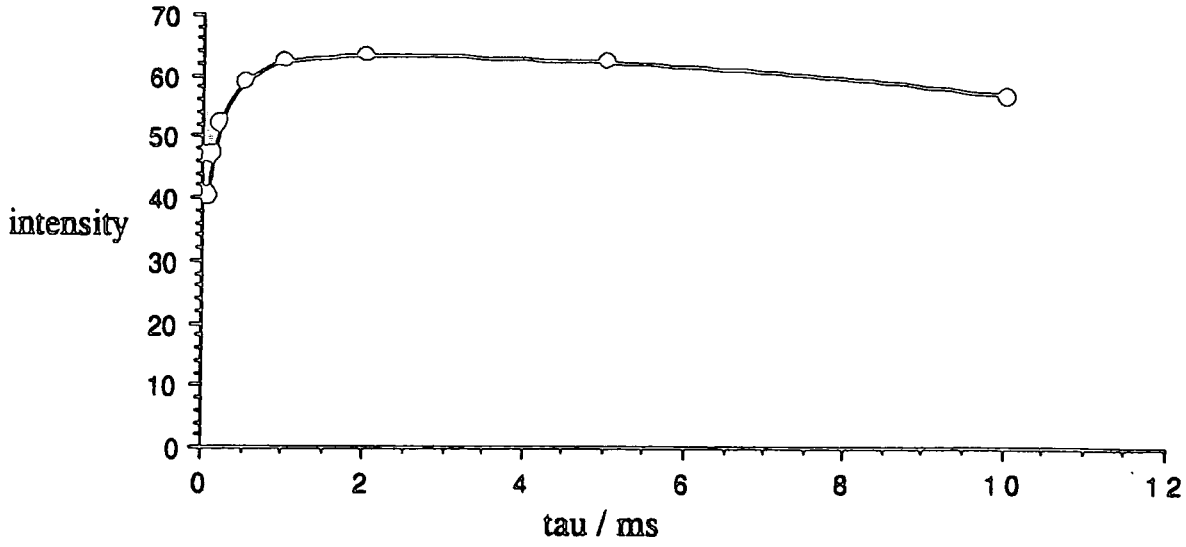

Methylene carbon at 36.60 ppm

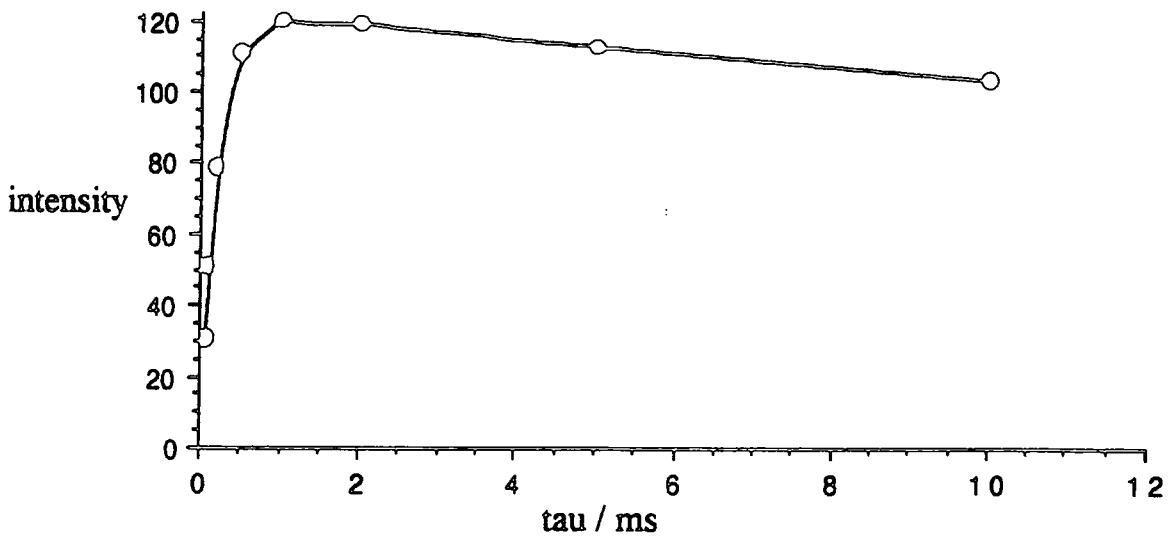

Methyl carbon at 19.81 ppm

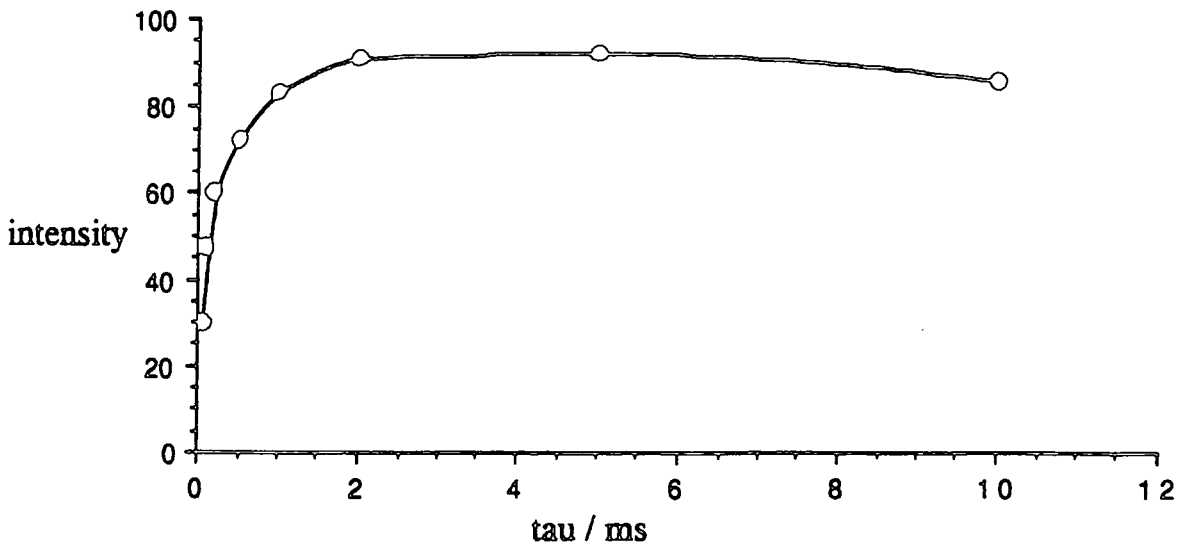

It is known[23] that if one or more protons are attached to a carbon atom, then the rate of cross polarisation will be dominated by these attached protons, and the effect of nearby protons will be negligible. However for non-protonated carbon atoms the only source of cross polarisation enhancement will be from more remote protons, and it is in these circumstances that the number of nearby protons becomes important. In principle the dipolar interactions by which cross polarisation occur could be either intramolecular or intermolecular. In practice however it is unlikely that intermolecular interactions would exceed one- or two-bond intramolecular interactions, unless rapid molecular motion made these intramolecular interactions ineffective. It seems that cross polarisation is still effective if a carbon atom is three or more bonds from the nearest proton, due to effective spin diffusion throughout the sample.

The data in table 4.11 show this trend i.e. that the fewer attached protons there are, the slower the rate of cross-polarisation (therefore leading to a greater rate constant T_{CH}). It can also be seen very clearly that the number of nearby protons is an important factor. If this were not the case then very little signal would be seen from non-protonated carbons. Also, the effect of rotation of methyl groups is seen, and marked with an asterisk in Table 4.11. Particularly noticeable is C22, which has a large value of T_{CH} greater than might have been expected from the number of attached and nearby protons. Note also that C8 in form IV_{ac} has a long T_{CH}. This may be due to experimental error.

The fitting routine also calculates the time $T_{1\rho}$. This varies in the range 10-70ms for the three forms studied. However, most $T_{1\rho}$ values for each form fall into a smaller range.

II	25-40 ms
IV_{et}	15-35 ms
IV_{ac}	10-30 ms

The exceptions are:

II	C4(66ms); C21(51ms); C23(62ms)
IV_{et}	C17(73ms); C22(52ms);
IV_{ac}	C8(48ms)

These exceptions do not correlate with any structural features, except for the fact that several of these large values occur in the side chain. This might be expected as the side chain could be more mobile, and so might have a slower rate of decay of proton magnetisation (i.e. a large $T_{1\rho}$). The error in the values of $T_{1\rho}$ is estimated to be ±5 ms.

4.11. Dipolar Dephasing

The strength of dipolar interactions in the solid state can provide much useful information. These interactions influence the rate of cross polarisation as discussed earlier, and also the rate at which dephasing occurs. The dipolar dephasing experiment (also known as non-quaternary suppression NQS) employs a gap in the decoupling that allows evolution of the spins under coupled conditions[27]. The strength of the dipolar interactions determines the rate at which dephasing occurs. The experiment is usually performed with a decoupling window of 50-60 μs so that signals from protonated carbons are dephased and therefore absent from the spectrum. However there is no reason why shorter windows of 30-40 μs should not be used that simply attenuate the signals from protonated carbons. Conditions can be chosen so that a spectrum may be obtained showing signals from non-protonated carbons, methyl carbons (due to motion they are not dephased) and small CH signals, whilst CH_2 signals are suppressed. A similar method for spectral editing has been described[28]. The explanation is identical to that given in explaining the rates of cross polarisation as both these experiments rely upon the strength of the dipolar interactions to distinguish the different types of carbon atom. Such experiments have been performed on cortisone acetate and the results of these are presented in chapter 6.

4.12. References

(1) Frye, J.S., Maciel G.E. *J. Magn. Reson.* 48, 125 (1982).

(2) Johnson, L.F., Jankowski W.C. *Carbon-13 NMR Spectra : a collection of assigned, coded and indexed spectra.*; Wiley Interscience: New York, (1972).

(3) Bremser, W., Franke B., Wagner H. *Chemical Shift Ranges in Carbon-13 NMR Spectroscopy*; Verlag Chemie: Basel, (1982).

(4) Blunt, J.W., Stothers J.B. *Org. Magn. Reson.* **9**, 439 (1977).

(5) Tori, K., Nishikawa J., Takeuchi Y. *Tetrahedron Letters* **22**, 2793 (1981).

(6) Wehrli, F.W., Marchand A.P., Wehrli S. *Interpretation Of Carbon-13 NMR Spectra;* 2nd ed.; J. Wiley & Sons: Chichester, (1983).

(7) Derome, A.E. *Modern NMR Techniques For Chemistry Research*; Pergamon Press: Oxford, (1987); Organic Chemistry Series; Vol. 6.

(8) Harris, R.K., Kenwright A.M., Say B.J., Yeung R.R., Fletton R.A., Lancaster R.W., Hardgrove G.L. Jnr. *Spectrochim. Acta* **46A**, 927 (1990).

(9) Callow, R.K., Kennard O. *J. Pharm. Pharmacol.* **13**, 723 (1961).

(10) Carless, J.E., Moustafa M.A., Rapson H.D.C. *J. Pharm. Pharmacol.* **18**, 190 (1966).

(11) Mesley, R.J. *J. Pharm. Pharmacol.* **20**, 877 (1968).

(12) Kuhnert-Brandstatter, M., Gasser P. *Microchem. J.* **16**, 590 (1971).

(13) Mesley, R.J., Johnson C.A. *J. Pharm. Pharmacol.* **17**, 329 (1965).

(14) Mesley, R.J. *Spectrochim. Acta* **22**, 889 (1966).

(15) Haw, J.F., Campbell G.C., Crosby R.C. *Analytical Chemistry* **58**, 3172 (1986).

(16) Campbell, G.C., Crosby R.C., Haw J.F. *J. Magn. Reson.* **69**, 191 (1986).

(17) Yeung, R.R., Harris R.K., Personal communication.

(18) Jiang, Y.J., Pugmire R.J., Grant D.M. *J. Magn. Reson.* **71**, 485 (1987).

(19) Morris, G.A. *J. Magn. Reson.* **80**, 547 (1988).

(20) Gibbs, A., Morris G.A. *J. Magn. Reson.* **91**, 77 (1991).

(21) Morris, G.A., Cowburn D. *Magn. Reson. Chem.* **27**, 1085 (1989).

(22) Hartmann, S.R., Hahn E.L. *Physical review* **128**, 2042 (1962).

(23) Alemany, L.B., Grant D.M., Pugmuire R.J., Alger T.D., Zilm K.W. *J. Am. Chem. Soc.* **105**, 2133 (1983).

(24) Alemany, L.B., Grant D.M., Pugmuire R.J., Alger T.D., Zilm K.W. *J. Am. Chem. Soc.* **105**, 2142 (1983).

(25) Alemany, L.B., Grant D.M., Alger T.D., Pugmuire R.J. *J. Am. Chem. Soc.* **105**, 6697 (1983).

(26) Clarke, P.G. *PhD. Thesis Univ. Durham* (1991).

(27) Opella, S.J., Frey M.H. *J. Am. Chem. Soc.* **101**, 5854 (1979).

(28) Hartman, J.S., Ripmeester J.A. *Chem. Phys. Lett* **168**, 219 (1990).

Chapter 5

Assignment Of NMR Spectra

Chapter 5 Assignment Of NMR Spectra

5.1 Introduction

The assignment of solution-state spectra is an important stepping stone to the assignment of solid-state spectra. There are very many techniques available, and some of the most commonly used pulse sequences are described in chapter 4. In this chapter, the aim is to show how these various experiments may lead to the full assignment of spectra. The example taken is the steroid Reichsteins d-diacetate (I). I will then proceed with a detailed summary of the assignments of cortisone acetate, cortisone and cefuroxime axetil then with a resumé of the work of others on testosterone, androstanolone and beclomethasone dipropionate. The final part of this chapter is concerned with a comparison of solution- and solid-state NMR spectra. Most figures are presented at the end of this chapter.

5.2 Reichsteins D-Diacetate

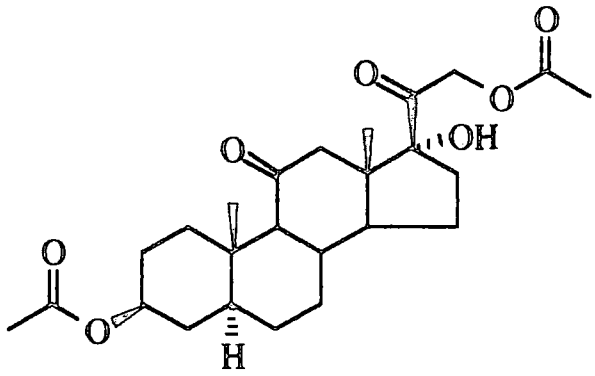

(I) 3β, 21-diacetoxy-17α-hydroxyallopregnane-11,20-dione

Reichsteins d-diacetate (I) has a molecular formula $C_{25}H_{36}O_7$ and there is no symmetry within the molecule. All carbon atoms are therefore different, so twenty five peaks should be expected in the ^{13}C spectrum (see figure 5.1). The peak listing shows the position of twenty eight peaks, three of which (77.32, 77.00, 76.69 ppm) correspond to d-chloroform, which is the solvent used in this study. The following numbering scheme will be adopted:

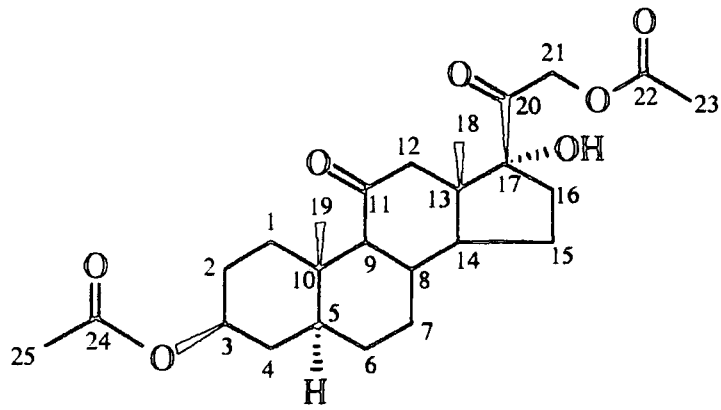

The starting point when making assignments is the fact that chemical shifts for specific structural units fall within certain ranges[1] and these are briefly summarised for steroids as follows:

CH_3	10 - 30 ppm
CH_2	15 - 55 ppm
CH	25 - 60 ppm
quaternary	30 - 40 ppm
C-OH	45 - 90 ppm
C=O	195 -220 ppm
CO_2C	160 - 180 ppm

As more data have been acquired over the years, databases of chemical shifts have been established and now chemical shifts can be predicted with much greater accuracy. Therefore one might start the process of assignment by using such a database. The programs compare fragments of the input structure with those in the database and suggest the expected chemical shifts. Output from such a program, called STN, for Reichsteins d-diacetate has been summarised in table 5.1.

Table 5.1 - Showing the output for Reichsteins d-diacetate obtained from the chemical shift database STN

carbon number	multiplicity	predicted chemical shift/ppm	error/ppm	number of matches in database
1	t	37.6	±1.8	36
2	t	26.7	±1.0	132
3	d	72.5	±1.3	128
4	t	33.9	±0.6	2
5	d	38.6	±2.5	54
6	t	26.8	±0.7	56
7	t	32.4 27.0	±0.5 ±0.2	15 4
8	d	36.5	±0.5	27
9	d	64.2 51.7	±0.5 ±0.4	12 5
10	s	36.1	±1.2	53
11	s	211.1	±0.8	48
12	t	49.8	±0.4	11
13	s	51.0	±0.3	10
14	d	49.6	±0.7	12
15	t	23.4	±0.4	37
16	t	33.8	±0.6	25
17	s	88.1	±0.7	8
18	q	15.5	±0.2	10
19	q	23.6 12.4	±0.7 ±0.8	45 12
20	s	205.7	±2.0	5
21	t	67.6	±0.2	7
22	s	170.1	±0.4	19
23	q	20.4	±0.2	20
24	s	170.3	±0.3	300
25	q	21.0	±0.3	2000

Notes: multiplicity is that arising from ^{1}J coupling, where 's' denotes a singlet, 'd' a doublet, 't' a triplet, and 'q' a quartet.

These estimated chemical shifts should now be compared with those obtained practically in the carbon-13 spectrum (see figure 5.1). For simple

structures the assignment may now be clear, but more often further experiments must be undertaken. Occasionally, the database suggests two different predicted chemical shifts for a particular atom. This occurs when the program finds chemical shifts that fall into two distinct groups. Then the number of matches for each range of chemical shifts is given. It can then be difficult to decide which is the more likely chemical shift for the molecule in question. The way to proceed from this point is to look at the experimentally observed chemical shifts to try to see if there is an obvious match. For example, the experimental spectrum shows a resonance at 12.0 ppm. The closest match is with one of those predicted for C19. Therefore one assumes that for Reichsteins d-diacetate, the C19 resonance is at 12.0 ppm. C9 may also be identified in a similar manner. The double entry for C7 is not so easy to resolve, and so the results of other experiments must be used. In this example the attached proton test (APT) and the DEPT experiments were performed (see figures 5.2, 5.3 and 5.4) in order to reveal the type (CH_3, CH_2, CH or quaternary) of each carbon resonance. A summary of the results of these experiments is given in table 5.2.

Table 5.2 - Showing the partial assignment of the carbon spectrum of Reichsteins d-diacetate based upon APT and DEPT spectra.

chemical shift / ppm	APT	DEPT	Assignment carbon no.
210.1	Q/CH_2	Q	11
204.5	Q/CH_2	Q	20
170.8	Q/CH_2	Q	22 or 24
170.5	Q/CH_2	Q	22 or 24
88.9	Q/CH_2	Q	17
73.3	CH	CH	3
67.4	Q/CH_2	CH_2	21
64.0	CH	CH	9
51.4	Q/CH_2	Q	13
50.5	CH	CH	14
49.8	Q/CH_2	CH_2	12
44.8	CH	CH	5 or 8
36.2	CH	CH	5 or 8
35.5	Q/CH_2	CH_2	*1,2,4,6,7 or 16
35.1	Q/CH_2	Q	10
35.05	Q/CH_2	CH_2	*
33.5	Q/CH_2	CH_2	*
32.8	Q/CH_2	CH_2	*
27.9	Q/CH_2	CH_2	*
27.2	Q/CH_2	CH_2	*
23.2	Q/CH_2	CH_2	15
21.4	CH_3	CH_3	23 or 25
20.4	CH_3	CH_3	23 or 25
15.5	CH_3	CH_3	18
12.0	CH_3	CH_3	19

Notes: 'Q' represents a quaternary carbon atom, and the assignment here is based upon expected chemical shift and the results of APT and DEPT experiments.

One feature of figure 5.1 is particularly noticeable, and that is that most of the peaks from the steroid molecule have very similar intensities but that a few peaks are much less intense. It is the quaternary carbons in the molecule that give peaks of low intensity since these atoms have longer relaxation times and so the

magnetisation (and hence the signal) becomes saturated more easily. One of the most important methods of relaxation is by dipolar coupling to protons, so if protons are distant then relaxation is slow and saturation may occur. It should be noted that relaxation times have not been measured and that the standard set-up conditions (using a recycle delay of 0.5 s) have been used in each case unless noted otherwise. It was considered unnecessary to use longer recycle delays in order to achieve accurate signal intensities, as only chemical shift information was required. Indeed, the deliberate use of short recycle delays may be considered advantageous as the average signal-to-noise ratio for the spectrum is greater and information is available on the presence of quaternary (or other slowly relaxing) nuclei. Thus from the intensities alone one may suggest that the peaks at 210.1, 204.5, 170.8, 170.5, 88.9, 51.4, and 35.1 ppm are from quaternary carbon atoms. These observations are confirmed by the DEPT experiment.

The results of APT and DEPT experiments are particularly useful for distinguishing C12, C13 and C14 that occur at about 50 ppm. APT spectra (figures 5.2 and 5.3) show that the central peak is from C14 but does not distinguish C12 and C13. The DEPT experiment however (figure 5.4) allows us to find that the C12 resonance occurs at 49.8 ppm. It also shows that C14 is at 50.5 ppm. One can also identify C13 (at 51.4 ppm) by its absence from the 'all protonated carbons' subspectrum.

One peak whose assignment is not clear from a comparison with the database chemical shifts is 44.8 ppm. From APT and DEPT it is known to be a CH resonance. This peak, along with that at 36.2 ppm must be C5 and C8 (both are CH groups), but the resonances are not necessarily in that order.

It is often helpful to assign the proton spectrum also, as carbon and proton shifts can be correlated. Thus a distinctive proton chemical shift may help the carbon assignment and vice versa. Particularly useful is the combination of the proton spectrum with the two dimensional techniques of COSY (^{1}H-^{1}H correlation) and HETCOR (^{1}H-^{13}C correlation), see figures 5.5, 5.6, 5.7, 5.8, 5.9

and 5.10. There is one apparent anomaly - the peak at 27.9 ppm is a CH_2 group according to DEPT, but only shows one cross peak in the HETCOR spectrum (suggesting that it is a CH group). This may be explained simply if both protons have the same chemical shift (or are not resolved) so that only one cross peak can be seen in the HETCOR spectrum.

We can now use the assignments of table 5.2 in conjunction with the proton and HETCOR spectra (figures 5.5,5.6,5.9 and 5.10) to see if the protons have the expected chemical shifts. Proton chemical shifts are often rather better documented than ^{13}C shifts so predicting proton shifts may be relatively straight forward, even though the chemical shift range is substantially smaller than for the carbon-13 nucleus.

One of the most noticeable features of the ^1H spectrum is the presence of four very intense singlets. These would be expected to arise from the methyl groups. In the HETCOR spectrum it can be seen that there are cross peaks connecting the following groups:

^{13}C shifts	12.0 ppm	↔	^1H shifts	1.03 ppm
	15.5 ppm	↔		0.62 ppm
	20.4 ppm	↔		2.16 ppm
	21.4 ppm	↔		2.02 ppm

All three hydrogens in a methyl group are equivalent due to internal rotation about the C_3 axis. Thus only one cross peak occurs. We can say with a fair degree of confidence that C19 resonates at 12.0 ppm and C18 at 15.5 ppm, as in most steroids studied so far C19 resonates at the lower frequency of the two[2-4]. In a similar way, C23 resonates to low frequency of C25 (and H23 to high frequency of H25), thus allowing assignments to be made.

Cross referencing between HETCOR (figures 5.9 and 5.10), COSY (figures 5.7 and 5.8), and the ^1H spectra (figures 5.5 and 5.6) allowed the assignment of both carbon and proton spectra. Carbon atoms C8 and C14 are easily identified as they give only single peaks in the HETCOR spectrum. This allowed H8 and H14 to be identified. As H14 couples to H8 and to H15 the chemical shift of H15 could be found. Similarly, the chemical shifts of C3 and

C5 are distinctive and, as the attached protons (H3 and H5) both couple to H4, this shift may be found too. Also, the coupling of H8 with H7 allowed the shift of H7 to be found, which by a process of elimination lead to the shift of H1. Coupling patterns are particularly useful for distinguishing the α and β protons.

Thus the spectrum can now be assigned. The assignment is presented in table 5.3.

Table 5.3 - The solution-state assignment of Reichsteins d-diacetate

Carbon atom no.	^{13}C shift /ppm	^{1}H shift /ppm α	β
1	35.5	0.91	2.52
2	27.2	1.76	1.54
3	73.3	4.68	-
4	33.5	1.58	1.36
5	44.8	1.16	-
6	27.9	1.26	1.26
7	32.8	1.12	1.80
8	36.2	-	1.72
9	64.0	1.72	-
10	35.1	-	-
11	210.1	-	-
12	49.8	2.87	2.18
13	51.4	-	-
14	50.5	2.36	-
15	23.2	1.88	1.40
16	35.05	1.60	2.76
17	88.9	-	-
18	15.5	0.62	
19	12.0	1.03	
20	204.5	-	-
21	67.4	4.63*	5.12*
22	170.5	-	-
23	20.4	2.16	
24	170.8	-	-
25	21.4	2.02	
OH	-	2.80	

The 'alpha' face of a steroid is below the plane of the ring system, and the 'beta' face is therefore above the plane, as defined in chapter 1.

*α and β are unsuitable terms for these protons as the side chain is not of a well defined conformation.

It is helpful to compare these assignments with those of other steroids of similar structure[5]. See table 5.4. There is good agreement between the chemical shifts obtained in solution and those reported for other steroids of similar

structure, so the assignments made are thought to be correct. The only large difference occurs for the hydroxyl proton, and the chemical shift of this proton is well known to be heavily solvent dependent[1].

Table 5.4 - The predicted chemical shifts for Reichsteins d-diacetate, based upon compounds of similar structure

Carbon atom no.	^{13}C shift /ppm	^{1}H shift (ppm) α	β	Source Structure
1	36.4	0.93	1.64	a
2	27.3	1.73	1.47	a
3	73.4	4.59	-	a
4	33.8	1.50	1.31	a
5	44.7	1.11	-	a
6	28.3	1.22	1.22	a
7	31.7	0.90	1.60	a
8	33.6	-	1.50	a
9	62.5	1.90	-	b
10	35.5	-	-	a
11	209.1	-	-	b
12	49.9	2.87	2.23	b
13	51.2	-	-	b
14	49.7	2.36	-	b
15	23.2	1.90	1.40	b
16	34.8	1.65	2.70	b
17	88.8	-	-	b
18	15.3	0.61		b
19	12.0	0.77		a
20	204.7	-	-	b
21	67.7	5.06	5.06	b
22	170.6	-	-	b
23	20.4	2.12		b
24	170.5	-	-	a
25	21.3	1.93		a
OH	-	3.57		b

The source structures a and b are as follows:

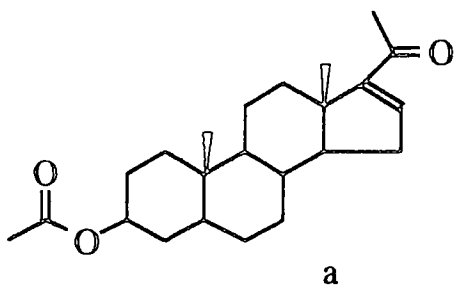

a

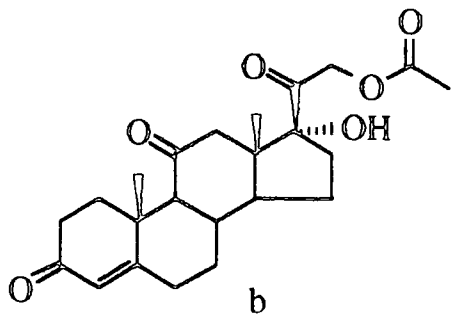

b

5.3 Assignment Of Cortisone Acetate

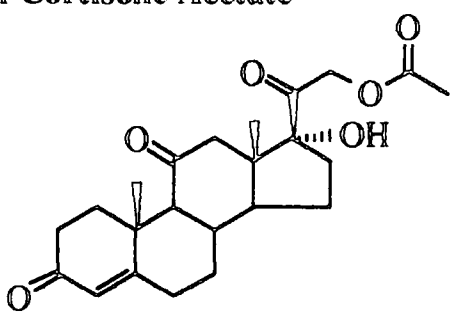

(II) 17α,21-dihydroxy-4-pregnene-3,11,20-trione,21-acetate

The assignment of the solution state NMR spectrum of cortisone acetate (II) has previously been reported[4-6]. However the reports are slightly different. As the solution state spectrum is used as the basis for making solid state assignments it was decided to carry out a wide range of experiments in order to clarify the assignments. Proton, carbon (both coupled and decoupled), COSY, HETCOR and NOE difference spectra have been recorded using d-chloroform as the solvent.

The following numbering scheme shall be adopted:

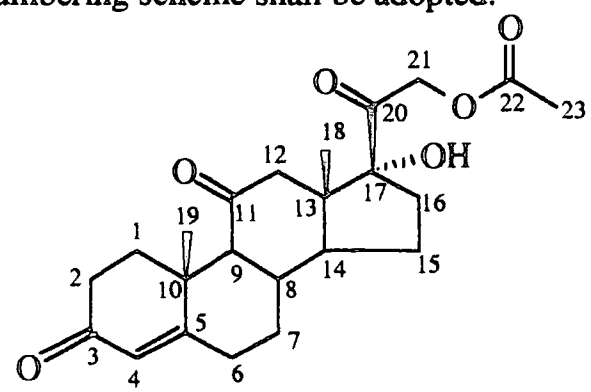

The differences in assignments can be resolved with the aid of a few experiments. C5 and C22 occur at ca. 170 ppm (see figure 5.11). They can be

distinguished with a carbon (proton-coupled) spectrum. See figure 5.12. One would expect C22 to show coupling to the three equivalent protons on C23, giving a quartet structure to the resonance, and some coupling to the protons on C21 (causing further splitting). However, C5 is expected to show coupling to the three nearest non-equivalent protons (H4 and both H6 protons), and also coupling with the protons on C1, C7, C9 and C19. Carbon-proton coupling constants are in the following ranges[1]: ^1J = 110 to 320 Hz (which are not of relevance here) and ^2J = -5 to 60 Hz. For sp^3 carbons ^2J is usually approximately the same as ^3J, whilst in aromatic compounds ^3J may be slightly greater than ^2J. Thus the range of couplings for C5 will give the resonance no clearly defined structure. The spectrum shows that the higher frequency peak (170.4 ppm) has a coupling pattern consistent with that expected for C22, whilst the lower frequency peak (168.4 ppm) does not show any clear structure and is consistent with the pattern expected for C5.

At ca. 50 ppm the discrepancies over C12 and C14 can be easily resolved with the HETCOR spectrum, which clearly shows that C12 occurs at 49.9 ppm (associated with two proton resonances) and C14 to lower frequency at 49.7 ppm (associated with only one proton resonance). The proton spectrum is presented in figure 5.13.

The assignment of the region 30-35 ppm is not straight forward. However the assignment made is proposed as follows. The HETCOR experiment allows C8 to be correlated with H8. Then use can be made of the COSY spectrum (see figure 5.14), since H8 will couple with H7 (and also with H9 and H14). Then, by returning to the HETCOR spectrum, knowing these proton shifts, C7 can be assigned as the peak at 32.2 ppm. Similarly, the coupling of H7 with H6 allows the identification of C6 as being at 33.7 ppm. This leaves two resonances (from C1 and C2) unassigned at 32.3 and 34.8 ppm. As the four attached protons do not couple strongly with any other protons, they cannot be distinguished. One must rely upon the fact that in steroids of similar structure, the H1 protons both resonate at ca. 2.3 ppm, whilst the H2 protons resonate at ca. 1.6 and 2.7 ppm

(these assignments have been established using the carbon-carbon INADEQUATE correlation experiment). As cortisone acetate shows resonances that are consistent with this pattern, one can conclude that C1 is at 32.3 ppm and C2 at 34.8 ppm. The assignments are summarised in table 5.5.

Table 5.5 - The assignment of cortisone acetate

Carbon atom no.	^{13}C shift / ppm	^{1}H shift / ppm α	β
1	32.3	2.43	2.24
2	34.8	2.70	1.59
3	199.6	-	-
4	124.5	5.68	
5	168.4	-	-
6	33.7	2.23	2.41
7	32.2	1.25	1.93
8	36.5	-	1.90
9	62.5	1.90	-
10	38.2	-	-
11	208.7	-	-
12	49.9	2.87	2.23
13	51.2	-	-
14	49.7	2.36	-
15	23.2	1.90	1.40
16	35.0	1.65	2.70
17	88.8	-	-
18	15.4	0.61	
19	17.2	1.36	
20	204.3	-	-
21	67.3	4.65*	5.06*
22	170.4	-	-
23	20.3	2.12	
17-OH		3.57	

* α and β are unsuitable terms for these protons as they are in the side chain.

The results are in agreement with the assignment made by Duddeck[5].

5.4 Assignment of Cortisone

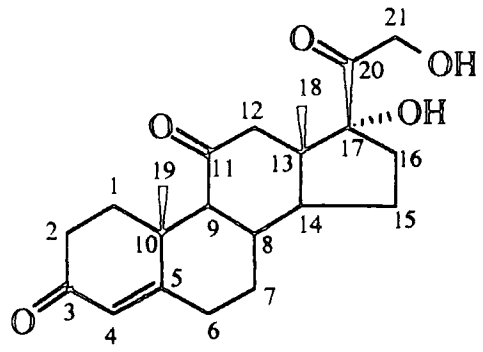

(III) 17α,21-dihydroxy-4-pregnene-3,11,20-trione

The assignment of cortisone (III) is quite straight forward as the structure is very similar to that of its derivative cortisone acetate. Therefore most peaks can be assigned by comparing the spectra of these two compounds. The following experiments were carried out - proton and carbon-13 spectra, COSY, HETCOR, long range HETCOR, TOCSY (total correlation spectroscopy), proton spin- decoupled spectra, and NOE difference spectroscopy. The carbon and proton spectra are shown in figures 5.15 and 5.16.

C11 and C20 could be distinguished in the long range HETCOR experiment as C20 shows correlations with the H21 protons, whilst C11 shows correlations with the H9 and H12 protons. C12, C13 and C14 can be distinguished with the HETCOR spectrum (shown in figure 5.17) as each shows a different number of proton correlations. The region about 30-35 ppm is again the most difficult to assign. As with cortisone acetate C16 is identified via H15, and C7 via H8, which also leads to the assignment of C6. As before, C1 and C2 can be assigned by comparing the proton chemical shifts with those of other steroids. The assignments made are supported by the long range HETCOR spectrum that shows correlations between C2 and H4, and also between H2 and C10. The assignments are summarised in table 5.6

Table 5.6 - The assignment of cortisone

Carbon atom no.	^{13}C shift / ppm	^{1}H shift / ppm α	β
1	33.4	2.41	2.12
2	33.9	2.53	1.66
3	198.2	-	-
4	123.7	5.63	
5	169.1	-	-
6	31.7	2.26	2.42
7	32.0	1.22	1.86
8	36.0	-	1.89
9	61.1	2.14	-
10	37.8	-	-
11	210.3	-	-
12	50.2	2.88	1.95
13	50.4	-	-
14	49.1	2.35	-
15	22.9	1.78	1.33
16	33.6	1.62	2.56
17	87.7	-	-
18	15.5	0.47	
19	16.9	1.32	
20	211.4	-	-
21	66.1	4.44	4.08
17-OH	-	5.58	
21-OH	-	4.64	
H_2O	-	3.30	

The results of all other experiments are consistent with the assignments made and serve to check that the assignments are correct.

5.5 Assignment Of Other Steroids

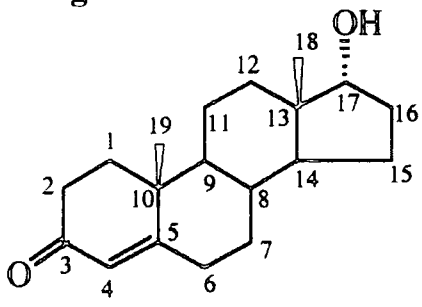

(IV) Testosterone

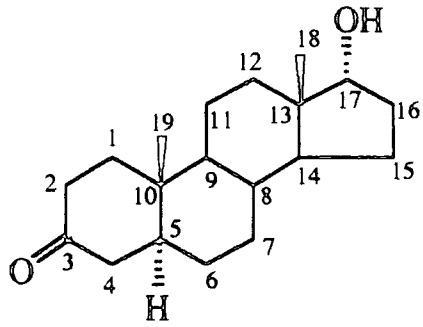

(V) Androstanolone

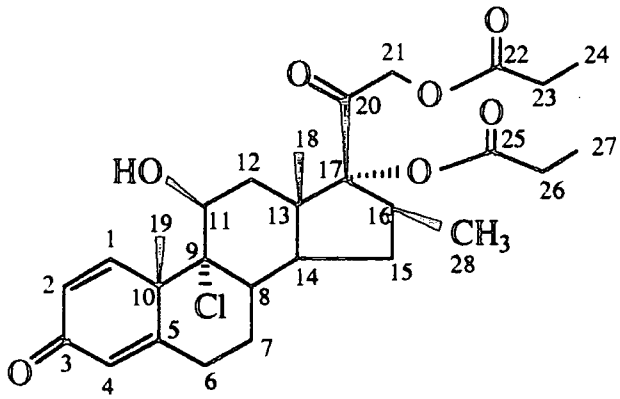

(VI) Beclomethasone Dipropionate

Other steroids (testosterone (IV), androstanolone (V) and beclomethasone dipropionate (VI)) have been studied in the solid state, and so the assignment of the solution state spectra[2,7] are summarised in table 5.7.

Table 5.7 - The assignment of other steroids

Carbon atom no.	BDP ^{13}C shift / ppm	testosterone ^{13}C shift / ppm	androstanolone ^{13}C shift / ppm
1	152.0	35.6	38.6
2	129.5	33.8	38.1
3	186.4	199.4	211.5
4	125.1	123.6	44.6
5	165.6	171.0	46.8
6	30.6	32.7	28.9
7	28.4	31.5	31.3
8	34.4	35.0	35.5
9	82.6	53.9	54.0
10	50.0	38.6	35.8
11	75.2	20.6	21.1
12	36.5	36.4	36.7
13	48.2	42.7	43.0
14	43.5	50.4	50.9
15	34.4	23.2	23.4
16	47.0	30.1	30.5
17	94.5	81.0	81.7
18	16.9	11.0	11.2
19	24.4	17.3	11.5
20	198.4		
21	67.8		
22	174.6		
23	27.5		
24	8.9		
25	174.1		
26	27.1		
27	8.7		
28	19.3		

The assignments made for the propionate side chains in BDP are uncertain and may be interchanged.

5.6 Assignment Of Cefuroxime Axetil

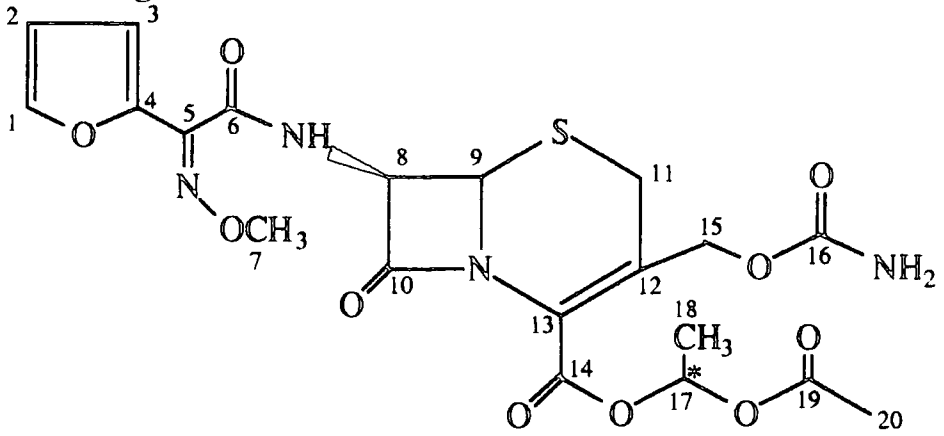

(VII) Cefuroxime Axetil

Cefuroxime axetil (VII) exists as two diastereoisomers and the solution state spectra of the two isomers are different. Both isomers are soluble in d_6-DMSO, but isomerisation occurs rapidly (over a few minutes) to form the Δ_2 product (see figure 5.18), and an equilibrium mixture of the Δ_2 and Δ_3 compounds is established. However, in order to make a full assignment it is necessary to have a stable solution, so other solvents were tried. Isomer A is not very soluble in $CDCl_3$, CD_3OD or CD_3CN, but isomer B is soluble in CD_3CN and the solution is stable for several hours. Therefore a solution of isomer B in CD_3CN was used for all further experiments.The following experiments were performed - proton and carbon-13 spectra, DEPT, HETCOR, long-range HETCOR, partial deuteration and carbon (proton-coupled) spectra. Carbon and proton spectra are shown in figures 5.19 and 5.20.

Figure 5.18 - The structure of the Δ_2 product and the original Δ_3 compound

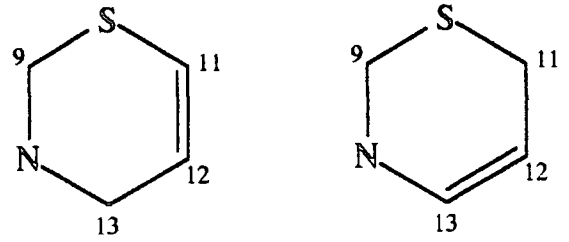

Δ_2 product Δ_3 compound

The proton spectrum is quite easy to assign as there are relatively few protons present in the molecule and the signals are generally well resolved. This allows the assignment of all the protonated carbon atoms via the HETCOR

spectrum. The five highest frequency peaks arise from carbonyl and ester carbons. Three of these (C10, C16 and C19) can be assigned simply from the long range HETCOR spectrum as C10 shows coupling with H9, C16 with H15 and C19 with H20. See figure 5.21. The remaining two carbons (C6 and C14) can be distinguished by the partial deuteration experiment that shows the expected splitting of C6 as the adjacent nitrogen atom undergoes deuteration to form two different species, one of which is protonated and the other deuterated. Note that the assignment of C16 is also confirmed by the partial deuteration experiment. The long range HETCOR experiment is useful for assigning the remaining non-protonated carbons. C12 and C13 occur at 125.5 and 129.5 ppm although it is not clear which is which, and C4 is identified at 146.6 ppm. Therefore by elimination C5 must occur at 145.4 ppm. This is confirmed by the carbon (proton coupled) spectrum that shows C5 as a clear singlet.

The unambiguous assignment of C12 and C13 is not possible based upon the experiments carried out, as the exact size of the ^{13}C-^{1}H coupling constants ^{2}J and ^{3}J are unknown. As these coupling constants are usually of approximately equal magnitude, one cannot distinguish these two peaks in either the long-range HETCOR or the proton-coupled carbon spectrum. One can only suggest that as C13 is adjacent to a nitrogen atom and a carbonyl group, both of which are electron withdrawing groups, that the C13 nucleus might be deshielded and so resonate at a higher frequency.

The assignments are summarised in table 5.8

Table 5.8 - The assignment of cefuroxime axetil

Carbon atom no.	^{13}C shift / ppm	^{1}H shift / ppm
1	146.2	7.63
2	112.9	6.55
3	114.3	6.73
4	146.6	-
5	145.4	-
6	162.6	-
7	63.4	3.95
8	60.1	5.87
9	58.3	5.13
10	164.7	-
11	27.1	3.57
12	125.5*	-
13	129.5*	-
14	160.6	-
15	63.7	4.80
16	157.4	-
17	89.6	7.05
18	19.7	1.52
19	170.0	-
20	21.0	2.05
NH_2	-	5.35
CONH	-	7.88

* These peaks have not been unambiguously assigned.

5.7 Comparison Of Solid And Solution State Spectra

There are often many similarities between the solid- and solution-state spectra. After all, the chemical structures (i.e. the configurations) are the same. But the differences are significant. In the solid state often one conformation is preferred, and even in the case of polymorphs where more than one conformation occurs, there are several discrete conformations. In the solution state there may be a whole range of conformations that exist in equilibrium, and the solution-state spectrum is that of the average conformation. The occurrence of different conformations is due to the differing molecular interactions that

occur. In the solid state it is the interaction between two like molecules in a particular packing arrangement, whilst in solution it is the interaction of solvent and solute molecules. The solvent/solute interactions are affected by polarity and molecular size, and this gives rise to 'solvent effects' that are well known. But there is little difference conceptually between solvent/solute interactions and the interactions that occur between molecules in a solid. Thus it should not be surprising that the differences between solid polymorph spectra and between solid and solution spectra are as large as the 'solvent effects' that are observed by changing the solvent.

In numerical terms the difference between solid polymorph resonances and between solid and solution resonances are usually up to 10 ppm for the carbon-13 nucleus. For a compound with a wide range of carbon chemical shifts, the similarities between solid and solution spectra are great, and a solution state assignment can often be easily transferred to the solid state spectrum.

Solid- and solution-state spectra of Reichsteins d-diacetate are presented together in figure 5.22 for comparison. Immediately obvious is the difference in linewidths. For solutions the widths at half height of carbon resonances are typically 0.03 ppm, that is 3 Hz (at 100 MHz), whilst for solids it is typically 0.3 ppm, that is 15 Hz (at a magnetic field corresponding to 50 MHz). Also for the solution-state spectrum most of the peak heights are approximately equal (except for quaternary carbons, as explained earlier in this chapter section 5.2), but the solid-state spectrum shows much greater variation in the peak heights. The reason for this is that the contact time cannot be the optimum for all atoms at any one value, this reduces the signal intensity to below the maximum. Another difference between solid and solution spectra is that spinning sidebands are present in the solid-state spectrum.

However, a closer examination of the two spectra shows that the differences in chemical shift are quite small, and are presented in table 5.9. The assignment of the solid-state spectrum is based upon the results of the NQS experiment (which shows peaks from quaternary and methyl peaks only), and

upon the measurement of line widths at half height. The peaks that remained in the NQS experiment are marked with an asterisk in table 5.9, and the linewidths are also given here. They are used as a basis for assignment since it is known that in steroids, the CH_2 carbons have much broader lines due to insufficient decoupler power (see chapter 4). This information does not give a full and unambiguous assignment, and those peaks whose chemical shifts are not sufficiently distinctive to allow assignment are indicated with brackets. In these cases the resonances are assumed to occur in the same order as in the solution, so that differences in the chemical shifts are minimised.

Table 5.9 - The solution- and solid-state chemical shifts of Reichsteins d-diacetate

carbon number	solution shift / ppm	solid shift / ppm	NQS	half-width / Hz	Δ / ppm
19	12.0	14.5	*	10	-2.5
18	15.5	16.5	*	15	-1.0
23	20.4	19.8	*	12	+0.6
25	21.4	20.2	*	15	+1.2
15	23.2	23.6		32	-0.4
2	27.2	26.9		22	+0.3
6	27.9	28.2		32	-0.3
7	32.8	33.0		41	-0.2
4	33.5	33.3			+0.2
16	35.05	35.1		20	-0.05
1	35.5	35.9		10	-0.4
10	35.1	36.6	*	25	-1.9
8	36.2	37.0		10	-0.4
5	44.8	47.4		15	-2.6
12	49.8	49.5		27	+0.3
14	50.5	51.0		15	-0.5
13	51.4	51.6	*	12	-0.2
9	64.0	65.0		15	-1.0
21	67.4	68.7		17	-1.3
3	73.3	78.6		22	-5.3
17	88.9	89.9	*	10	-1.0
22	170.5	171.3	*	22	-0.8
24	170.8	173.9	*	32	-3.1
20	204.5	202.7	*	32	+1.8
11	210.1	209.5	*	22	+0.6

where Δ = solution shift - solid shift

The largest differences are summarised in table 5.10.

Table 5.10 - The largest differences between solid- and solution-state chemical shifts for Reichsteins d-diacetate

solid shift / ppm	carbon atom number	Δ / ppm
12.0	19	-2.5
35.1	10	-1.9
44.8	5	-2.6
77.3	3	-5.3
170.5 / 170.8	22 / 24	-3.4 / -3.1
204.5	20	+1.8

It is interesting to see that the largest differences occur in the A ring of the steroid, its substituents and in the other side chain. This suggests that the A ring has a slightly different conformation in the solid from that in the solution. This could be explained by the fact that a high frequency shift of 3 ppm at C24 in the solid state suggests that a hydrogen bond is formed (probably to the C17 alcohol). Similar high frequency shifts are seen for other steroids (notably cortisone acetate), where the crystal structure is known (see chapter 8). However, as it has not been possible to definitely distinguish C24 from C22, the possibility remains that it is the C22 carbonyl involved in any hydrogen bonds, and not C24. The large difference at C20 is not unexpected as this side chain does not have a rigid conformation in solution.

5.8 References

(1) Silverstein, R.M., Bassler G.C., Morrill T.C. *Spectrometric identification of organic compounds;* 4th ed.; J. Wiley & Sons: New York, (1981).

(2) Blunt, J.W., Stothers J.B. *Org. Magn. Reson.* 9, 439 (1977).

(3) Page, J.E. *NMR spectra of steroids*; Academic Press: London, (1970); Annual reports on NMR spectroscopy; Vol. 3, pp 149.

(4) Hickey, J.P., Butler I.S., Pouskouleli G. *J. Magn. Reson.* 38, 501 (1980).

(5) Duddeck, H., Rosenbaum D., Hani M., Elgamal A., Fayez M.B.E. *Magn. Reson. Chem.* 24, 999 (1986).

(6) Johnson, L.F., Jankowski W.C. *Carbon-13 NMR Spectra : a collection of assigned, coded and indexed spectra.*; Wiley Interscience: New York, (1972).

(7) Fletton, R. *Glaxo Internal Report* (1989).

Figure 5.1 - ^{13}C spectrum of Reichsteins d-diacetate.
Operating conditions were as follows : pulse width = 2.5 ms; acquisition time = 1.5 s; recycle delay = 0.5 s; no. of points = 75K; no. of transients = 960. The solvent is $CDCl_3$ and is marked with //.

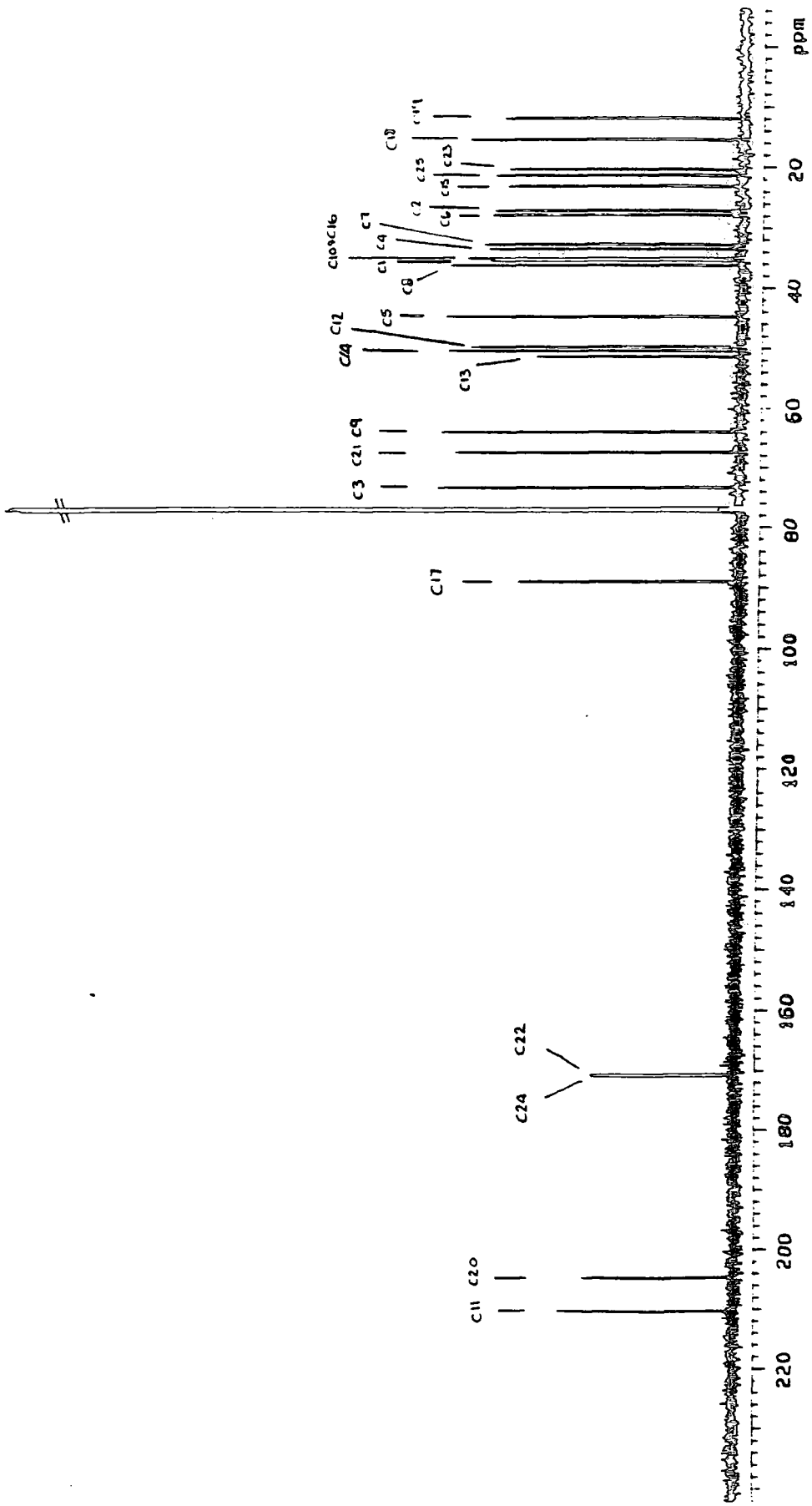

Figure 5.2 - ^{13}C APT spectrum of Reichsteins d-diacetate.
Operating conditions were as follows : 180° pulse width = 10.6 μs; acquisition time = 1.5 s; recycle delay = 0.5 s; τ = 7 ms; no. of points = 75K; no. of transients = 480. The solvent is $CDCl_3$ and is marked with //.

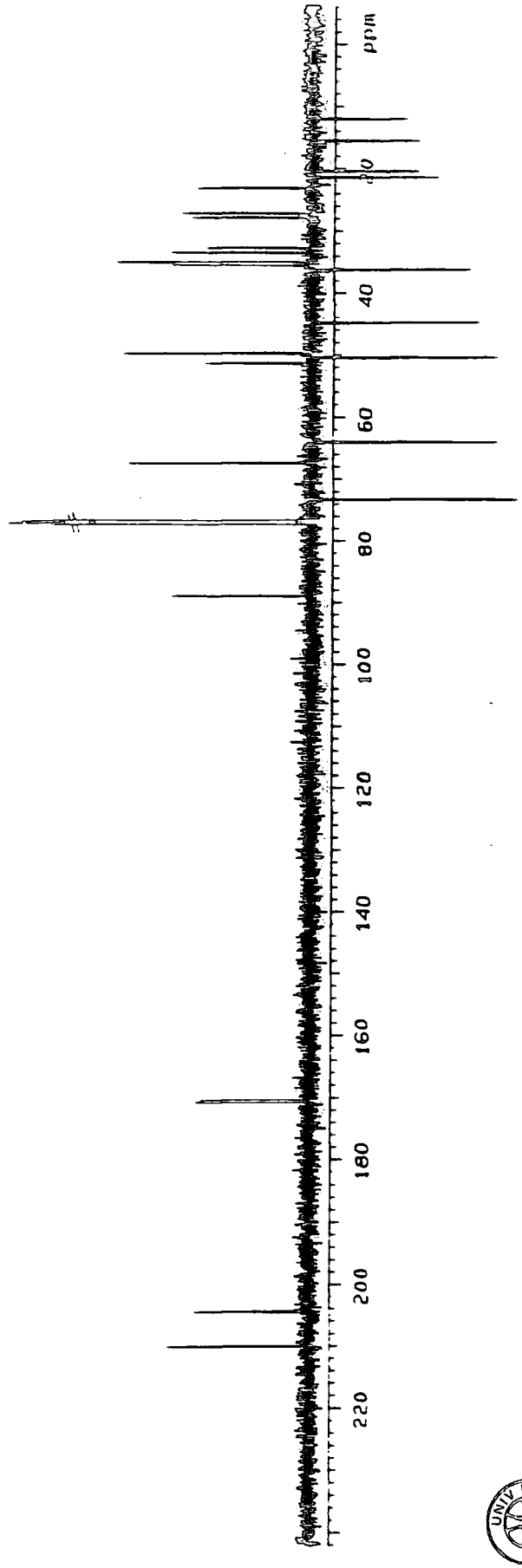

Figure 5.3 - Expansion of the ^{13}C APT spectrum of Reichsteins d-diacetate . Operating conditions were as follows : 180° pulse width = 10.6 μs; acquisition time = 1.5 s; recycle delay = 0.5 s; τ = 7 ms; no. of points = 75K; no. of transients = 675. The solvent is $CDCl_3$ and is marked with //.

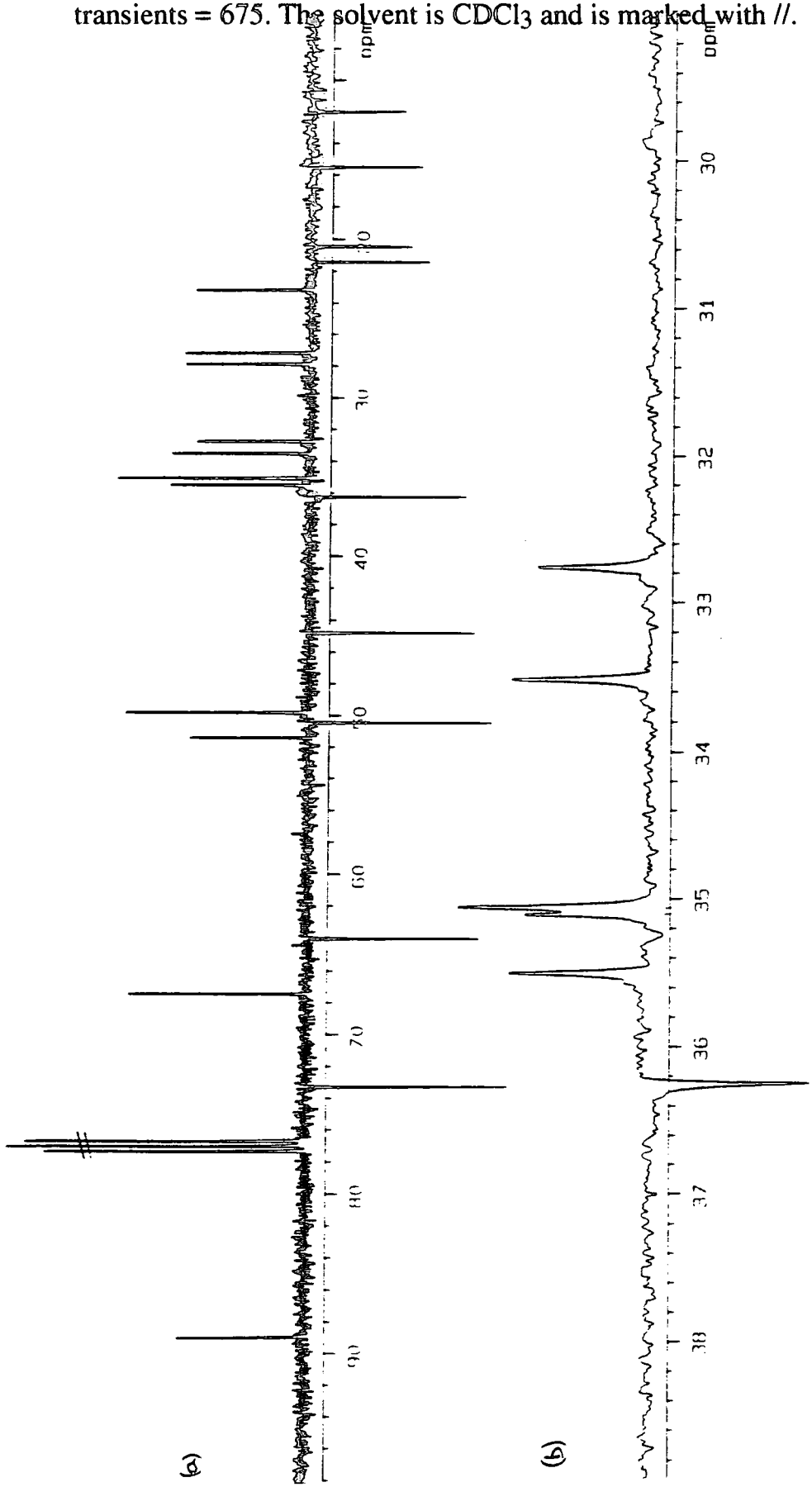

Figure 5.4 - ^{13}C DEPT spectrum of Reichsteins d-diacetate. Operating conditions were as follows : carbon 90° pulse width = 5.3 μs; proton 90° pulse width = 19.1μs; τ = 3.5 ms; acquisition time = 1.5 s; recycle delay = 2 s; no. of points = 75K; no. of transients = 320. The solvent is $CDCl_3$.

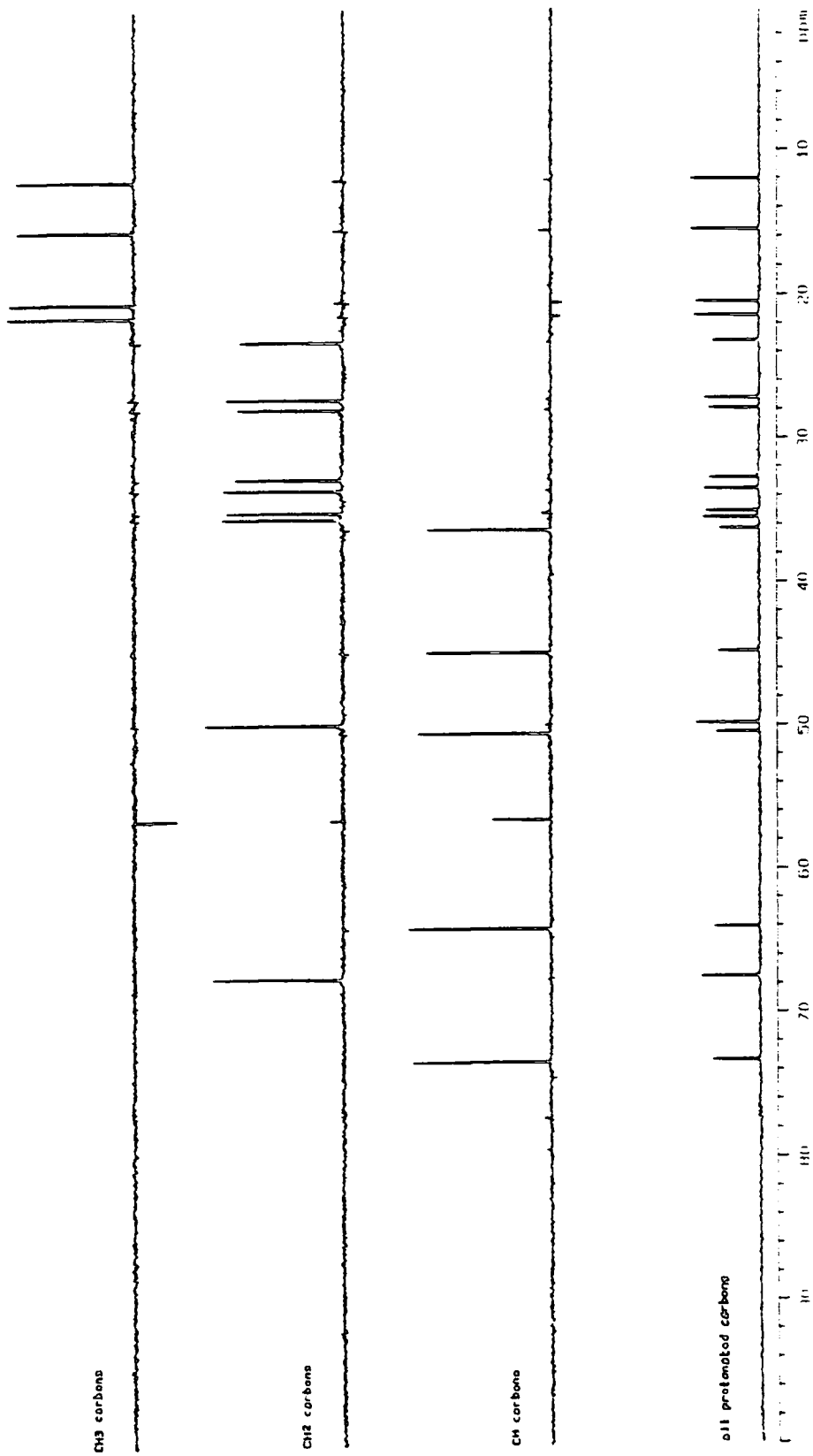

Figure 5.5 - ^{1}H solution spectrum of Reichsteins d-diacetate. Operating conditions were as follows : pulse width = 10 μs; acquisition time = 4 s; recycle delay = 0 s; no. of points = 64K; no. of transients = 112. The solvent is $CDCl_3$.

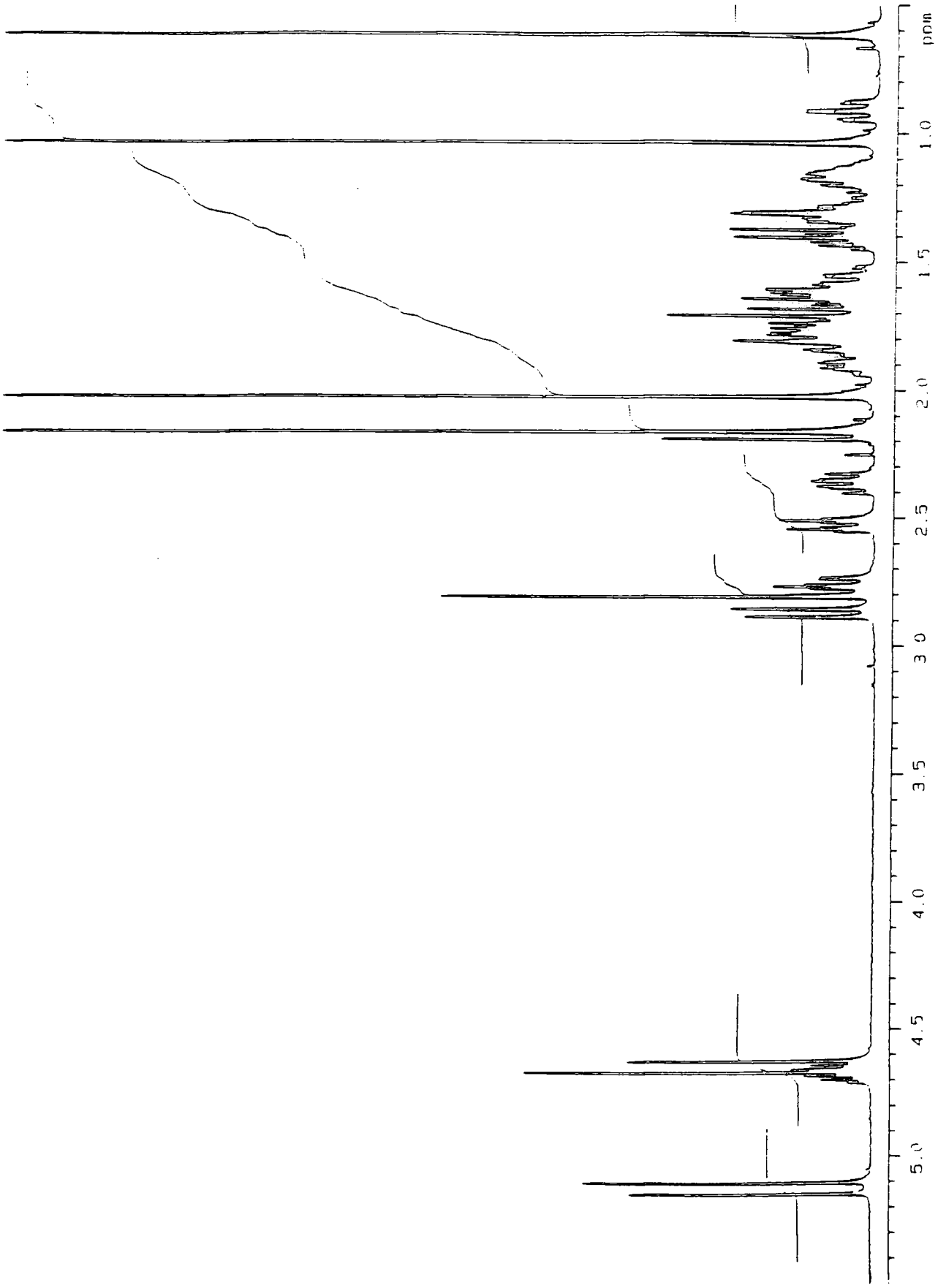

Figure 5.6 - Expansion of the ^1H spectrum of Reichsteins d-diacetate. Operating conditions were as follows : pulse width = 10 μs; acquisition time = 4 s; recycle delay = 0 s; no. of points = 64K; no. of transients = 112. The solvent is $CDCl_3$.

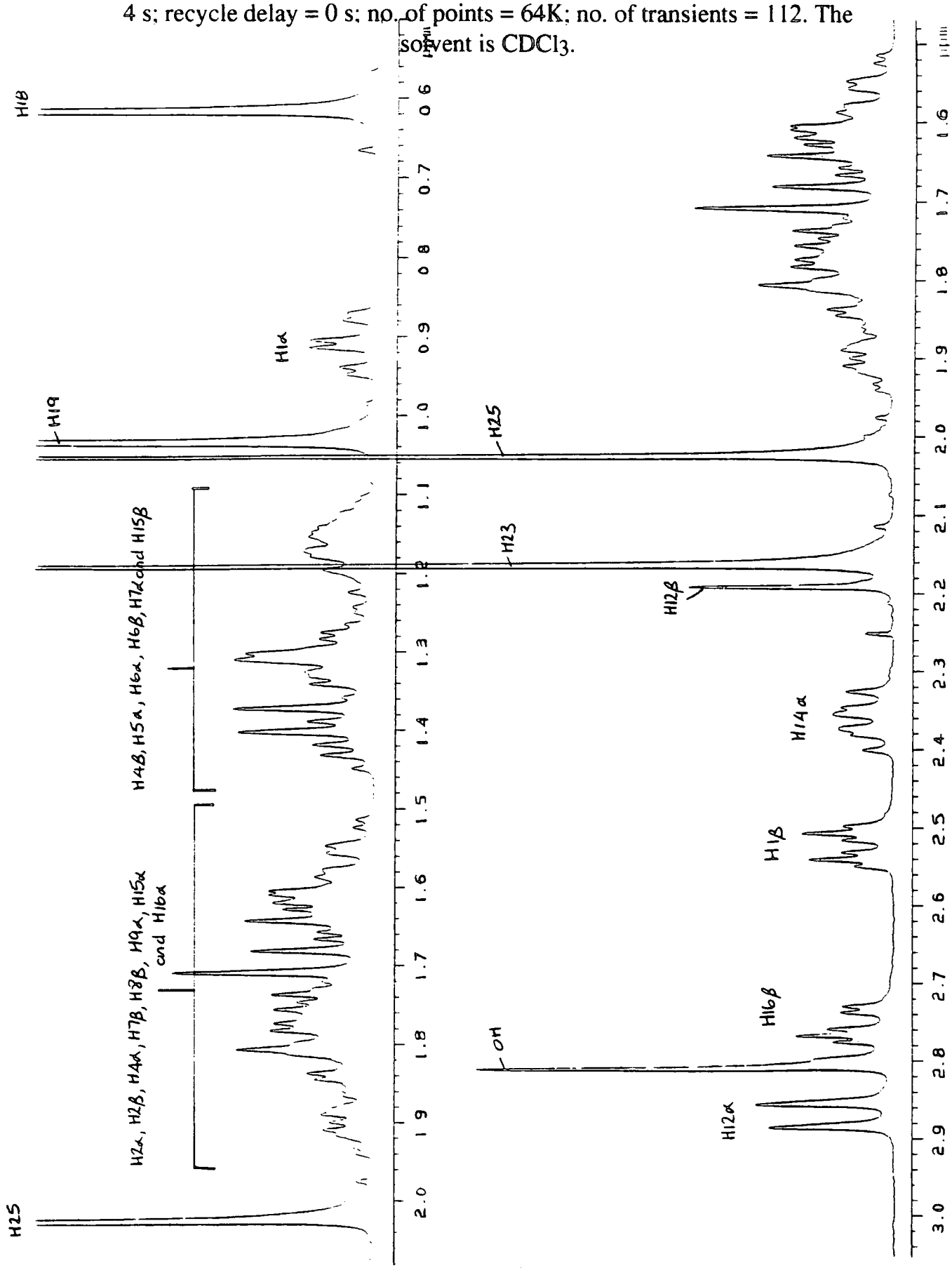

Figure 5.7 - ^{1}H COSY spectrum of Reichsteins d-diacetate. Operating conditions were as follows : 90° pulse width = 19.1 μs; acquisition time = 0.232 s; recycle delay = 1.5 s; no. of points = 1K in each dimension; no. of transients = 8 for each of 256 increments. The solvent is $CDCl_3$.

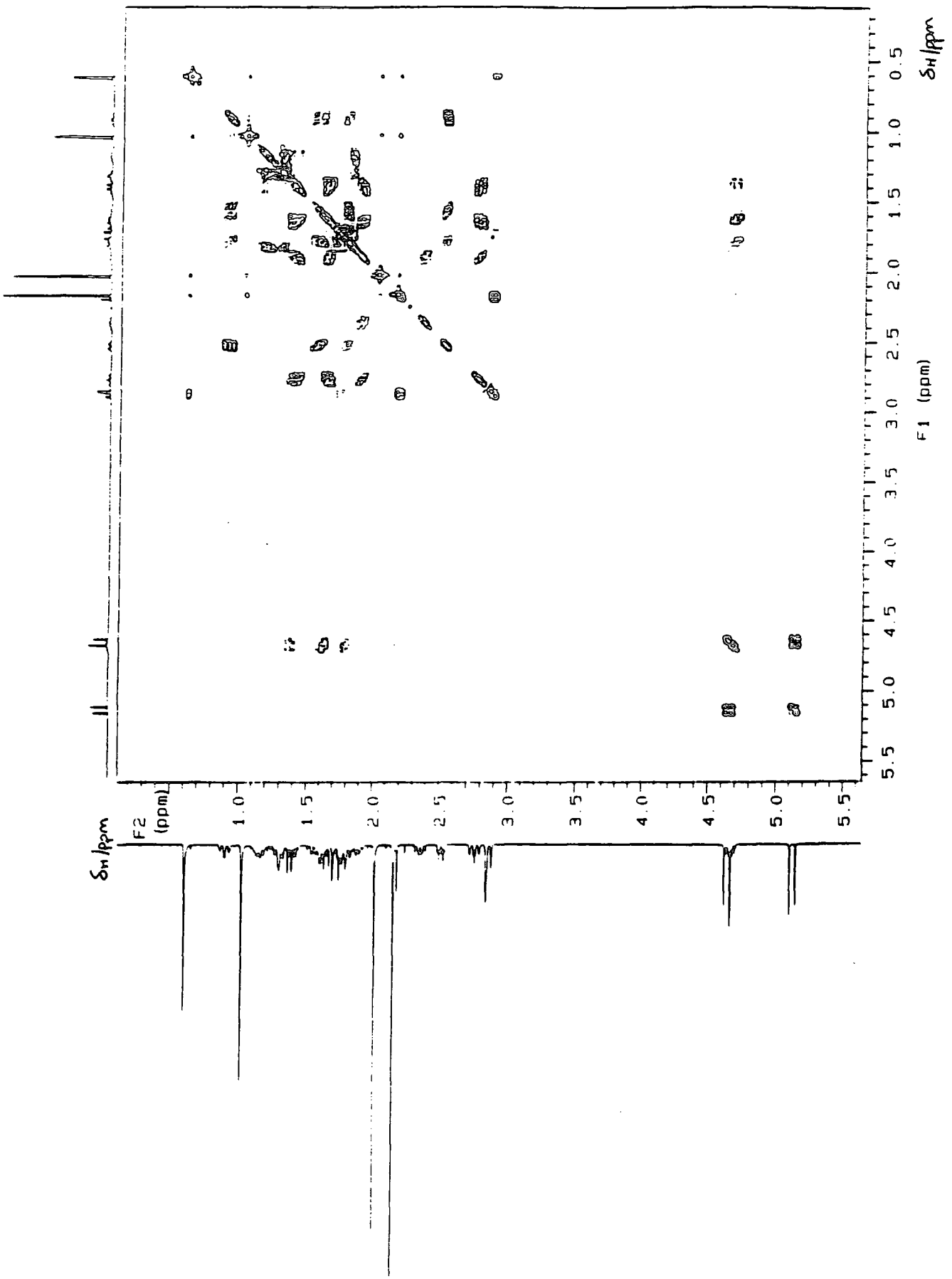

Figure 5.8 - Expansion of the ^1H COSY spectrum of Reichsteins d-diacetate. Operating conditions were as follows : 90° pulse width = 19.1 μs; acquisition time = 0.232 s; recycle delay = 1.5 s; no. of points = 1K in each dimension; no. of transients = 8 for each of 256 increments. The solvent is $CDCl_3$.

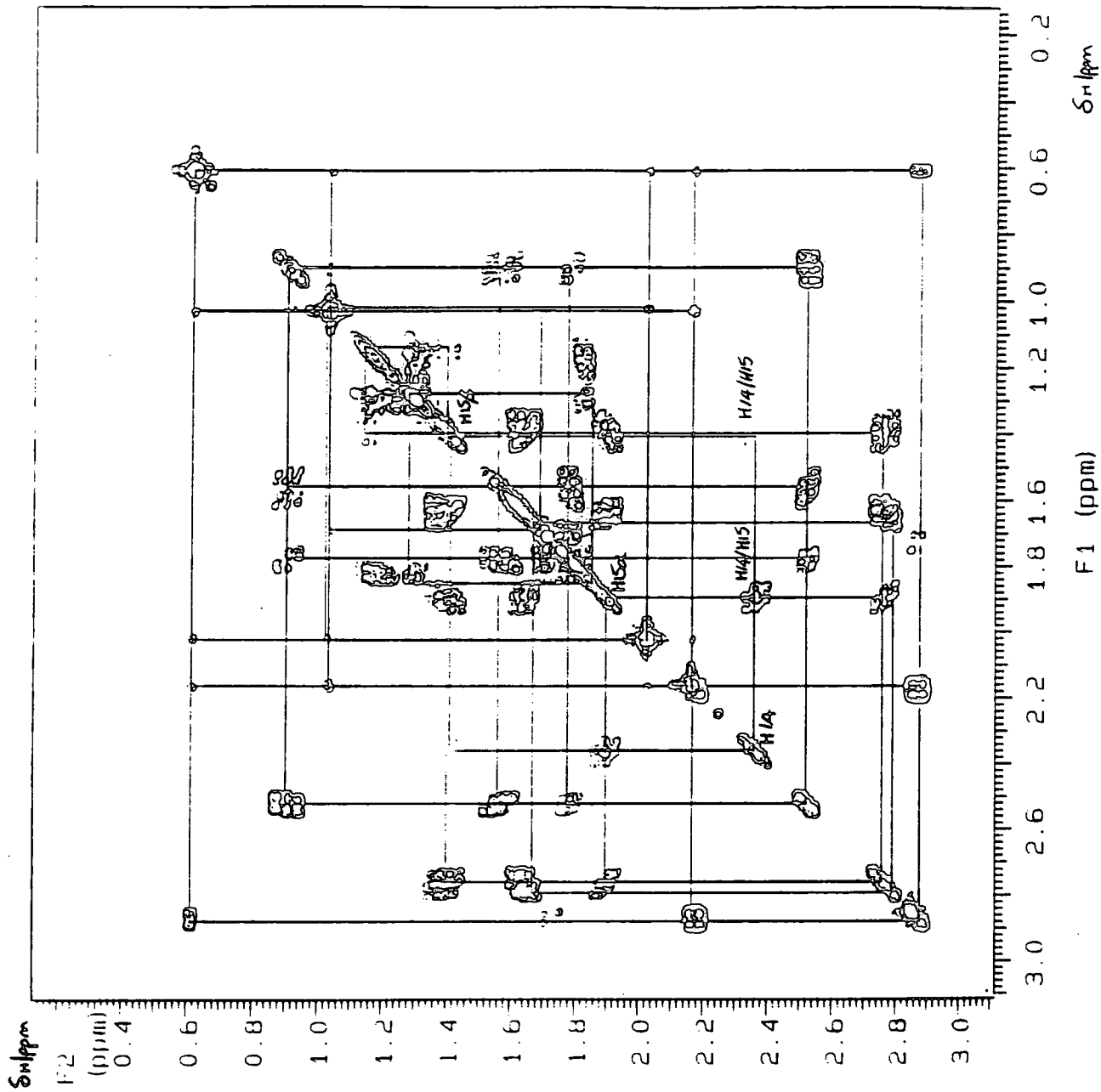

Figure 5.9 - HETCOR spectrum of Reichsteins d-diacetate. Operating conditions were as follows : carbon 90° pulse width = 5.3 μs; proton 90° pulse width = 19.1 μs; acquisition time = 0.088 s; recycle delay = 1.0 s; no. of points = 256W in the f1 dimension and 2K in the f2 dimension; no. of transients = 60 for each of 128 increments. The solvent is $CDCl_3$ and is marked with //.

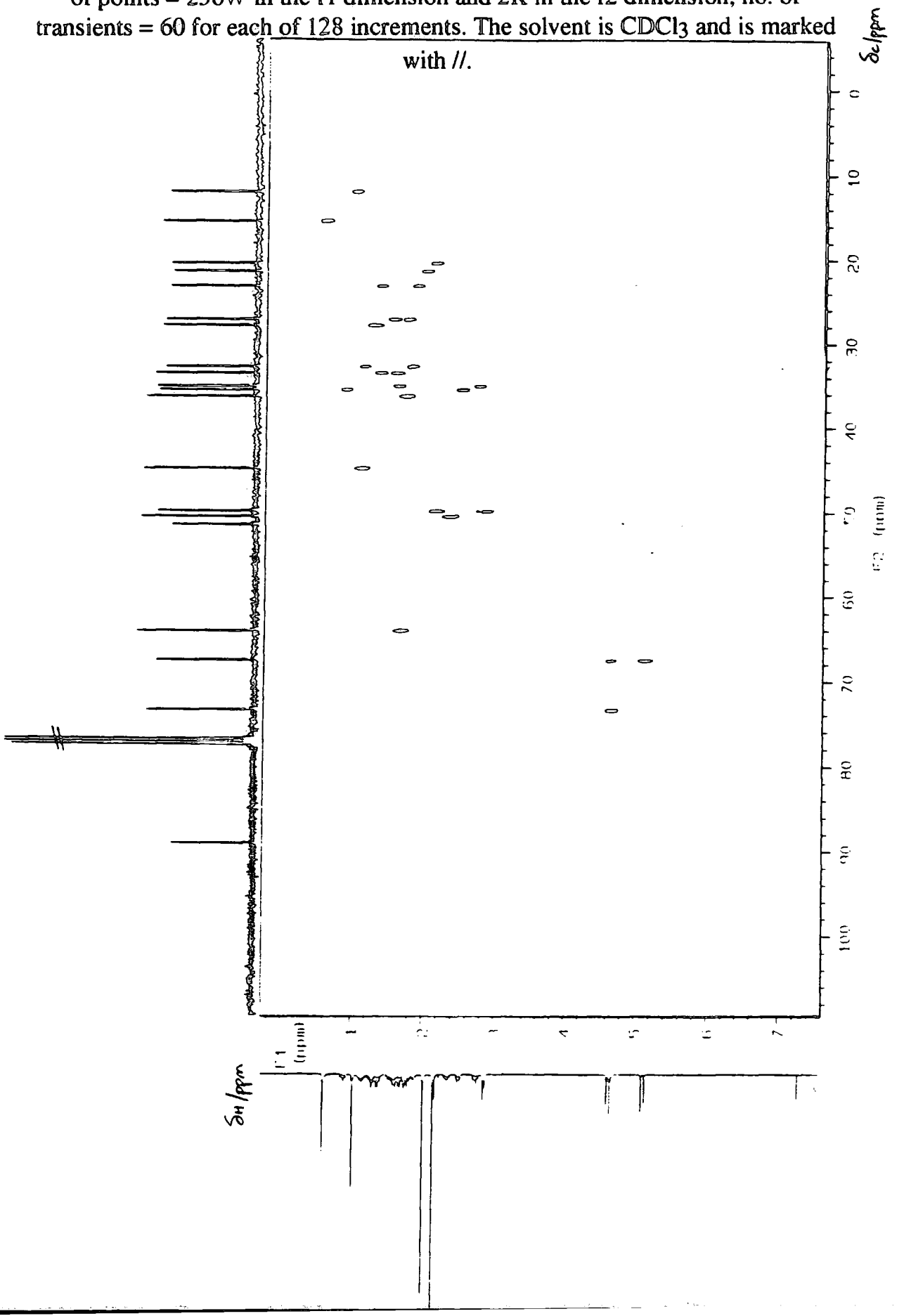

Figure 5.10 -Expansion of the HETCOR spectrum of Reichsteins d-diacetate. Operating conditions were as follows : carbon 90° pulse width = 5.3 μs; proton 90° pulse width = 19.1 μs; acquisition time = 0.088 s; recycle delay = 1.0 s; no. of points = 256W in the f1 dimension and 2K in the f2 dimension; no. of transients = 60 for each of 128 increments. The solvent is $CDCl_3$.

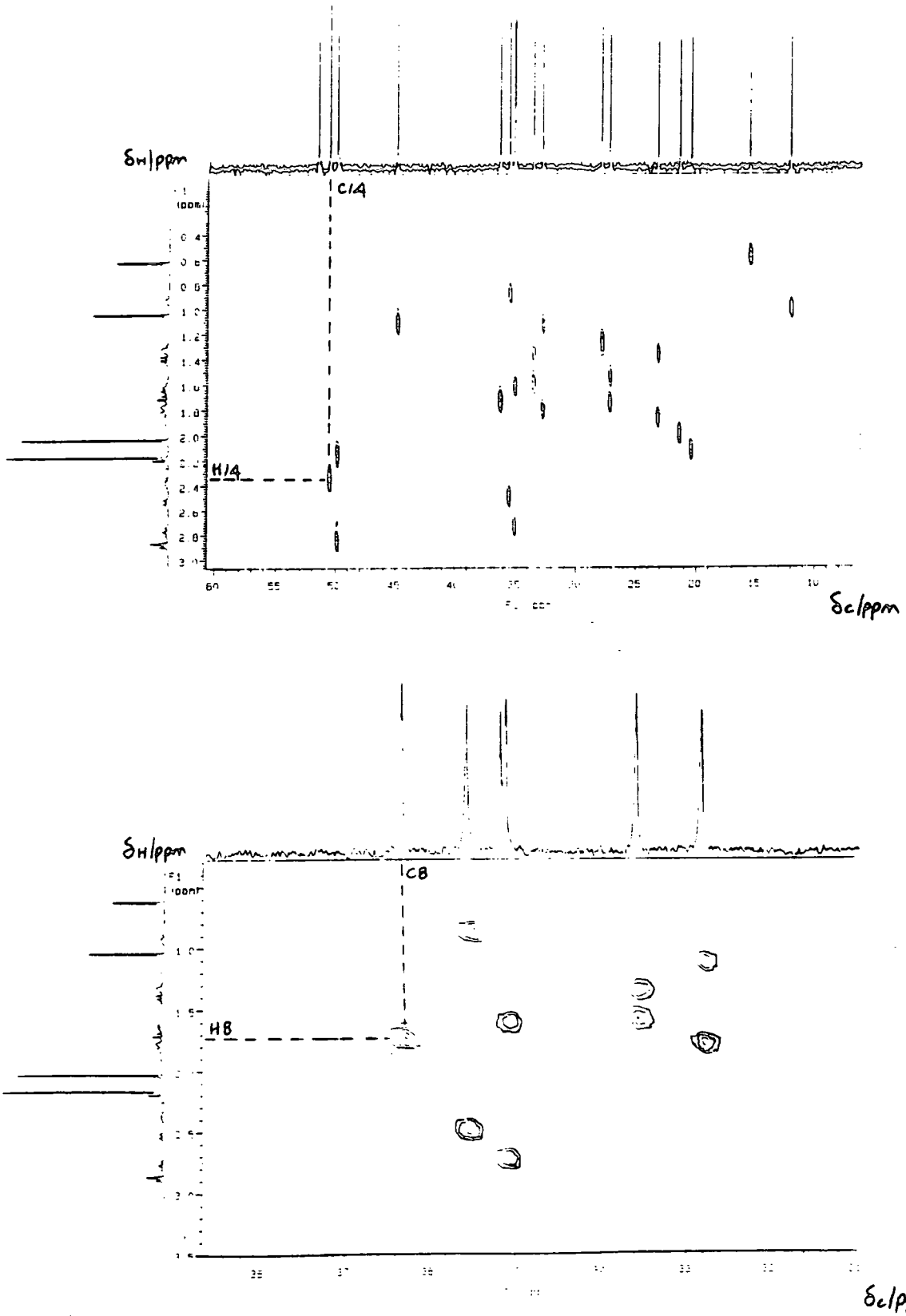

Figure 5.11 -^{13}C spectrum of Cortisone acetate.
Operating conditions were as follows : pulse width = 2.5 μs; acquisition time = 1.5 s; recycle delay = 0.5 s; no. of points = 75K ; no. of transients = 2944. The solvent is $CDCl_3$ and is marked with //.

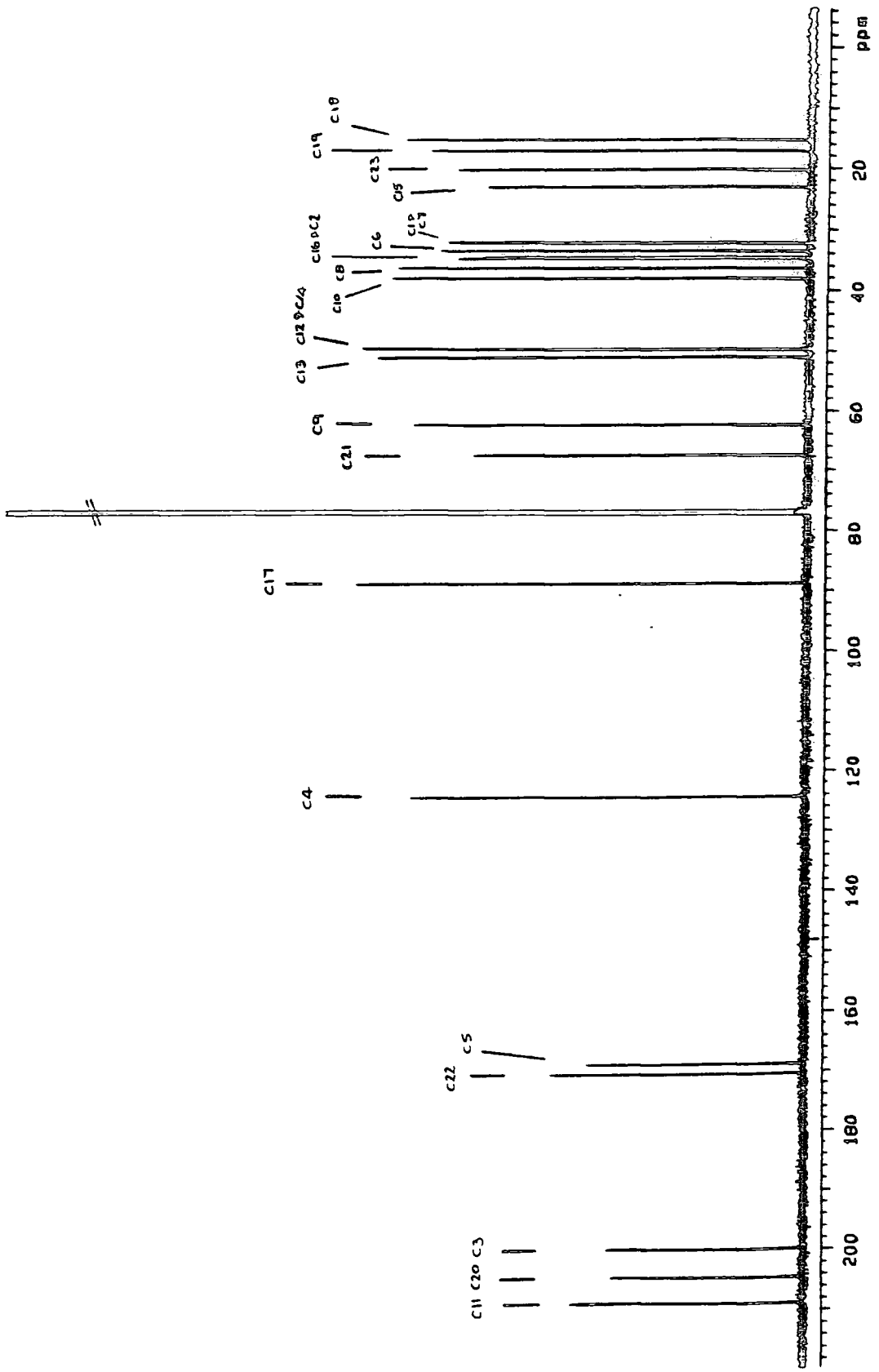

Figure 5.12 -^{13}C (proton coupled) spectrum of Cortisone acetate. Operating conditions were as follows : pulse width = 2.5 μs; acquisition time = 1.5 s; recycle delay = 0.5 s; no. of points = 75K ; no. of transients = 15424. The solvent is $CDCl_3$.

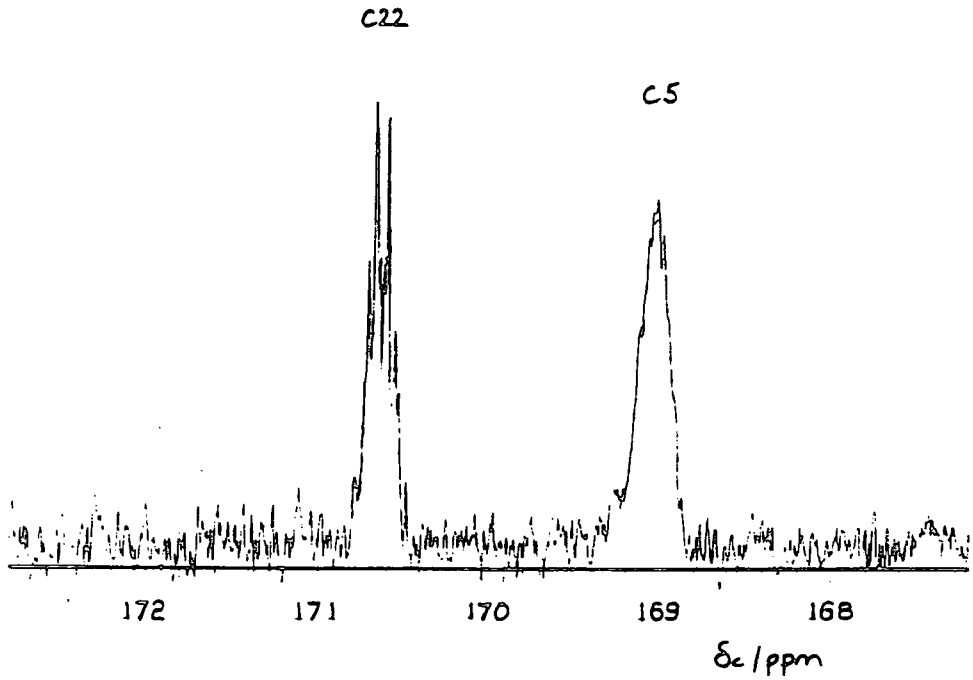

Figure 5.13 - ^{1}H spectrum of Cortisone acetate.
Operating conditions were as follows : pulse width = 10 μs; acquisition time = 4 s; recycle delay = 0 s; no. of points = 64K ; no. of transients = 128. The solvent is $CDCl_3$.

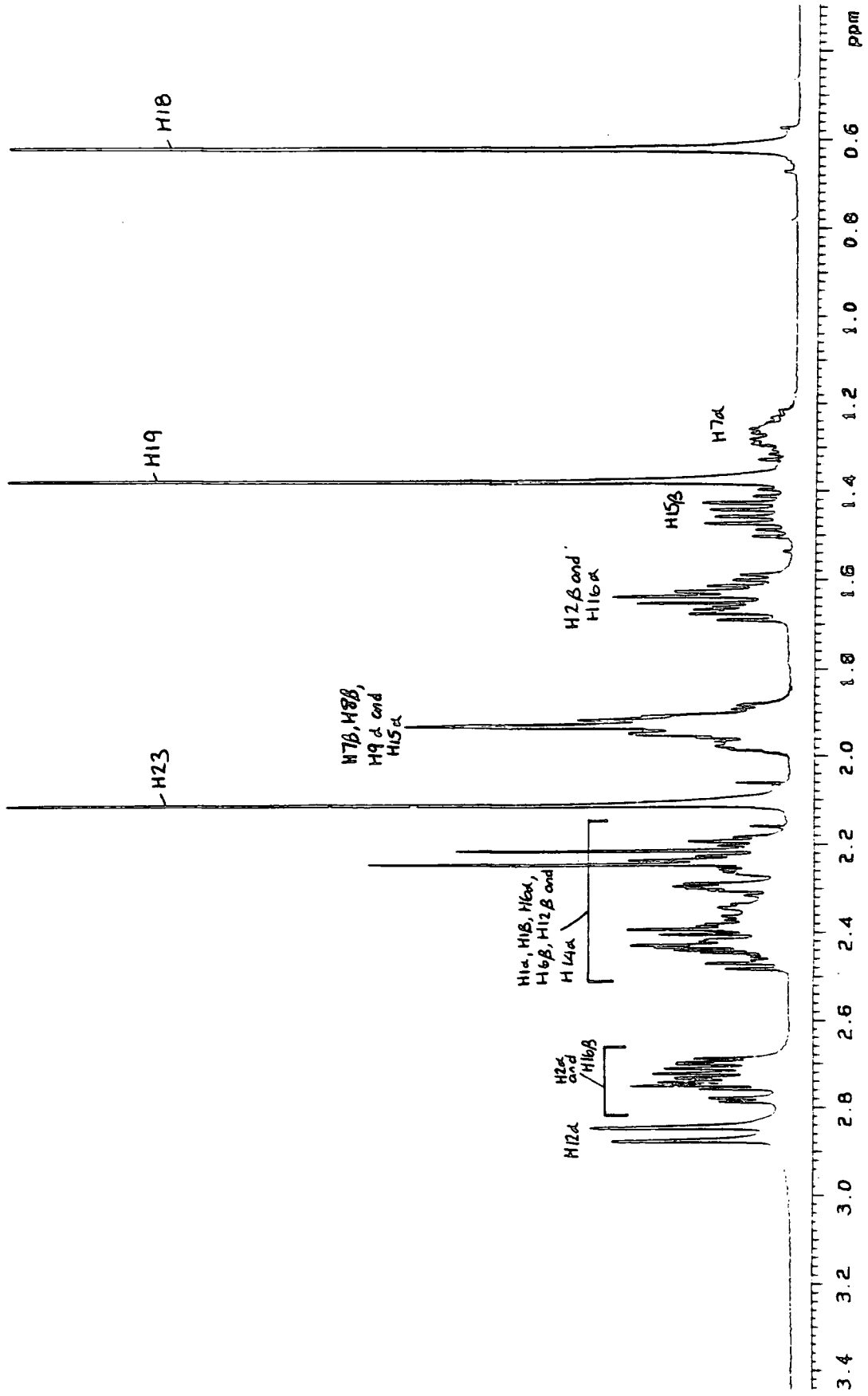

Figure 5.14 - ^{1}H COSY spectrum of Cortisone acetate.
Operating conditions were as follows : 90° pulse width = 26.0 μs; acquisition time = 0.203 s; recycle delay = 1 s; no. of points = 1K in each dimension; no. of transients = 16 for each of 419 increments. The solvent is $CDCl_3$.

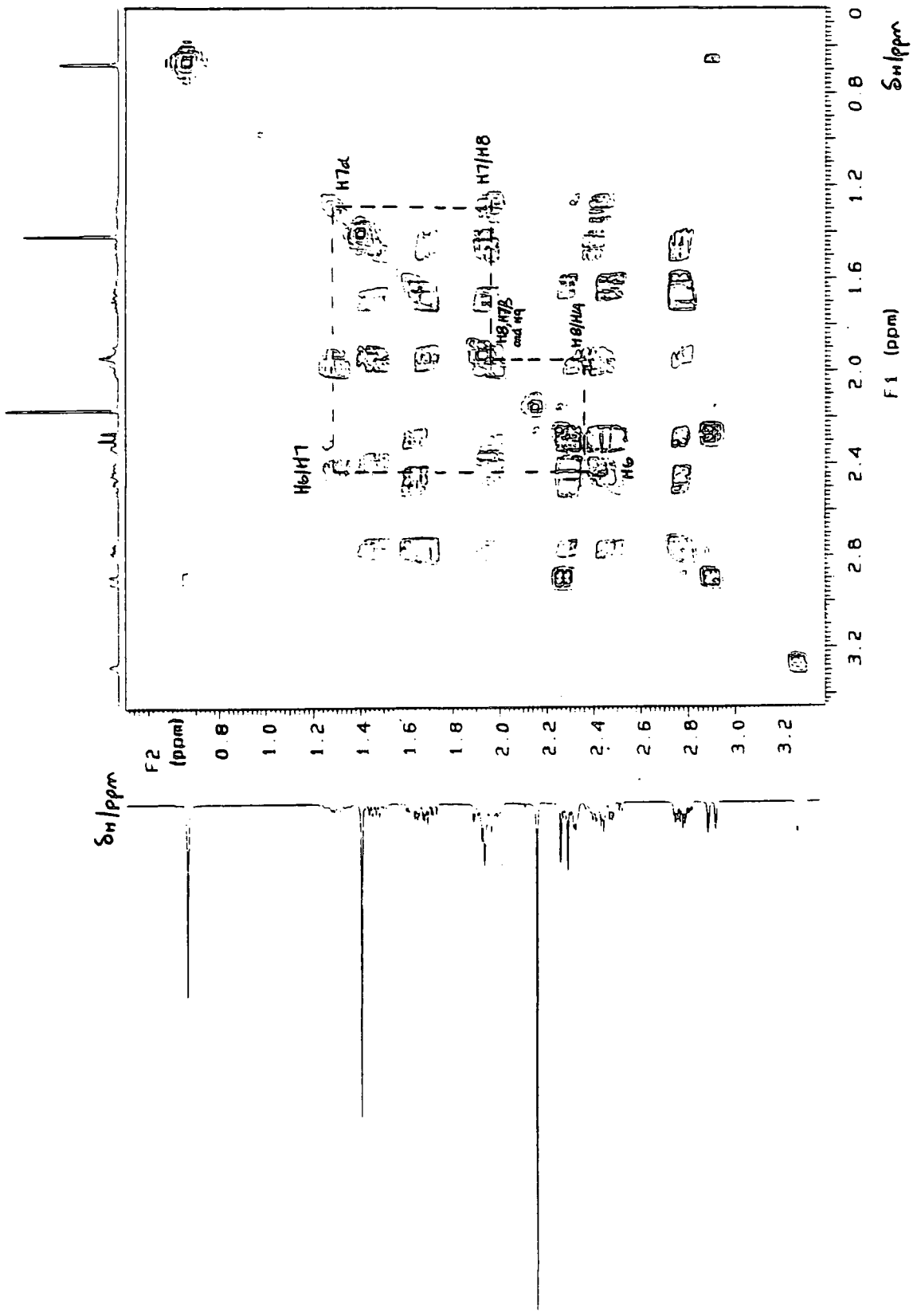

Figure 5.15 -^{13}C spectrum of Cortisone.
Operating conditions were as follows : pulse width = 2.5 μs; acquisition time = 1.5 s; recycle delay = 0.5 s; no. of points = 75K; no. of transients = 256. The solvent is DMSO and is marked with //.

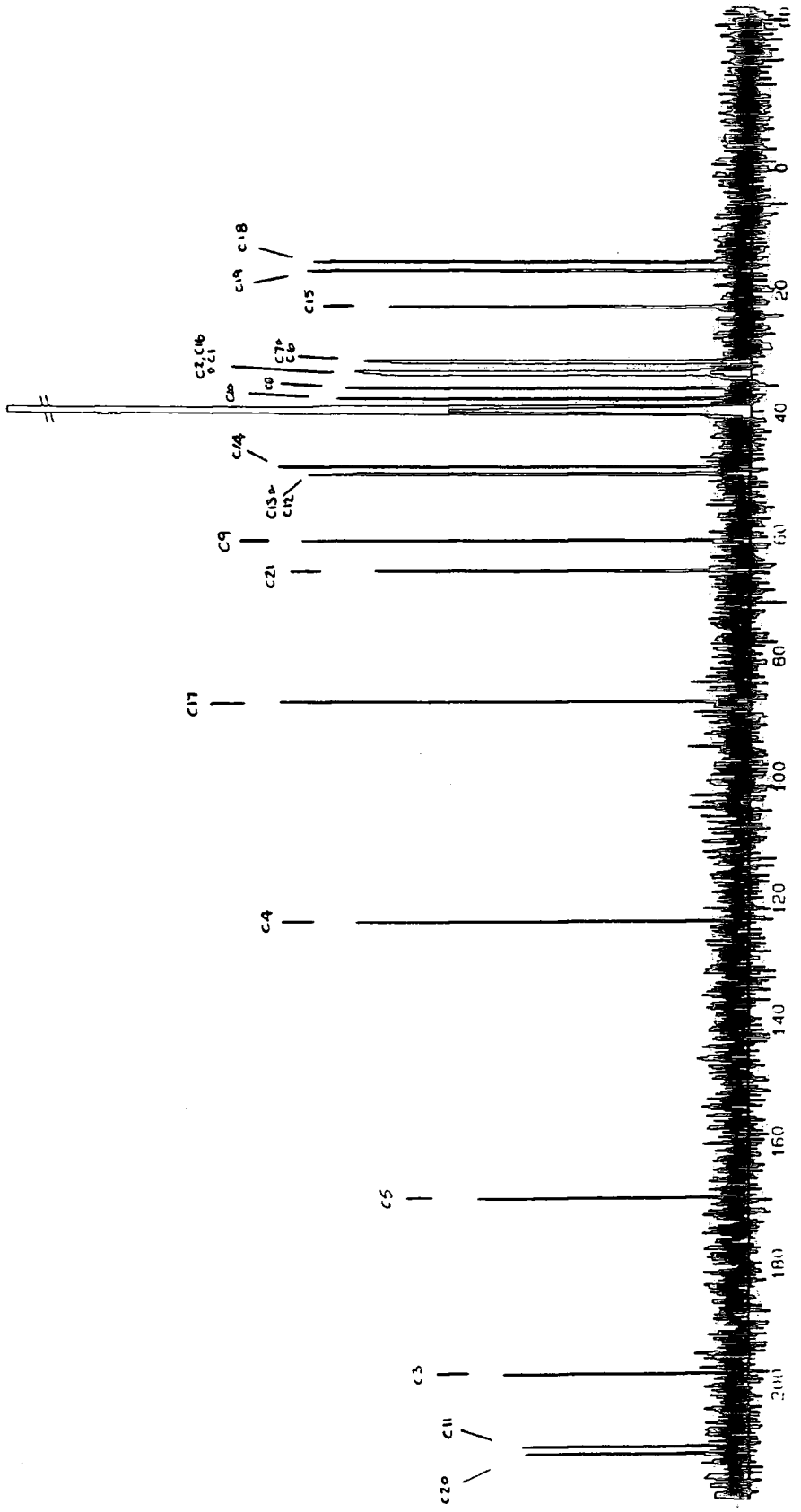

Figure 5.16 - ^{1}H spectrum of Cortisone.
Operating conditions were as follows : pulse width = 10 μs; acquisition time = 4 s; recycle delay = 0 s; no. of points = 64K; no. of transients = 272. The solvent is DMSO and is marked with //.

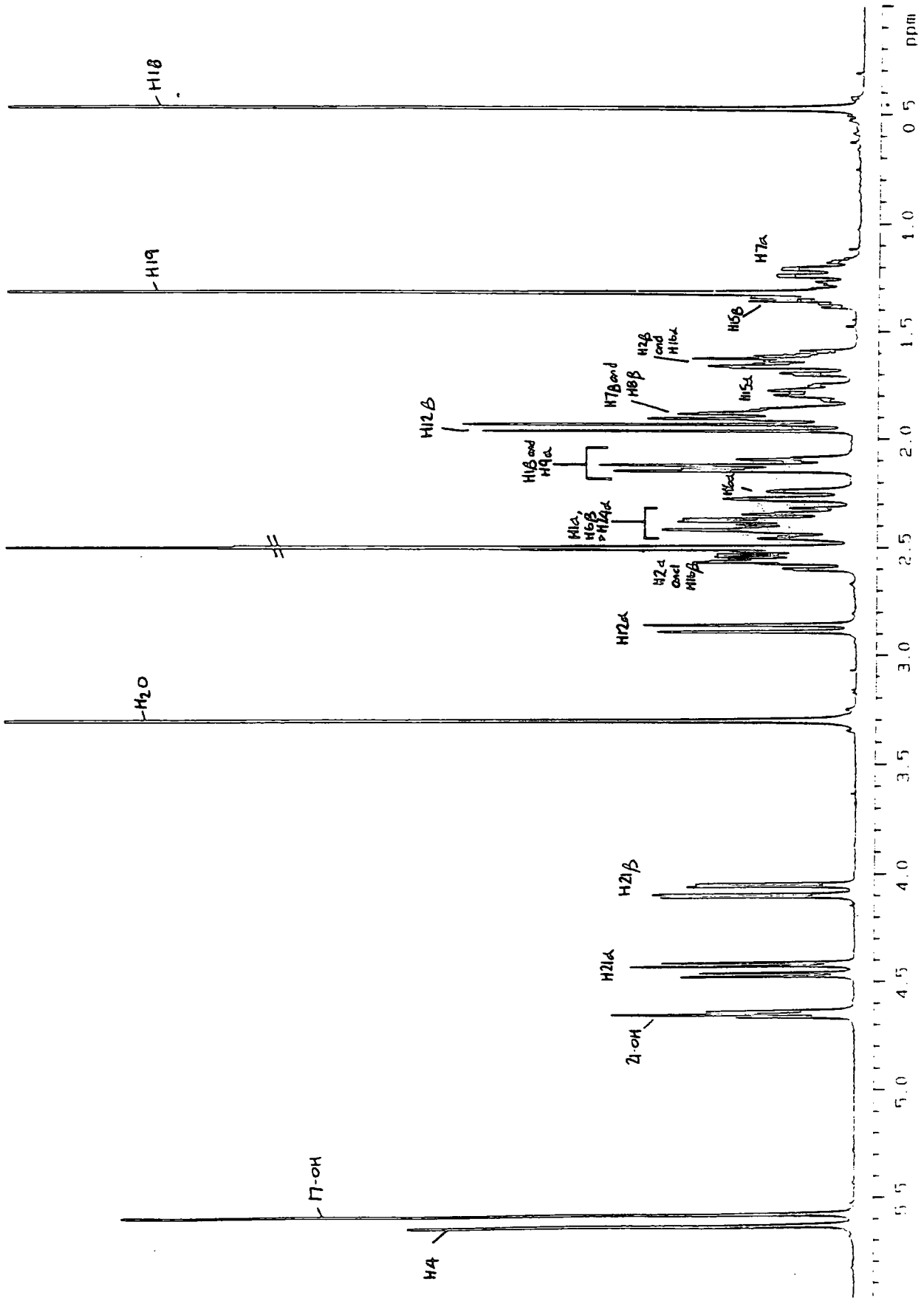

Figure 5.17 -HETCOR spectrum of Cortisone.
Operating conditions were as follows : carbon 90° pulse width = 5.3 μs; proton 90° pulse width = 19.1 μs; acquisition time = 0.084 s; recycle delay = 1 s; no. of points = 512W in each dimension; no. of transients = 120 for each of 128 increments. The solvent is DMSO and is marked with //.

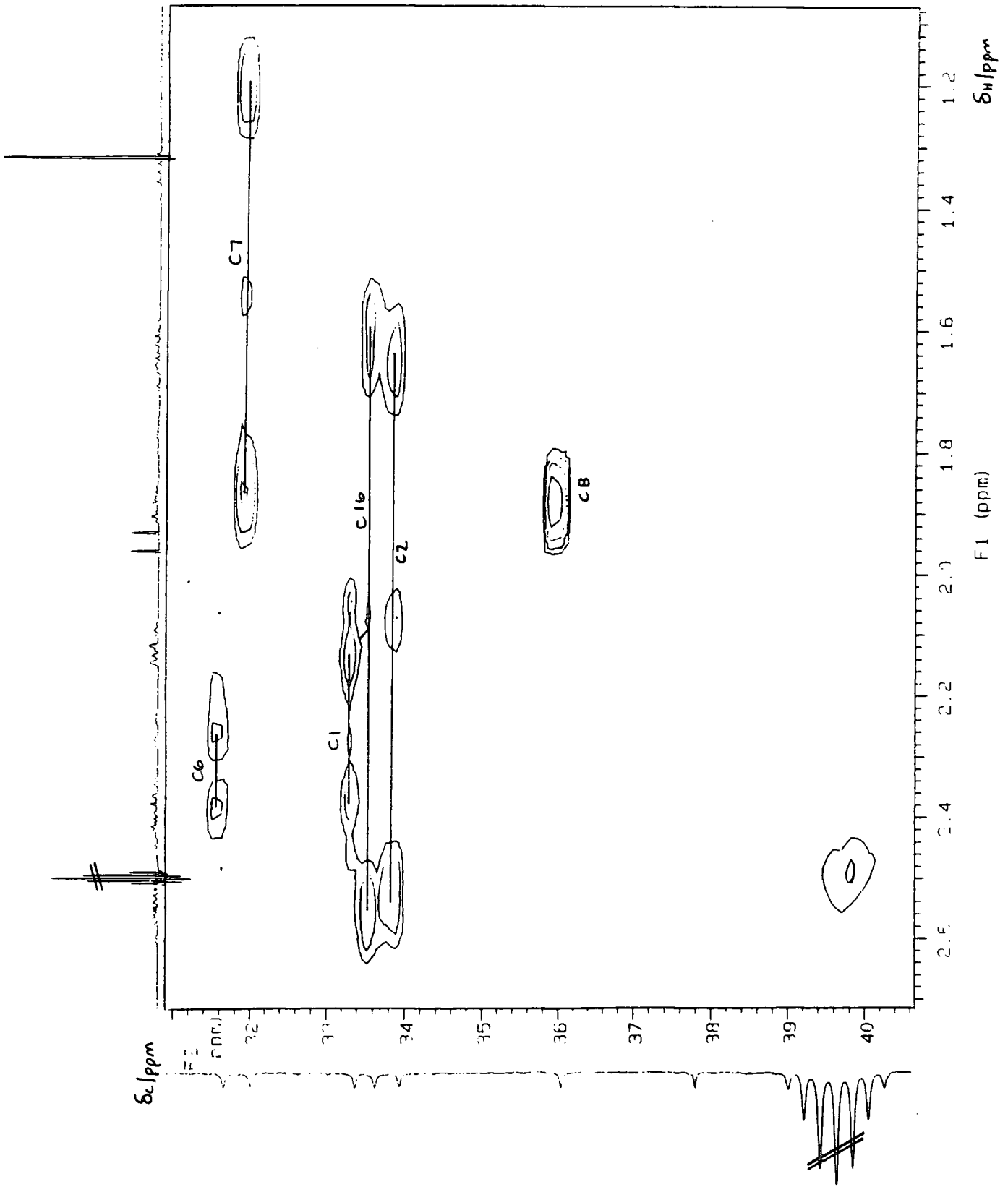

Figure 5.19 -^{13}C spectrum of Cefuroxime axetil.
Operating conditions were as follows : pulse width = 2.5 μs; acquisition time = 1.5 s; recycle delay = 0.5 s; no. of points = 75K; no. of transients = 576. The solvent is CD_3CN and is marked with //.

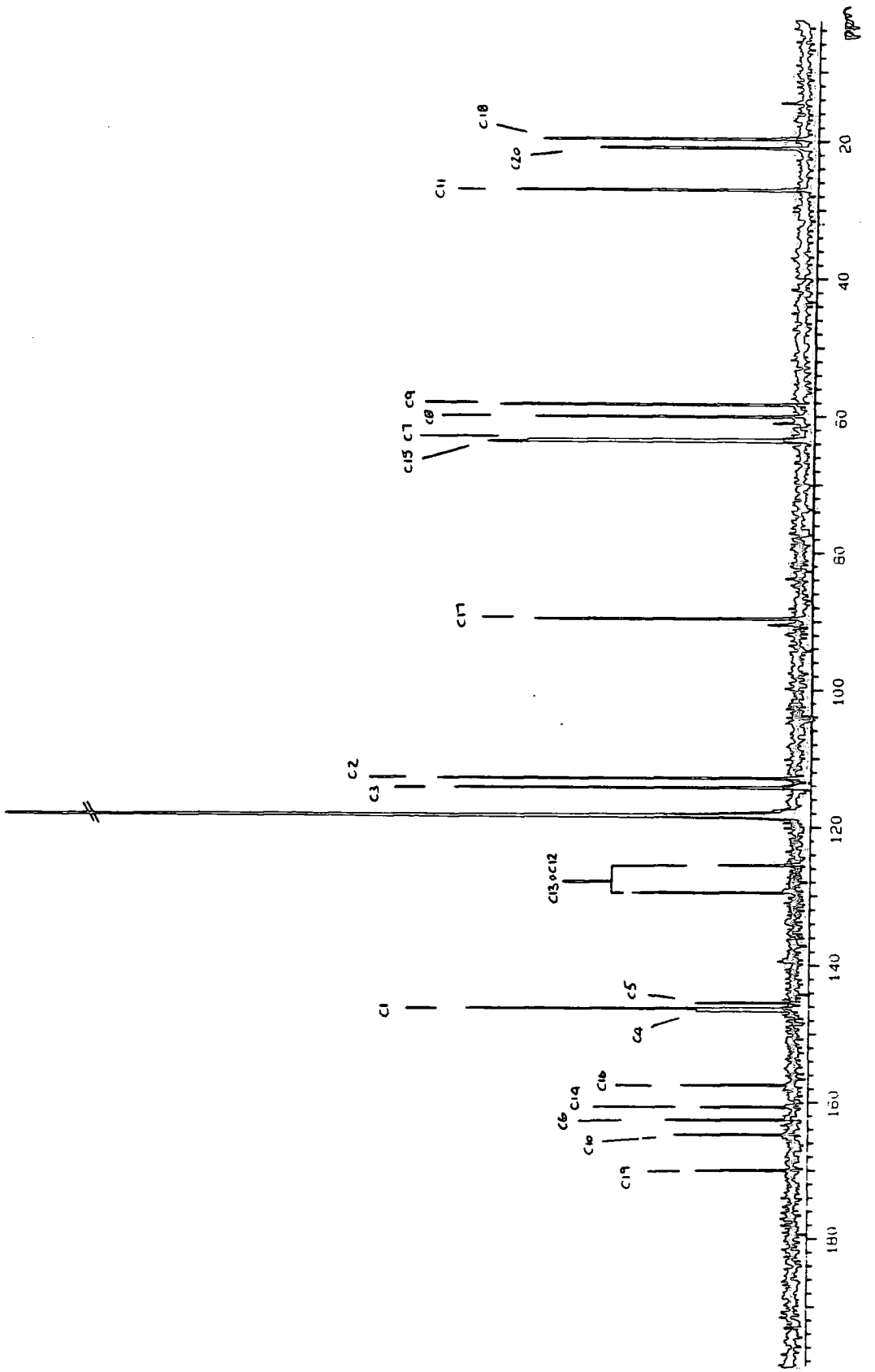

Figure 5.20 -^{1}H spectrum of Cefuroxime axetil.
Operating conditions were as follows : pulse width = 10 μs; acquisition time = 4 s; recycle delay = 0 s; no. of points = 64K; no. of transients = 48. The solvent is CD_3CN and is marked with //.

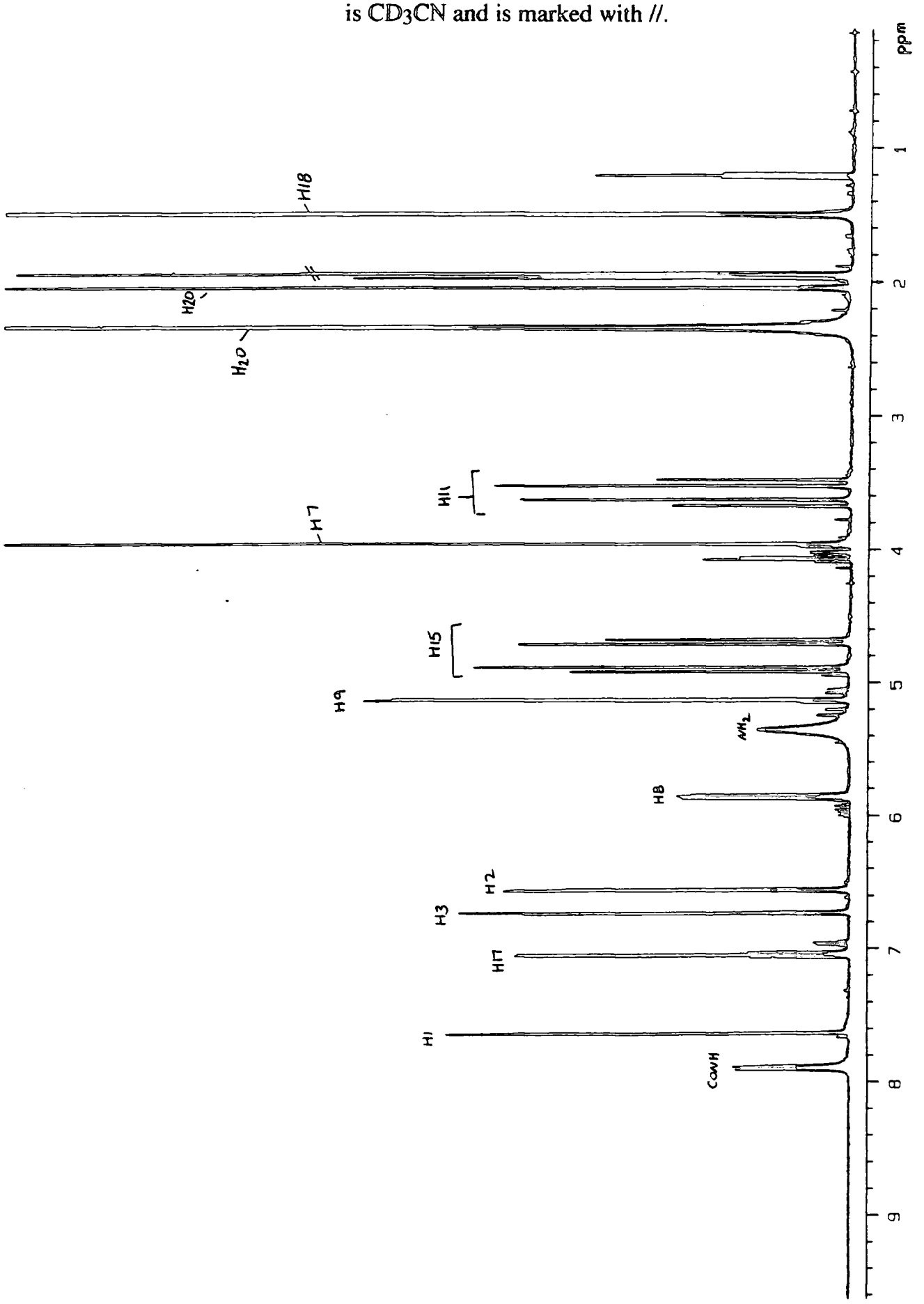

Figure 5.21 - Long range HETCOR spectrum of Cefuroxime axetil. Operating conditions were as follows : carbon 90° pulse width = 5.3 μs; proton 90° pulse width = 19.1 μs; τ = 0.05 s; acquisition time = 0.084 s; recycle delay = 1 s; no. of points = 512W in each dimension. The solvent is CD_3CN and is marked with //.

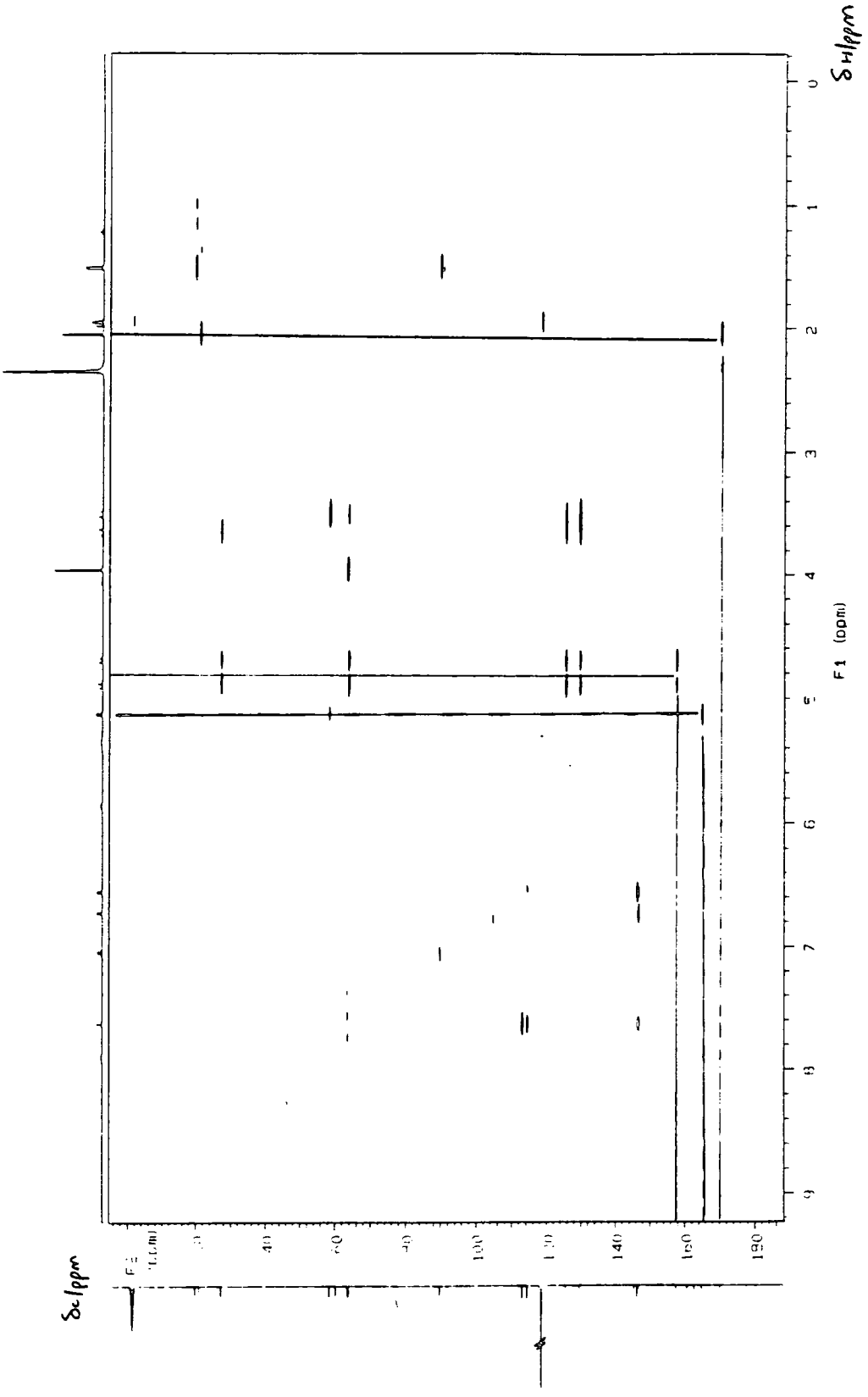

Figure 5.22 - ^{13}C solution- and solid-state spectrum of Reichsteins d-diacetate. Operating conditions for the solution state spectrum were as follows : pulse width = 2.5 μs; acquisition time = 1.5 s; recycle delay = 0.5 s; no. of points = 75K; no. of transients = 960. The solvent is $CDCl_3$ and marked with //. The operating conditions for the solid-state spectrum are as follows: 90° proton pulse =4 μs; contact time = 2 ms; dead time = 50 μs; aquisition time = 0.164 s; decycle delay =5 s; no. of transients = 11132. The spinning speed is 3025 Hz and spinning sidebands are marked with a *.

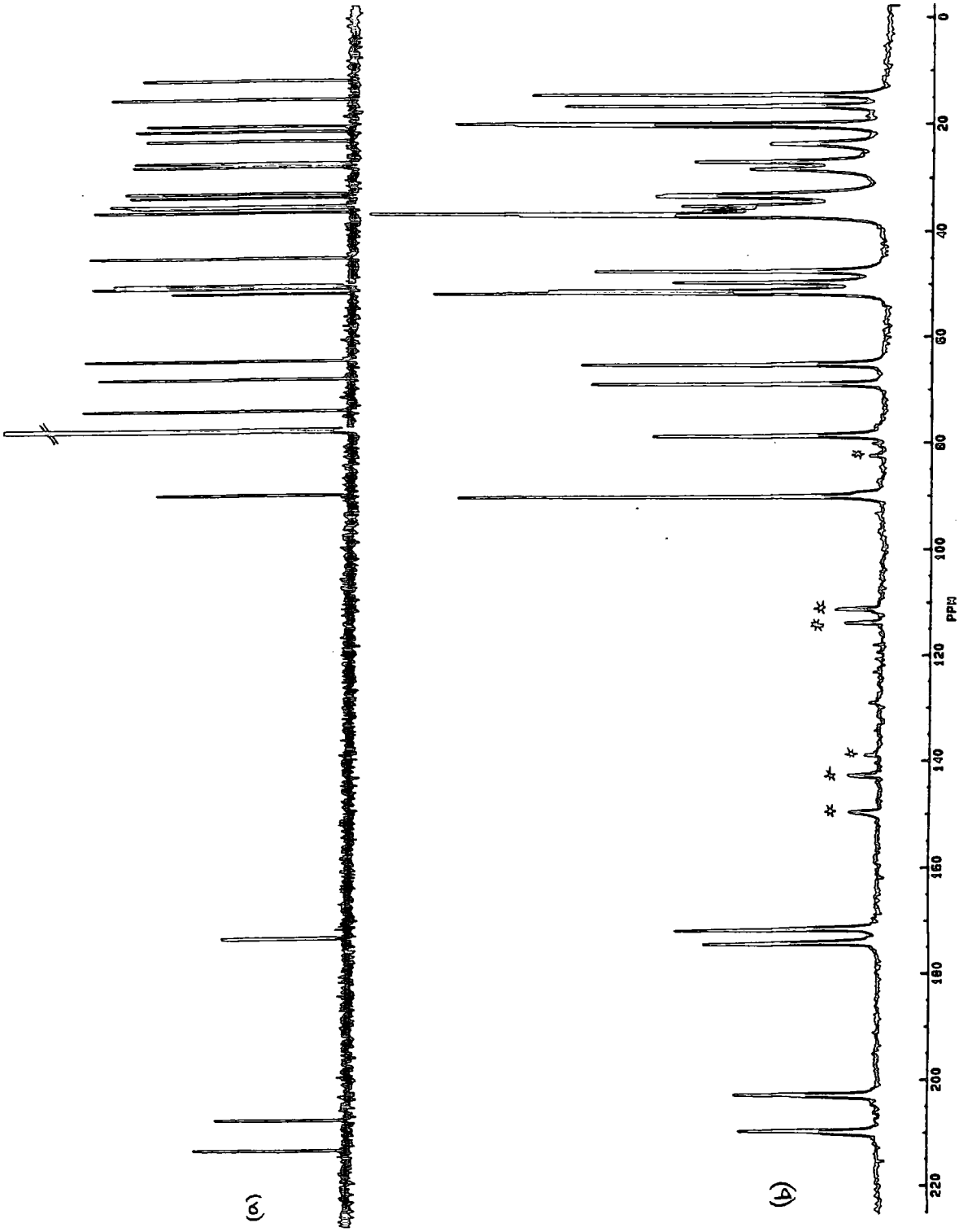

Chapter 6

Cortisone Acetate

Chapter 6 Cortisone Acetate

6.1. Introduction

The existence of polymorphs of cortisone acetate has been known for many years[1-8]. There are at least seven different crystalline forms, each of these having been studied in this work. Previously there has been some confusion over the naming of the forms, but this problem has been addressed by Harris et al[9]. The nomenclature that has been more generally adopted in recent years is that of Carless[4], and will be used here. It is unusual to find a compound with so many polymorphs (both true polymorphs and polymorphic solvates) that have had their crystal structure determined. This is the reason cortisone acetate is such a good compound to study.

6.2. Sample Characterisation

6.2.1. Crystallography

To date, the full single crystal structure determinations have been successfully performed for four forms[10-13]. Powder diffraction studies have also been made of several forms[1]. Attempts have been made during the course of this work to produce high quality single crystals of other forms for the purpose of X-ray diffraction. However, problems have been encountered with structure refinements and so the full structures remain elusive, although the unit cell dimensions and the space group have been found for form IV_{et}. These data are presented below. The known crystallographic data for all forms are summarised in table 6.1.

Table 6.1 - Crystallographic data for polymorphs of cortisone acetate

form	space group	unit cell dimensions a/Å	b/Å	c/Å	β	Z	N	sample type	reference
I	$P2_12_12_1$	8.018	12.579	20.963		4	1	single	11
II	$P2_12_12_1$	11.048	7.102	27.095		4	1	single	10
III	$P2_1$	15.68	7.52	26.58	97°	6	3	powder	1
IV_{ac}	$P2_1$	9.820	7.661	16.648	94°	2	1	single	13
IV_{et}	$P2_1$	9.842	7.578	16.391	94°	2	1	single	this work
V_{aq}	$P2_12_12_1$	7.548	9.863	30.648		4	1	single	12

Notes: Z is the number of molecules in the unit cell, whilst N is the number of molecules in the asymmetric unit. For the sample type, 'single' refers to single crystals, whilst 'powder' refers to a crystalline powdered sample. Unit cell dimensions are known to an accuracy of ±1 in the last quoted decimal place.

It was desirable to compare the conformation of the molecules in the various forms. A computer program 'SYBYL' (available at Glaxo Group Research Ltd.) that draws upon data in the Cambridge Crystallographic Database, was used to overlay the molecules matching atoms in the B and C rings.

Figure 6.1 - Showing the conformations of the cortisone acetate polymorphs. Structures are overlaid matching atoms in the B and C rings

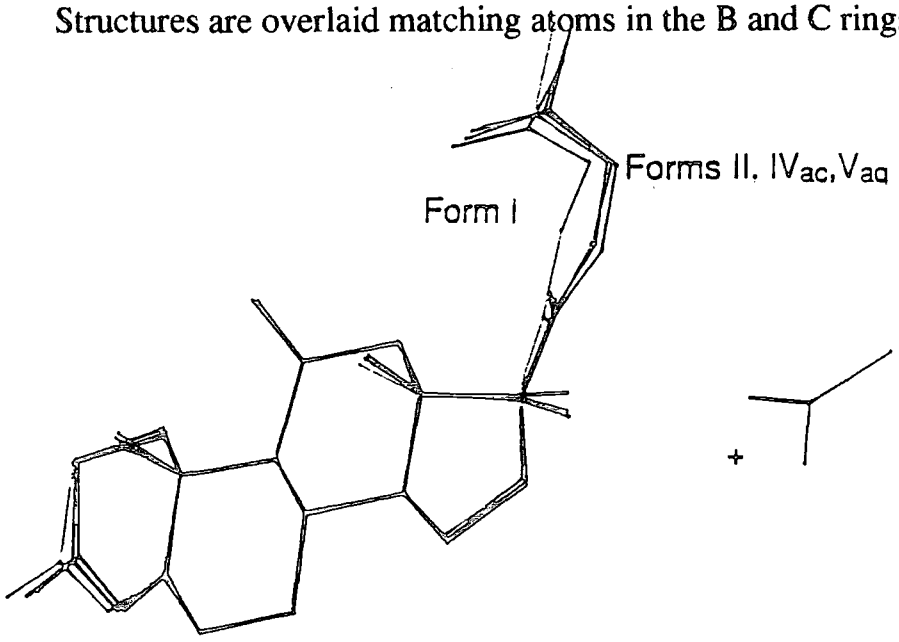

The overlaid structures match closely for forms II, IV_{aq} and V_{aq} (including the conformation of the side chain). However, form I deviates from this conformation in the A and D rings and also in the side chain conformation. Figure 6.1 shows the overlaid structures. This figure shows the limited differences between conformations.

The conformations of the rings have been described[14] as follows: the A ring has a 1α-sofa conformation and the B and C rings both have slightly distorted chair conformations. The main difference between forms I and II is in the conformation of the D rings. Form I exists as a 13β-envelope (i.e. C14, C15, C16 and C17 lie in a plane, with C13 out of the plane), whilst form II is a 13β,14α-half chair (i.e. C15, C16 and C17 lie in a plane, with C13 and C14 out of the plane). These conformations are shown in figure 6.2.

Figure 6.2 - Showing the ring conformations

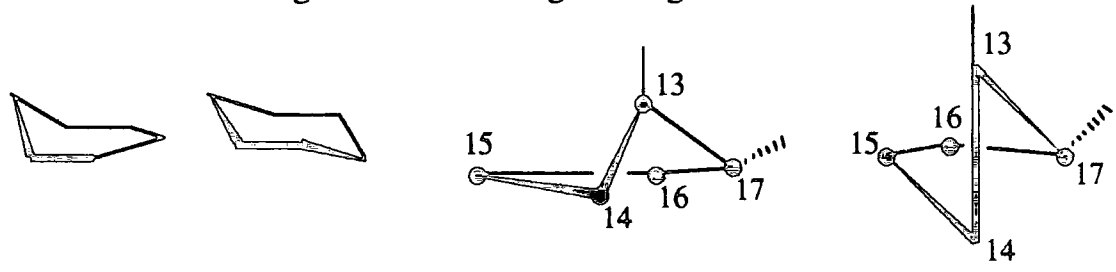

1α-sofa distorted chair 13β-envelope (4 atoms in a plane) 13β-14a-half chair (3 atoms in a plane)

6.2.2. Infra-Red Spectroscopy

X-ray crystallography, particularly that on single crystals, is not a quick and simple technique that can be used routinely to identify samples. Other techniques have been used in order to accomplish this. Infra-red (IR) spectroscopy is one such technique, each polymorph giving a characteristic spectrum[1-4]. Particularly useful for identifying the form present in a sample is the carbonyl region (1550 - 1800 cm^{-1}). The carbonyl region of the IR spectra of cortisone acetate polymorphs as nujol mulls are presented in figure 6.3. These reference spectra have been used to identify quickly the content of the sample. However, there is one significant disadvantage of this technique, and that is that

Figure 6.3 - The infra-red spectra of cortisone acetate polymorphs recorded as nujol mulls (at 2 cm^{-1} resolution)

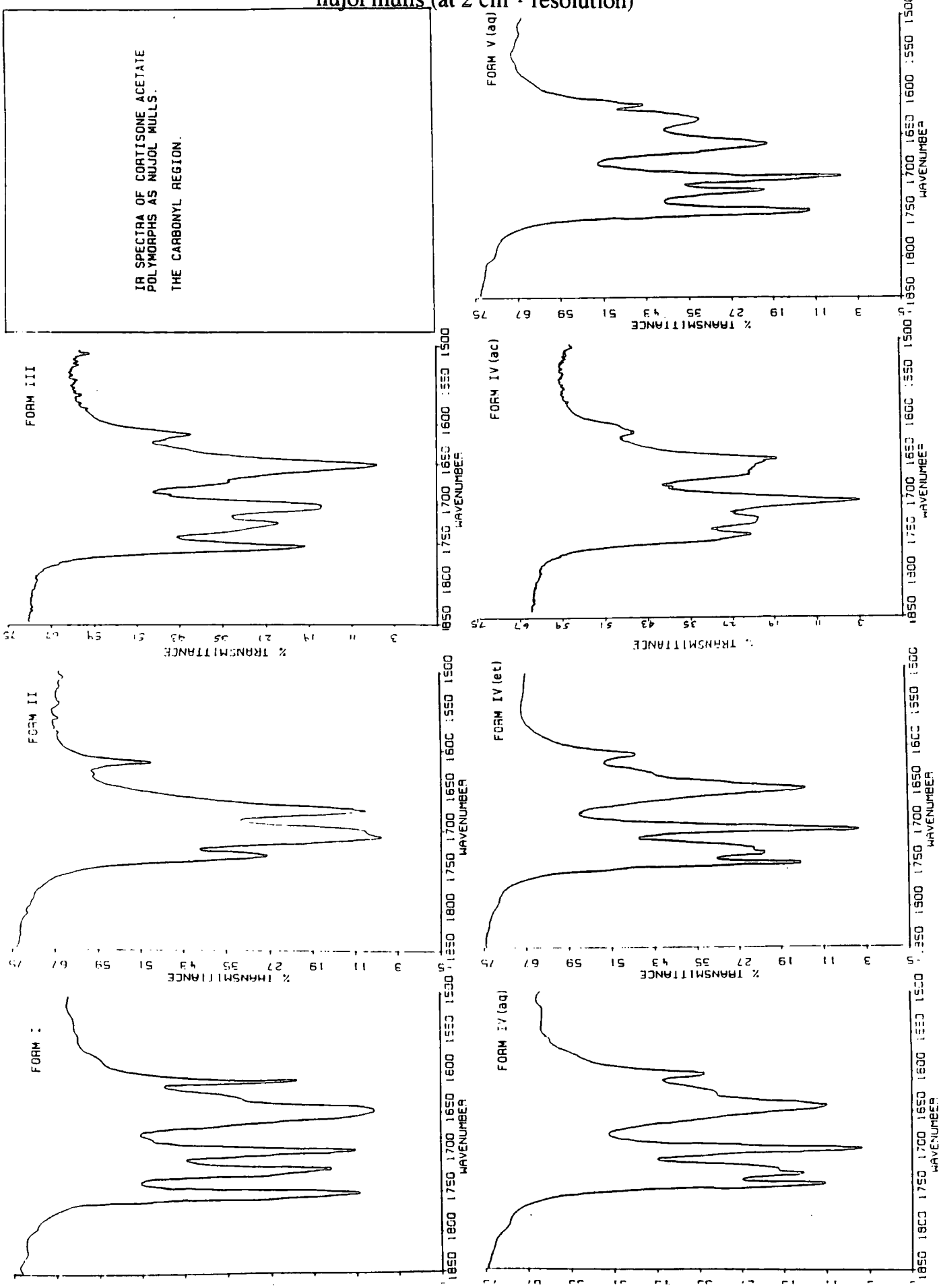

small amounts (<10%) of impurities of other polymorphs are not readily detectable and even moderate amounts (20-30%) may not be identifiable. Quantification of the relative proportions of polymorphs in a mixture is theoretically possible, but in practical terms is very difficult. Other possible problems may arise if the polymorphs undergo phase transformations when ground, although this is not generally a problem with cortisone acetate polymorphs.

6.2.3. Differential Scanning Calorimetry

Differential scanning calorimetry (DSC) has also been used to characterise samples, particularly those that contain solvate molecules. Table 6.2 summarises the DSC data for cortisone acetate polymorphs.

Table 6.2 - The temperatures (in °C) of endotherms in the DSC data of cortisone acetate polymorphs

form	low temperature	melting point	literature[1] values / °C
I	-	246	251-253
II (ex $CHCl_3$)	-	237	241-246
II (ex EtOAc)‡	-	242	
II (ex C_6H_6)	-	234-235	
III	-	241-246	241-245
IV_{et}	111-115	240-244	111-116 and 245-247
V_{aq}	99	238	105-110 and 238-242

‡ EtOAc represents ethyl acetate. Form II may be prepared by recrystallising from any of the three solvents stated above. The melting points are rather different in each case, the reason being unclear.

6.2.4. Karl-Fischer Analysis

Samples have also been studied by Karl-Fischer analysis to find the water content of the samples. The results are presented in table 6.3.

Table 6.3 - Results of Karl-Fischer analysis for percentage water (by weight)

form	% water	no. of samples
IV_{aq}	7.5	3
IV_{et}	3.2	1
V_{aq}	4.4	1

Note that DSC and Karl-Fischer analysis experiments were performed by technical personnel at Glaxo Group Research.

If the ratio of cortisone acetate to water is 1:1, then the sample would contain 4.5% water by weight. Therefore form IV_{aq} seems to contain 1.7 molecules of water per cortisone acetate molecule whilst IV_{et} contains less than 1 molecule of water per cortisone acetate molecule. Form V_{aq} contains almost equimolar proportions of water and cortisone acetate.

The significant amount of water present in the sample of form IV_{et} is rather surprising as this form is not hydrated. However, this form is known to undergo loss of ethanol quite readily, water being attracted in its place so that form IV_{aq} is produced. Therefore the water content of samples is very variable.

6.2.5. Solution-State Proton NMR

Samples have also been studied by quantitative solution-state proton NMR, to estimate the solvate content. The samples are dissolved in 99% $CDCl_3$ (with TMS) and spectra recorded using a recycle delay of 2 s (to allow complete relaxation to occur). The peak integrals are then proportional to the number of nuclei giving rise to that resonance. As chloroform attracts a small amount of water, the amount of water present in the solvent is found by studying a sample of the solvent only (referred to here as a 'blank' sample). In the case of hydrated forms of cortisone acetate, when the water content is being estimated, account must be taken of the water arising from purely from the solvent. Also the number of equivalent nuclei in the molecule giving rise to that resonance must be accounted for. Thus to estimate the solvate content of samples one must compare the peak integrals per molecule of the resonance in question. An example calculation is given in table 6.4. The results for all forms are summarised in table 6.5.

Table 6.4 - Example of the estimation of water content of cortisone acetate form I by ^1H NMR in solution

	blank			I		
	$CHCl_3$	H_2O	CA	$CHCl_3$	H_2O	CA
peak integral	30	40	154	35	50	220
number of protons	1	2	3	1	2	3
integral / number of protons	30	20	51	35	25	73
ratio of water to chloroform in blank solvent		0.66:1				
predicted amount of water in solution (arising from solvent)				0.66 x 35 =		23
water arising from sample				25 - 23 =		2
cortisone acetate : H_2O ratio				73 / 2 =		37:1

Table 6.5 - Water (and ethanol) content of samples of cortisone acetate by ^1H NMR in solution

form	CA : H_2O	CA : ethanol
I	37:1	
I and II (mixture)	11:1	
I and III (mixture)	11:1	
II (micronised)	11:1	
II (ex C_6H_6)	4:1	
II (ex EtOAc)	9:1	
II and III (mixture)	10:1	
IV_{aq}	1:1	
IV_{et}	1:1	3:1
V_{aq}	0.7:1	

The peak integrals show that the anhydrous forms (I, II and III) contain little water. As the amount of absorbed water in the solution will change with time, there will be inaccuracy in finding the exact water content. Therefore, it is likely that the water present has been absorbed from the air. The hydrated forms IV_{aq} and V_{aq} show approximately equimolar proportions of cortisone acetate and water. Somewhat surprising is that form IV_{et} contains so much water, and relatively little ethanol. However, as discussed above, this form is known to be rather unstable, losing ethanol and transforming to form IV_{aq}.

6.3. Solid-State ^{13}C NMR

6.3.1. Acquisition of Spectra

Solid-state NMR spectra of seven polymorphs of cortisone acetate have been recorded with the cross-polarisation and magic angle spinning (CPMAS) technique as described in chapters 3 and 4. The non-quaternary suppression (NQS) experiment has also been performed in order to aid the assignment of spectra. Single pulse and variable contact time experiments have also been performed on certain samples where appropriate. The solid-state NMR spectra have been acquired using standard conditions of a 3 or 5 s recycle delay (longer delays were found not to affect peak intensities) and a 2 ms contact time (found to be the optimum from variable contact experiments). The CPMAS spectra are presented in figures 6.4 - 6.10. The differences between the spectra mean that samples can easily be identified. The high-frequency region is particularly useful in this respect. Figure 6.11 shows an expansion of the high-frequency region of the spectra of all seven forms. Solid-state NMR is a particularly useful technique for identifying small amounts of impurities of other forms in the sample. An estimate can also be made of the percentage of impurity present. Even small amounts (about 2%) can be identified. Also transformations of one form into another can be monitored. An example of the transformation of form IV_{aq} into form III is given in figure 6.12. The peak arising from form IV_{aq} is marked with a # sign.

Figure 6.4 - The solid-state ^{13}C NMR spectrum of cortisone acetate form I. Spinning sidebands are marked with an asterisk.

operating conditions	^{1}H 90° pulse	contact time	acquisition time	recycle delay	number of transients	spin rate
50 MHz	4 μs	2 ms	0.16 s	3 s	3000	3.0 kHz

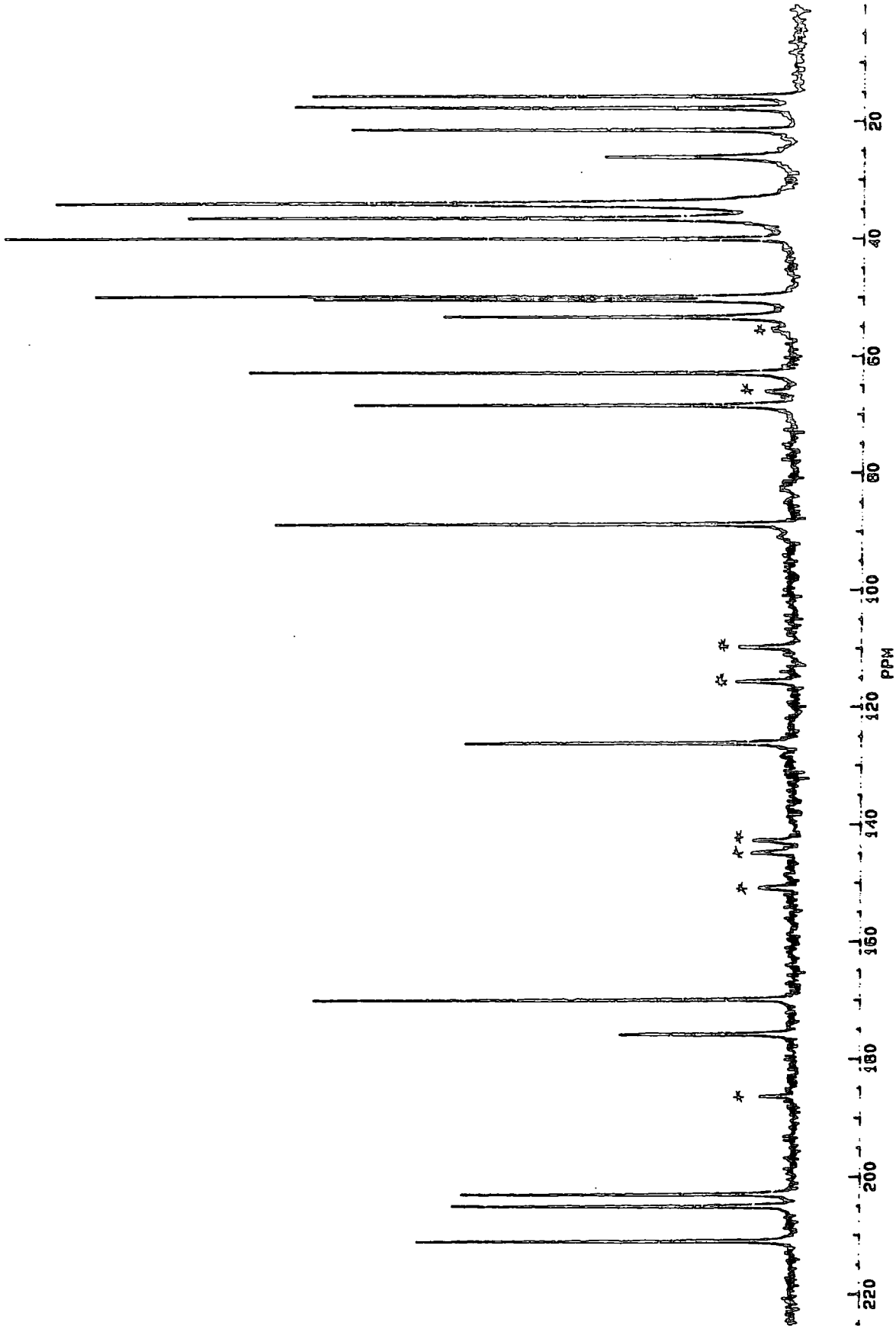

Figure 6.5 - The solid-state ^{13}C NMR spectrum of cortisone acetate form II. Spinning sidebands are marked with an asterisk.

operating conditions	^{1}H 90° pulse	contact time	acquisition time	recycle delay	number of transients	spin rate
50 MHz	4 μs	2 ms	0.16 s	5 s	11051	3.1 kHz

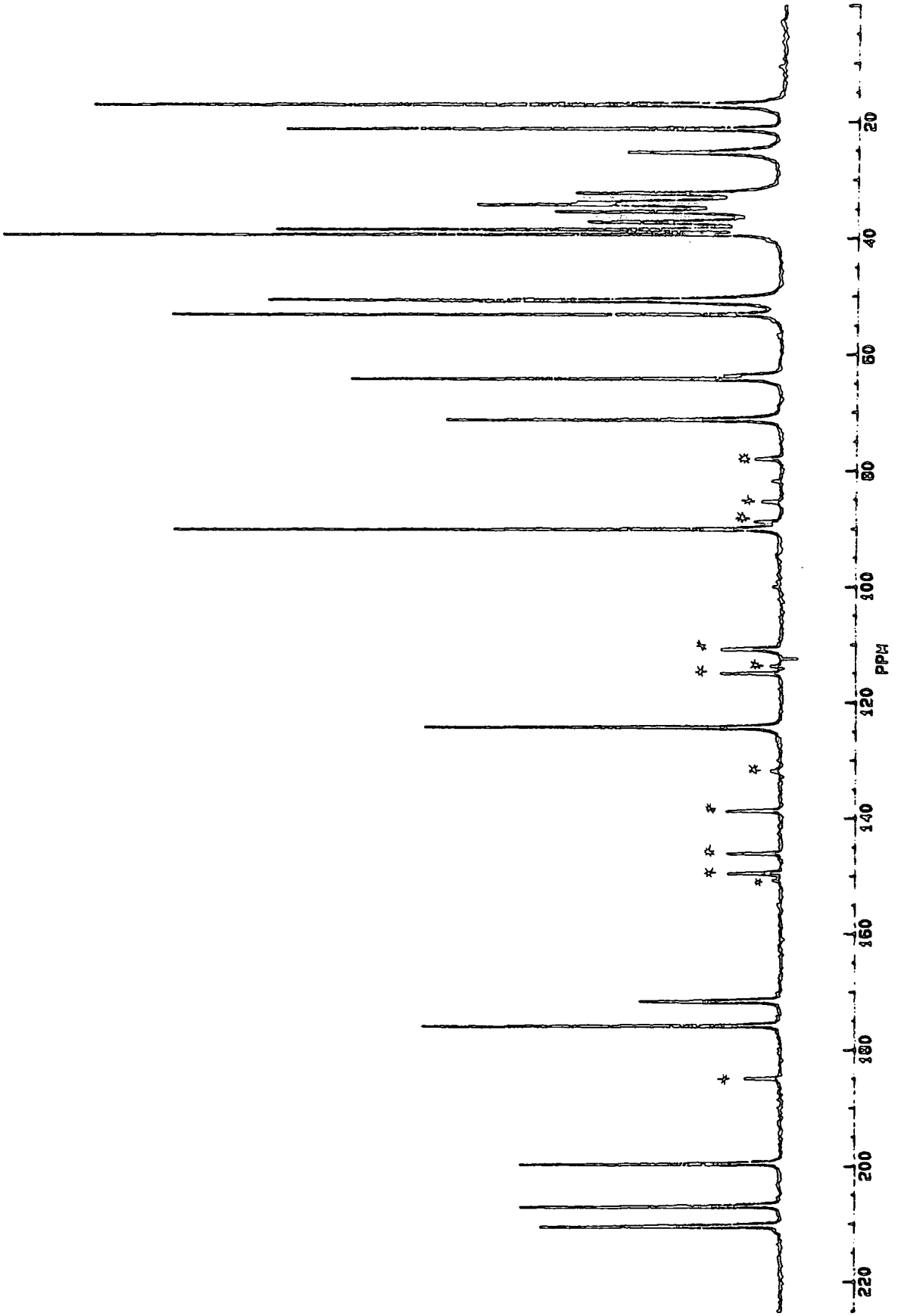

Figure 6.6 - The solid-state ^{13}C NMR spectrum of cortisone acetate form III. Spinning sidebands are marked with an asterisk.

operating conditions	^{1}H 90° pulse	contact time	acquisition time	recycle delay	number of transients	spin rate
50 MHz	4 μs	2 ms	0.16 s	5 s	18550	3.0 kHz

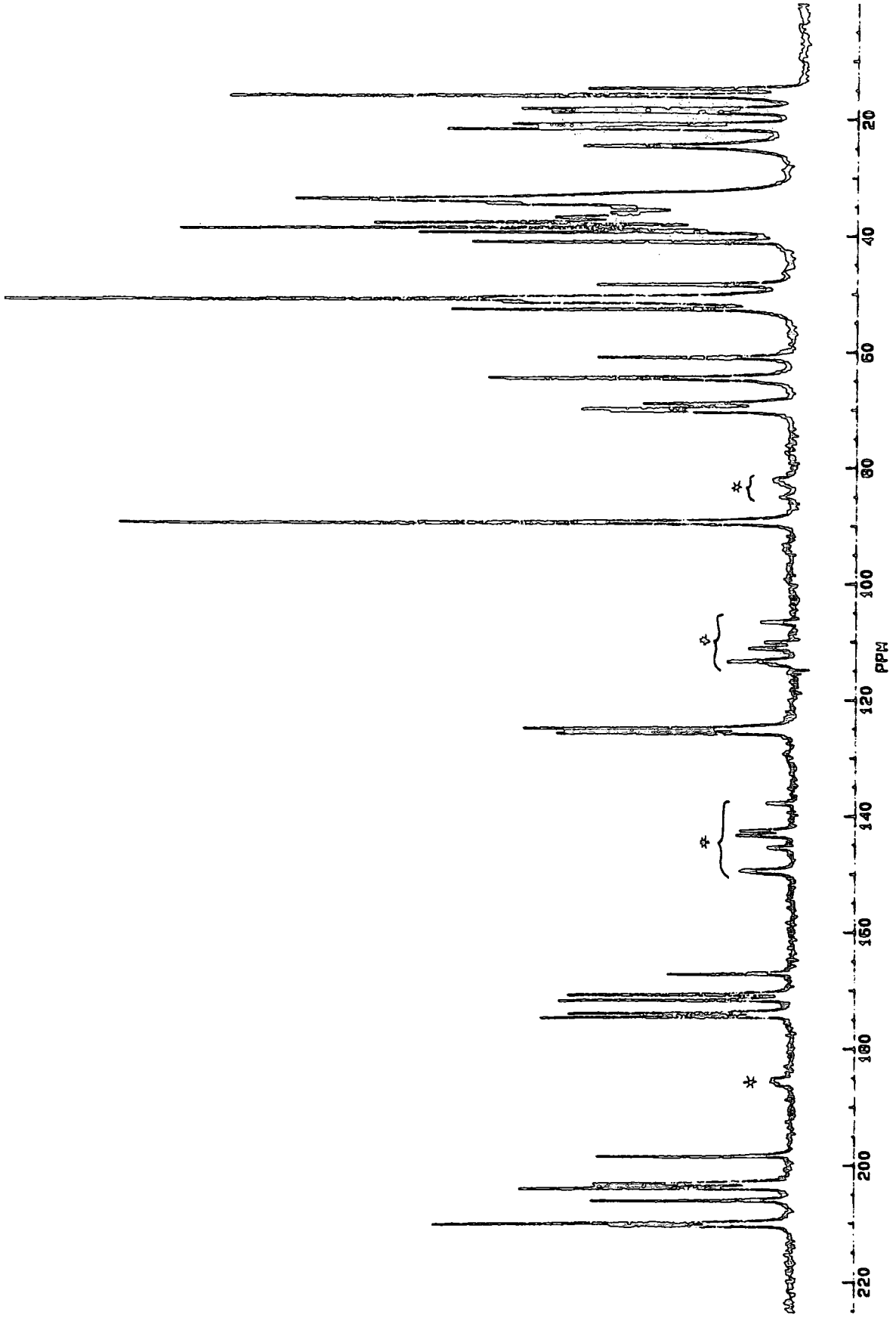

Figure 6.7 - The solid-state ^{13}C NMR spectrum of cortisone acetate form IV_{aq}. Spinning sidebands are marked with an asterisk.

operating conditions	^{1}H 90° pulse	contact time	acquisition time	recycle delay	number of transients	spin rate
50 MHz	4 μs	2 ms	0.16 s	5 s	3620	3.0 kHz

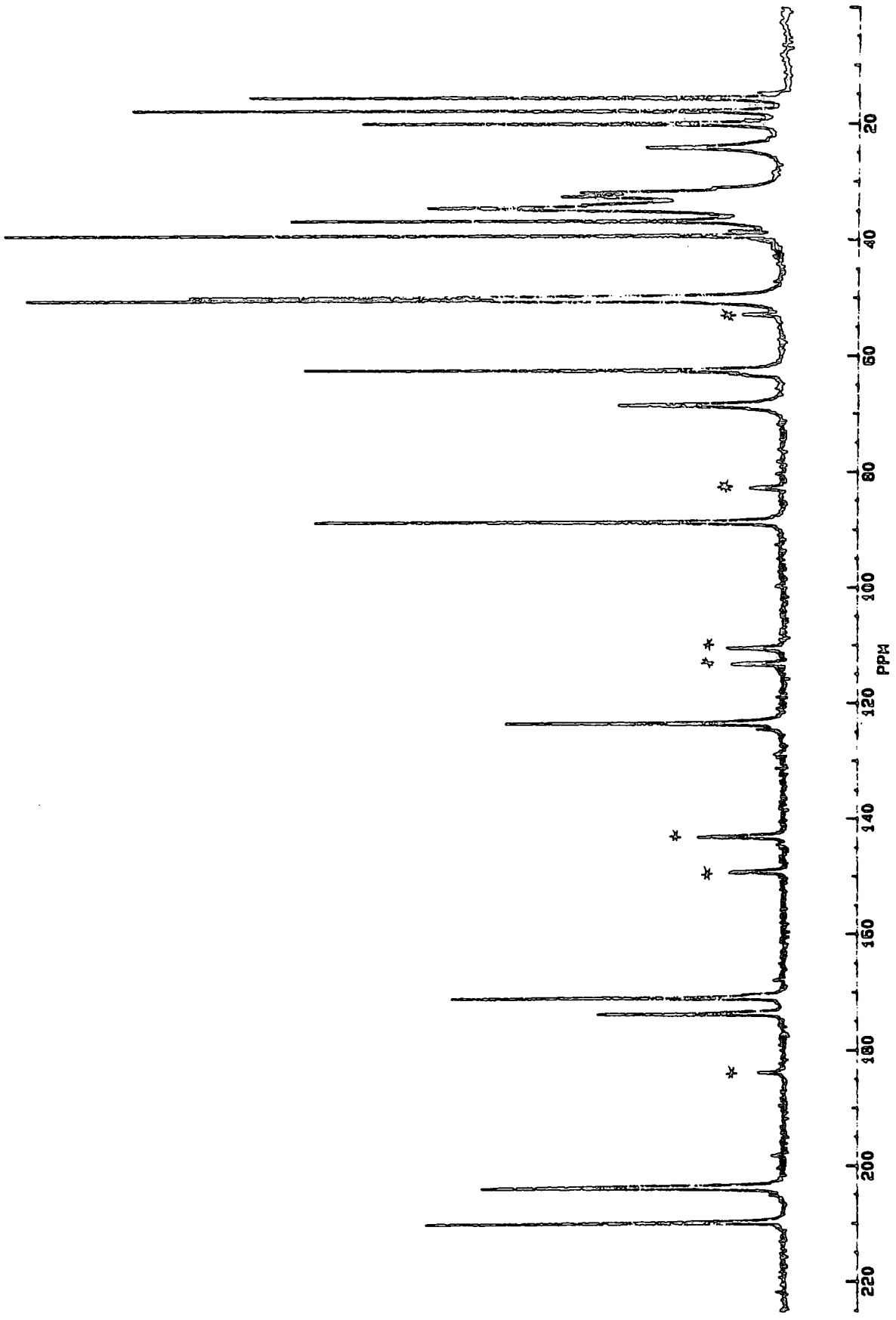

Figure 6.8 - The solid-state ^{13}C NMR spectrum of cortisone acetate form IV_{et}. Spinning sidebands are marked with an asterisk.

operating conditions	^{1}H 90° pulse	contact time	acquisition time	recycle delay	number of transients	spin rate
50 MHz	4 µs	2 ms	0.16 s	3 s	5900	3.0 kHz

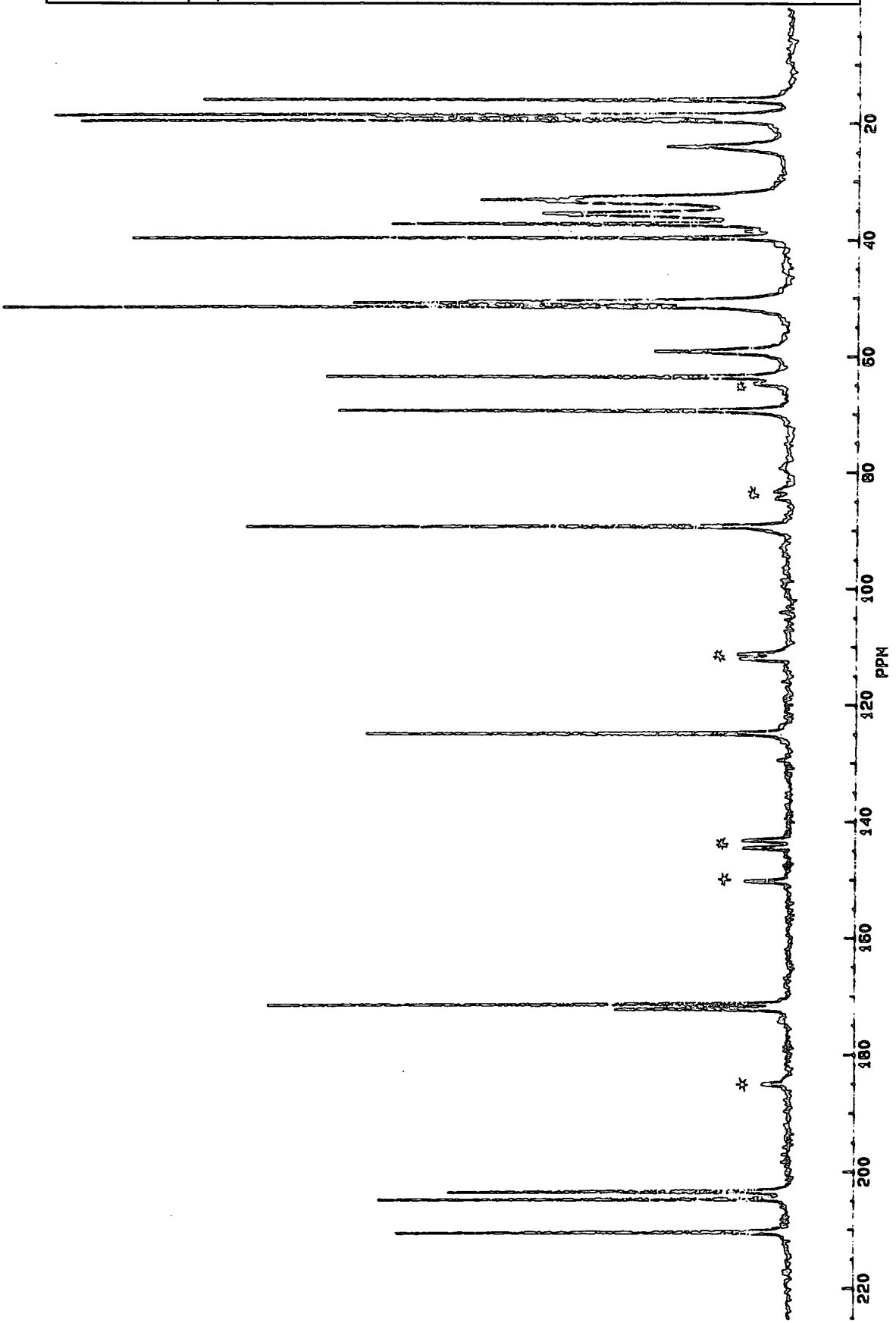

Figure 6.9 - The solid-state ^{13}C NMR spectrum of cortisone acetate form IV_{ac}. Spinning sidebands are marked with an asterisk.

operating conditions	^{1}H 90° pulse	contact time	acquisition time	recycle delay	number of transients	spin rate
50 MHz	4 μs	2 ms	0.16 s	3 s	5500	3.2 kHz

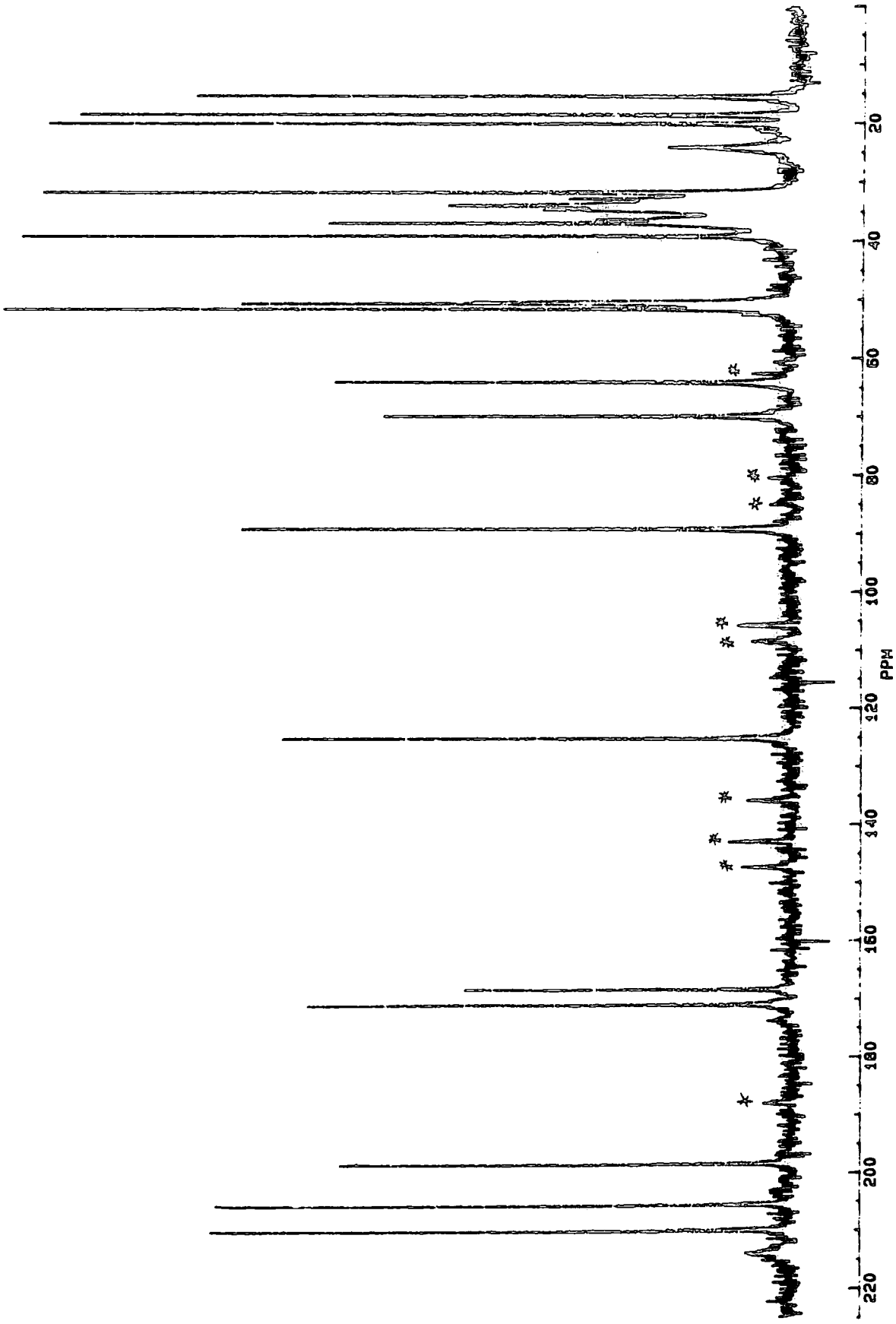

Figure 6.10 - The solid-state ^{13}C NMR spectrum of cortisone acetate form V_{aq}. Spinning sidebands are marked with an asterisk.

operating conditions	^{1}H 90° pulse	contact time	acquisition time	recycle delay	number of transients	spin rate
50 MHz	4 µs	2 ms	0.16 s	3 s	2200	3.0 kHz

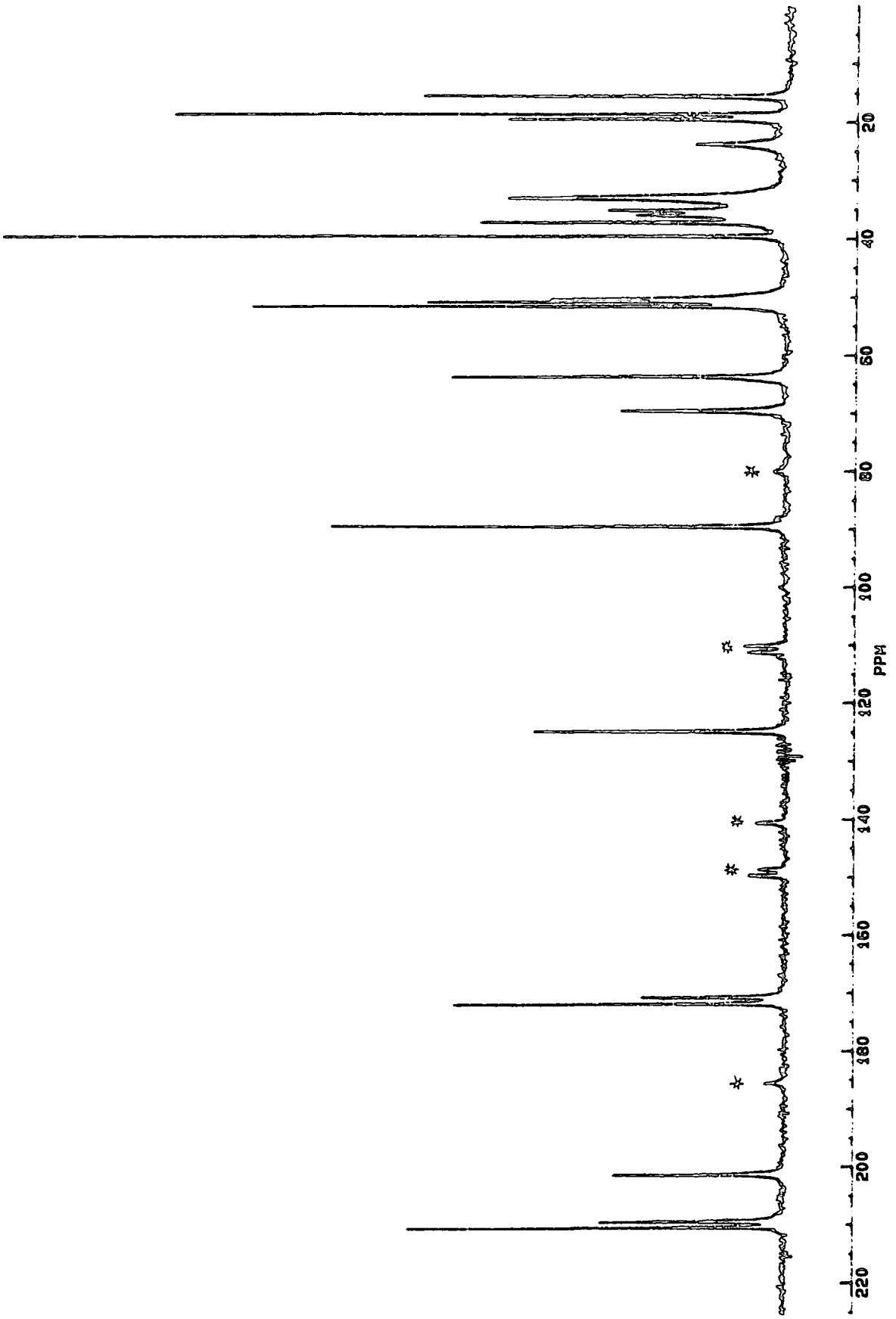

Figure 6.11 - Expansion of the high frequency region of the solid-state ^{13}C NMR spectrum of cortisone acetate polymorphs.

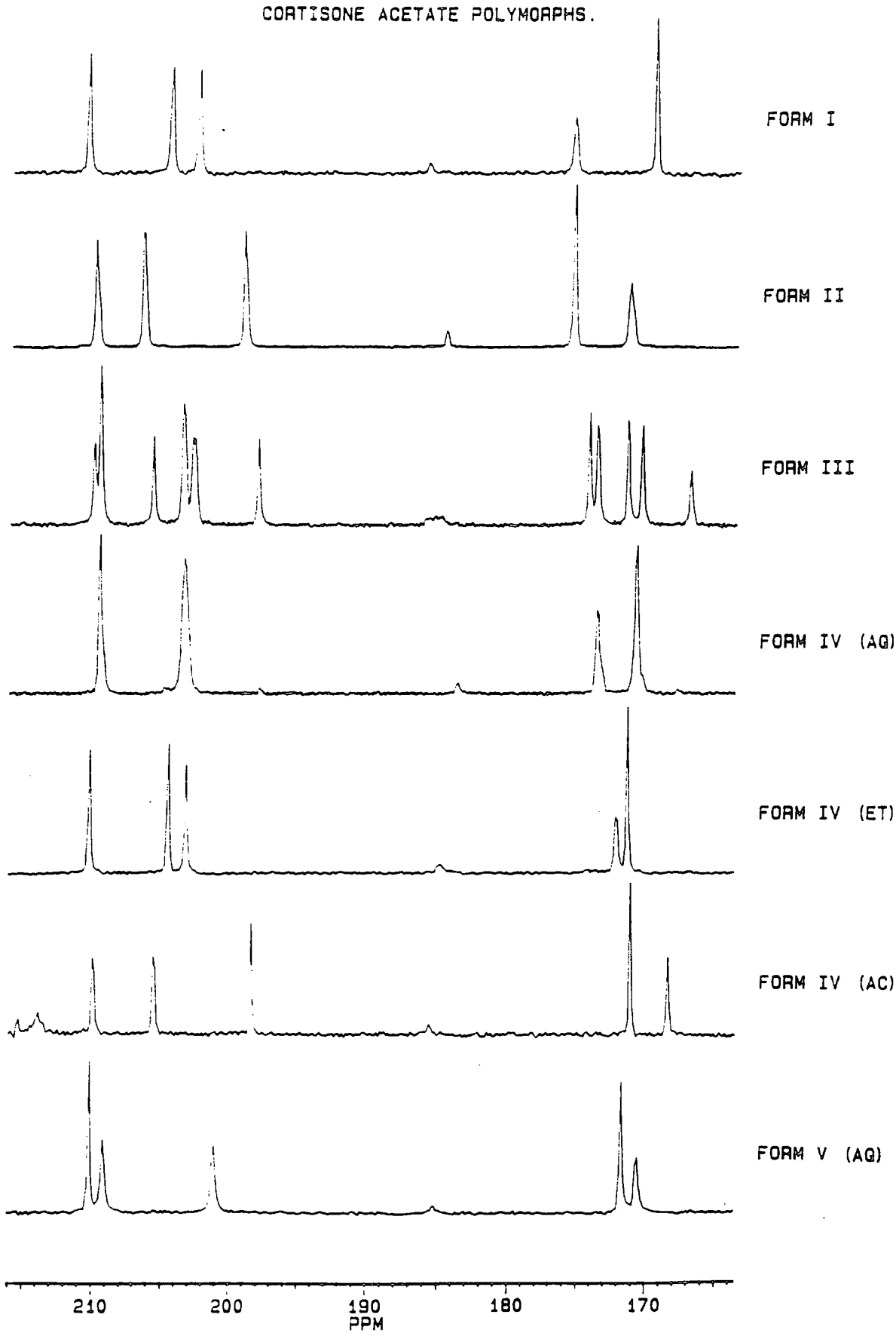

Figure 6.12 - The solid-state ^{13}C NMR spectrum of cortisone acetate form IV_{aq} undergoing transformation to form III. The peak from form IV_{aq} is marked with an asterisk. Standard operating conditions

sample	(a)	(b)	(c)	(d)	(e)
time from preparation	day 1	day 145	day 161	day 174	day 191
% of form IV_{aq} present	100%	43%	14%	6%	0%

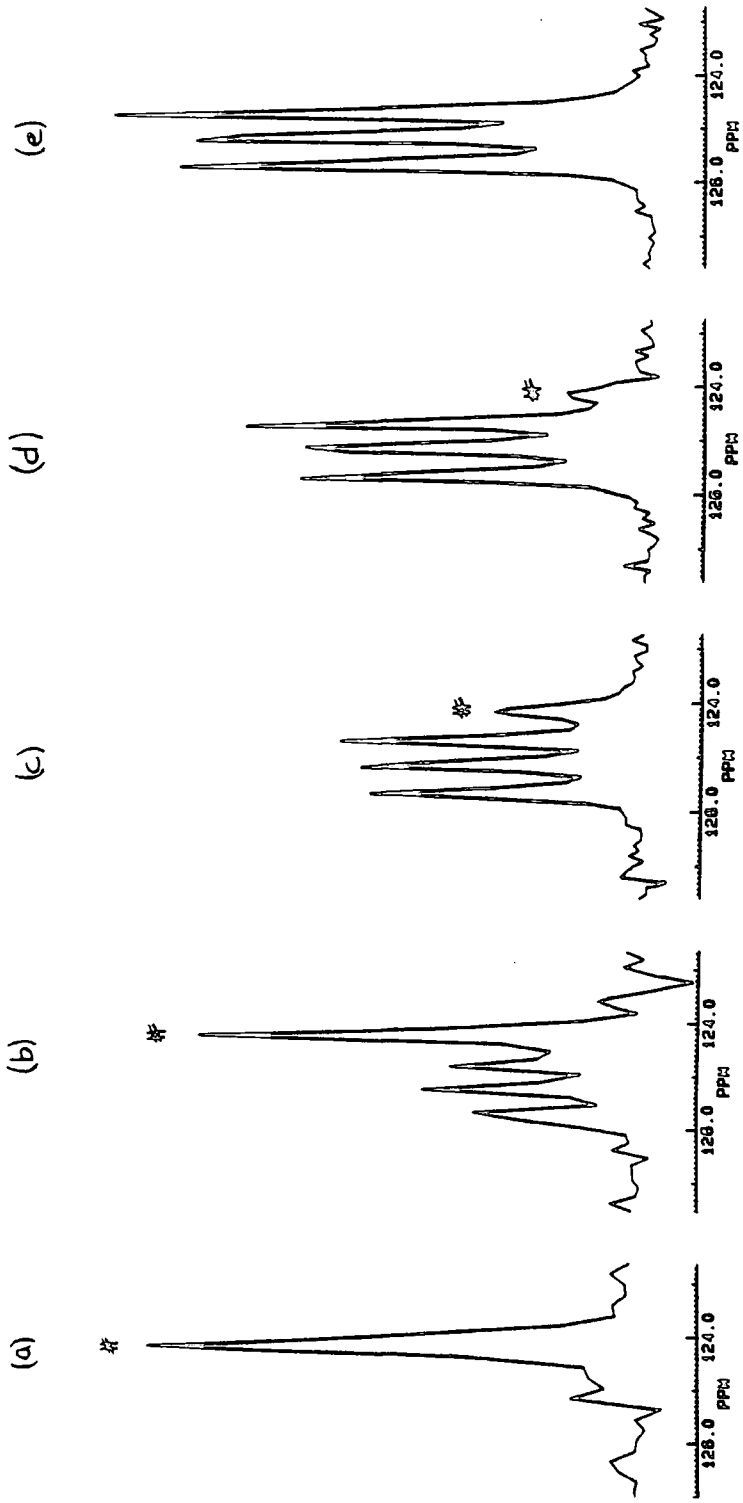

Figure 6.13 - Expansion of the solid-state ^{13}C NMR spectrum of cortisone acetate form III. Operating conditions as in figure 6.6

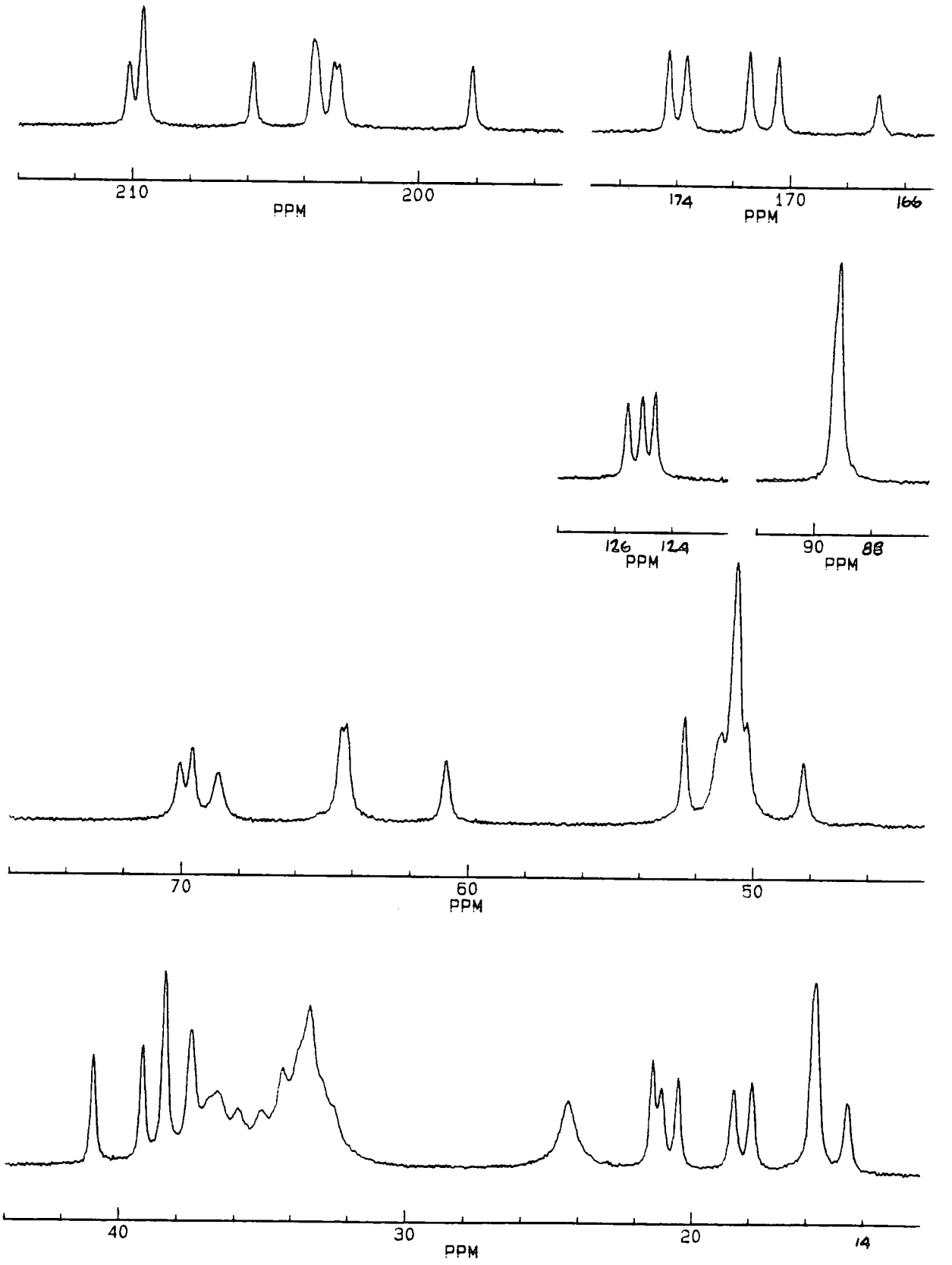

6.3.2. Form III

One would normally expect to see 23 peaks in the carbon spectrum of the compound $C_{23}H_{30}O_6$ when there is no symmetry within the molecule. However, for form III of cortisone acetate there are considerably more than 23 peaks present. A closer inspection reveals that there are often three peaks where only one might be expected. This is crystallographic splitting. There are two possible causes of these splittings. The first being that symmetrically related atoms have become inequivalent due to packing constraints, and the second is that there is more than one molecule in the crystallographic asymmetric unit. As there is no symmetry within the molecule, the first explanation cannot be the correct one. The origin of the splittings is that in form III there are three molecules in the asymmetric unit. This is consistent with the space group $P2_1$ and 6 molecules in the unit cell. Each of the three molecules has a different conformation and gives rise to a unique set of resonances. The spectrum is the composite of these individual molecules. An expanded spectrum is given in figure 6.13.

6.3.3. Polymorphic Solvates

The ^{13}C spectra of the polymorphic solvates (i.e forms IV_{ac} and IV_{et}) show peaks arising from the solvate molecules. The chemical shifts are given in table 6.6 and the solvate peaks are highlighted in figure 6.14. (the spectrum of form IV_{aq} is also shown for comparison). The similarities in chemical shift between solution and solid-state are quite good.

Table 6.6 - Chemical shifts of solvate molecules in solid and in solution (neat liquids)

form	solvate	C type	solution shift[15] /ppm	solid shift /ppm
IV_{et}	ethanol	CH_3	17.6	18.6‡
	"	CH_2	57.0	59.1
IV_{ac}	acetone	CH_3	30.6	31.8
	"	C=O	205.8	214.1

‡ See section on form IV_{et} (6.3.6.)

Figure 6.14 - The solid-state ^{13}C NMR spectrum of cortisone acetate form IV_{aq}, IV_{et} and IV_{ac}. The peaks from the solvate molecules are highlighted. Standard operating conditions have been used.

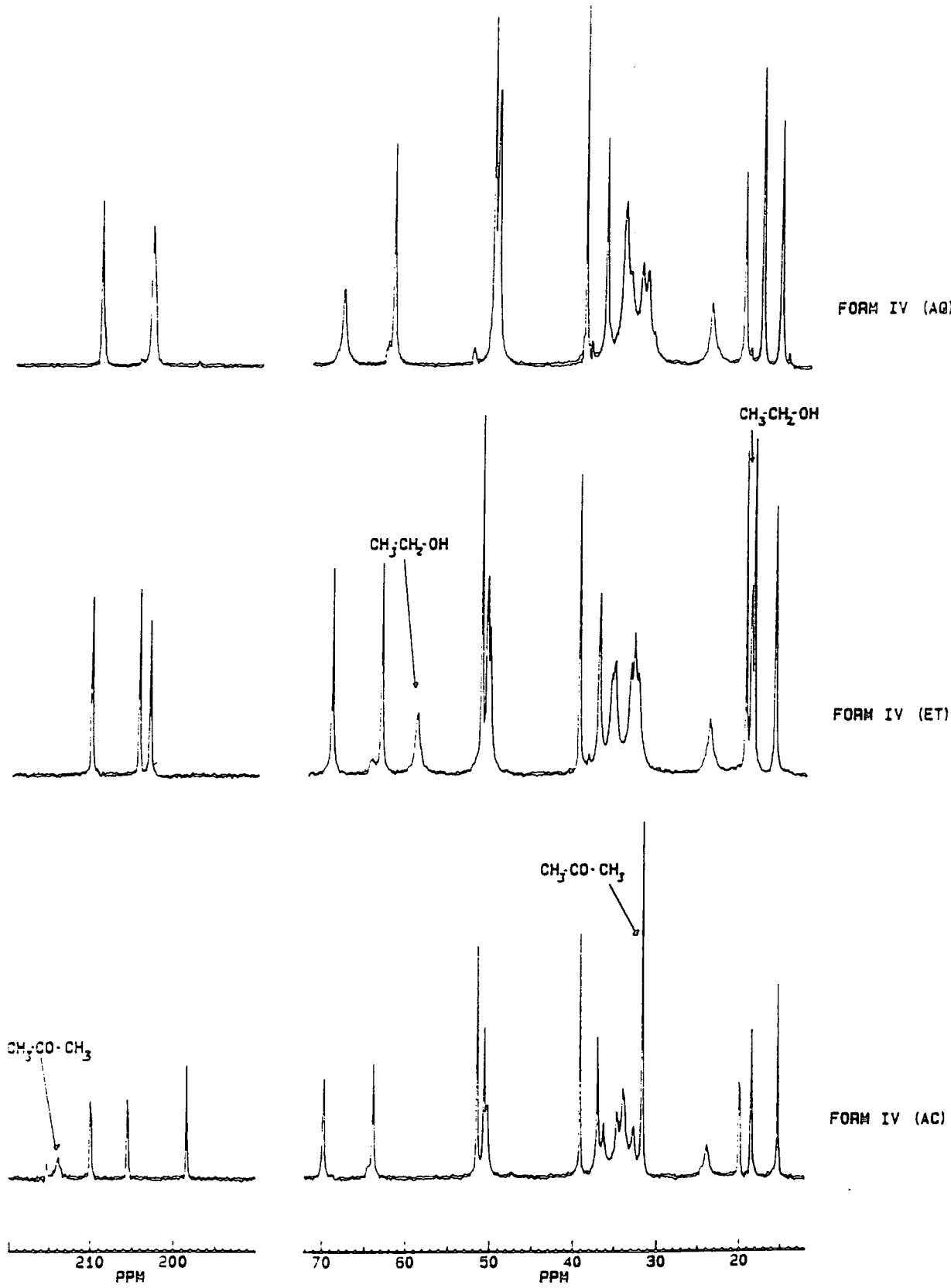

6.3.4. Assignment of Spectra

Now if chemical shifts are to be related to structure, i.e. conformation, packing, and intermolecular interactions, then the resonances must be assigned to specific carbon atoms. The assignment of solid-state NMR spectra is not straightforward. The fully assigned solution-state spectrum (discussed in chapter 5) is particularly useful for comparison, and the solid-state NQS spectrum is also very helpful. However, full assignment may still not be possible. Take, for example, the three resonances at about 50 ppm arising from C12, C13 and C14. These three peaks arise from a CH_2, a quaternary and a CH group respectively. Therefore as these three resonances are from carbons of rather different character, it may be possible to distinguish them. Suitable methods will be based upon proton-carbon interactions. For example the NQS experiment relies upon the dephasing of the carbon magnetization due to ^{1}H-^{13}C dipolar interactions. The strength of the dipolar interaction (which depends upon the number and distance of protons from the carbon atom) may be utilised to differentiate these carbon atom types. If a long window in decoupling (50-60 μs) is employed then the spectrum is of quaternary and methyl groups only, the CH_2 and CH carbon signals being completely dephased. But if shorter windows are used, (20-30 μs) the spectrum will contain peaks from protonated carbons, but with attenuated intensity. The longer the window the greater will be the attenuation of protonated signals. Therefore at 20 μs the spectrum will show resonances of all carbon types, but at 30 μs the intensity of CH_2 signals is attenuated more than those of CH signals. Therefore CH carbons can be identified, and thence by elimination the CH_2 carbons can also be identified. This method has been used to distinguish the carbons at about 50 ppm. A series of spectra with different decoupling windows are shown in figure 6.15 for form V_{aq}. The results for all forms are given in table 6.7.

Figure 6.15 - The solid-state ^{13}C NQS spectrum of cortisone acetate form V_{aq} with different decoupling windows. (a) 60 μs (b) 30 μs (c) 20 μs and (d) CPMAS spectrum for reference.

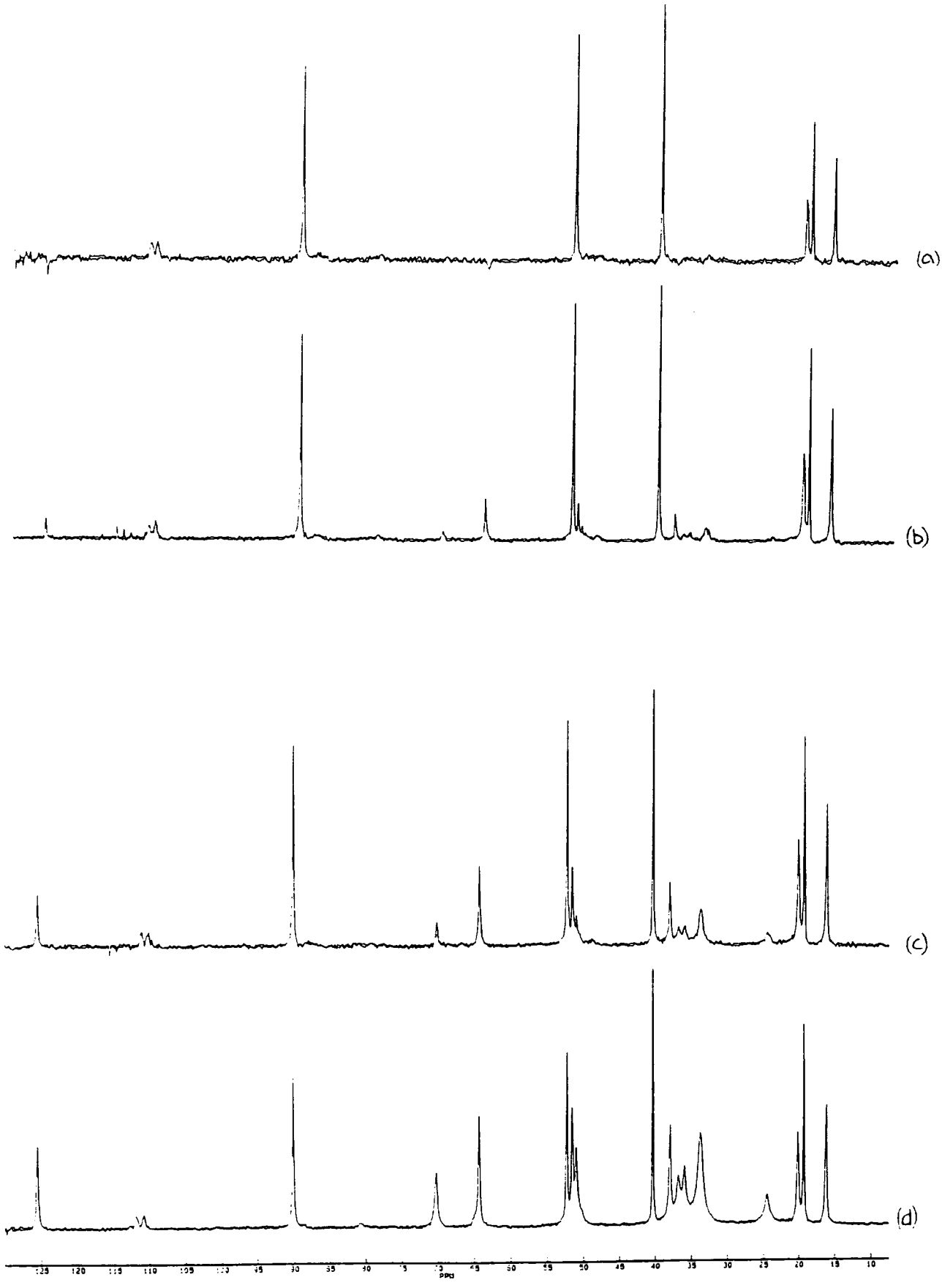

Table 6.7 - The chemical shifts of C12, C13, C14 and C8 for cortisone acetate polymorphs

form	C12	C13	C14	Order of chemical shift	C8
I	53.3	49.8	50.5	C12>C14>C13	36.5
II	50.3	52.5	50.5	C13>C12>C14	37.9
IV_{ac}	50.4	51.6	50.7	C13>C14>C12	37.0
IV_{et}	50.4	51.4	50.7	C13>C14>C12	37.3
IV_{aq}	50.6	51.1	50.6	C13>C12=C14	37.5
V_{aq}	50.3	51.7	50.8	C13>C14>C12	37.3
III	48.3	52.5	-		37.5
		50.6			

For forms I, II, IV_{ac}, IV_{et}, IV_{aq} and V_{aq}, each peak in this region may be assigned. For form III, the tripling of peaks leads to overlapping of some resonances. Consequently only the lowest and highest peaks in this region are well resolved and could be easily studied by this method. The NQS spectrum shows that the other two resonances from C13 are coincident at 50.6 ppm.

Note also that C8 (which occurs at about 37 ppm) may also be identified in this way. The chemical shift of C8 in each form is given in table 6.7.

The variable contact-time experiment may also be useful for distinguishing the three carbon atoms at about 50 ppm. The rate of cross-polarisation depends upon the number and distance of nearby protons (both those bonded directly to the carbon, and those on adjacent atoms). C13, being quaternary, can be easily distinguished as it has a slow rate of cross polarisation (T_{CH} = 0.5 - 0.6 s). C12 and C14 are not easily distinguished (for both carbons T_{CH} = 0.05 - 0.10 s) as C12 has two attached protons, with none on adjacent carbons, whilst C14 has only one attached proton but three on adjacent carbons. Therefore the rates of cross polarisation of C12 and C14 are very similar. The full results for forms II, IV_{et} and IV_{ac} are given in chapter 4 (table 4.11), and not reproduced here.

The chemical shifts of most carbon atoms are distinctive and so can be assigned. However, ambiguities remain over the assignment of C3, C11 and C20 (211-198 ppm); C5 and C22 (176-167 ppm) and C1, C2, C6, C7 and C16

(37-32 ppm). The assignment of peaks with high chemical shift anisotropies can be aided by the determination of the shielding tensor components (see chapter 7 for a full discussion). This has allowed the high-frequency region to be assigned. However, the low-frequency region (32-37 ppm) arising from CH_2 groups cannot be assigned with any certainty.

6.3.5. ^{13}C-Enriched Samples

The assignment of the spectrum can be further helped by the preparation of samples that have been selectively labelled with the ^{13}C isotope. Cortisone acetate was prepared, ^{13}C-enriched at C22, as forms II and IV_{aq}, and the chemical shift anisotropy determined (see chapter 7). Also cortisone acetate was prepared labelled at both C22 and C23 so that these resonances could be identified. In addition, form IV_{et} has been prepared with enriched ethanol so that the ethanol resonances may be unambiguously identified. Unfortunately, the doubly-enriched samples show broader resonances, due primarily to ^{13}C-^{13}C dipolar interactions. Therefore there is no simple enhancement of signal intensities, as all peaks close by are enhanced by overlapping with the broad signal. The ^{13}C-enriched samples are shown in table 6.8.

Table 6.8 - ^{13}C enriched samples

enrichment	form	labelled positions	% of ^{13}C
natural abundance	all forms	-	1%
labelled	II and IV_{aq}	C22	20%
doubly labelled	IV_{et}	C22 and C23 in the same molecule	20%‡
doubly labelled	IV_{et}	ethanol, both atoms in the same molecule	6%‡

‡ For the doubly labelled samples, the percentage of the ^{13}C isotope has been enriched to 6 or 20%. However, the probability of the two ^{13}C nuclei being at adjacent sites is >99%.

6.3.6. Form IV_{et}

A sample of form IV_{et} has been prepared with enriched ethanol. The aim here was to identify definitely the methyl resonance from the ethanol. Attempts had been made previously to identify the ethanol methyl resonance by studying a

sample when 'wet' (i.e. immediately after separation from the mother liquor by buchner funnel under water pressure), and after drying (on a vacuum line). The experiment proved to be inconclusive. One peak (at 18.6 ppm, the third peak from low frequency) underwent a change in intensity, but apparently there was more of this nucleus in the dry sample. Therefore the results of the enrichment were hoped to clarify the matter. Figure 6.16 shows the spectra of form IV_{et} for the natural abundance and the doubly enriched ethanol samples. The doubly enriched cortisone acetate sample is also shown for comparison. However, due to the broadening of signals the results are still not conclusive. It seems unlikely that the C23 resonance will have shifted to such an extent from the solution state position, that it will not be the highest frequency resonance in the group. Similarly C18 is likely to be the lowest frequency peak in the group. The singly-labelled sample shows that the C23 resonance has increased in intensity significantly when compared to the intensity of the C18 peak. The C19 and ethanol methyl peaks are then the two middle peaks of the group, but it is not immediately clear which peak is which. The higher-frequency peak has a variable intensity between samples and so it is proposed that this is the ethanol peak, as the samples each contain slightly different amounts of ethanol. The ethanol-enriched sample has a broad resonance that will also have increased the intensity of the C19 resonance by overlapping with this broad peak.

Therefore one can only conclude that the results of these experiments on enriched samples are not at variance with those of other naturally abundant samples, but also that the results are not conclusive.

Figure 6.16 - The solid-state ^{13}C NMR spectrum of cortisone acetate form IV_{et}. (a) Enriched ethanol, (b) enriched cortisone acetate and (c) natural abundance. Standard operating conditions have been used.

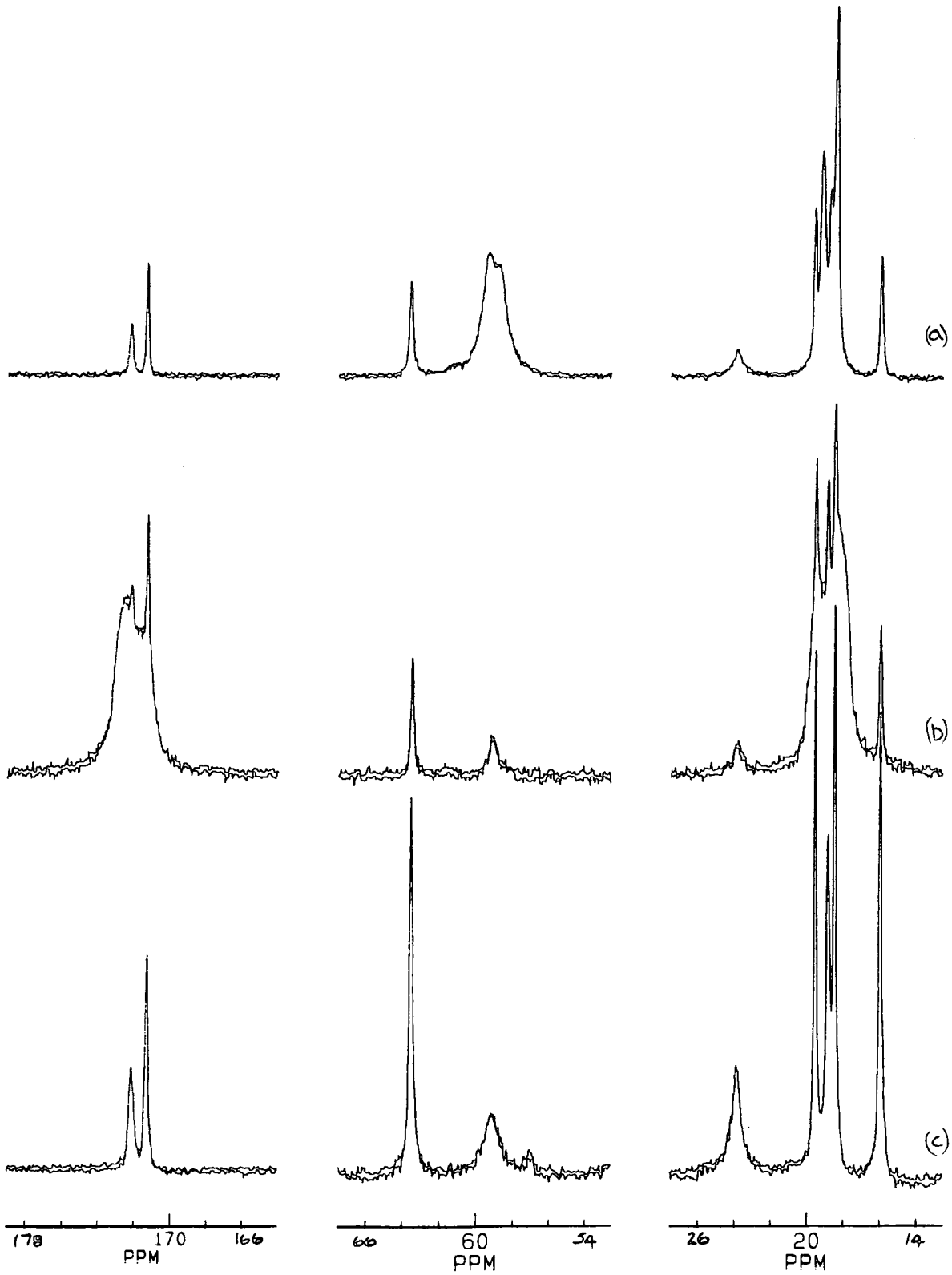

Figure 6.17 - The solid-state ^{13}C NMR spectrum of cortisone acetate form IV_{et}. (a) 'dry' and (b) 'wet' samples. Number of transients: (a) 11450 and (b) 2220.

operating conditions	^1H 90° pulse	contact time	acquisition time	recycle delay	spin rate
50 MHz	4 μs	2 ms	0.16 s	5 s	3.0 kHz

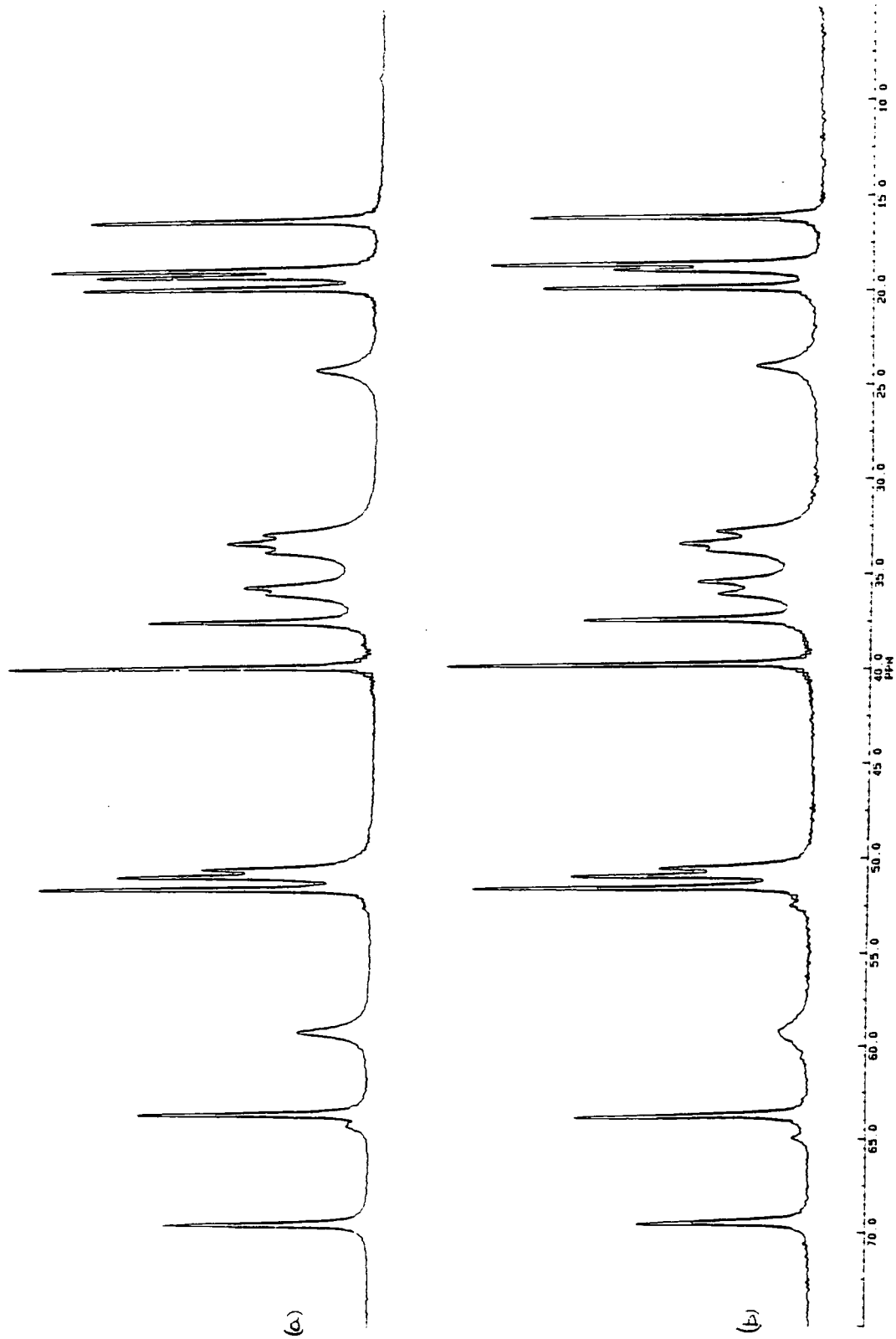

The study of wet and dry samples of form IV_{et} has also turned up an interesting situation. The spectra were expected to be different only in the intensity of the ethanol peak. However, figure 6.17 shows that there are other small (though significant) differences in the spectra of these forms. Note the differences between the peaks at 32.5-36 ppm. The differences are attributed to small changes in the crystal structure that occur when solvent is removed. The two samples have been studied by DSC and the traces are not identical (see figure 6.18). Both samples show a low temperature endotherm: for the wet sample at 113.0°C and 121.0°C and for the dry sample at 114.0°C and 122.0°C. These endotherms arise from ethanol bonded to the cortisone acetate. However, the main difference is in the temperature of the final melting endotherm, which varies by 9°C. The higher temperature transition for the wet sample indicates that the sample has transformed, upon loss of solvent, to form I or III whilst the lower melting dry sample has transformed to form II. These results are in agreement with the suggestion that the wet and dry samples have slightly different crystal structures.

Of course, the initial aim of the experiment to produce wet and dry samples was to identify the ethanol peak in the NMR spectrum. It has already been stated that unexpectedly there is apparently more ethanol in the dry sample than the wet one. As solid-sate NMR peak integrals are not normally quantitative, this phenomenon could have been attributed to experimental error. However, the two samples were also studied by solution-state proton NMR, which can be quantitative.The result was that there is indeed slightly more ethanol in the dry sample. Also the DSC peak integral shows the same trend, though only fractionally more in the dry sample. This result is seemingly inexplicable, particularly when one considers the method of preparation of the two samples. They were made by simply dividing one sample in half after separating from solution. One half is called 'wet', the other half is dried under vacuum for one hour and called 'dry'. Therefore it is hard to understand how the dry sample can contain more ethanol than the wet sample.

Figure 6.18 - The DSC traces of cortisone acetate form IV_{et}. (a) 'wet' and (b) 'dry' samples

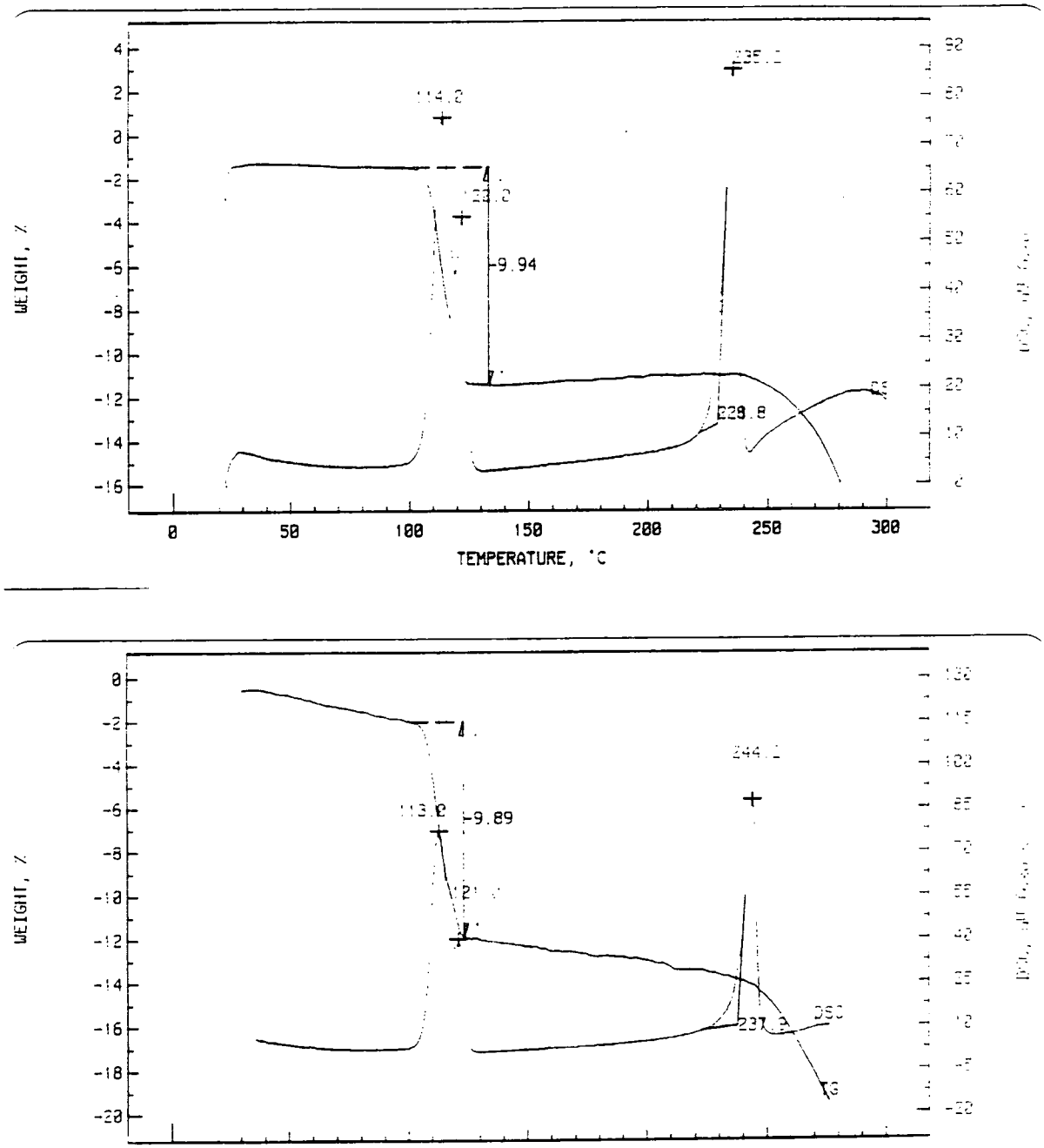

Figure 6.19 - The IR spectra of cortisone acetate form IV_{et}. (a) 'wet' and (b) 'dry' samples.

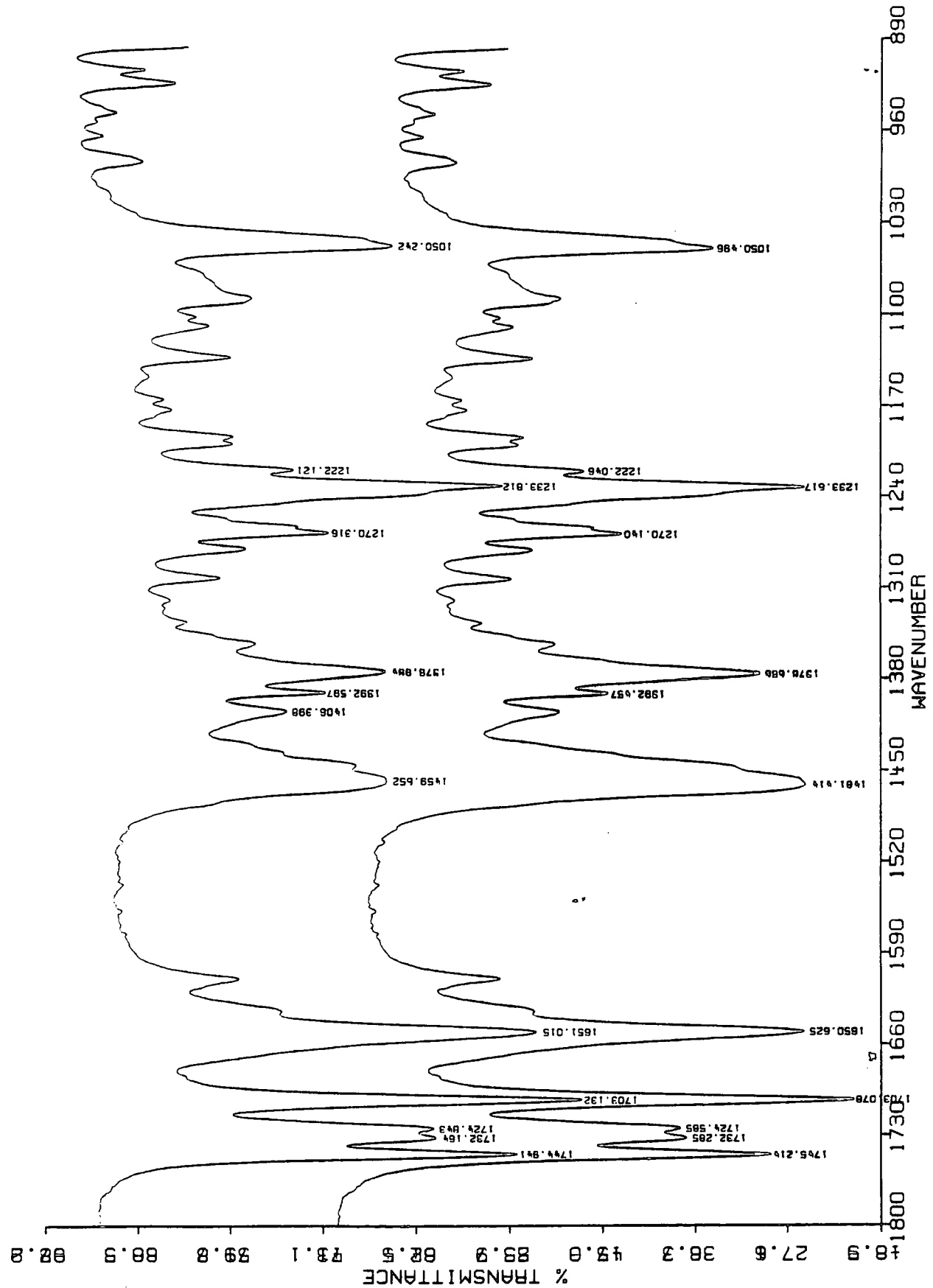

Table 6.9 - Peak integrals of ^1H NMR in solution for wet and dry samples of cortisone acetate form IV_{et}

	chemical shift / ppm	Carbon atom no.	No. of protons	integral	integral / no. of protons	EtOH:CA
dry	4.65	C21	1	7	7	0.9:1
	3.66	‡CH_2	2	13	6.5	
	1.23	‡CH_3	3	19	6.3	
	0.61	C18	3	20	6.6	
wet	4.63	C21	1	10	10	0.8:1
	3.60	‡CH_2	2	13	6.5	
	1.23	‡CH_3	3	25	8.3	
	0.61	C18	3	28	9.3	

‡ denotes carbon atoms in the ethanol molecule. The assignment of the proton spectrum of cortisone acetate was presented in chapter 5, and the chemical shifts of the ethanol peaks are well known.

Figure 6.19 shows the infra-red spectra of the two samples, which are identical. Therefore, the differences must be very small, and are probably in the packing rather than the conformation. Infra-red spectroscopy is very sensitive on a short range, but longer range differences are more difficult to detect.

6.4. References

(1) Callow, R.K., Kennard O. *J. Pharm. Pharmacol.* 13, 723 (1961).

(2) Mesley, R.J., Johnson C.A. *J. Pharm. Pharmacol.* 17, 329 (1965).

(3) Mesley, R.J. *Spectrochim. Acta* 22, 889 (1966).

(4) Carless, J.E., Moustafa M.A., Rapson H.D.C. *J. Pharm. Pharmacol.* 18, 190 (1966).

(5) Mesley, R.J. *J. Pharm. Pharmacol.* 20, 877 (1968).

(6) Carless, J.E., Moustafa M.A., Rapson H.D.C. *J. Pharm. Pharmacol.* 20, 630 (1968).

(7) Carless, J.E., Moustafa M.A., Rapson H.D.C. *J. Pharm. Pharmacol.* 20, 639 (1968).

(8) Kuhnert-Brandstatter, M., Gasser P. *Microchem. J.* 16, 590 (1971).

(9) Harris, R.K., Kenwright A.M., Say B.J., Yeung R.R., Fletton R.A., Lancaster R.W., Hardgrove G.L. Jnr. *Spectrochim. Acta* 46A, 927 (1990).

(10) Declercq, J.P., Germain G., van Meerssche M. *Cryst. Struct. Commun.* 1, 59 (1972).

(11) Kanters, J.A., de Koster A., van Geerestein V.J., van Dijck L.V. *Acta Cryst.* C41, 760 (1985).

(12) van Geerestein, V.J., Kanters J.A. *Acta Cryst.* C43, 936 (1987).

(13) van Geerestein, V.J., Kanters J.A. *Acta Cryst.* C43, 136 (1987).

(14) Bernstein, J. In *Organic Solid State Chemistry*; Eds. Desiraju, G.; Elsevier: New York, (1987); Vol. 32; chap. 13; pp 471.

(15) Silverstein, R.M., Bassler G.C., Morrill T.C. *Spectrometric identification of organic compounds;* 4th ed.; J. Wiley & Sons: New York, (1981).

Chapter 7

Chemical Shift Anisotropy

Chapter 7 Chemical Shift Anisotropy

7.1. Theory Of Anisotropy

The chemical shift is affected by the interaction of the nucleus with the surrounding electrons. The induced motion of electrons around the nucleus generates a magnetic field that may oppose that of the applied field, thus reducing the field experienced by the nucleus i.e. shielding from the applied field. If the distribution of electron density around the nucleus is not spherical, as is usually the case, then the shielding effect of the electrons will be orientation dependent[1-6]. The shielding may be represented by a tensor that can be expressed as a diagonalised 3×3 matrix by the choice of a suitable axis system. The three non-zero terms are called the principal components of the tensor and given the symbols σ_{11}, σ_{22}, and σ_{33}. The shielding tensor components may be used to describe the local environment of the nucleus.

In solutions, rapid molecular motion averages the shielding tensor to an isotropic value (σ_{iso}), which is given by the trace of the tensor (given in equation (1)).

$$\sigma_{iso} = \frac{1}{3}(\sigma_{11} + \sigma_{22} + \sigma_{33}) \quad \text{..... (1)}$$

However, in solids motion is generally restricted and so the principal tensor components are not averaged and may be determined from the spectrum.

Since the shielding of the nucleus is orientation dependent, different orientations of a molecule in the applied field will experience different shielding. This can be visualised by considering a simple molecule such as $CHCl_3$. There are two clearly different orientations of the molecule with respect to the magnetic field, as shown in figure 7.1, and the chemical shift of the carbon nucleus is different for the two orientations.

Figure 7.1 - Showing two different orientations of the $CHCl_3$ molecule in an applied magnetic field

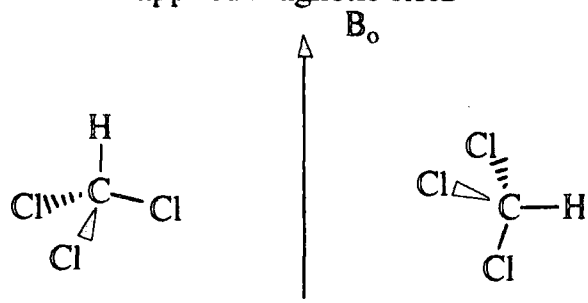

If a single crystal is placed in an applied magnetic field B_0, then the shielding will change as the orientation of the crystal with respect to B_0 changes. In a powdered crystalline sample, all possible orientations of the microcrystallites will occur and so each crystal will experience different shielding, and hence resonate at a different frequency from all the other orientations. The resulting spectrum will be composed of the superposition of all the resonance frequencies, and so appear as a broad line, which is known as a powder pattern. The shape of the powder pattern will be dependent upon the values of the principal tensor components. Although the values of the principal tensor components may be obtained from the spectrum, the direction of the components with respect to the molecular axis system cannot be simply found from the powder pattern (although there are some sophisticated two dimensional experiments that are able to do this). The direction of the components with respect to the molecular axis system may be determined from single crystal NMR work (which is very time consuming).

Depending upon the molecule in question the environment of the nucleus will fall into one of the following categories (see also figure 7.2):

(a) Isotropic: (i.e. cubic symmetry exists) in which case the shielding is independent of orientation

(b) Axial symmetry exists. An example is the carbon atom of a methyl group, which often has this symmetry, or the carbon or hydrogen atoms of a $CHCl_3$ molecule mentioned earlier.

(c) General non-symmetric case

Figure 7.2 - Schematic diagram showing solid-state NMR powder patterns

(a) isotropic case

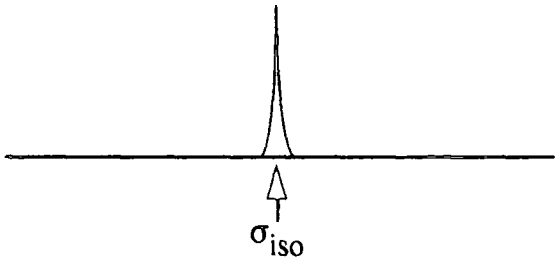

(b) axially symmetric case

$\sigma_{||}$ is the parallel component
$\sigma_{\perp}$ is the perpedicular component

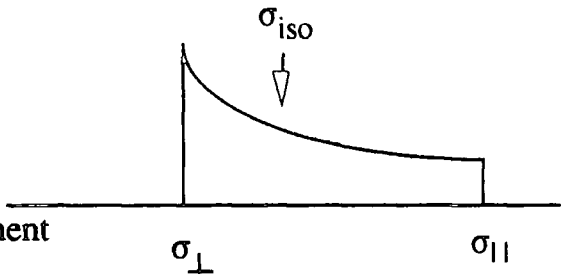

(c) general non-symmetric case

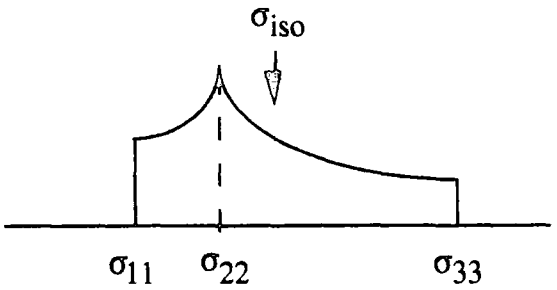

Two parameters are often used to describe the powder pattern, the anisotropy ($\Im$) and the asymmetry (η), which are defined in equations (2) and (3) as follows:

$$\Im = \sigma_{33} - \sigma_{iso} \quad \text{.....} \quad (2)$$

$$\eta = \frac{\sigma_{22} - \sigma_{11}}{\Im} \quad \text{.....} \quad (3)$$

The convention used here and throughout this thesis is that of Haeberlen [7], where $|\sigma_{33} - \sigma_{iso}| \geq |\sigma_{11} - \sigma_{iso}| \geq |\sigma_{22} - \sigma_{iso}|$ and $0 \leq \eta \leq 1$. Note that $\sigma_{iso} = -\delta$, where δ is the chemical shift.

7.2. Anisotropy And Magic Angle Spinning

The interaction of the magnetic moment of the nucleus and the external magnetic field can be represented by a Hamiltonian operator. The spatial part of

the Hamiltonian[2] referring to shielding anisotropy has a $(3\cos^2\theta - 1)$ dependence upon the orientation, where θ is the angle between a particular axis in the sample and B_0. However, the orientation dependence may be averaged over time as follows:

$$\langle\cos^2\theta\rangle = \cos^2\beta\cos^2\chi + 2\sin\beta\cos\beta\sin\chi\cos\chi\langle\cos\omega t\rangle + \sin^2\beta\sin^2\chi\langle\cos^2\omega t\rangle \ldots\ldots \quad (4)$$

but as $\langle\cos\omega t\rangle = 0$ and $\langle\cos^2\omega t\rangle = \frac{1}{2}$, the average orientation dependence of the shielding can be expressed as follows:

$$\langle 3\cos^2\theta - 1\rangle = \frac{1}{2}(3\cos^2\beta - 1)(3\cos^2\chi - 1) \ldots\ldots (5)$$

where β is the angle between B_0 and the rotor axis, χ is the angle between the dipole and the axis of rotation, ω is the spinning frequency and t is time. The angles are shown in figure 7.3.

Figure 7.3 - Diagram showing the definition the angles χ, β and θ.

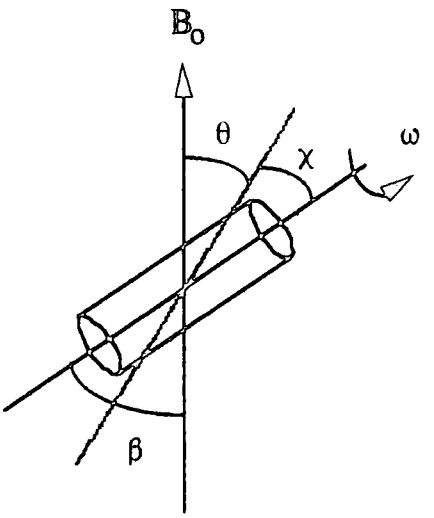

In a powdered sample, all values of θ and χ are present. The angle β takes only one value and may be chosen by the operator. If $\beta = 54.7°$ then

$$\frac{1}{2}(3\cos^2\beta - 1)(3\cos^2\chi - 1) = 0 \ldots\ldots (6)$$

This angle of β is called the magic angle. The second and third terms in the equation 4 will average to zero if ω is greater than the shielding anisotropy ($\omega > \aleph$). In this case the spectrum will consist of a single sharp line at the isotropic frequency, but spinning speeds of several kiloHertz are required. In general, the spinning speed will be less than the anisotropy, and so the final terms are only

partly averaged, which leads to spinning sidebands in the spectrum. The spinning sidebands are spaced at the spinning frequency and the intensities follow approximately the shape of the powder pattern.

Magic angle spinning is commonly used in order to simplify the spectrum from the effects of chemical shift anisotropy[8-10]. In general, fast spinning speeds are used in order to obtain the minimum number of sidebands possible. This has the effect of simplifying the spectrum and increasing the intensity of the centreband.

7.3. Finding The Shielding Tensor Components

Several methods for finding the shielding tensors are available, and are described briefly as follows:

(i) From the static spectrum. The powder pattern is obtained and if S/N is high, the tensor components are easily found[6,11]. However if the spectrum contains more than one peak, the powder patterns may overlap considerably, and obscure the features of each pattern. Moreover, other interactions (e.g. dipolar interactions) may cause additional broadening of the spectrum. Thus this method has rather restricted use.

(ii) Slow magic angle spinning. This results in the occurrence of spinning sidebands[1,12,13]. Analysis of the intensities of the spinning sideband manifold can yield the values of the tensor components.

(iii) Off angle fast spinning. The sample is spun rapidly but not at the magic angle[14]. This gives a spectrum that is similar in appearance to the static powder pattern, but with the width of the powder patterns reduced, so scaling down the effect. If there are several peaks close together in a spectrum then this method would not be suitable as overlap of patterns will still occur.

(iv) Two-dimensional experiments. The complete static powder pattern is obtained in one of the dimensions whilst the other dimension contains only

the isotropic chemical shifts[15]. Such an experiment can be performed on a static sample that undergoes 120° jumps in orientation.

(v) Single crystal NMR. Only this method allows the orientation of the tensor components to be found with respect to the molecular axis system.

The relative merits of the various methods have been investigated[11,13,16,17]. The method of slow magic angle spinning has been used in this work, and the method is described briefly as follows. A slow spinning speed is chosen so that the sidebands of one peak do not overlap with those of another resonance in the spectrum. For steroids, the high frequency region of the spectrum contains the peaks with the largest anisotropies. As often there are several peaks close together, the spinning speed must be chosen with care. A simple Pascal computer program was used for this purpose. Slow spinning speeds are used because more spinning sidebands are seen, and so the shielding tensors can be found more accurately as more data is available. However, as the total intensity of the spinning sideband manifold is constant, if there are more spinning sidebands present, each will have a reduced intensity. This adversely affects the overall S/N. Therefore many more transients are required to achieve the same S/N ratio than for the same sample when spun faster. Generally steroids give resonances that are narrow in the fast spinning case, and so a high quality spectrum with good S/N can be acquired quite quickly (perhaps 1000 transients are necessary, taking about 90 minutes). In the slow spinning experiments, 10000-20000 transients are usually acquired (taking 14-28 hours) depending upon the time available.

The method adopted for analysing the sideband patterns in order to reveal the tensor components is to use computer simulation of the spectra by iterative fitting to the experimental spectra. A mathematical expression for the pattern of spinning sideband intensities has been derived by Maricq and Waugh[12] but is not reproduced here. This provides the basis for the computer program used. The program has been described elsewhere[18,19], and was used without any major

modifications. The program requires the following input information: Larmor frequency of the nucleus, spinning speed, number of sidebands, sideband intensities and an initial estimate of the anisotropy and the asymmetry. The program produces output of simulated intensities of the sidebands, the tensor components, the anisotropy, the asymmetry, and (in order to give an indication of the quality of the fit) the sum of the squared differences. A diagram of the simulated and experimental peaks is also produced.

An investigation of the accuracy of such fitting programs[11,18-20] has revealed that for asymmetric cases, both the asymmetry and the anisotropy can be found quite accurately, as there is a clear minimum in the sum of the squared differences. However, for the axially symmetric case, there is not a sharp minimum in the sum of squared differences, and so the axial case cannot be distinguished from a near axial case, i.e. values of $\eta < 0.2$ are unreliable. Generally, the asymmetric case is much less sensitive to errors in peak intensities. For example[18], a 5% error in measuring sideband intensities would lead to ±2.0 ppm for $\Im$, and ±0.15 for η, whereas for a symmetric case, a 5% error in intensity leads to an error of ±11.0 ppm in $\Im$, and ±0.2 in η. Thus the intensity differences between axial ($\eta = 0$) and near-axial ($\eta = 0.2$) symmetry cases are too small to detect. The accuracy of the fitting procedure is dependent upon accurate signal intensities being available. Hence high S/N spectra would have least error in measured intensities and should give the most accurate fits.

7.4. Results Of Computer Fitting

7.4.1. The Results

The shielding tensor components of the highest frequency peaks in cortisone acetate have been determined and the full results are presented in appendix 2 (tables A2.1-A2.7). Generally, each form has been studied at three spinning speeds in order to reduce experimental error. For comparison purposes, the steroids testosterone, cortisone, androstanolone and ^{13}C-labelled cortisone acetate (labelled at C22) have also been studied, and the results are presented in

appendix 2 (tables A2.8-A2.11). All the data are summarised here in tables 7.3 - 7.13. Solid-state NMR spectra of testosterone, a cortisone and androstanolone are presented in figures 7.4 - 7.6.

The following abbreviations have been used: RO, the spinning speed; $\Re$, the anisotropy; η, the asymmetry; σ_{ii}, the shielding tensor components; δ, the chemical shift; ssd, the sum of square differences; range, the number of sidebands used for fitting.

Two examples of the fitting of experimental and calculated patterns are shown in figure 7.7 for the axial symmetry case, and a general non-symmetric case.

7.4.2. Summary Of Results and Discussion

The shielding tensor components can be used to make assignments of the solid state spectra of cortisone acetate polymorphs. The high frequency region of the solution-state spectrum is assigned as follows (see chapter 5):

Table 7.1 - The solution-state chemical shifts of the five highest frequency peaks of cortisone acetate

Carbon Number	Chemical Shift / ppm
C11	208.7
C20	204.3
C3	199.6
C22	170.4
C5	168.4

Figure 7.4 - Solid-state ^{13}C NMR spectrum of α-testosterone. Spinning sidebands are marked with an asterisk.

operating conditions	^{1}H 90° pulse	contact time	acquisition time	recycle delay	number of transients	spin rate
50 MHz	4 μs	2 ms	0.16 s	3 s	5600	3.5 kHz

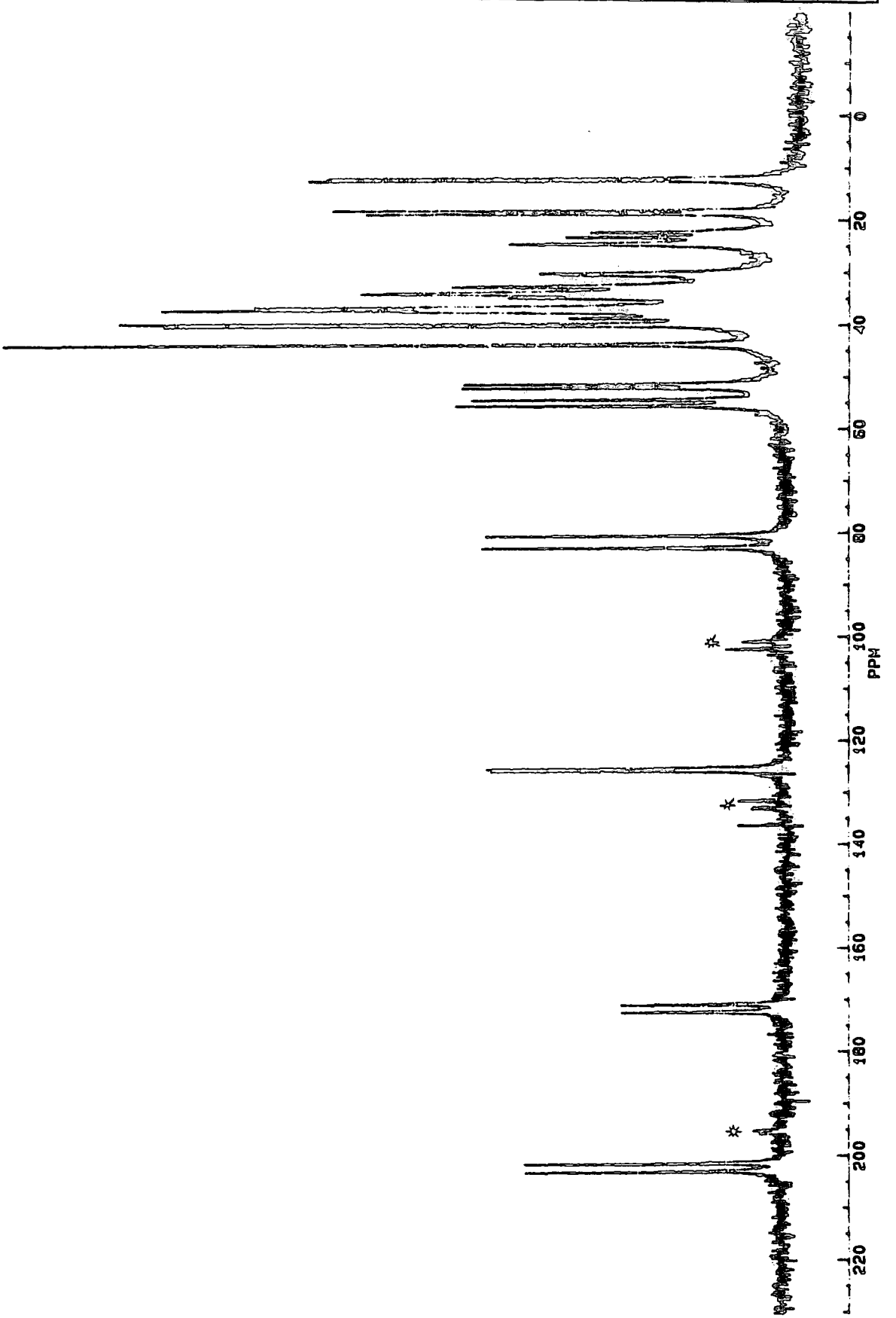

Figure 7.5 - Solid-state ^{13}C NMR spectrum of cortisone. Spinning sidebands are marked with an asterisk.

operating conditions	^{1}H 90° pulse	contact time	acquisition time	recycle delay	number of transients	spin rate
50 MHz	4 μs	2 ms	0.16 s	4 s	5630	3.5 kHz

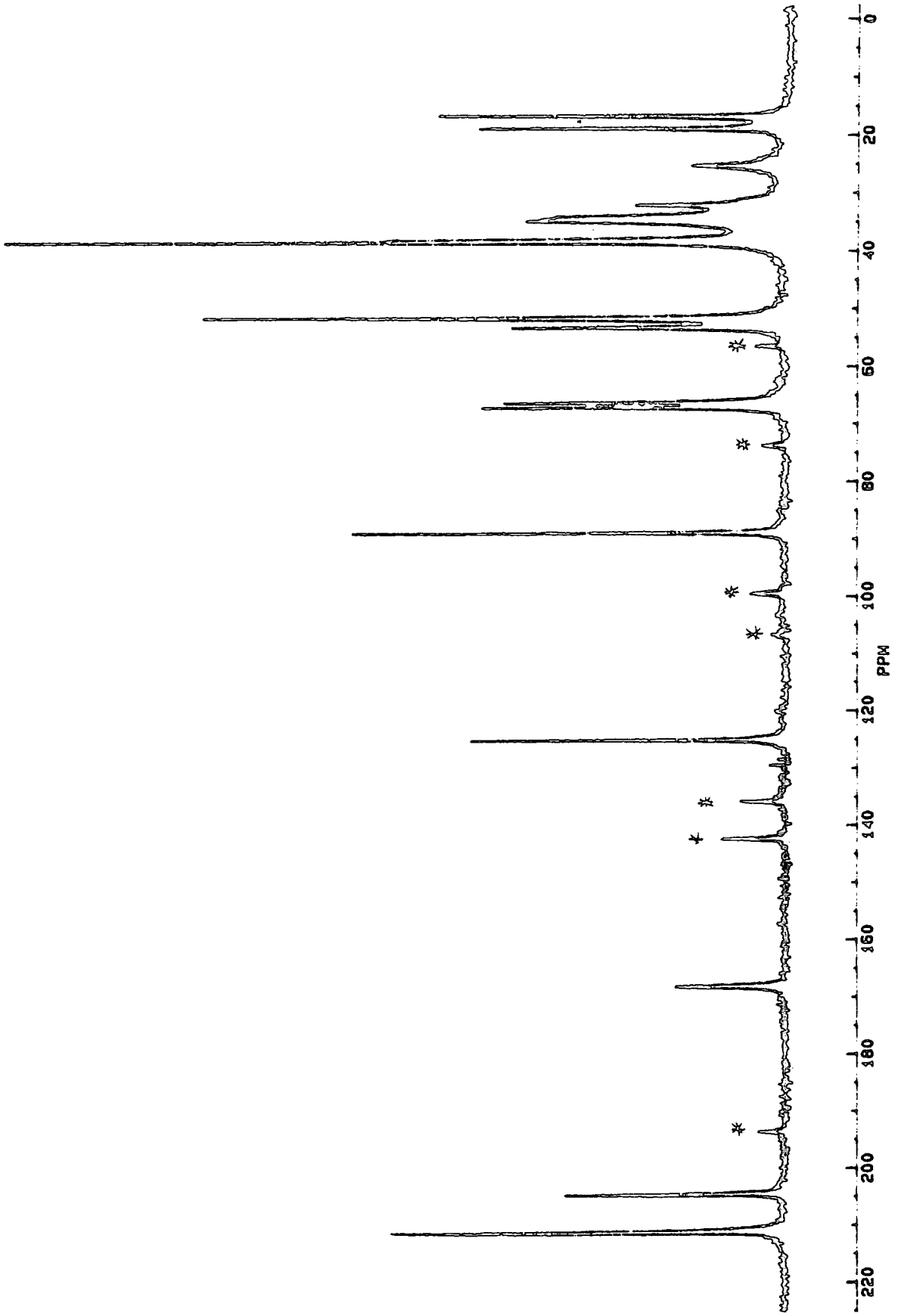

Figure 7.6 - Solid-state ^{13}C NMR spectrum of androstanolone hydrate. Spinning sidebands are marked with an asterisk.

operating conditions	^{1}H 90° pulse	contact time	acquisition time	recycle delay	number of transients	spin rate
50 MHz	4 µs	2 ms	0.16 s	4 s	2000	3.1 kHz

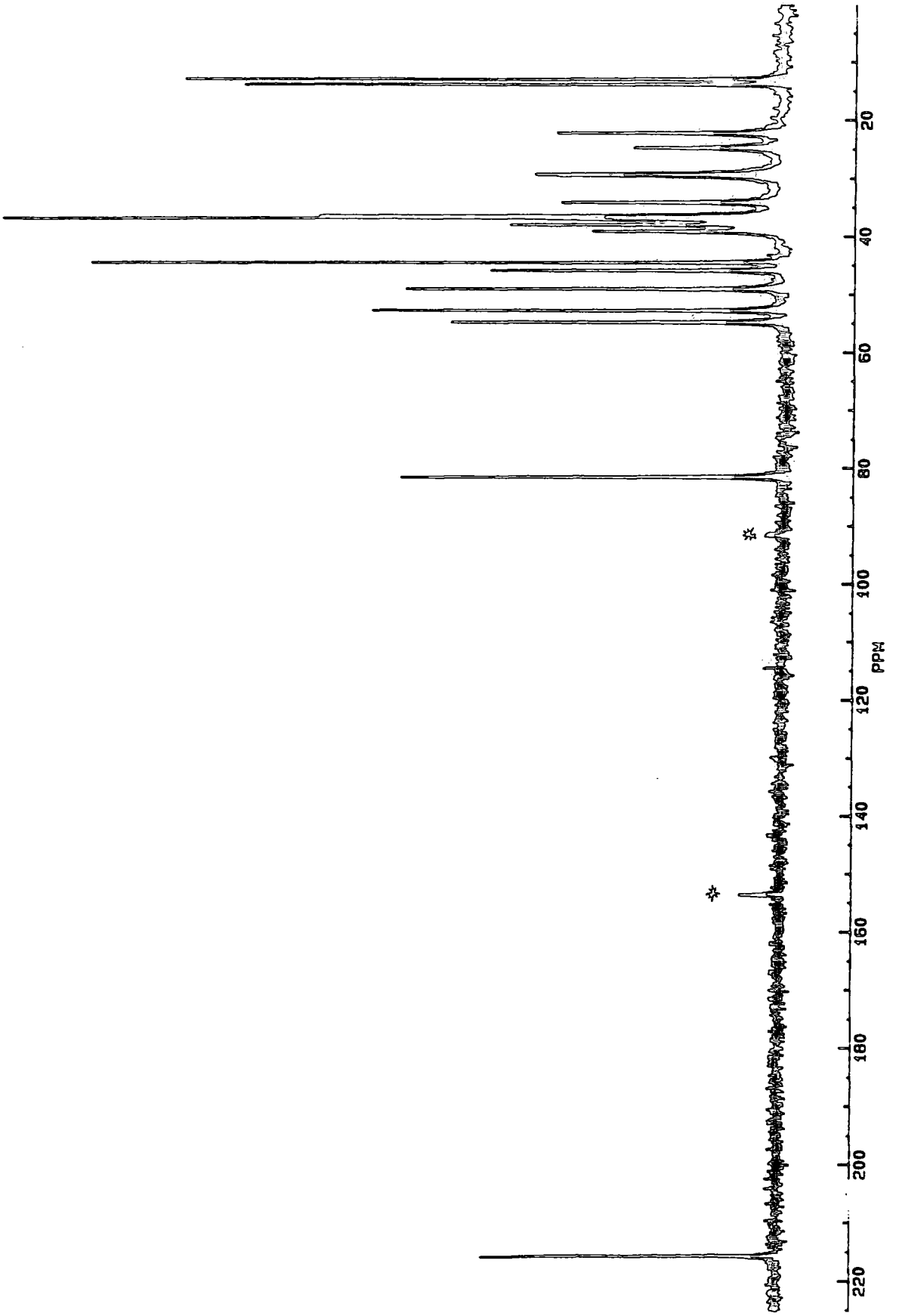

Figure 7.7 - Showing the fitting of experimental and calculated patterns. (a) Axial symmetry and (b) non-symmetric case.

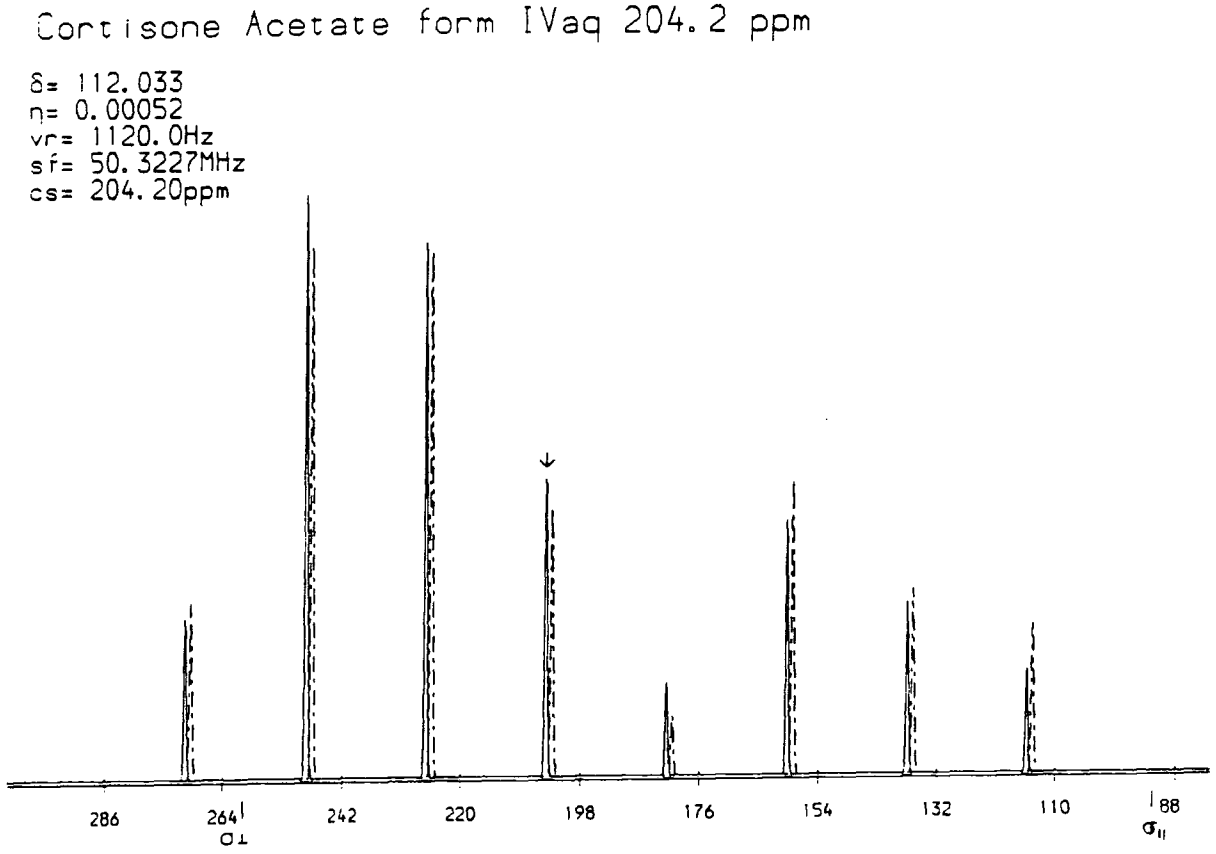

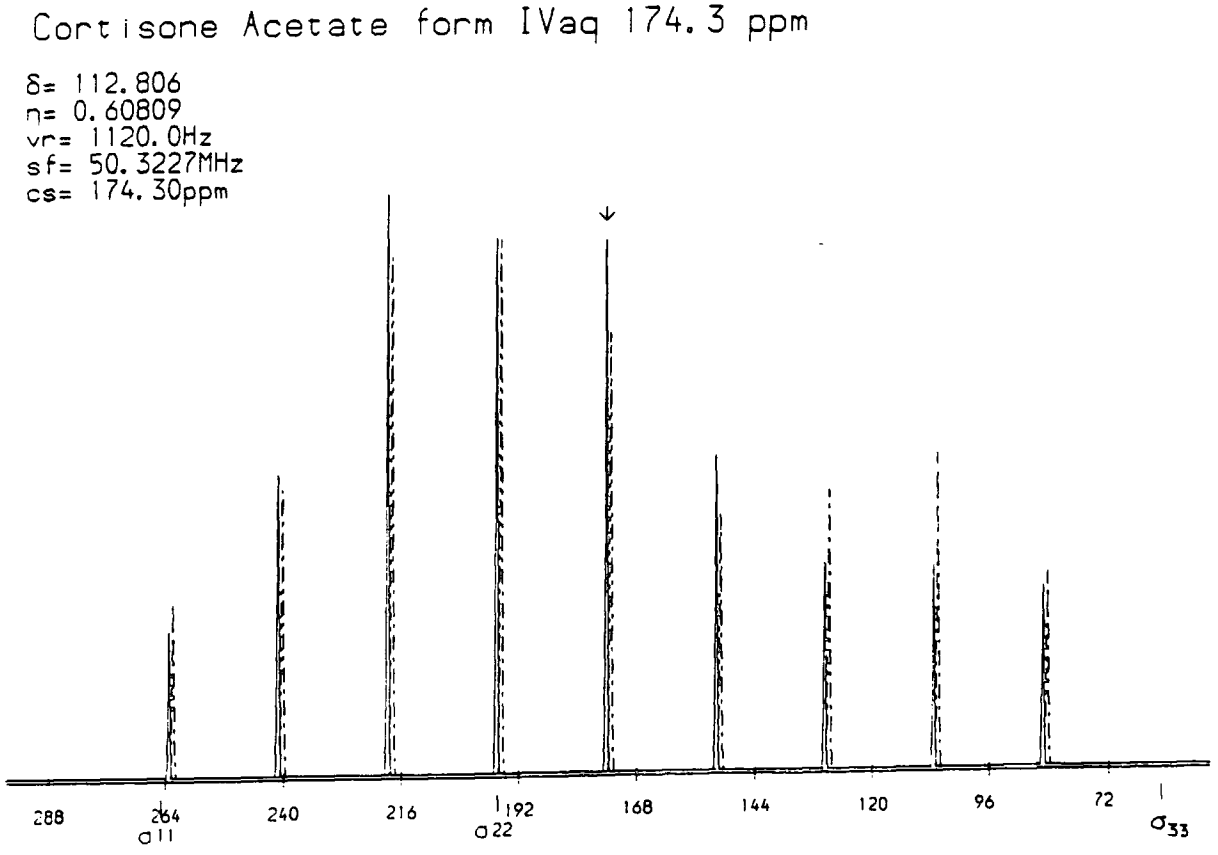

By comparison with the solution-state spectrum, the three highest frequency peaks are likely to be C11, C20, and C3 from the highest frequency. The peaks are reasonably well separated, by 4-5 ppm, so crossing over of the peaks is unlikely, but not impossible. However the lower two frequency peaks are much closer together and differences in conformation, packing, and intermolecular interactions could cause crossing over of these two peaks. Cortisone and testosterone were studied in order to reveal the likely parameters to be expected for C5, as C22 is not present in either of these compounds. Also, the C3 resonance can be distinguished easily in testosterone and cortisone. These values should be compared with those available in the literature[1,4,6,21,22], the review by Duncan[22] being particularly recent and extensive.

The average values of the relevant shielding tensor components taken from the literature are summarised in table 7.2.

Table 7.2 - Average shielding tensor components from the literature[22] and the calculated $\Im$ and η.

carbon atom type	shielding components σ_{11}	σ_{22}	σ_{33}	$\Im$	η	δ_{iso}
ketone	-279	-245	-85	118	0.29	203
ester	-257	-131	-107	-91	0.26	166
olefinic‡	-224	-134	-37	±94	0.96	131
alcohol(1°)	-78	-72	-15	40	0.15	55
alcohol(2°)	-92	-76	-47	25	0.64	72

‡ The large asymmetry of the olefinic carbon atoms means that $|\sigma_{33} - \sigma_{iso}| \approx |\sigma_{11} - \sigma_{iso}|$ and so, in practical terms, it is difficult to decide which is the larger due to experimental error. This means that the sign of $\Im$ is uncertain (although the magnitude is quite well known).

A summary of the results of the experiments on testosterone, cortisone and androstanolone are given in tables 7.3 - 7.5.

Table 7.3 - Summary of shielding tensor components of α-testosterone‡

	C3	C3	C5	C5	C4	C4
$\Re$	109	103	117	111	-67	-69
η	0.00	0.00	0.65	0.66	0.86	0.75
σ_{11}	-257	-253	-269	-263	-69	-65
σ_{22}	-257	-253	-193	-189	-166	-177
σ_{33}	-94	-98	-55	-60	-193	-195
δ_{iso}	202.8	201.4	172.2	170.7	125.8	125.3

‡ the α-form of testosterone contains two molecules in the asymmetric unit which leads to crystallographic splittings

Table 7.4 - Summary of shielding tensor components of cortisone and androstanolone

					androstanolone		
	Cortisone				anhydrous	hydrate	
	C11/20	C3	C5	C4	C3	C3	C17
$\Re$	108	111	121	-66	121	122	±40
η	0.00	0.00	0.59	0.75	0.03	0.12	0.69
σ_{11}	-265	-260	-264	-67	-278	-284	-76
σ_{22}	-265	-260	-193	117	-275	-270	-79
σ_{33}	-103	-93	-47	-191	-94	-93	-89
δ_{iso}	211.0	204.5	168.1	124.9	215.8	215.5	81.5

Table 7.5 - Summary of shielding tensor components of ^{13}C labelled cortisone acetate samples

	form II	form IV_{aq}
	C22	C22
$\Re$	-72.5	-87.5
η	0.46	0.17
σ_{11}	-122.1	-120.2
σ_{22}	-155.8	-135.5
σ_{33}	-247.7	-259.1
δ_{iso}	175.2	171.6

The structures of these molecules are shown in figure 7.8, along with the numbering of functional groups. The full numbering scheme is given in chapter 5.

Figure 7.8 - Showing the structure of the steroids studied, and the numbering of functional groups.

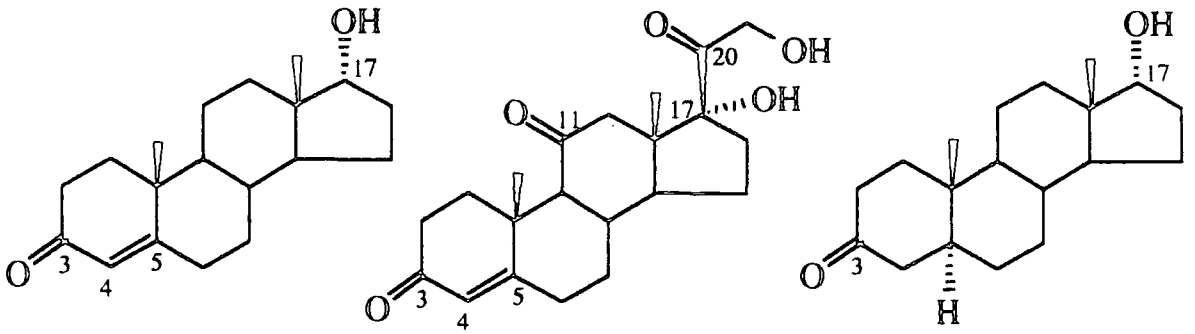

Testosterone Cortisone Androstanolone

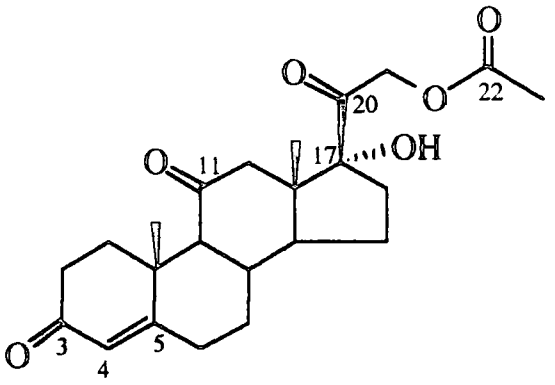

Cortisone Acetate

The results show that the carbonyl groups (C3, C11 and C20) have similar anisotropy and asymmetry parameters to those in the literature. It should be noted however, that C3 has a slightly smaller anisotropy in testosterone and cortisone than in androstanolone (and also the literature value). This might be due to conjugation with the carbon-carbon double bond or simply that C3 in androstanolone has a different conformation. Unfortunately, the literature is not so extensive that a distinction between conjugated and non-conjugated carbonyl and olefinic carbons is possible on the basis of the shielding tensor components. Also, the literature data for olefinic carbons has not been divided into those that carry a proton and those that are quaternary. The data above shows that there is significant difference between these two types of olefinic carbon, at least when conjugation is involved. The C4 atom is protonated and has a smaller anisotropy

(and of opposite sign) to that for C5, which is quaternary. Also the protonated carbons have a slightly larger asymmetry than the quaternary carbons.

The anisotropy data of C17 in androstanolone is in agreement with the literature value for an alcoholic carbon atom.

There are no ester carbons in these compounds with which to compare the literature value. In order to be certain of the assignment of C22, a ^{13}C enriched sample was prepared of cortisone acetate enriched at this position, and the shielding tensor components found. The sample was present as form II, but was also studied after being recrystallised as form IV_{aq}. The summary of these results is given in table 7.5.

As the anisotropy and asymmetry have characteristic values for certain carbon atom types (e.g. carbonyl, ester and olefinic carbons), these values may be used to identify a resonance. The literature values for the anisotropy and asymmetry along with those determined in this work on other steroids will be used to assign the high frequency region of the spectra of cortisone acetate. The assignment is made by comparing the anisotropy and asymmetry parameters obtained for a peak with those expected for specific carbon atom types. This has meant that resonances, particularly those of C5 and C22, cross-over between forms. It is expected that the shielding parameters for cortisone acetate may agree rather better with those of other steroids, rather than with those from the literature that are found from compounds of very different overall structure.

The results of the studies of shielding tensor components, anisotropy and asymmetry parameters for cortisone acetate are summarised in tables 7.6 - 7.13.

Table 7.6 - Summary of the shielding tensor data for cortisone acetate form I

δ_{iso}	210.8	204.9	202.9	175.7	169.9
$\Re$	99	94	109	106	-74
η	0.16	0.35	0.08	0.76	0.06
σ_{11}	-268	-269	-263	-268	-129
σ_{22}	-252	-235	-252	-189	-134
σ_{33}	-112	-111	-94	-70	-247
assignment	C11	C20	C3	C5	C22

Table 7.7 - Summary of the shielding tensor data for cortisone acetate form II

δ_{iso}	209.7	206.2	198.9	170.9	175.2
$\Im$	110	101	106	116	-78
η	0.18	0.32	0.25	0.71	0.47
σ_{11}	-274	-273	-265	-269	-118
σ_{22}	-255	-240	-239	-188	-155
σ_{33}	-100	-105	-93	-55	-253
assignment	C11	C20	C3	C5	C22

Table 7.8 - Summary of the shielding tensor data for cortisone acetate form III

δ_{iso}	210.3	209.8	205.9	203.8	203.0	198.2
$\Im$	110	106	102	105	121	104
η	0.11	0.08	0.11	0.23	0.07	0.12
σ_{11}	-271	-268	-262	-269	-268	-257
σ_{22}	-259	-258	-251	-244	-260	-243
σ_{33}	-101	-104	-104	-98	-82	-95
assignment	C11	C11	C20	C20	C3	C3
intensity	1	2	1	2	2	1

Table 7.9 - Summary of the shielding tensor data for cortisone acetate form III

δ_{iso}	174.4	173.7	171.5	170.5	167.0
$\Im$	-73	111	-79	-73	104
η	0.57	0.52	0.11	0.62	0.63
σ_{11}	-117	-258	-128	-114	-250
σ_{22}	-159	-201	-137	-155	-188
σ_{33}	-248	-63	-250	-243	-63
assignment	C22	C5	C22	C22	C5
intensity	1	2	1	1	1

Table 7.10 - Summary of the shielding tensor data for cortisone acetate form IV$_{aq}$

δ_{iso}	210.3	204.2	174.4	171.6
$\Im$	99	109	109	-80
η	0.31	0.25	0.73	0.00
σ_{11}	-275	-272	-268	-131
σ_{22}	-244	-245	-189	-131
σ_{33}	-112	-95	-66	-252
assignment	C20	C11/3	C5	C22

Table 7.11 - Summary of the shielding tensor data for cortisone acetate form IV_{et}

δ_{iso}	210.3	204.6	203.3	172.1	171.3
$\Re$	99	97	110	108	-74
η	0.26	0.33	0.15	0.67	0.00
σ_{11}	-273	-270	-267	-264	-134
σ_{22}	-247	-237	-250	-189	-134
σ_{33}	-111	-107	-93	-64	-246
assignment	C11	C20	C3	C5	C22

Table 7.12 - Summary of the shielding tensor data for cortisone acetate form IV_{ac}

δ_{iso}	210.1	205.6	198.6	168.4	171.2	214.1	207.2*
$\Re$	92	93	95	93	-74	87	128
η	0.20	0.29	0.11	0.69	0.15	0.14	0.11
σ_{11}	-266	-266	-252	-248	-128	-265	-279
σ_{22}	-246	-238	-241	-182	-141	-252	-265
σ_{33}	-118	-113	-103	-75	-245	-126	-79
assignment	C11	C20	C3	C5	C22	acetone	* solid acetone

* Solid Acetone[21] (at 87K, after correction for referencing)

Table 7.13 - Summary of the shielding tensor data for cortisone acetate form V_{aq}

δ_{iso}	209.5	210.4	201.6	171.1	171.8
$\Re$	107	98	109	101	-78
η	0.13	0.19	0.08	0.79	0.13
σ_{11}	-270	-269	-261	-260	-127
σ_{22}	-256	-250	-252	-182	-138
σ_{33}	-103	-112	-93	-71	-250
assignment	C11	C20	C3	C5	C22

These results show that the C5 and C22 carbons can easily be distinguished as C5 has a large, positive anisotropy and a large asymmetry, whilst the ester carbon, C22, has a smaller, negative anisotropy and a small asymmetry. These agree well with the expected values. The figures also show however, that the three carbonyl carbon atoms (C3, C11 and C20) are very difficult to distinguish. If one assumes that the resonances have not swapped over in forms I, II, IV_{et}, and IV_{ac}, then perhaps the only distinguishing feature is that generally, C20 has a slightly lower anisotropy and a slightly higher

asymmetry. The assignment of the high frequency region of the spectra of forms IV_{aq} and V_{aq} are particularly interesting. In form IV_{aq} two peaks are known to be coincident at 204.2 ppm from the double intensity of this peak. The slightly smaller anisotropy and larger asymmetry of the 210.3 ppm peak suggests that this may be from C20. This conclusion must be regarded as only tentative as the differences in anisotropy and asymmetry between the carbon types are small. In form V_{aq} the C20 resonance has moved to high frequency. The question is whether this resonance occurs at 209.5 or 210.4 ppm. The higher frequency peak has a smaller anisotropy and a slightly larger asymmetry than the other peak and so it is suggested that the high frequency peak is assigned to C20. Again this must be regarded as only a tentative assignment, and further evidence should be sought in order to confirm the assignment.

The assignment of the spectrum of form III is also very interesting and made even more difficult by the tripling of peaks due to there being three molecules in the crystallographic asymmetric unit. The peak integrals of the highest frequency peaks (from C3, C11 and C20) are consistent with there being no crossing over of peaks. They seem to show a trend of two peaks close together, and then one further away. The peaks at 205.9 and 203.8 ppm have slightly smaller anisotropies and larger asymmetries than most of the other peaks and so are assigned to C20. Again it must be stressed that these assignments are tentative. The assignment of the peaks from C5 and C22 are rather easier as ester and olefinic carbons have anisotropies of opposite sign. This region also shows the trend of two resonances close together whilst the other is shifted away.

The assignments that have been made on the basis of the shielding parameters will be discussed further in chapter 8.

7.5. The Effect Of Spinning Speed On The Centreband Intensity.

The centreband intensities alone have been used previously by workers in this group to make assignments of the C5 and C22 resonances of cortisone acetate[23]. However, their work relied upon the naive assumption that the

centreband intensity reflects in a simple manner the anisotropy of the nucleus at all spinning speeds. Therefore, an investigation was carried out as part of this project, to study the effect of spinning speed, anisotropy and asymmetry on the centreband intensity.

It has already been stated that the total intensity of the spinning sideband manifold is constant, and if there are more spinning sidebands present, each sideband will have a reduced intensity. There are three obvious factors that determine the number of sidebands that are present. The spinning sidebands are spaced at the spinning frequency, and so if the spinning speed is reduced, the separation of the sidebands goes down. This means that there are more spinning sidebands present and thus the intensity of the centreband goes down. However, at low spinning speeds the intensities of the sidebands follow, approximately, the shape of the powder pattern. So if the anisotropy goes up, more spinning sidebands will occur, and so again the intensity of the centreband is expected to go down. The asymmetry also affects the number of sidebands that occur. If the asymmetry is increased, then the width of the spinning sideband manifold increases, reducing the centreband intensity further. In order to find out if changes in centreband intensity can be easily and simply attributed to changes in the anisotropy and asymmetry, the centreband intensity, at a given spinning speed, has been studied as the anisotropy and asymmetry are varied.

A computer program, called SIMUL, based upon the one used to find the shielding tensor components was used to calculate the sideband pattern at a specific spinning speed, whilst the anisotropy and asymmetry are varied. A listing of the program SIMUL is given in Appendix 1. The calculated centreband intensity, the anisotropy and asymmetry are written to a file. The data are plotted on a three-dimensional graph with the computer program UNIPLOT, which is available in the University of Durham Computer Centre on the UNIX system. The variations in centreband intensity were studied at a range of spinning speeds (from 500 Hz to 1800 Hz at 100 Hz intervals). Figure 7.9 shows how the centreband intensity (at 1250 Hz, chosen as a typical 'slow' spinning speed)

varies as the anisotropy changes from 0 to 150 ppm, and as the asymmetry varies over the complete range from 0 to 1. As expected, as the anisotropy increases, the centreband intensity decreases. One can also see that the asymmetry has little effect on the centreband intensity. Figure 7.10 show the expanded region (anisotropies varying from 70 to 130 ppm) at spinning speeds of 1600, 1200, 1000, 800 and 500 Hz. This range of anisotropies was chosen as most of the high frequency peaks in the spectra of steroids have large anisotropies that fall within this range. Note that the graphs each have different vertical scales with respect to centreband intensity. The important points that are illustrated by the graphs are as follows:

i) 1600 Hz. At high spinning speeds, the centreband intensity varies predictably with changes in anisotropy and asymmetry. Generally the trend is that as the anisotropy increases, the centreband intensity decreases as a smooth curve. At low anisotropies (70 ppm), the centreband intensity decreases with increasing asymmetry. At higher anisotropies (130 ppm) the asymmetry has little effect on the centreband intensity.

ii) 1200 Hz. At this spinning speed the centreband intensity varies so that as the anisotropy increases, the centreband intensity decreases. At low anisotropies, an increase in the asymmetry causes a decrease in intensity, as expected. At higher anisotropies, an increase in asymmetry causes an increase in intensity. The overall result is that there is the beginnings of a plateau developing at high anisotropies and asymmetries.

iii) 1000 Hz. The graph is similar to that at 1200 Hz, only the features are more pronounced at the lower spinning speed. There is a sharp drop in intensity at high anisotropies and low asymmetries. There is also a shallow valley developing at high asymmetry and moderate anisotropy (ca. 90 ppm).

iv) 800 Hz. The plateau and valley have now disappeared. The graph shows that as the asymmetry increases, the centreband intensity also increases. This is not what would be intuitively expected.

Figure 7.9 - Showing variations in the centreband intensity with changing anisotropy and asymmetry. The lower graph shows the centreband intensity at a spinning speed of 1250 Hz and a wide range of anisotropies (0 - 150 ppm). The upper graph shows an expanded region (anisotropies of 70 - 130 ppm) at a spinning speed of 1600 Hz.

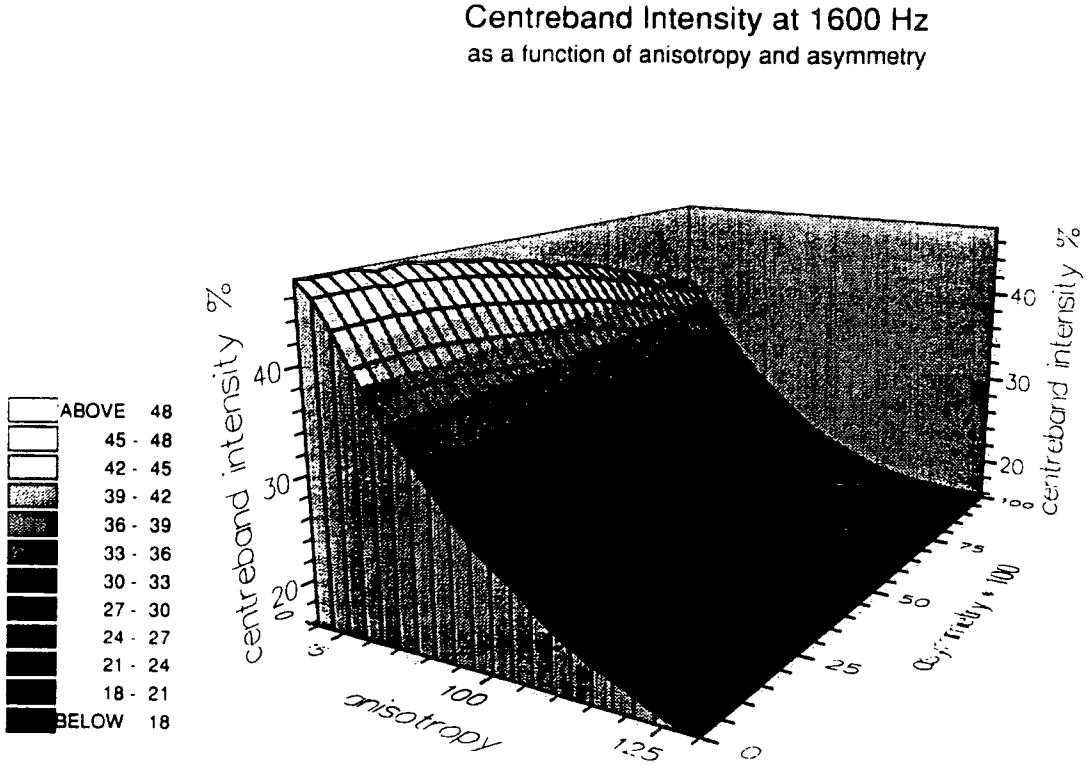

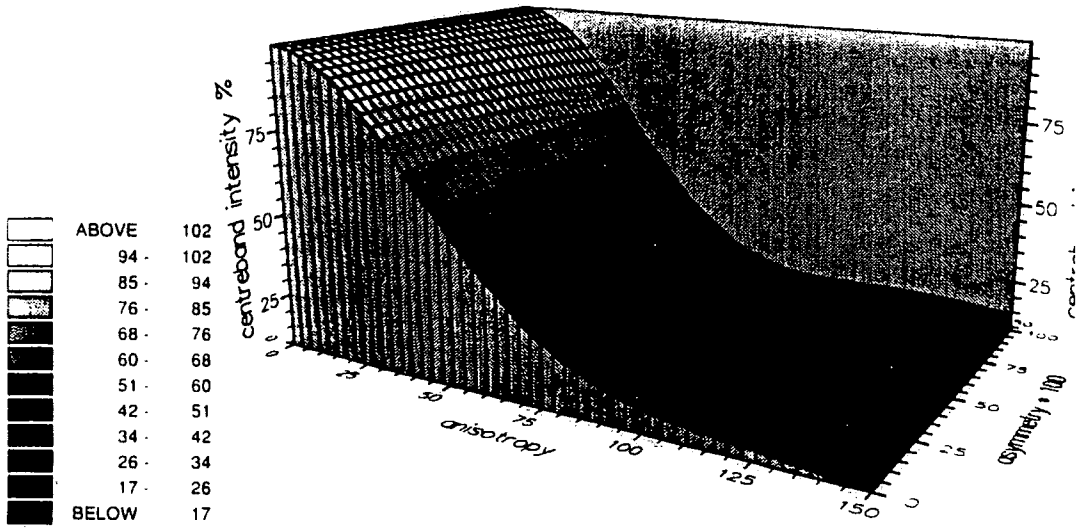

Figure 7.10 - Showing variations in the centreband intensity with changing anisotropy and asymmetry, at spinning speeds of 1200 Hz and 1000 Hz.

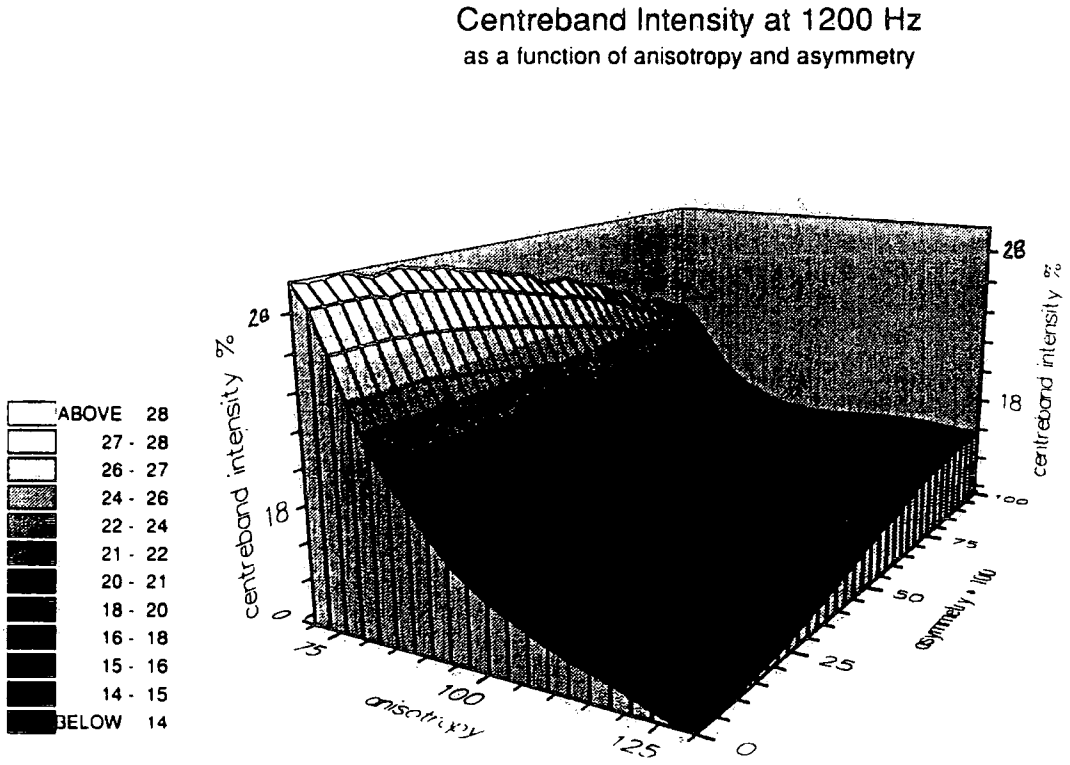

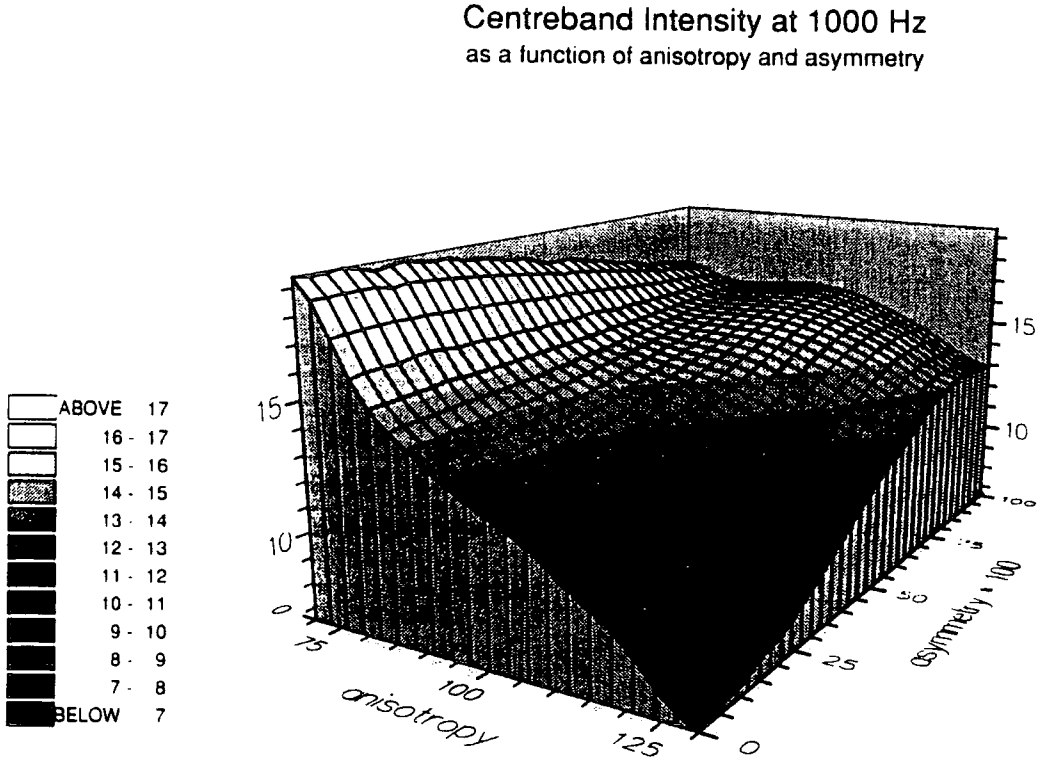

Figure 7.10 continued - Showing variations in the centreband intensity with changing anisotropy and asymmetry, at spinning speeds of 800 Hz and 500 Hz.

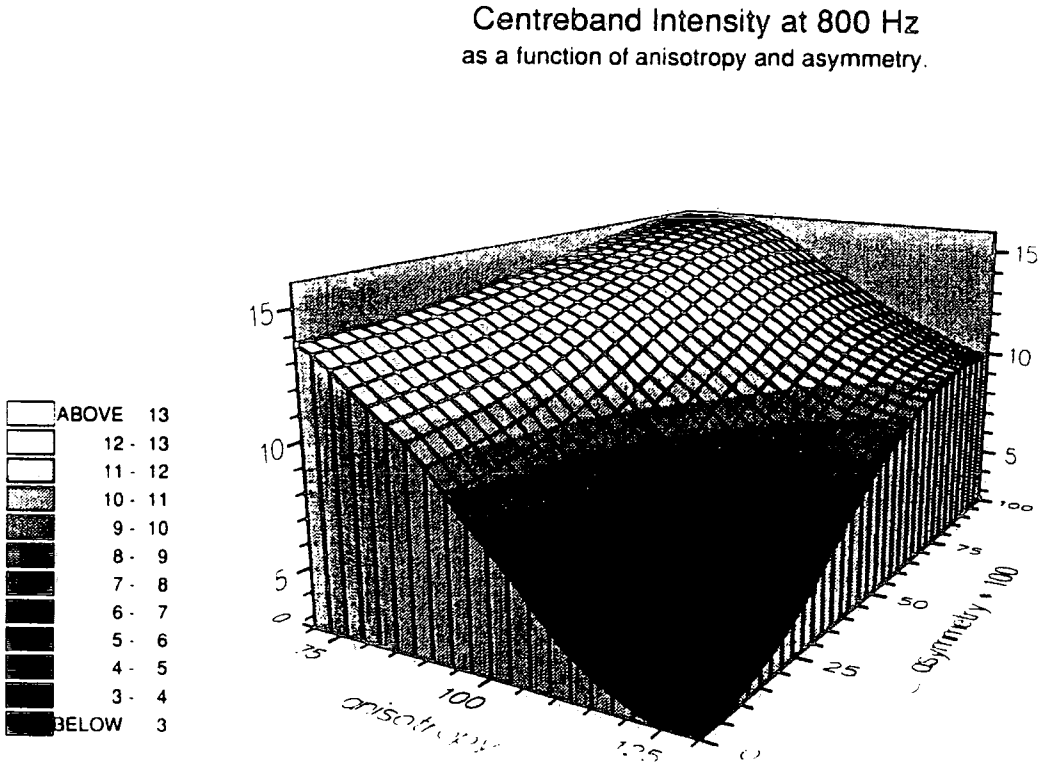

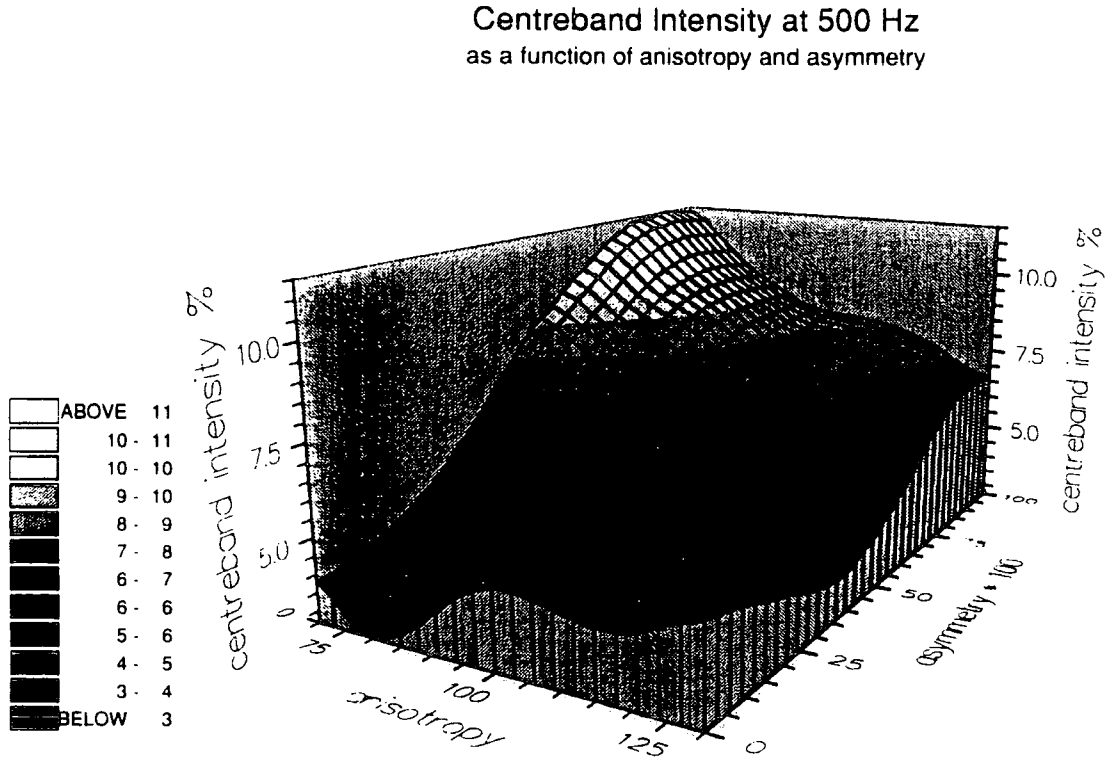

v) 500 Hz. At this low spinning speed the centreband intensity varies considerably as the anisotropy and asymmetry are varied. There are a number of local minima in the intensity. Generally the intensity does not vary in an easily predictable way.

The graphs show that, as expected, the centreband intensity decreases as the spinning speed decreases. However, the graphs also show that the initial assumptions (a) that as the anisotropy increases, the intensity of the centreband decreases, and (b) that as the asymmetry is increased, there is a reduction in the centreband intensity, are not necessarily correct in all circumstances. The assumptions are generally correct at higher spinning speeds (above 1200 Hz), but at low spinning speeds the intensity can vary considerably with changes in both anisotropy and asymmetry. Therefore at low spinning speeds it is inadvisable to make the assumption that a lower centreband intensity implies a larger anisotropy or asymmetry. However, it should be pointed out that at low spinning speeds, there are many sidebands and so the centreband intensity is very low. Therefore, small predicted changes in centreband intensity would, in most experiments, be within the experimental error of the measurement of the centreband intensity. An important principle has been demonstrated by this work, and that is that the anisotropy and asymmetry should be found by the full analysis of the sideband intensities of the entire sideband manifold, and not assumed to be larger or smaller that those of other peaks in the spectrum, based purely on the centreband intensity.

7.6. Conclusions

The measurement of shielding tensor components has allowed the high frequency region of the spectra of cortisone acetate polymorphs to be assigned. The C5 and C22 resonances are easily distinguishable, but the carbonyl resonances of C3, C11 and C20 have very similar tensor components, and their assignment must be regarded as only tentative.

The variation in the centreband intensity at different spinning speeds has been found to vary in a complicated manner (at low speeds) with changes in anisotropy and asymmetry. Therefore it is considered advisable to find the shielding tensor components in full when making assignments based upon anisotropy and asymmetry.

7.7. References

(1) Veeman, W.S. *Prog. NMR Spectr.* 16, 193 (1984).

(2) Harris, R.K. *Nuclear magnetic resonance spectroscopy*; Pitman: London, (1983).

(3) Shaw, D. *Fourier Transform NMR Spectroscopy;* 2nd ed.; Elsevier: Amsterdam, (1984); Studies in Physical and TheoreticalChemistry; Vol. 30.

(4) Mehring, M. *C-13 shielding tensors*; Springer-Verlag: Heidelburg, (1976); NMR Basic Principles and Progress; Vol. 11, pp 183.

(5) Lounila, J., Jokisaari J. In *Progress in NMR spectroscopy*; Eds. Emsley, J.W., Feeney, J. and Sutcliffe, L.H.; Pergamon: Oxford, (1983); Vol. 15; pp 249.

(6) Pines, A., Gibby M.G., Waugh J.S. *J. Chem. Phys.* 59, 569 (1973).

(7) Haeberlen, U. *High Resolution NMR in Solids: Selective Averaging*; Academic Press: New York, (1976); Advances in Magnetic Resonance; Vol. Supplement 1.

(8) Andrew, E.R., Bradbury A., Eades R.G. *Nature* 182, 1659 (1958).

(9) Lowe, I.J. *Phys. Rev. Lett.* 2, 285 (1959).

(10) Andrew, E.R., Firth M., Jasinski A., Randall P.J. *Phys. Lett.* 31A, 446 (1970).

(11) Clayden, N.J., Dobson C.M., Lian L.Y. *J. Magn. Reson.* 69, 476 (1986).

(12) Maricq, M.M., Waugh J.S. *J. Chem. Phys.* 70, 3300 (1979).

(13) De Groot, H.J.M., Smith S.O., Kolbert A.C., Courtin J.M.L., Winkel C., Lugtenburg J., Herzfeld J., Griffin R.G. *J. Magn. Reson.* 91, 30 (1991).

(14) Opella, S.J., Frey M.H. *J. Am. Chem. Soc.* 101, 5854 (1979).

(15) Bax, A., Szeverenyi N.M., Maciel G.E. *J. Magn. Reson.* 52, 147 (1983).

(16) Jakobsen, H.J., Ellis P.D., Inners R.R., Jensen C.F. *J. Am. Chem. Soc.* 104, 7442 (1982).

(17) Marchetti, P.S., Ellis P.D., Bryant R.G. *J. Am. Chem. Soc.* 107, 8191 (1985).

(18) Bai, H. Ph.D. Thesis, Univ. Durham, (1991).

(19) Merwin, L. Ph.D. Thesis, Univ. Durham, (1987).

(20) Harris, R.K., Jackson P., Merwin L.H., Say B.J., Hägel G. *J. Chem. Soc. Faraday Trans. I* 84, 3649 (1988).

(21) Pines, A., Gibby M.G., Waugh J.S. *Chem. Phys. Lett* 15, 373 (1972).

(22) Duncan, T.M. *A Compilation Of Chemical Shift Anisotropies*; Farragut Press: Chicago, (1990).

(23) Harris, R.K., Kenwright A.M., Say B.J., Yeung R.R., Fletton R.A., Lancaster R.W., Hardgrove G.L. Jnr. *Spectrochim. Acta* 46A, 927 (1990).

Chapter 8

Cortisone Acetate Conclusions

Chapter 8 Cortisone Acetate Conclusions

8.1. Introduction

The aim of much of the work on cortisone acetate has been to assign the solid-state NMR spectra. The solution-state NMR spectrum has been fully assigned for comparison. The solid-state NMR techniques that have been used to make assignments are NQS (with varying lengths of decoupling window), slow spinning and determination of the shielding anisotropy and asymmetry, single pulse experiments and variable contact cross-polarisation. The aims of the experiments can be summarised as follows:

i) NQS: to identify quaternary and methyl carbon atoms

ii) NQS (with a variable decoupling window): to identify CH_2 and CH carbons

iii) single pulse: to identify solvate molecules

iv) variable contact cross-polarisation: to distinguish CH, CH_2, CH_3 and quaternary carbon atoms

v) shielding anisotropy: to distinguish peaks with distinctive anisotropies and asymmetries (usually quaternary carbon atoms).

The peak assignments are given in table 8.1.

The ultimate aim of this work is to deduce crystallographic information from the solid-state NMR spectrum. Therefore, first the known crystal structures[1-4] must be related to the spectra, before going on to make predictions about other forms, where the crystal structure is not known.

Table 8.1 - The peak assignments from cortisone acetate polymorphs. Chemical shifts are given in ppm.

C no.	soln	I	II	III			IV_{ac}	IV_{et}	IV_{aq}	V_{aq}
11	208.7	210.8	209.7	210.2	209.7‡		210.1	210.3	210.3	209.6
20	204.3	204.9	206.2	205.8	203.7‡		205.6	204.6	204.2‡	210.4
3	199.6	202.9	198.9	203.0‡	198.2		198.5	203.3	204.2‡	201.9
5	168.4	175.7	171.0	173.7‡	167.0		168.4	172.2	174.3	171.2
22	170.4	169.8	175.2	174.3	171.5	170.5	171.1	171.3	171.6	171.9
4	124.5	126.2	123.6	125.6	125.1	124.6	125.2	124.8	124.1	124.8
17	88.8	88.8	89.4	89.2¶			89.3	89.3	89.3	89.5
21	67.3	68.4	70.6	70.1	69.7	68.8	69.9	69.4	69.1	69.6
9	62.5	62.8	63.6	64.5	64.3	60.8	64.1	63.5	63.1	63.6
13	51.2	49.8	52.5	52.5	50.6§		51.6	51.4	51.1	51.7
14	49.7	50.5	50.5	51.2	50.3		50.7	50.7	50.6‡	50.8
12	49.9	53.3	50.3	48.3			50.4	50.4	50.6‡	50.3
10	38.2	40.1	38.8	40.9	39.2		39.2	39.7	40.0	39.6
8	36.5	36.5	37.9	38.5			37.0	37.3	37.5	37.3
1	32.3		36.7				36.4	35.8	35.2	
2	34.8		34.9	36.6	35.9		34.7	35.4	34.5	35.9
6	33.7	34.0	33.7	37.5	34.3	33.4	34.0	33.5	33.2	35.2
7	32.2		33.2	35.1			32.8	33.1	32.5	32.9
16	35.0		31.8					32.6		
15	23.2	26.0	24.7	24.4¶			23.9	23.9	24.7	23.8
23	20.3	21.4	20.6	21.4	21.1	20.5	20.0	19.6	20.7	19.7
19	17.2	17.7	16.5	18.5	17.9		18.6	18.6	18.5	18.5
18	15.4	15.7		15.7¶	14.6		15.4	16.0	16.3	15.7
solvate							214.1 31.8	59.1 18.6		

Notes: ‡ shows a double intensity peak, ¶ a triple intensity peak and § a quintuple intensity peak.

8.2. Conformation

In chapter 6, the conformations of the molecules were compared. Forms II, IV_{aq} and V_{aq} have almost the same conformation, whilst form I has a different conformation in the A- and D-rings, and also in the side chain. In particular the

different conformations of the D-ring were illustrated: form I is a 13β-envelope (i.e. four atoms in a plane, with C13 out of the plane), and forms II, IV_{ac} and V_{aq} have 13β,14α-half chair conformations (with three atoms in a plane and C13 and C14 out of the plane). Therefore, differences in chemical shift at any carbon atom in the D-ring may be distinctive of the adopted conformation.

Table 8.2 - The chemical shifts (in ppm) of atoms in the D-ring

Carbon atom	I	II	IV_{ac}	V_{aq}	comments	average difference‡
C13	49.8	52.5	51.6	51.7	form I to low frequency	2.1
C14	50.5	50.5	50.7	50.8	all shifts are very similar	~0
C15	26.0	24.7	23.9	23.8	form I to high frequency	1.9
C16	not unambiguously assigned				-	-
C17	88.8	89.4	89.3	89.5	form I to low frequency	0.6

Notes: ‡ the average difference is that of the chemical shift of form I from those in the other three forms.

These differences between form I and forms II, IV_{ac} and V_{aq} may be coincidental. But as the similarities between forms II, IV_{ac} and V_{aq} are quite good, it may be assumed that the chemical shifts reflect the conformation of the D-ring. Therefore, can any conclusions be drawn about the D-ring conformation in the forms where the crystal structure is not known? No other C15 atom has such a high chemical shift as in form I. Neither of forms IV_{aq} or IV_{et} show a low frequency resonance for C13. However, the double intensity peak for C13 in form III is to lower frequency (although it is still 0.8 ppm higher than form I). The differences at C17 are too small to allow extrapolation of the trend to other forms (particularly when one bears in mind that chemical shifts are only known to an accuracy of ca. 0.5 ppm by external referencing). Therefore, the conclusion must be that no other form shows any clear evidence in the chemical shifts of the D-ring that this ring adopts the 13β-envelope, as in form I. As the chemical shifts are generally rather closer to those of forms II, IV_{ac} and V_{aq}, I tentatively suggest that the other polymorphs adopt the 13β,14α-half chair conformation of the D-ring. The A-ring conformation in form I is only slightly different from the other known forms, and as C1 and C2 are not identifiable, and C3, C4 and C5 are

likely to be influenced by hydrogen bonding and varying conjugation, no conclusions may readily be drawn regarding the exact A-ring conformation. The side chain conformation is variable between all forms (although quite similar in forms II, IV_{ac} and V_{aq}), and as there is the possibility of hydrogen bonding at C20 and C22, it is not possible to determine conformational information of the side chain.

8.3. Hydrogen Bonding

When one compares the chemical shifts for any particular carbon atom between forms, in most cases the shifts are generally quite similar. However, wider variations in chemical shift are apparent for the high frequency peaks C3, C4, C5, C11, C20 and C22. These carbon atoms are part of the functionalities of the molecule, and therefore might be expected to show more variation in chemical shift as the functional groups interact with those nearby. The main differences between C3, C11, C20 and C22 will arise when these groups are involved in hydrogen bonding, and differences at C3, C4 and C5 will also arise with the effect of varying conjugation. The position of the hydrogen bonds is known for the forms where the crystal structure has been determined. This information is given in table 8.3.

Table 8.3 - The modes and lengths of hydrogen bonds[1-4].

form	mode of hydrogen bonding	bond length / Å
I	C(17)-OH···O=C(3)	2.761
II	C(17)-OH···O=C(22)	2.757
IV_{ac}	C(17)-OH···O=$C(CH_3)_2$	2.801‡
	C(17)-OH···O=$C(CH_3)_2$	2.59‡
V_{aq}	C(17)-OH···OH_2	2.742
	HOH···O=C(3)	2.87

Notes: ‡ the acetone molecule occupies two sites, with occupancy in a ratio of 2:1. The molecule involved in the longer bond has double the site occupancy of the one with the shorter bond.

Now C22 has been definitely assigned from its distinctive anisotropy and asymmetry. In form II, the chemical shift of this atom (175.2 ppm) is much

higher in frequency than the other peaks (typically 171 ppm, except for one peak in form III). Of particular significance is that the chemical shift in the solid is much higher than in solution (by 4.8 ppm), which will generally not be involved in hydrogen bonds. A high frequency shift caused by hydrogen bonding can be explained naively as follows: the electrophilic hydrogen atom withdraws electron density away from the oxygen atom. But as oxygen is more electronegative than the carbon atom to which it is bonded, electrons will be withdrawn from the double bond, thereby reducing the electron density at the carbon atom. The chemical shift is affected by the shielding of the nucleus, from the applied magnetic field, by the electrons. If the electron density is reduced, the nucleus is deshielded, and so experiences a stronger magnetic field that increases the Zeeman splitting of the nuclear magnetic moments and thus the transition frequency is increased. Hence the formation of a hydrogen bond causes the nucleus to resonate at a higher frequency by typically[5] 2-4 ppm.

One resonance of form III at C22 is at a high frequency, similar to that of form II. Therefore, it is proposed based upon isotropic chemical shifts, that only form II and one molecule of form III are involved in hydrogen bonds at C22. A similar high frequency shift might be expected for C3 in forms I and V_{aq} (compared with solution and forms II and IV_{ac}, none of which are involved in hydrogen bonds at this position) - see table 8.4.

Table 8.4 - Chemical shifts (in ppm) of C3

non-hydrogen bonded			hydrogen bonded	
solution	form II	form IV_{ac}	form I	form V_{aq}
199.6	198.9	198.5	202.9	201.9

The difference in chemical shift is quite striking. Thus it should be possible to predict the mode of hydrogen boding in the other forms. Forms IV_{et} and IV_{aq} each show high frequency positions, along with the double intensity peak of form III. The single intensity peak of form III occurs to low frequency. Therefore it is predicted that forms IV_{et}, IV_{aq} and two molecules of form III are hydrogen bonded via C3. The other form III molecule is not hydrogen bonded at C3.

Carbon atoms C11 and C20 are also possible sites that may be involved in hydrogen bonding. The chemical shifts of all C11 atoms show very little variation. The case is the same with the C20 chemical shifts except that the C20 resonance in form V_{aq} has shifted to high frequency (even if the C11 and C20 assignments, which are not certain, are transposed). The reason for such a large frequency shift is unknown. This atom is not involved in hydrogen bonding, the side chain conformation is the same as that in forms IV_{ac} and no such shift is seen in this molecule. Therefore the difference must be attributed to packing effects (which are not very well understood).

Therefore the mode of hydrogen bonding in each form is summarised in table 8.5.

Table 8.5 - Summary of the modes of hydrogen bonding

form	mode of bonding	comments
I	C(17)-OH···O=C(3)	known from the crystal structure
II	C(17)-OH···O=C(22)	known from the crystal structure
III ‡	C(17)-OH···O=C(3)	predicted based on δ_{iso}
III ‡	C(17)-OH···O=C(3)	predicted based on δ_{iso}
III ‡	C(17)-OH···O=C(22)	predicted based on δ_{iso}
IV_{ac}	C(17)-OH···O=C(CH_3)2	known from the crystal structure
IV_{et} §	(C(17)-OH)···(EtOH)···O=C(3)	predicted based on δ_{iso}
IV_{aq} §	(C(17)-OH)···(H_2O)···O=C(3)	predicted based on δ_{iso}
V_{aq}	C(17)-OH···H_2O···O=C(3)	known from the crystal structure

Notes: δ_{iso} is the isotropic chemical shift.

‡ For form III, it is not known if the proposed hydrogen bonds are formed with one per molecule, or whether one molecule forms two bonds whilst another does not form any hydrogen bonds.

§ For forms IV_{et} and IV_{aq} the C17 and solvate molecules are in brackets because the exact mode of bonding is not known. For these two forms, there may be two hydrogen bonds present, as shown, or only one, in which case the bond could be to either C17 or the solvate molecule.

Note that there is very little variation in the chemical shift of C17. Therefore, modes of hydrogen bonding have been proposed for each form that

involve the hydroxyl group, and so it is not surprising that the chemical shifts should be similar.

8.4. The Effect of Hydrogen Bonding on the Shielding Tensor Components

The effect of the formation of hydrogen bonds on the isotropic chemical shift has been explained in terms of the deshielding of the nucleus. Therefore, the different shielding experienced by the nuclei in the hydrogen bonded and non-bonded situations should be reflected, in some way, in the shielding tensor components. This effect has indeed been observed. The effect of hydrogen bonding upon the shielding tensor components of a few compounds has previously been studied[6-12]. The general view is that σ_{22} tends to lie along (or close to) the C=O bond, with σ_{11} also in the sp^2 plane, perpendicular to σ_{22}, and σ_{33} is perpendicular to the sp^2 plane, being orthogonal to the other two axes. In Meldrums acid[11], σ_{22} shows a high frequency shift of 40 ppm when compared with malonic acid (which is not hydrogen bonded). Similarly, σ_{22} in hydrous oxalic acid[6] shows a high frequency shift when compared with that in anhydrous oxalic acid (which is more weakly hydrogen bonded). A reference to the study of dimedone[10] puts σ_{11} along the C=O bond, and this component experiences a high frequency shift when compared with similar non-bonded compounds. However, there are many more references that place σ_{22} along the C=O bond in carbonyl and ester groups. There are many examples of hydrogen bonding being accompanied by a high frequency shift in the isotropic chemical shift[13-15]. If σ_{22} is the only tensor component that is affected by hydrogen bond formation, then a 2-4 ppm shift in the isotropic chemical shift will cause a 6-12 ppm shift in σ_{22} (as $\delta_{iso} = -\frac{1}{3}(\sigma_{11} + \sigma_{22} + \sigma_{33})$).

The effect of the formation of a hydrogen bond upon the shielding tensor components may be explained by the electrophilic hydrogen withdrawing electrons from the C=O bond, and as σ_{22} lies approximately along this bond, σ_{22}

is the tensor component that is most affected by the formation of the hydrogen bond.

For the most part of this work it will be more convenient to refer to the chemical shift anisotropy (described by tensor components δ_{ii}) rather than the shielding anisotropy (with tensor components σ_{ii}). In chapter 7 it was stated that the relationship between shielding and chemical shift anisotropy is described by $\delta_{ii} = -\sigma_{ii}$. The δ_{22} components for cortisone acetate polymorphs are presented in table 8.6.

Table 8.6 - The δ_{22} components of cortisone acetate polymorphs

form	C11	C20	C3	C22
I	252.1	235.2	252.3	133.9
II	254.7	240.4	238.8	154.5
III	259.0	251.4	259.6‡	158.8
III	258.1‡	244.3‡	243.4	136.8
III				154.8
IV_{et}	246.9	239.2	250.0	134.2
IV_{ac}	246.2	238.4	240.0	140.5
IV_{aq}	245.3	245.2	245.3	131.4
V_{aq}	255.6	249.6	251.8	138.1

‡ denotes a double intensity peak in form III

For C3, the tensor component δ_{22} is clearly higher for those forms that are known to be hydrogen bonded (i.e forms I and V_{aq}), at about 252 ppm, compared with those that are known not to be involved in hydrogen bonding (i.e. forms II and IV_{ac}) at about 239 ppm. Therefore, the presence, or absence of hydrogen bonds may be predicted for the forms where the mode of bonding is not already known. The double intensity peak for form III and the resonance for form IV_{et} fall clearly in to the high frequency group, thereby implying hydrogen bonding at C3. The single intensity peak in form III is clearly in the low frequency group (therefore it is not bonded at C3). Form IV_{aq} falls inbetween these two ranges, and so it is not clear whether this carbonyl group is involved in hydrogen bonding. This ambiguity may be resolved. The C3 resonance overlaps with that of C11, and so tensor components found for the combined peak would be the

average of those for the two individual resonances. Therefore the intermediate value of δ_{22} for form IV_{aq} indicates that one of C3 or C11 is involved in hydrogen bonding. The tensor components alone do not allow one to be distinguished from the other. However, the isotropic chemical shift of C3 has moved to high frequency, whilst that of C11 is close to that of the non-bonded solution-state. Therefore a reasonable conclusion is that C3 is involved in a hydrogen bond, and that δ_{22} has moved to high frequency, although the exact value may not be found.

For C22, the tensor component δ_{22} is shifted to high frequency in form II, when compared with forms I, IV_{ac} and V_{aq}. This is as expected. Other forms that fall into the low frequency group (130-140 ppm) are forms III (single intensity), IV_{et} and IV_{aq}. Two peaks from form III occur at high frequency (154-158 ppm).

For C11, none of the forms with known crystal structures, are hydrogen bonded at this position. For these forms δ_{22} = 246-256 ppm. The δ_{22} component for all other forms fall within , or close to this range. The situation is similar at C20. Therefore no hydrogen bonds are predicted to occur at either C11 or C20 in any forms. One must recognise, however, that the ranges of δ_{22} values for C11 and C20 are quite wide and could conceal the effect of hydrogen bonding on the tensor components in other forms.

The hydrogen bonds are summarised as follows:

Table 8.7 - Known and predicted hydrogen bonds

form	hydrogen bonding based on δ_{22}		hydrogen bonding based on the isotropic shift	
I	C3	‡	C3	‡
II	C22	‡	C22	‡
III	C3	two molecules	C3	two molecules
III	C22	two molecules	C22	one molecule
IV_{et}	C3		C3	
IV_{aq}	C3		C3	
IV_{ac}	acetone	‡	acetone	‡
V_{aq}	C3	‡	C3	‡

Note: ‡ signifies that the mode of hydrogen bonding is known from the crystal structure.

The hydrogen bonds proposed based upon the values of the chemical shift tensor component δ_{22}, are generally in agreement with those predicted by the isotropic chemical shift. The case of form III is worthy of further comment. The chemical shift tensor component, δ_{22}, allows one to predict the presence of four hydrogen bonds per asymmetric unit. However, it is not clear how the hydrogen bonds are distributed amongst the molecules. It is possible that two molecules each form two hydrogen bonds (at C3 and C22) and that the other molecule in the asymmetric unit forms no hydrogen bonds. It is also possible that only one molecule is involved in two bonds, whilst the other two molecules are each involved in only one bond. Now, the isotropic shift suggests that there are two bonds via C3 and one via C22. This contradicts the proposed hydrogen bonding based upon δ_{22}. So which method will be the most reliable? The isotropic chemical shift can be found unambiguously from the spectrum (the accuracy being dependent upon the method of external referencing of peaks). However the chemical shift tensors are found by fitting experimental and theoretical slow spinning spectra. The quality of the fitting depends upon the quality (S/N ratio) of the spectrum. The value of δ_{22} is also dependent, as with the isotropic chemical shift, upon the method of external referencing of peaks. Also as the orientation of the chemical shift tensors is not found, only assumed, then if δ_{22} is not along the C=O bond, δ_{22} will not be a suitable method for predicting the mode of hydrogen bonding in the samples. Therefore, on balance, the predictions based upon the isotropic chemical shift should be given greater weight.

Now that the positions of hydrogen bonds have been predicted, can one say anything about the strength of the bonds? A relationship between chemical shift and hydrogen bond length has been established for homopolypeptide chains[16]. If a similar relationship can be established, then it might be possible to predict not only the presence of hydrogen bonds, but also their length.

The hydrogen bonding in a number of steroids has been studied. The results are presented in table 8.8. In order to take account of different underlying chemical shifts of carbonyl and ester carbons, the difference between the solid and solution state chemical shifts (Δ) has been calculated, and this is plotted, in figure 8.1, against the hydrogen bond length.

Table 8.8 - The chemical shifts and hydrogen bond lengths of selected steroids.

compound	form		δ (solid)	δ (solution)	Δ/ ppm	length/Å
cortisone	I	C3	202.9	199.6	3.3	2.761
acetate	II	C22	175.2	170.4	4.8	2.757
	V_{aq}	C3	201.9	199.6	2.3	2.87
testosterone	α	C3	200.6	199.3	1.3	3.00
	α	C3	202.1	199.3	2.8	2.793
	δ	C3	201.8	199.3	2.5	2.98
androstanolone	anhydrous	C3	215.6	211.7	3.9	2.75
	anhydrous	C3	215.6	211.7	3.9	2.82
	hydrate	C3	215.4	211.7	3.7	2.83

Figure 8.1 - Graph of hydrogen bond lengths (in Å) vs. difference from solution of the chemical shift

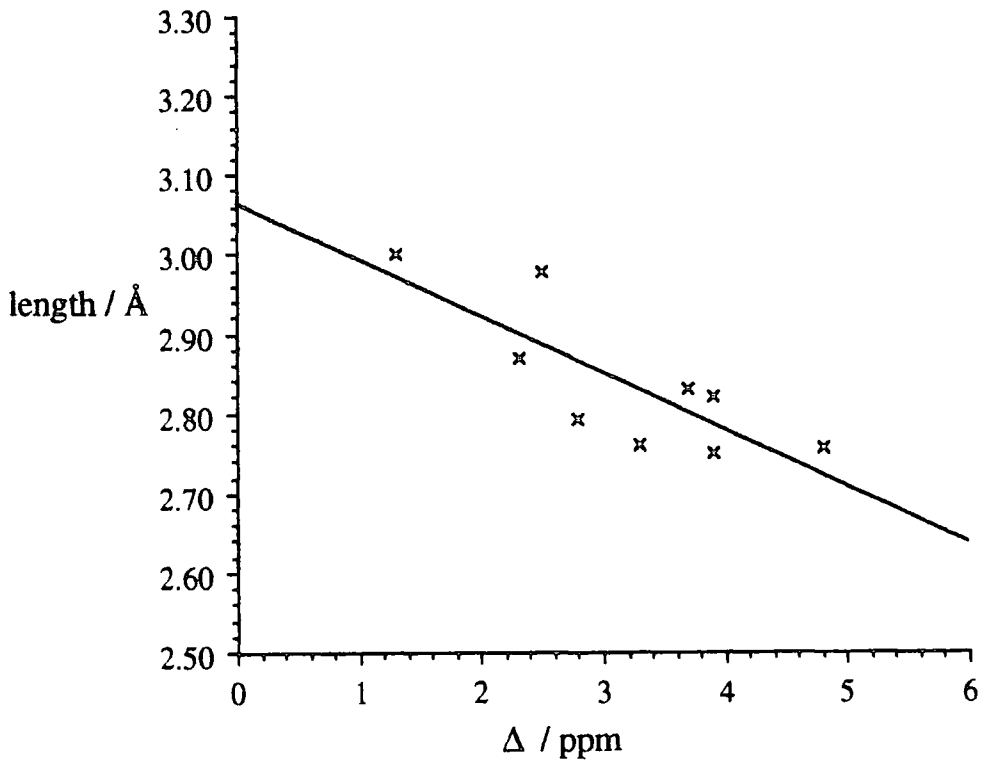

The graph clearly shows a trend that as the hydrogen bond becomes stronger (i.e. shorter bond lengths), there is an increase in Δ. This means that the solid-state chemical shift has increased. This is consistent with the explanation already given regarding the deshielding of the carbon nucleus.

The straight line is that of the least squares fit of the data. The equation of the line is $y = -0.071x + 3.07$ ($R^2 = 0.65$). The correlation of the data with the line is quite low, but this is not surprising when one considers that the packing and conformation will be slightly different in these compounds. The line may now be used to estimate the hydrogen bond lengths for those forms for which the crystal structure is not available. The results are summarised in table 8.9.

Table 8.9 - Predicted hydrogen bond lengths

form		solid-state chemical shift	solution-state chemical shift	Δ / ppm	predicted length / Å
III	C3	203.0	199.6	3.4	2.83 ± 0.05
III	C22	174.3	170.4	3.9	2.79 ± 0.05
IV_{et}	C3	203.3	199.6	3.7	2.81 ± 0.05
IV_{aq}	C3	204.2	199.6	4.6	2.74 ± 0.05

The error is estimated from the scatter of the data about the straight line. Of course, this data does not provide an accurate means of estimating the hydrogen bond lengths, but it does give an indication of the length of the predicted bonds.

8.5. The Effect of Conjugation on Isotropic Chemical Shifts

The isotropic chemical shift of C3, C4 and C5 atoms has been studied with respect to conjugation. The chemical shifts of C3 and C5 have been plotted in figure 8.2.

Figure 8.2 - Graph of chemical shift of C3 vs. that of C5

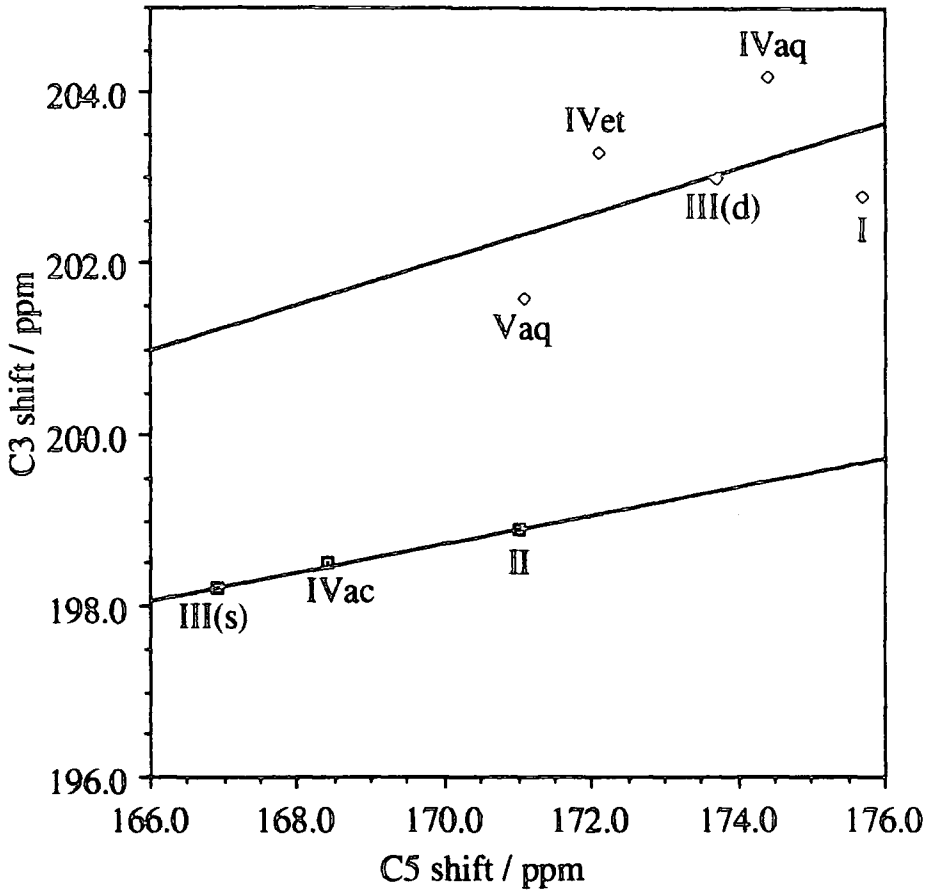

The graph shows that as the chemical shift of C3 increases, so does the shift of C5. This is the effect of conjugation. As the degree of conjugation increases, the chemical shifts of both C3 and C5 rise. However, it can also be seen clearly from the graph that the resonances fall into two groups. Of the lower group forms II and IV_{ac} are known to be not hydrogen bonded via C3, whilst of the upper group forms I and V_{aq} are hydrogen bonded via C3. So one might suggest that the other polymorphs in a particular group may follow a similar hydrogen bonding scheme. Therefore forms I, IV_{aq}, IV_{et} and the double intensity peak of form III (in the upper group) might all be involved in hydrogen bonding via C3, whilst the single intensity peak of form III (in the lower group) are not.

For the forms where the crystal structure is known, the torsion angle of the conjugated system is known. These data are given in table 8.10.

Table 8.10 - Torsion angles about the conjugated system in cortisone acetate.

form	O(3)-C(3)-C(4)-C(5) torsion angle
I	-172.6°
II	-176.6°
IV_{ac}	-175.4°
V_{aq}	-179.3°

For the non-hydrogen bonded carbon atoms, the three points on the graph of chemical shift of C3 vs. C5 fall close to a straight line. It might be possible in this case to relate the chemical shifts of C3 or C5 to the torsion angle. Torsion angles of 0 (or -180°) show that the atoms are coplanar. If the atoms are coplanar, then the conjugation is likely to be the greatest in this case.

Figure 8.3 - Graph of chemical shift of C3+C5 vs. torsion angle.

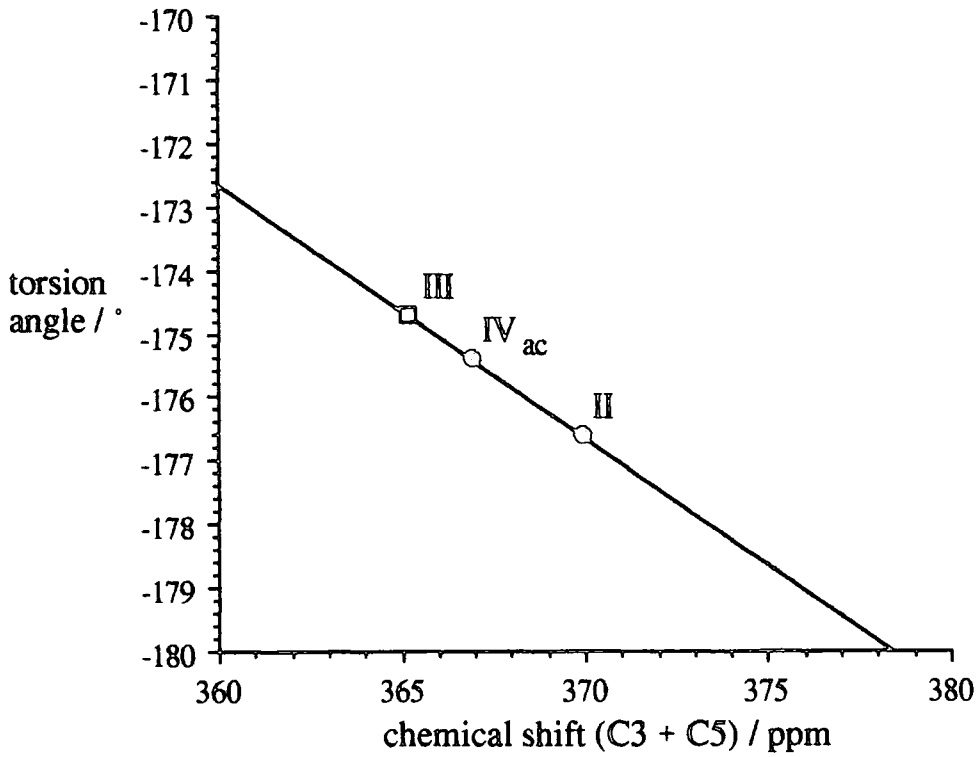

The effect of increasing conjugation on the chemical shifts of C3 and C5 will be to deshield these nuclei, as electron density is withdrawn from the double bonds, and towards the central single bond. Therefore, the chemical shift of the C4 atom will be shielded, and consequently move to lower frequency. This effect is observed, with C4 in form II resonating to lower frequency (at 123.6 ppm) compared with form IV_{ac} (at 125.2 ppm).

The torsion angle for one molecule in form III is predicted to be -174.7°. The error in such an estimation is likely to be quite large as there is so little data available with which to compare.

For the case of the hydrogen bonded carbonyls, the chemical shifts are influenced by the strength of the hydrogen bond and so no simple relationship between torsion angle and chemical shift is available.

8.6. References

(1) Declercq, J.P., Germain G., van Meerssche M. *Cryst. Struct. Commun.* 1, 59 (1972).

(2) Kanters, J.A., de Koster A., van Geerestein V.J., van Dijck L.V. *Acta Cryst.* C41, 760 (1985).

(3) van Geerestein, V.J., Kanters J.A. *Acta Cryst.* C43, 936 (1987).

(4) van Geerestein, V.J., Kanters J.A. *Acta Cryst.* C43, 136 (1987).

(5) Etter, M.C., Hoye R.C., Vojta G.M. *Cryst. Reviews* 1, 281 (1988).

(6) Griffin, R., Pines A., Pausak S., Waugh J. *J. Chem. Phys.* 63, 1267 (1975).

(7) Torman, J.v.D., Veeman W., Boer E.d. *J. Magn. Reson.* 32, 49 (1978).

(8) Veeman, W. *Phil. Trans. R. Soc. Lond.* A299, 629 (1981).

(9) Nagaoka, S., Terao T., Imashiro F., Saika A., Hirota N., Hayashi S. *Chem. Phys. Lett* 80, 580 (1981).

(10) Takegoshi, K., Naito A., McDowell C. *J. Magn. Reson.* 65, 34 (1985).

(11) Takegoshi, K., McDowell C.A. *J. Am. Chem. Soc.* 108, 6852 (1986).

(12) Jagannathan, N.R. *Magn. Reson. Chem.* 27, 941 (1989).

(13) Imashiro, F., Maeda S., Takegoshi K., Terao T., Saika A. *Chem. Phys. Lett* 92, 642 (1982).

(14) Imashiro, F., Maeda S., Takegoshi K., Terao T., Saika A. *Chem. Phys. Lett* 99, 189 (1983).

(15) Imashiro, F., Maeda S., Takegoshi K., Terao T., Saika A. *J. Am. Chem. Soc.* 109, 5213 (1987).

(16) Ando, S., Ando I., Shoji A., Ozaki T. *J. Am. Chem. Soc.* 110, 3380 (1988).

Chapter 9

Beclomethasone Dipropionate

Chapter 9 Beclomethasone Dipropionate

9.1. Introduction

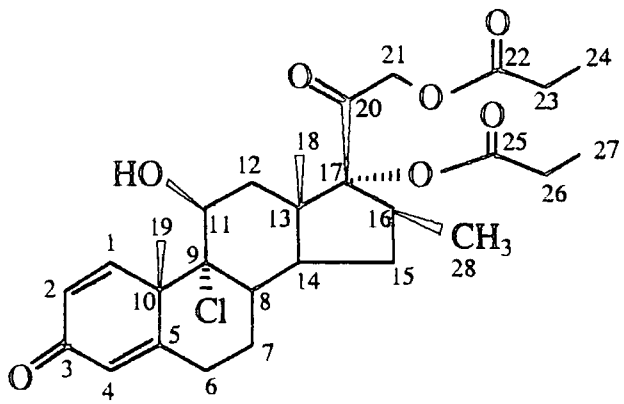

Beclomethasone dipropionate (BDP) is an important substance in the pharmaceutical industry as an anti-inflammatory agent. It was identified by infra red spectroscopy as existing in three main forms: anhydrous, monohydrate, and several solvates. The IR spectra are shown in figure 9.1 - for comparison purposes, the spectra of solvates with organic solvents are included. Many solvents can be incorporated in the crystal[1] including alkanes (5 to 8 carbon atoms long), alcohols (2 to 5 carbon atoms long), ethers and ketones (each 2 to 5 carbon atoms long), and halo-alkanes (1 to 2 carbon atoms and containing various combinations of hydrogen, fluorine, chlorine and bromine). Indeed, the most interesting aspect of the study of BDP solvates might be considered to be that non-stoichiometric amounts of these solvents can be incorporated in the solid and that they can be lost progressively (as measured by elemental microanalysis and quantitative gas chromatography). Similarities in the IR spectra have lead to the proposal that the solvates with organic solvents share a common crystal structure. Accordingly, single crystal X-ray studies of the anhydrate, monohydrate and ethyl acetate solvate have been done to determine the crystal structures[1,2]. The crystal structure information is summarised in table 9.1.

Figure 9.1 - The infra-red spectra of BDP polymorphs recorded from nujol mulls at 2 cm^{-1} resolution (a) anhydrate, (b) monohydrate, (c) ethyl acetate solvate and (d) Arcton solvate for comparison (opposite page).

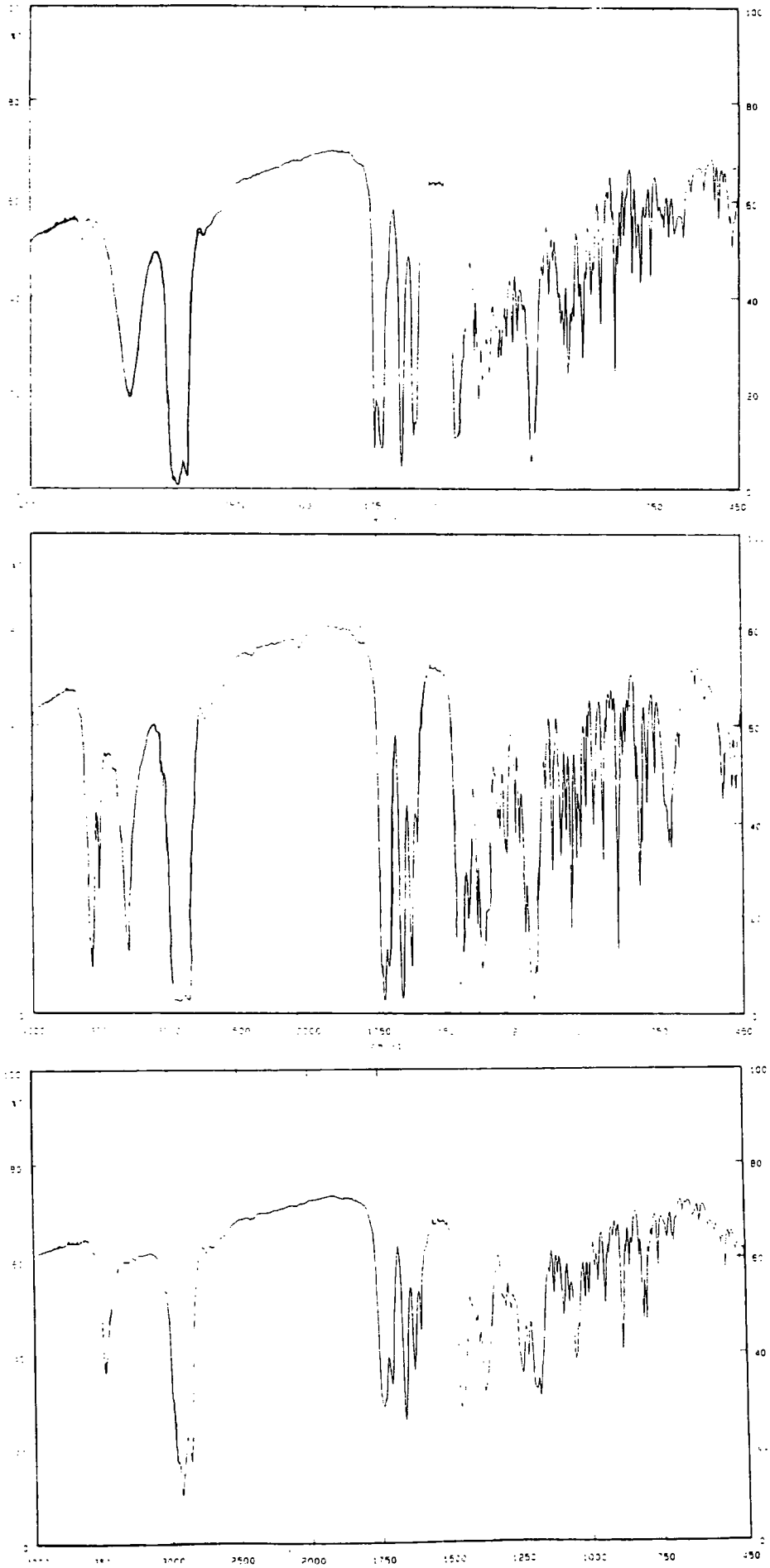

Figure 9.2 - Showing the modes (and lengths) of hydrogen bonds in BDP polymorphs (a) anhydrate, (b) monohydrate and (c) ethyl acetate solvate

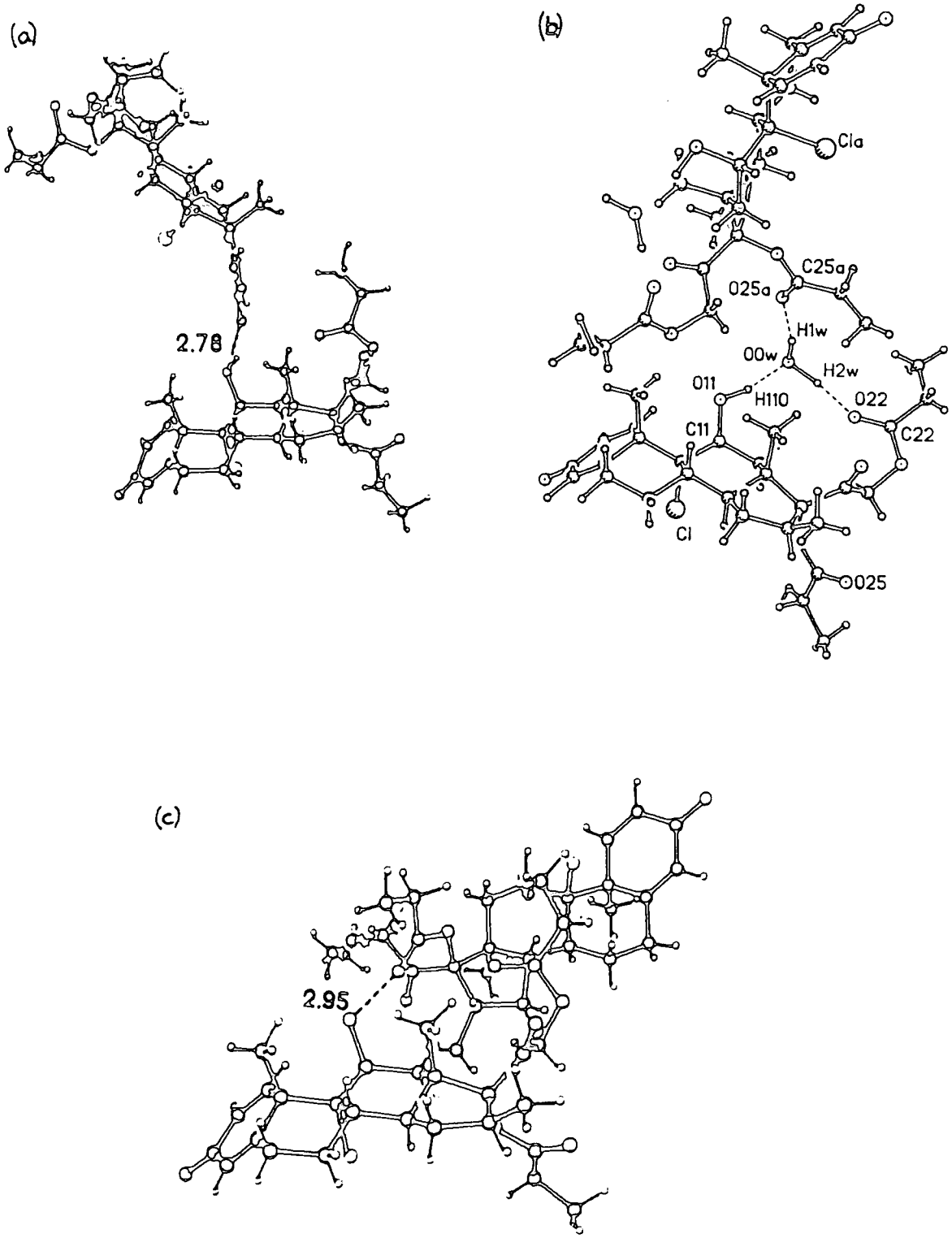

Figure 9.3 - Showing the channels present in crystals of BDP ethyl acetate solvate

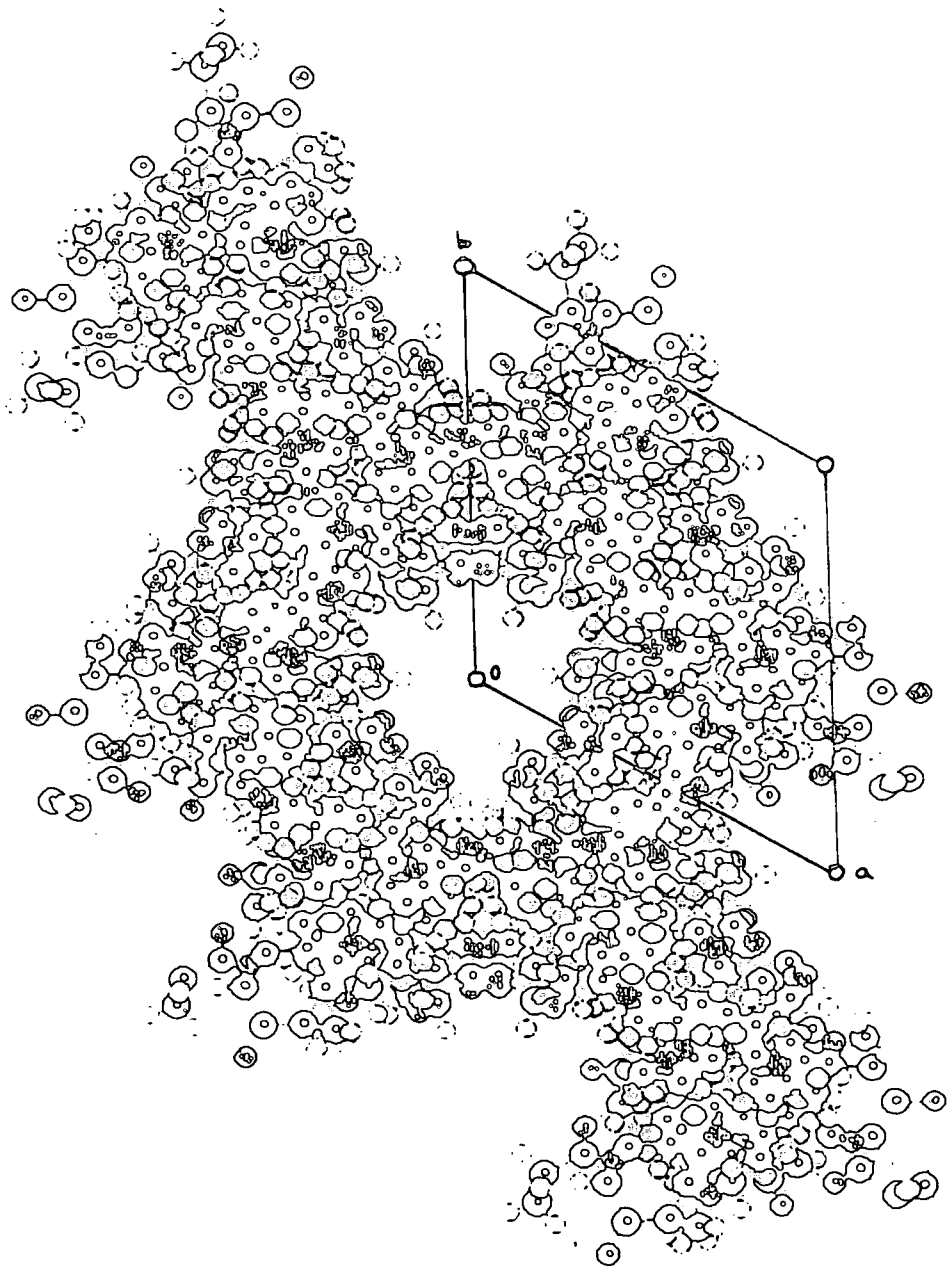

Table 9.1 - The crystal structures of BDP polymorphs[1,2]

form	space group	unit cell dimensions§						Z	N
		a / Å	b / Å	c / Å	α / °	β / °	γ / °		
anhydrate	$P2_12_12_1$	14.116	15.542	12.013	90	90	90	4	1
monohydrate	$P2_12_12_1$	14.152	16.268	12.085	90	90	90	4	1
ethyl acetate solvate	$P3_121$	13.570	13.570	31.081	90	90	120	6	1

§ unit cell dimensions are known to an accuracy of ±0.001Å.

The hydrogen bonds formed are presented in table 9.2 and are also shown in figure 9.2. It is interesting to note that the water molecule in the monohydrate acts as a bridge between C11 and C22 in the same molecule, and as a bridge to a neighbouring molecule.

Table 9.2 - The hydrogen bonding present in BDP polymorphs

Form	Atoms involved in the hydrogen bond	O-O distance / Å	Notes
anhydrate	C(11)-OH···O=C(3)	2.78	Bonding is between adjacent molecules.
monohydrate	C(11)-OH···OH_2	2.770	The C(11) and C(22) are in the same molecule, whilst C(25) is in an adjacent molecule. Each water molecule is involved in three hydrogen bonds.
	H_2O···O=C(22)	2.881	
	H_2O···O=C(25)	2.917	
ethyl acetate solvate	C(11)-OH···O=C(25)	2.95	Bonding is between adjacent molecules.

The crystal structure of the ethyl acetate solvate contains long channels where the ethyl acetate molecules are present (see figure 9.3). The diameter of the channels, as estimated from a space-filling model, is about 6 Å. Thus the ethyl acetate can easily leave the crystal, to be replaced by other species.

All forms can be readily identified by IR spectroscopy[3] as follows:

The anhydrate shows a single O-H stretch at 3280 cm^{-1}.

The monohydrate shows a splitting of the O-H stretch into three bands: 3560, 3510 and 3300 cm^{-1}. This is due to there being three different hydrogen bonds present. The highest frequency stretch corresponds to the shortest O-H

distance[4] as expected (the longer the O-O distance is, the shorter the O-H distance will be).

The solvates each show a single O-H stretch at 3483 cm^{-1} and many absorptions of the steroid molecule are the same in all the solvates:

1712 and 1665 cm^{-1} are the carbonyl stretches at C3 and C20

1630 and 1607 cm^{-1} are the stretches of the C=C double bonds

1750 and 1742 cm^{-1} are the carbonyl stretches of the propionate groups

Absorptions arise from the other molecule in the solvate, e.g. for the ethyl acetate solvate a broad band at 1740 cm^{-1} arises from the ethyl acetate, but also overlaps with the absorptions from the propionate side chains. The Arcton ($CFCl_3$) solvate of BDP, used in aerosol formulations of Becotide*, Becloforte* and Ventide* inhalers for the treatment of asthma, shows a band for C-Cl at 837 cm^{-1} arising from the Arcton.

In order to understand BDP by solid-state NMR one must first assign the spectrum. The solution state spectrum has already been assigned as mentioned in chapter 5. One can compare the assigned solution spectrum with the solid-state chemical shifts, in order to begin to make an assignment. The chemical shifts of anhydrous, monohydrate and ethyl acetate solvates are presented in table 9.3, and those peaks that remained in the non-quaternary suppression (NQS) experiment are indicated with an asterisk. The solid-state NMR spectra of the three forms are presented in figure 9.4, 9.5 and 9.6.

Figure 9.4 - The solid-state ^{13}C NMR spectrum of BDP anhydrate. Spinning sidebands are marked with an asterisk.

operating conditions	^{1}H 90° pulse	contact time	acquisition time	recycle delay	number of transients	spin rate
50 MHz	4 μs	2 ms	0.16 s	5 s	11132	3.0 kHz

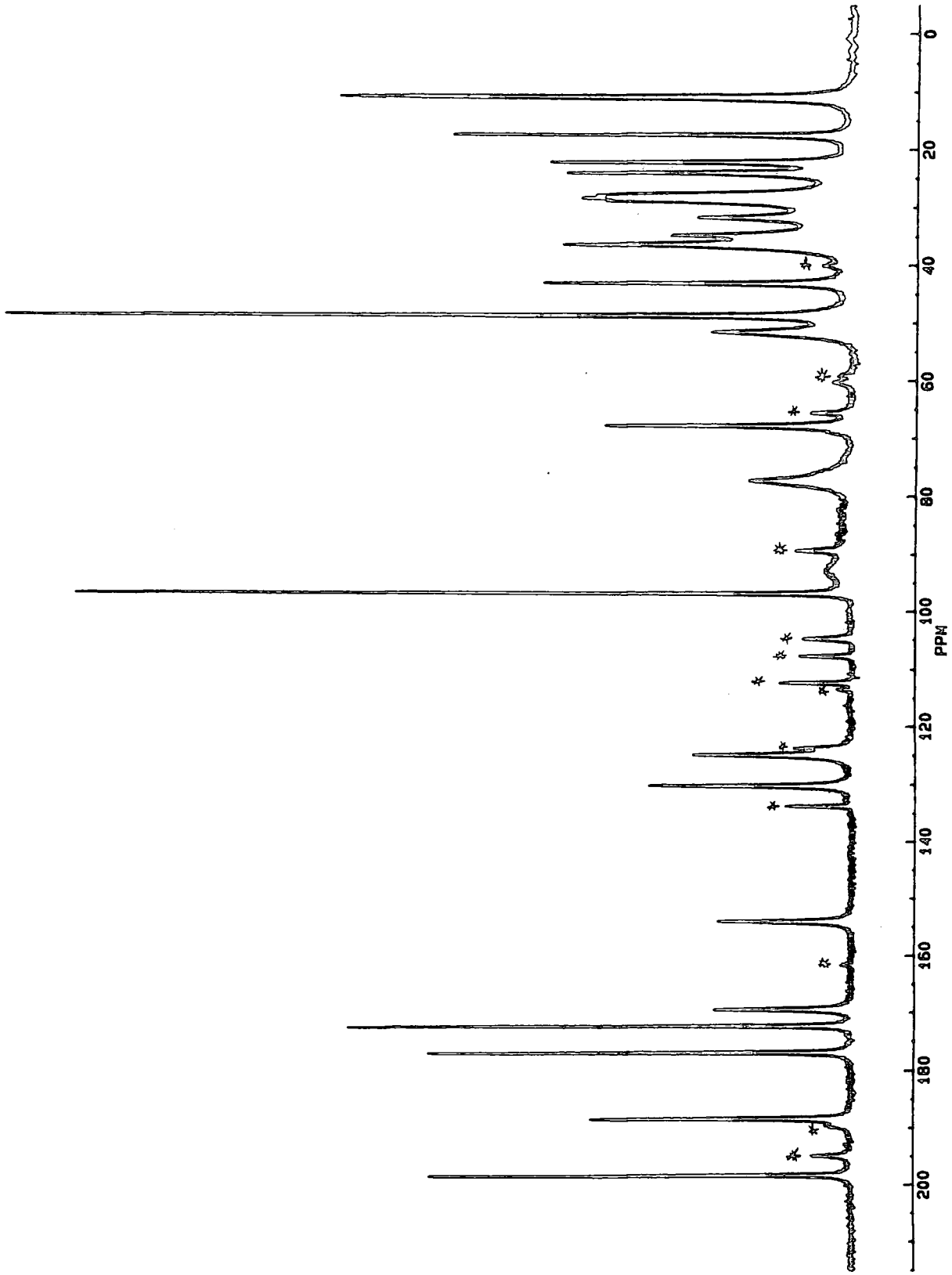

Figure 9.5 - The solid-state ^{13}C NMR spectrum of BDP monohydrate. Spinning sidebands are marked with an asterisk.

operating conditions	^{1}H 90° pulse	contact time	acquisition time	recycle delay	number of transients	spin rate
50 MHz	4 μs	2 ms	0.16 s	5 s	11664	3.8 kHz

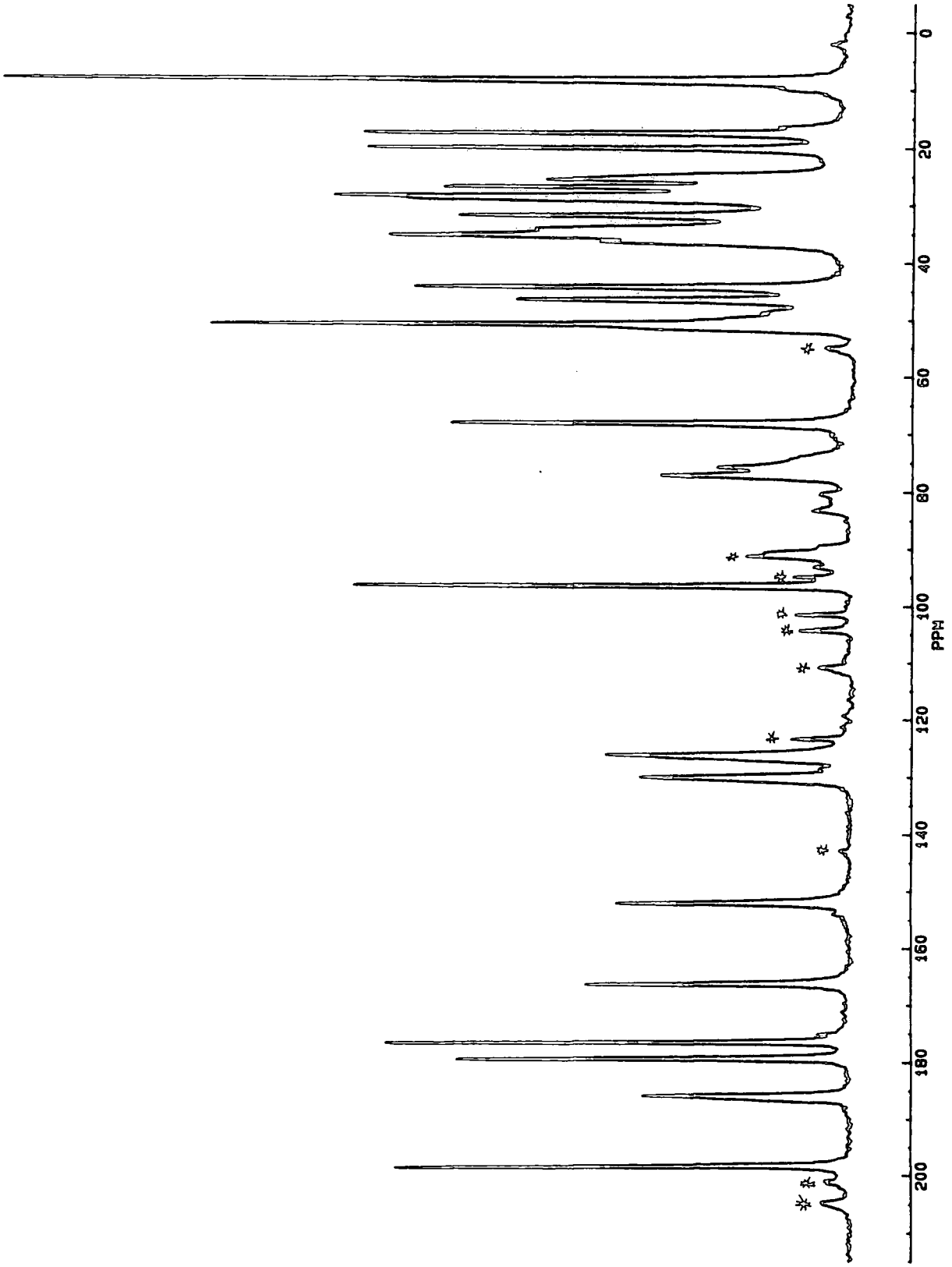

Figure 9.6 - The solid-state ^{13}C NMR spectrum of BDP ethyl acetate solvate. Spinning sidebands are marked with an asterisk.

operating conditions	^{1}H 90° pulse	contact time	acquisition time	recycle delay	number of transients	spin rate
50 MHz	4 μs	2 ms	0.16 s	5 s	1000	3.2 kHz

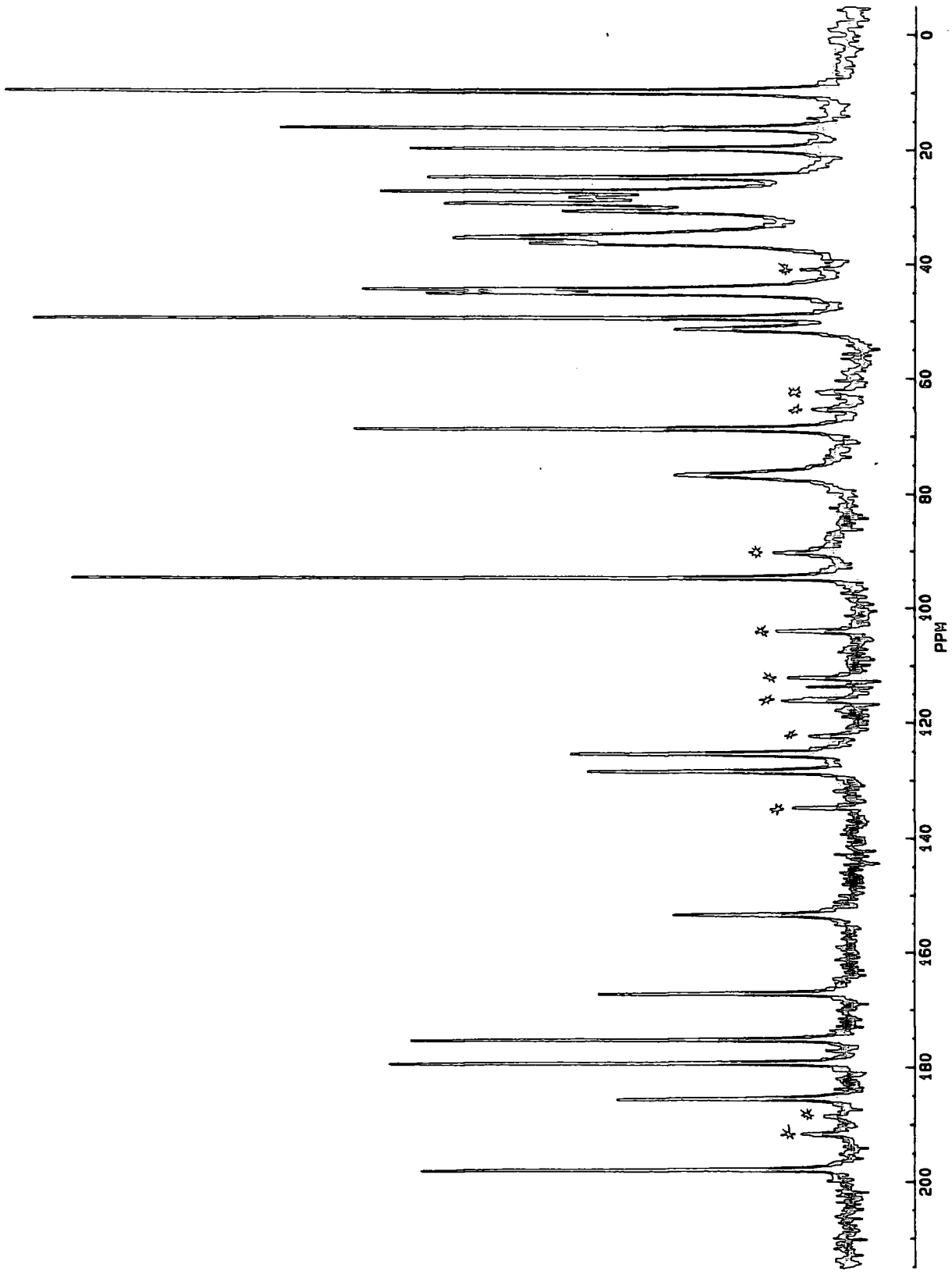

Table 9.3 - The ^{13}C chemical shifts in ppm of BDP polymorphs

Carbon number	solution[5]	anhydrate	NQS	monohydrate	NQS	ethyl acetate solvate	NQS
20	198.4	198.5	*	198.4	*	197.8	*
3	186.4	188.4	*	185.9	*	185.5	*
25	174.6	177.0	*	179.4	*	179.2	*
22	174.1	172.4	*	176.5	*	175.2	*
5	165.6	169.5	*	166.3	*	167.2	*
1	152.0	154.0		152.1		153.4	
2	129.5	130.2		130.1		128.4	
4	125.1	124.9		126.3		125.4	
17	94.5	96.8	*	96.5	*	94.7	*
9	82.6	~92.5		86.9		~90.0	
11	75.2	77.3		76.6		76.6	
21	67.8	67.8		68.2		68.7	
10	50.0	51.3	*	50.9	*	51.2	*
13	48.2	48.7	*	50.9	d	49.4	*
16	47.0	48.7	d	46.5		45.0	
14	43.5	43.1		44.3		44.3	
12	36.5	36.4		36.5		36.3	
8	34.4	34.8		35.4		35.4	d
15	34.4	31.7		34.3		30.8	
6	30.6	28.9		32.0		29.5	
7	28.4	28.5		30.0		28.4	
23	27.5	28.0		28.6		27.4	
26	27.1			27.0			
19	24.4	24.1	*	25.3	*	24.9	*
28	19.3	22.3	*	20.2	*	19.8	*
18	16.9	17.5	*	17.7	*	16.2	*
24	8.9	10.9	* d	8.4	* d	9.9	*
27	8.7					9.7	*

Note that the assignments are uncertain within the brackets. The 'd' represents a peak with approximately double intensity. Solid-state data acquired on the Bruker CXP-200, and solution-state data on the Varian VXR-400. A fuller discussion of the assignments is given in sections 9.3, 9.4, 9.5 and 9.7.

9.2. Shielding Anisotropy

Assignment of the spectra is aided by the investigation of shielding tensors as the study of cortisone acetate, cortisone, testosterone and androstanolone (see chapter 7) and the work of others[6] has shown. The following anisotropy and asymmetry parameters, given in table 9.4, are typical of particular structural groups.

Table 9.4 - Typical anisotropy and asymmetry parameters based upon structure[6]

	anisotropy / ppm	asymmetry
carbonyl	107	0.2
ester	-82	0.2
sp^2 quaternary carbon	113	0.7
sp^2 protonated carbon	-88	0.8

These typical values for the anisotropy and asymmetry are based upon the work presented in chapter 7 on steroids and the review of Veeman[6] that covers many varied compounds.

Even when the shielding tensors are known, C3 and C20 in BDP still cannot be distinguished (except on the basis of the chemical shift) as both are carbonyls, and the same is true of C1, C2 and C4, which are all sp^2 hybridized protonated carbons. The atoms C22 and C25 cannot be distinguished by either chemical shift or shielding anisotropy. However one may be able to distinguish C22 and C25 in the solvate, as only C25 is involved in hydrogen bonding. As the formation of hydrogen bonds causes a deshielding of the nucleus and a subsequent increase in the chemical shift by about 3 ppm, one would expect C25 to resonate at the higher frequency of the pair, i.e. at 179.2 ppm. Further discussion of this topic is to be found later in this chapter.

The shielding anisotropy of the highest frequency peaks has been found for each of the three forms, as described in chapter 7. The full results are presented in appendix 1 tables A1.12 -A1.14. The average tensors are presented in tables 9.5 - 9.7. The chemical shifts, anisotropy and shielding tensors are given in ppm, but the asymmetry is dimensionless.

Table 9.5 - Shielding tensors of BDP Anhydrate

δ	198.5	188.5	177.1	172.5	169.5	154.1	130.3	125.0
$\Im$	92	106	-91	-77	126	97	-78	-77
η	0.55	0.30	0.26	0.08	0.66	0.95	0.75	0.37
σ_{11}	-270	-257	-120	-131	-274	-249	-62	-72
σ_{22}	-219	-226	-144	-137	-191	-156	-120	-101
σ_{33}	-107	-82	-268	-250	-43	-57	-209	-202
	C20	C3	C25	C22	C5	C1	C2	C4

Table 9.6 - Shielding tensors of BDP Micronised Monohydrate

δ	198.7	185.9	179.3	176.5	166.3	152.1	130.1	126.3
$\Im$	95	106	-88	-86	126	-130	-89	-79
η	0.46	0.32	0.45	0.28	0.71	0.96	0.66	0.52
σ_{11}	-268	-256	-115	-122	-273	-32	-56	-66
σ_{22}	-224	-222	-155	-146	-185	-142	-115	-107
σ_{33}	-104	-80	-268	-262	-41	-283	-219	-205
	C20	C3	C25	C22	C5	C1	C2	C4

Table 9.7 - Shielding tensors of BDP ethyl acetate solvate

δ	197.8	185.4	179.2	175.1	167.1
$\Im$	90	100	-84	-85	116
η	0.43	0.36	0.33	0.09	0.66
σ_{11}	-262	-253	-123	-129	-263
σ_{22}	-223	-217	-151	-136	-187
σ_{33}	-108	-86	-263	-260	-51
	C20	C3	C25	C22	C5

Notes for tables 9.5 - 9.7: Data acquired on the Bruker CXP-200. The 'range' shows which sidebands were used in the fit and 'ssd' represents the sum of the squared differences for each fit. δ, $\Im$, and all σ values are in ppm.

The average values of the anisotropy and asymmetry are summarised in table 9.8.

Table 9.8 - The average values of the anisotropy and asymmetry for the polymorphs of BDP.

	anisotropy / ppm			asymmetry		
carbon no.	anhydrate	mono-hydrate	ethyl acetate solvate	anhydrate	mono-hydrate	ethyl acetate solvate
C20	92	95	90	0.55	0.46	0.43
C3	106	106	100	0.30	0.32	0.36
C25	-91	-88	-84	0.26	0.45	0.33
C22	-77	-86	-85	0.08	0.28	0.09
C5	126	126	116	0.66	0.71	0.66
C1	97	-130	-	0.95	0.96	-
C2	-78	-89	-	0.75	0.66	-
C4	-77	-79	-	0.37	0.52	-

The average values of the anisotropy and asymmetry agree quite well with those predicted[6]. The carbonyls C20 and C3 have large, positive anisotropies, although the asymmetries are perhaps a little larger than might have been expected. The ester groups (C22 and C25) have anisotropies that are smaller than for the carbonyls and of opposite sign. Also the asymmetries are quite small. The other carbon atoms in the A ring also exhibit some interesting properties. The quaternary sp^2 atom (C5) has, as expected, a large, positive anisotropy and a moderately large asymmetry. The protonated sp^2 atoms (i.e. C1, C2 and C4) have, generally, somewhat lower anisotropies than C5. This is to be expected from the predicted values. The sign of the anisotropy of C1 is uncertain as the asymmetry is approaching unity. It is interesting to note the similarity in the values for C2 and C4, as might be expected from the similarity in structure. However, it is clear that C1 has a significantly larger anisotropy (whatever the sign) than C2 and C4, and is much closer to that of C5. Perhaps this is not unexpected as C1 and C5 are both at the termini of the conjugated system and so there is some similarity in the environment of these atoms.

It has been noted (see chapter 8) that the formation of hydrogen bonds causes, along with a high frequency shift of about 3 ppm, an increase in the asymmetry of the the carbonyl group involved i.e. a move away from axial

symmetry ($\eta = 0$) that is often observed for carbonyl groups. This may help with the assignment of C22 and C25 as the hydrogen bonding is known. For the ethyl acetate solvate, only C25 is involved in hydrogen bonds, and so the peak with an asymmetry of 0.3 is likely to be C25. This point is discussed further in section 9.7. The hydrogen bond angles are given in table 9.9.

Table 9.9 - The hydrogen bond angles in BDP polymorphs

anhydrate	C11-O11-O3	117°
monohydrate	C22-O22-O(water)	155°
monohydrate	C25-O25-O(water)	144.4°
monohydrate	C11-O11-O(water)	112°
ethyl acetate solvate	C25-O25-O11	135.3°

The figures show that the hydrogen bonds are not at 180° to the C=O bond. Neither are the C=O···H angles 180°, where these can be found (hydrogen atoms are often not located in the crystal structure, but are added on in suitable positions later). Thus deformation of the axial symmetry of the carbonyl is to be expected. As was found for cortisone acetate, the formation of hydrogen bonds has the effect of increasing the value of δ_{22}. This effect has been discussed in chapter 8 and is useful in the identification of hydrogen bonds.

9.3. BDP Anhydrate

There are a number of points worthy of note for each polymorph. For the anhydrate (see figure 9.4), the first point is that the resonance from C9, expected at around 82 ppm, appears to be absent. The second point is that several peaks are much broader than others the spectrum, namely C11 (at 77.3 ppm) which is about 80 Hz wide at half height, and C10 (at 51.3 ppm) which is about 65 Hz wide, compared with the typical line width of 15-20 Hz. Now of course both C10 and C11 are adjacent to C9-Cl, so one might expect some broadening due to the close proximity of the quadrupolar chlorine nucleus. (The effect of a quadrupolar nucleus is discussed in greater detail in the following section.) This raises the important question again of the C9 resonance that is not readily observable. If the broadening of adjacent carbons due to the quadrupolar nucleus is significant, then how much more broadening would one expect for the carbon that is directly

bonded to the quadrupolar nucleus? A close inspection of the spectrum does reveal a very broad resonance (220 Hz wide approximately), at about 92.5 ppm which, as it remains in the NQS spectrum, might be assigned as arising from C9. A third point of interest is that if broadening of signals occurs at C10 and C11, both of which are adjacent to the quadrupole, then one might expect to see broadening of the C8 resonance that is expected at about 34 ppm. Now the region of the spectrum from 40 to 25 ppm cannot normally be assigned to individual carbon atoms. In this case there appears to be one too few resonances in this region and this could be explained if the C8 resonance has been broadened so that it does not give a distinct peak and is lost amongst the other peaks in the region.

9.4. BDP Monohydrate

Now the situation with the monohydrate is slightly different from that of the anhydrate. Again the resonance from C9 appears to be absent (see figure 9.5). Also one notices a number of broad lines in the spectrum. These correspond to the C11 and C10 resonances, but the difference is that there are two peaks for the former, at 77.3 and 75.8 ppm, and two shoulders for the latter, one on each side of the 50.9 ppm resonance. The C11 peaks at 77.3 and 75.8 ppm (that is C11 has a chemical shift midway between these peaks at 76.6 ppm) have widths at half height of about 70 and 90 Hz respectively, compared with a typical line width for the spectrum of about 30 Hz. Neither the exact chemical shift, nor the width at half height of the C10 resonances can be found due to overlap with the C13 resonance. Also the resonances of C2,3 and C4 are unusually broad at around 60 Hz each, although the reason for this is unknown.

9.4.1. The Effect Of Quadrupolar Nuclei On The Spectrum Of A Spin-1/2 Nucleus

Now the effect of a quadrupolar nucleus upon NMR spectra of a nearby spin-$\frac{1}{2}$ nucleus is dependent upon the magnetic field strength. Magic angle spinning is used to average the dipolar interactions, but quadrupolar interactions

are much greater and cannot always be completely averaged in this way, although they may be reduced. The use of higher magnetic fields can be helpful in reducing the effect of the quadrupolar interactions and thereby causing simplification of the spin-$\frac{1}{2}$ NMR spectrum.

The spectrum of a spin-$\frac{1}{2}$ nucleus coupled to a nucleus of spin S will be split into 2S+1 lines by indirect ("scalar") coupling. These lines are affected by 'second-order effects' arising from the quadrupolar interactions[7]. The ^{35}Cl nucleus has spin-$\frac{3}{2}$ and so the carbon spectrum is split into four lines by the spin-spin coupling. The second-order effects cause the outer two lines (corresponding to $m_S = \pm \frac{3}{2}$) to shift in one direction, whilst the inner two lines (corresponding to $m_S = \pm \frac{1}{2}$) shift in the other direction. As the second-order effects cause shifts that are greatly in excess of the spin-spin coupling constant, the smaller spin-spin coupling cannot be distinguished, and the spectrum takes the form of a 1:1 doublet. The splitting gives rise to the second-order shift (symbol Δ). See figure 9.7. As Δ is orientation dependent, each of these lines is, in principle, a powder pattern due to the different orientations of each microcrystallite in the magnetic field. The lines may appear as a single broad line if relaxation of the quadrupolar chlorine nucleus is rapid.

Figure 9.8 - Expansion of the solid-state ^{13}C NMR spectrum of BDP monohydrate

operating conditions	^{1}H 90° pulse	contact time	acquisition time	recycle delay	number of transients	spin rate
(a) 125 MHz	4.8 µs	3 ms	0.04 s	5 s	1680	9.5 kHz
(b) 75 MHz	4 µs	1 ms	0.07 s	2 s	1600	9 kHz
(c) 50 MHz	4 µs	2 ms	0.16 s	5 s	11664	3.8 kHz

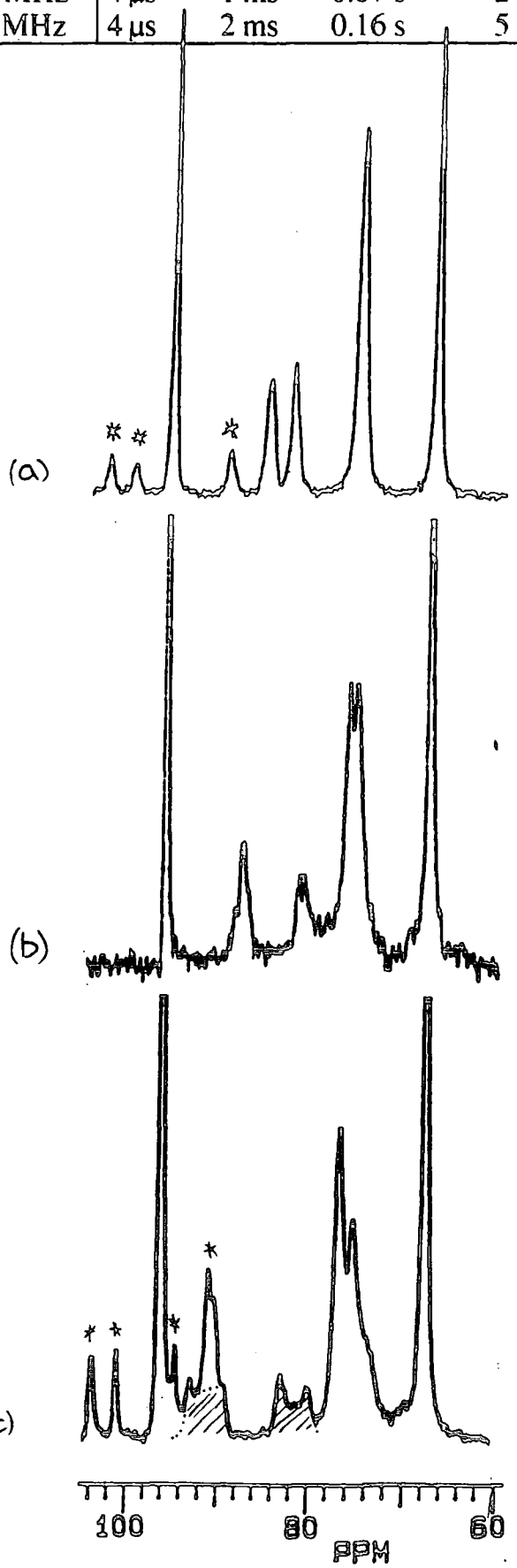

Figure 9.9 - The 125 MHz solid-state ^{13}C NMR spectrum of BDP monohydrate. Spinning sidebands are marked with an asterisk.

operating conditions	^{1}H 90° pulse	contact time	acquisition time	recycle delay	number of transients	spin rate
125 MHz	4.8 μs	3 ms	0.04 s	5 s	1680	9.5 kHz

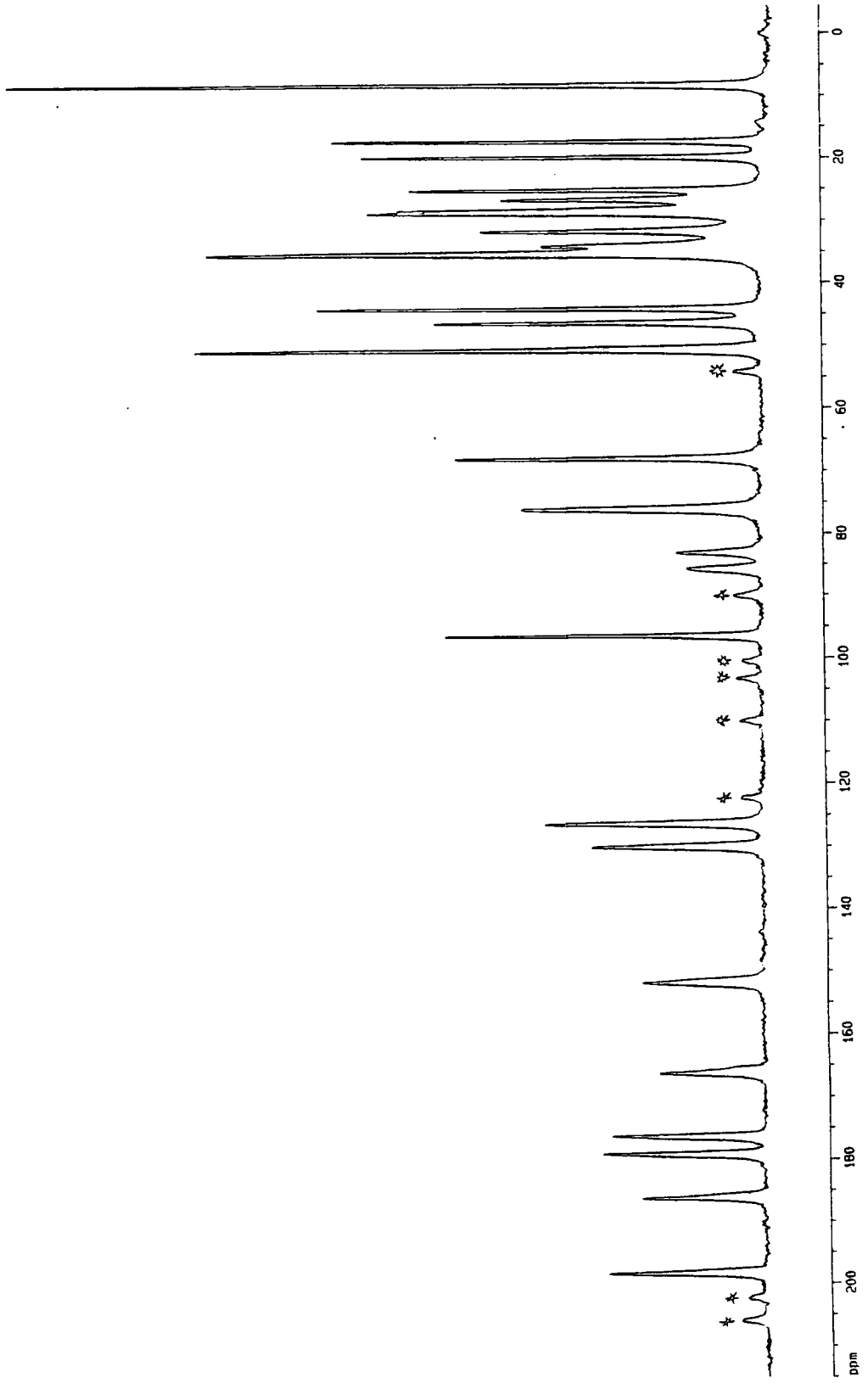

Figure 9.7 - Schematic diagram showing the effect of a quadrupolar nucleus ($S = \frac{3}{2}$) upon the spectrum of a spin-$\frac{1}{2}$ nucleus

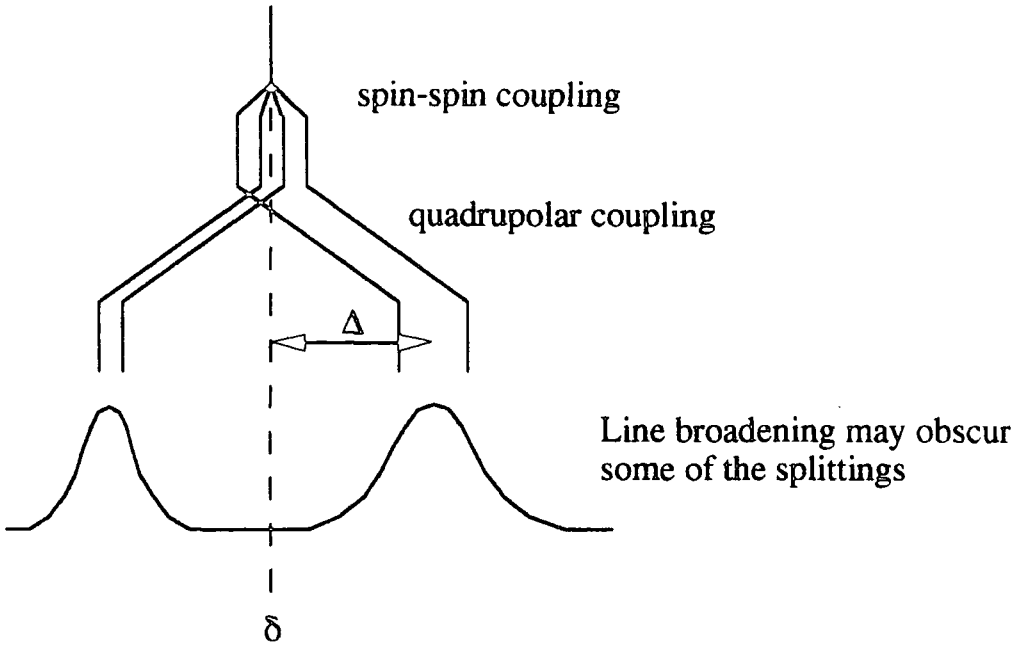

The spectrum of the monohydrate form of BDP acquired at 50 MHz carbon frequency, shows several peaks in the region around where the C9 resonance is expected. I believe that the C9 resonance is split into two lines, each of which can be described as a powder pattern. This is shown in figure 9.8(c) as the shaded areas. The chemical shift should be given as halfway between these two patterns at 86.9 ppm.

The spectrum should be simplified by working at higher magnetic field. Accordingly the ^{13}C spectrum of the monohydrate was recorded at 125 MHz carbon frequency (see figure 9.9). Now the region of the spectrum at around 80-100 ppm is much simpler than at lower field, and two peaks can be clearly seen at 85.9 and 83.3 ppm that should be assigned to C9. Therefore the chemical shift should be recorded as 84.6 ppm. This is lower than that found at lower field and the reason for this is not clear although it may be because of breakdown of the perturbation treatment on which the above discussion is based[8]. The ^{13}C spectrum has also been recorded at 75 MHz carbon frequency for comparison.

Figure 9.8 shows the 60-100 ppm region of the spectrum of the monohydrate at these three different field strengths.

At higher fields, one also notices that the C11 and C10 resonances have been simplified. Now one sees only a single broad peak at 76.3 ppm corresponding to C11 (and at about 140 Hz wide, twice the typical line width of the narrow lines in the spectrum). Also the shoulders on each side of the 50.9 ppm peak (assigned as C10) have now disappeared, and so the C10 resonance is overlapping exactly with the C13 resonance. Also the 25-35 ppm region of the spectrum is simplified at higher field, in particular, the changes around the highest frequency peaks in this region suggest that C8 is indeed present here at 35.4 ppm. There is also a sharpening of the C19 resonance at 25.6 ppm at high field.

Now the line splittings (Δ_m) are given by equation (1)[9] as follows:

$$\Delta_m = \frac{3\chi D'}{20\nu_S}\frac{(S(S+1)-3m_S^2)}{S(2S-1)}(3\cos^2\beta^D-1+\eta\sin^2\beta^D\cos 2\alpha^D) \quad \ldots\ldots (1)$$

where χ is the quadrupolar coupling constant, ν_S is the Larmor frequency of the quadrupolar nucleus, D' is the effective dipolar coupling constant (that takes account of the anisotropy of the spin-spin coupling constant ΔJ), S is the nuclear spin quantum number of the quadrupolar nucleus, m_S is the component of the nuclear spin quantum number, and the angles α^D and β^D describe the orientation of the internuclear distance with respect to the electric field gradient (see figure 9.11).

So for a spin-$\frac{1}{2}$ nucleus coupling to a spin-$\frac{3}{2}$ nucleus, the second-order shift (Δ) for the outermost lines is given by the following expression[7].

$$\Delta = \frac{-3\chi D'}{10\nu_S} \quad \ldots\ldots (2)$$

as $S=\frac{3}{2}$ and $m_S = \pm\frac{3}{2}$. One must also assume that there is axial symmetry of the electric field gradient (i.e. $\eta=0$) and that the electric field gradient is along the internuclear distance (i.e. $\beta^D=0$). These are considered reasonable assumptions for a univalent quadrupolar nucleus such as ^{35}Cl.

Note that $D' = D - \frac{1}{3}\Delta J$ ..... (3)

and $D = \frac{\mu_0 r^{-3} \gamma_1 \gamma_2 \hbar}{8\pi^2}$ ..... (4)

where μ_0 is the permeability of a vacuum, γ_1 and γ_2 are the magnetogyric ratios of ^{13}C and ^{35}Cl and r is the internuclear distance ^{13}C-^{35}Cl.

So, if r is known, the dipolar coupling constant D can be calculated. Moreover, if Δ can be measured, and χ estimated, then a value for the effective dipolar coupling constant D' can be found. This may be used to estimate the anisotropy of the spin-spin coupling constant ΔJ. The anisotropy of the spin-spin coupling constant gives valuable information, to add to the isotropic value J for testing theoretical calculations. Fuller discussions of the theory have appeared elsewhere[10-16].

The second-order splitting (Δ), measured at three field strengths is given in table 9.10 along with the calculated effective dipolar coupling constant (D') and the calculated values of ΔJ. D' has been obtained using equation (2) and assumes a quadrupolar coupling constant (χ) of 65 ± 2.5 MHz, which is based upon the measured values of the quadrupolar transition frequency (ν) for compounds of similar structure[17]. The quadrupolar coupling constant is twice the transition frequency[18,19] for the case of a spin-$\frac{3}{2}$ nucleus.

i.e. $\chi = \frac{e^2 q_{zz} Q}{h}$ ..... (5)

and $\nu = \frac{e^2 q_{zz} Q}{2h}$ ..... (6)

so $\chi = 2\nu$ ..... (7)

where e is the unit electric charge, q_{zz} is the component of the electric field gradient (arising from the quadrupole) that is along the z direction, and Q is the electric quadrupole moment.

Table 9.10 - The second-order splitting at different magnetic fields.

^{13}C magnetic field	Δ / ppm	Δ / Hz	D' / Hz	ΔJ_-	ΔJ_+	error in ΔJ
50 MHz	±4.8	±241	±242	2163	711	±66
75 MHz	±3.3	±246	±371	2550	324	±104
125 MHz	±1.3	±163	±410	2667	207	±111

Notes: ΔJ_- represents the case when D' is negative, and ΔJ_+ is when D' is positive (since γ_C and γ_{Cl} are both positive, so D must also be positive).

The dipolar coupling constant (D) was calculated using equation (3) as follows:

$$D = \frac{\mu_0 r^{-3} \gamma_1 \gamma_2 \hbar}{8\pi^2} = 479 \text{ Hz}$$

$\mu_0 = 4\pi \times 10^{-7}$ kg m s^{-2} A^{-2}

$r = 1.836 \times 10^{-10}$ m (known from the crystal structure determination[2])

γ_1 (^{13}C) $= 6.728 \times 10^7$ rad T^{-1} s^{-1}

γ_2 (^{35}Cl) $= 2.624 \times 10^7$ rad T^{-1} s^{-1}

$\hbar = 1.055 \times 10^{-34}$ J s

$\nu_S = 9.8 \times 10^{-2} \times \nu_H$ (where ν_H is the proton Larmor frequency)

Now for each calculated value of D', the anisotropy in the spin-spin coupling constant (ΔJ) can be calculated. If Δ is positive then either χ is negative and D and D' have the same sign, or χ is positive and then D and D' will have opposite signs[7]. However, the signs of Δ and χ are unknown (the sign of Δ is only obtainable if J_{iso} is observable), and so there is ambiguity over the value of ΔJ (these are given the symbols ΔJ_- and ΔJ_+ in the table 9.10).

An estimate of the errors involved in the calculation of ΔJ has been carried out as follows:

Δ measured to $\pm$ 0.1 ppm	i.e. a maximum of 8 % error
r has been found to $\pm$ 0.01 Å	i.e. an error of 0.5 %
χ is estimated to $\pm$ 2.5 MHz	i.e. an error of 4 %

If $D = C r^{-3}$

(where C represents several constants) then the error is given by

$$f_D^2 = f_C^2 + 3f_r^2$$

(where f represents the fractional error in the quantity given by the subscript). If the constants are assumed to be known accurately, then f_C is zero and so

$$f_D = 8.6 \times 10^{-3} \text{ (i.e. D} = 479 \pm 4 \text{ Hz)}$$

Similarly, if $D' = \frac{C\Delta}{\chi}$

(where C represents other constants)

then $f_{D'}^2 = f_C^2 + f_\Delta^2 + f_\chi^2$

Hence $f_{D'} = 0.089$ (i.e. $D' = 410 \pm 37$ Hz for the case of the 125 MHz spectrum)

The absolute error in a sum (E_x) for the equation

$$x = D - D'$$

is given by $E_x^2 = E_D^2 + E_{D'}^2$

thus $E_x = 37$

so $x = 889 \pm 37$ or $x = 69 \pm 37$

(depending upon the sign of D'). These correspond to fractional errors of 0.042 or 0.536 respectively. Therefore, the final stage is to find the error in ΔJ ($\Delta J = 3x$), i.e. the fractional error in ΔJ is equal to the fractional error in x.

So $\Delta J_- = 2267 \pm 111$ H or $\Delta J_+ = 207 \pm 111$ Hz.

Similar calculations have given the estimates for the spectra acquired at other field strengths.

Now the quantity $\Delta \nu_s$ should be constant (and equal to $\frac{-3}{10} \chi D'$). The agreement at the two highest fields is good (7987×10^6 s^{-2} and 7232×10^6 s^{-2}), but $\Delta \nu_s$ at 200 MHz is very low (at only 4724×10^6 s^{-2}). This discrepancy may be accounted for by the fact that the equations used, which are based upon perturbation theory, could only be expected to be true at high magnetic field[7]. Thus one should give greater weight to the values of ΔJ obtained in the 125 MHz carbon spectrum. One should also note that the calculations make the assumptions that the principal components of the J and D tensors are coaxial with the internuclear distance.

A review of the literature yields few references to the effect of chlorine on a carbon spectrum[20]. One compound studied was poly(chlorotrifluoroethylene) and a broadening of the carbon resonance from the CFCl group is reported and attributed to the influence of the quadrupolar chlorine nucleus, although the

magnitude of the effect is not quoted. However a review[21] in 1982 gives some values for ΔJ for the following cases:

C-C	2.5 - 88.7 Hz
C=N	-32.6 Hz
C-N	-10.5 Hz
C-Hg	650 - 1150 Hz

Thus on reflection, the lower values of ΔJ based upon calculations of D' being positive seem more reasonable (and especially those obtained at higher field strengths) as ΔJ is unlikely to be as large as for carbon bonded to a very heavy nucleus such as mercury.

9.4.2. Long Range Quadrupolar Effects

The effect of the quadrupolar chlorine nucleus upon the resonances of the carbons adjacent to C9 have also been noted. There is evidence in the monohydrate that broadening and even splitting of the carbon resonances has been observed at C8, C10 and C11. The quadrupolar effects are however rather weaker than are observed for C9. The larger distance between the carbon and chlorine nuclei is certainly one cause and another factor will be that the internuclear distance will not be along the quadrupolar axis. See figure 9.10.

Figure 9.10 - Showing the environment of the chlorine nucleus

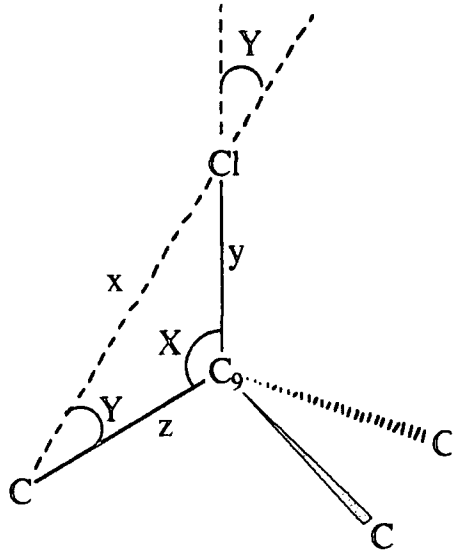

By trigonometrical relations the internuclear distance 'x' and the angle Y can be calculated, as distances y and z and the angle X are known from the

crystal structure. These values are given in table 9.11. The Cl-C9 distance (y) = 1.836 Å.

Table 9.11 - The internuclear distances and angles around the chlorine nucleus

A	C9-A distance z / Å	Cl-C9-A angle X / °	Cl-A distance x / Å	C9-A-Cl angle Y / °
C8	1.563	108.0	2.755	39.3
C10	1.591	105.4	2.730	40.4
C11	1.546	105.3	2.694	41.1

Now equation (1) is based upon the assumptions that there is axial symmetry of the electric field gradient (i.e. that the asymmetry parameter, $\eta = 0$) and that the electric field gradient is aligned along the internuclear axis. These seem reasonable assumptions for a univalent atom such as chlorine. However, if one is considering the effect of the quadrupolar nucleus on carbons more distant than C9 one must consider other terms in the expression given in equation (8).

$$\Delta = \frac{-3\chi D'}{20\nu_S}.(3\cos^2\beta^D - 1 + \eta\sin^2\beta^D\cos 2\alpha^D) \quad \text{..... (8)}$$

The angle α^D and β^D are defined in figure 9.11.

Figure 9.11 - Showing the α^D and β^D angles

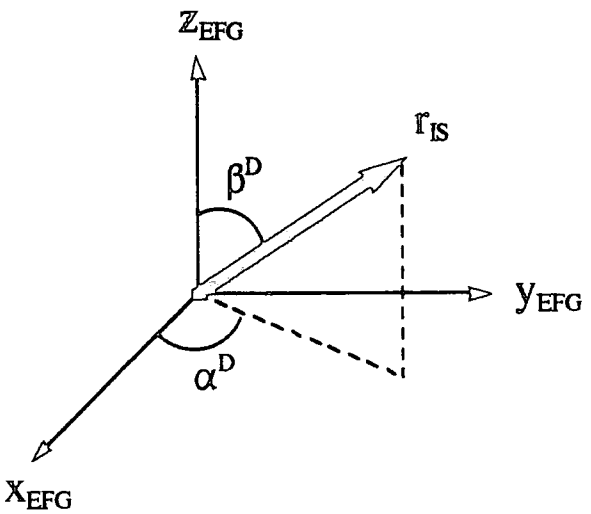

So if $\eta = 0$ and $\beta^D = 0$ (these are the usual assumptions) then equation (1) reduces to the familiar form of equation (2). But for more distant carbons $\beta^D \neq 0$, although η remains equal to zero.

Hence $\Delta = \frac{-3\chi D'}{20\nu_S}(3\cos^2\beta^D - 1)$ ..... (9)

$$\text{or } \Delta = \frac{-3\chi D'}{10\nu_S}\frac{(3\cos^2\beta^D - 1)}{2} \quad \text{.....(10)}$$

The quadrupolar splitting is dependent upon the dipolar interaction. This has a r^{-3} dependence. The quadrupolar splitting is greatest when the internuclear distance is along the quadrupolar axis, i.e. the splitting is also dependent upon $(3\cos^2 Y - 1)$. Thus an estimate of the expected splitting can be made by substituting the appropriate values in equation (11).

$$\Delta = \frac{-3\chi}{20\nu_S}\left(\frac{\mu_o\gamma_1\gamma_2\hbar r^{-3}}{8\pi^2} - \frac{1}{3}\Delta J\right)(3\cos^2\beta^D - 1) \quad \text{.....(11)}$$

The average of the two high field values of ΔJ has been used in the calculations as it is considered that these are more reliable than the figure found at the lower field strength. Therefore $\Delta J = 265$ Hz and r and β are given by the values of x and Y in table 9.11.

The calculated splittings compare favourably with the observed splittings that are given in table 9.12.

Table 9.12 - Observed and calculated long range quadrupolar splittings in Hz

carbon	δ / ppm	50 MHz		75 MHz		125 MHz	
		Δ (calc)	Δ (obs)	Δ (calc)	Δ (obs)	Δ (calc)	Δ (obs)
C8	~35	21	*	14	*	9	*
C10	50.9	21	17	14	*	9	*
C11	76.6	22	33	15	28	9	*

An asterisk shows that no splitting was observable. The observed splittings are small and difficult to measure accurately, so an error of 10-15% in the observed Δ is likely. With this in mind, the observed and calculated values agree quite well, but in many cases the effect is too small to be observed.

9.4.3. The Effect Of Chlorine-37

One must also consider the possible effect of the ^{37}Cl nucleus on the spectrum. Some of the relevant physical properties of the two isotopes are given in table 9.13.

Table 9.13 - Some physical properties of the chlorine isotopes[22]

property	^{35}Cl	^{37}Cl
NMR frequency / MHz (relative to ^{1}H = 100 MHz)	9.809	8.165
Q (quadrupole moment) x 10^{-28} / m^2	-0.10	-0.079
γ (magnetogyric ratio) x 10^{-7} / rad T^{-1} s^{-1}	2.624	2.184
natural abundance as %	75.53	24.47

The quadrupolar coupling constant is given by $\chi = \frac{e^2 q_{zz} Q}{h}$, and if the anisotropy in the spin-spin coupling is assumed to be zero then D = D' and so $D' = \frac{\mu_0 r^{-3} \gamma_1 \gamma_2 \hbar}{8\pi^2}$. Thus if $\Delta = \frac{-3 \chi D'}{10 \nu_s}$ then $\Delta \propto \frac{Q\gamma}{\nu_s}$.

For the ^{35}Cl $\Delta_{35} \propto -0.02675$

whilst for ^{37}Cl $\Delta_{37} \propto -0.02113$

Thus $\frac{\Delta_{37}}{\Delta_{35}} = 0.79$, so the quadrupolar splitting arising from the ^{37}Cl nucleus would be only 79% of that arising from ^{35}Cl and accounting for only quarter of the total intensity (due to the lower natural abundance). Calculated splittings for the ^{37}Cl nucleus are presented in table 9.14 along with a schematic diagram (figure 9.12) showing the expected spectrum.

Table 9.14 - The quadrupolar splittings arising from the chlorine isotopes

	Δ_{35} / ppm	Δ_{37} / ppm	(Δ_{35} - Δ_{37}) / ppm
50 MHz	4.8	3.8	1.0
75 MHz	3.3	2.6	0.7
125 MHz	1.3	1.0	0.3

Figure 9.12 - A schematic diagram showing the expected spectrum arising from the chlorine isotopes

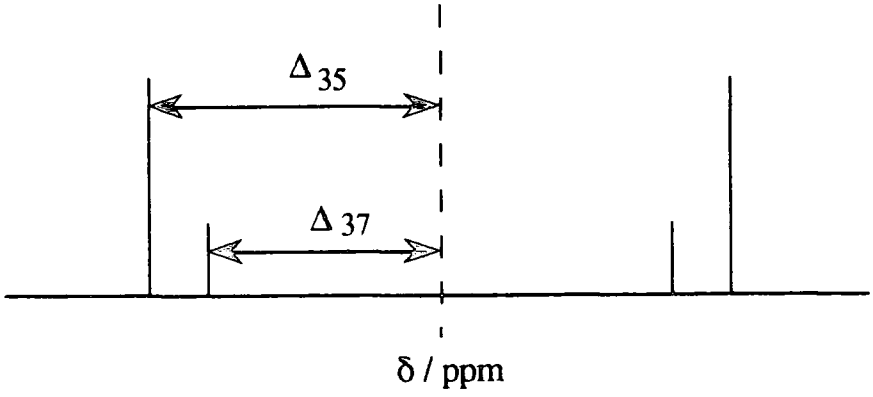

Therefore for the 50 MHz spectrum a splitting caused by ^{37}Cl of 1 ppm from the ^{35}Cl peak might be expected. This is a very small additional effect, both in terms of the splitting and the intensity. A close inspection of the spectrum does not reveal any peaks in the expected position with a suitable intensity. However, the occurrence of a number of unexplained peaks in this region and the relatively low signal-to-noise ratio leads to an amount of confusion, and so the effect of ^{37}Cl cannot be entirely ruled out at this field strength. For the 75 and 125 MHz spectra, again there is no clear evidence for the existence of peaks arising from ^{37}Cl quadrupolar effects. But, the effect could be masked by the broadness of the main peaks. To conclude, the effect of the ^{37}Cl quadrupolar interaction is too small to observe[15,23], and at best it seems that it would only be a small shoulder on the side of the main peak.

9.5. BDP Ethyl Acetate Solvate

As with the anhydrate and monohydrate forms, the ethyl acetate solvate does not show a clear resonance from C9, and as with the anhydrate, the signals from C11 (at 76.6 ppm) and C10 (at 51.2 ppm) are broad at about 60 and 50 Hz respectively compared with the typical peak width of 15-20 Hz (see figure 9.6). If C8 is broadened also, then it may be the resonance at 35.4 ppm as this peak is broad and to the high frequency end of the suitable range. (Note however that the 35.4 ppm peak represents two carbon atoms as judged from the integral, the other carbon being C15). One might conclude that the C9 resonance has been broadened to such an extent that it is not normally visible, although some spectra do show what might be a very broad peak at about 90 ppm and 200-300 Hz wide. Note that this peak should not be confused with the sharp spinning sideband that is often present in this region of the spectrum.

When suitable acquisition parameters are used (i.e. a long contact time of 10 ms in the cross polarization experiment or a single pulse experiment), peaks from the ethyl acetate molecule can also be seen (see figures 9.13 and 9.14), and

the chemical shifts are given in table 9.15 and the numbering scheme used for ethyl acetate assignments is shown in figure 9.15.

Table 9.15 - Solid- and solution-state ^{13}C chemical shifts of ethyl acetate

	δ_C / ppm	δ_C / ppm	δ_C / ppm	δ_C / ppm
BDP ethyl acetate solvate solid-state	14.2	20.4	60.3	169.7
ethyl acetate solution-state[24]	13.8	20.0	60.0	170.3
carbon atom assignment	1	4	2	3

Figure 9.15 - The numbering scheme for ethyl acetate

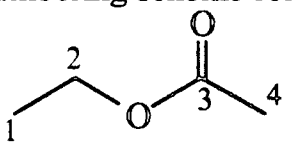

There is a very close agreement between solid- and solution-state chemical shifts. Indeed, as the chemical shifts are so very close, one might suggest that the ethyl acetate is in a solution-like environment when in the solvate, i.e. with no strong interactions with the steroid and possibly with rapid motion. The possibility of motion is supported by the linewidths of the ethyl acetate resonances, which are each 10-15 Hz, and are slightly narrower than the resonances of the steroid that are generally 15-20 Hz.

Most attempts to study the proton spectra of solid steroids produce no useful results even with magic angle spinning, with at best a very broad and ill-defined peak. The proton spectrum of the ethyl acetate solvate of BDP is a very different case. There are three clearly resolved lines each about 80 Hz wide (see figure 9.16). The chemical shifts are presented in table 9.16 along with the proton chemical shifts of ethyl acetate in solution.

Table 9.16 - Solid- and solution-state ^{1}H chemical shifts of ethyl acetate

	δ_H / ppm	δ_H / ppm	δ_H / ppm
Ethyl acetate solvate of BDP in the solid-state	1.14	1.85	4.08
Ethyl acetate in solution[24]	1.21	1.93	4.03
proton assignment	1	4	2

Figure 9.13 - The solid-state ^{13}C NMR spectrum of BDP ethyl acetate solvate. Spinning sidebands are marked with an asterisk.

operating conditions	^{1}H 90° pulse	contact time	acquisition time	recycle delay	number of transients	spin rate
50 MHz	4 μs	10 ms	0.04 s	3 s	200	3.2 kHz

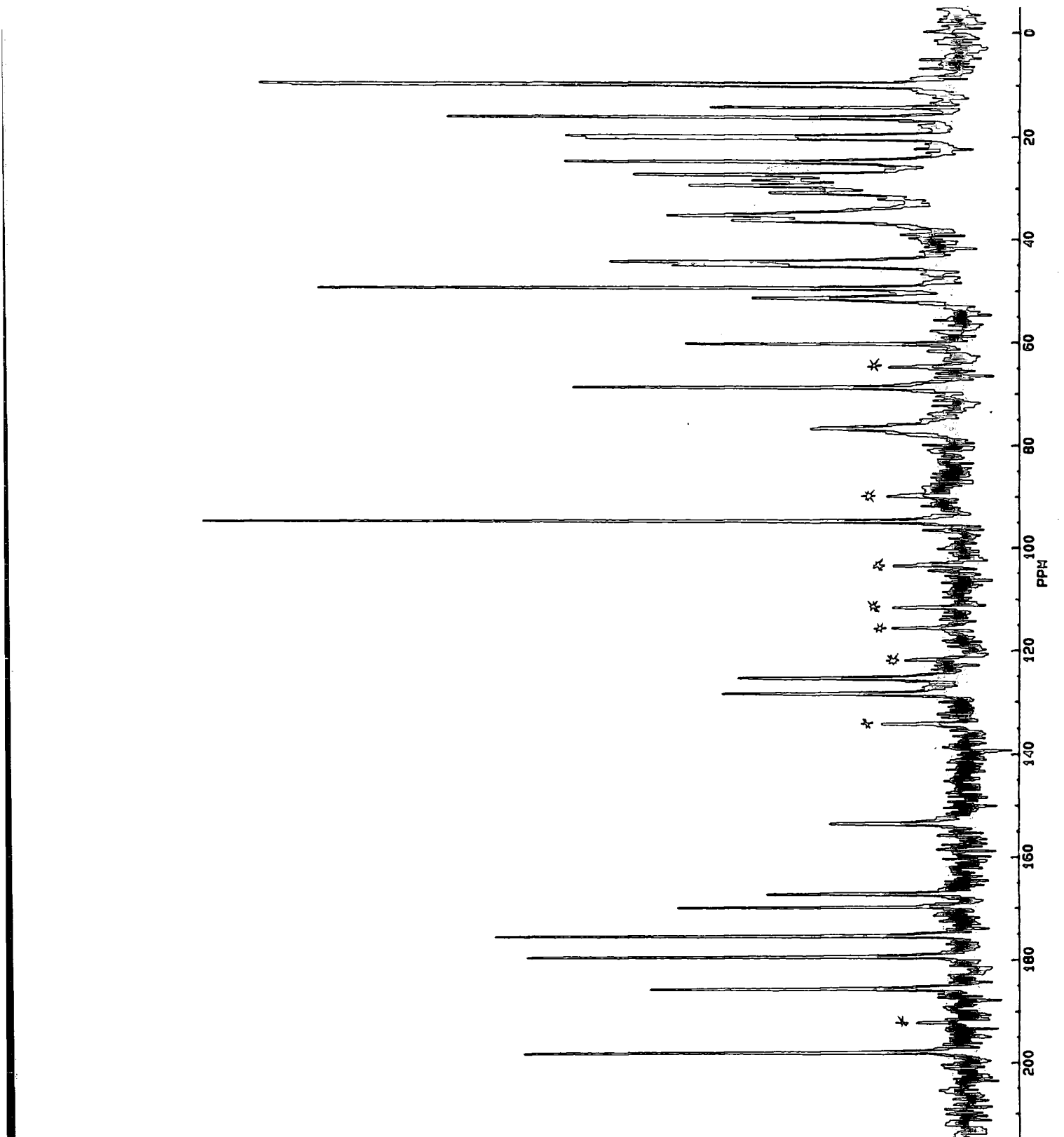

Figure 9.14 - NQS solid-state ^{13}C NMR spectrum of BDP ethyl acetate solvate. Spinning sidebands are marked with an asterisk.

operating conditions	^{1}H 90° pulse	contact time	dead time	acquisition time	recycle delay	number of transients	spin rate
50 MHz	4 μs	10 ms	55 μs	0.04 s	3 s	410	3.2 kHz

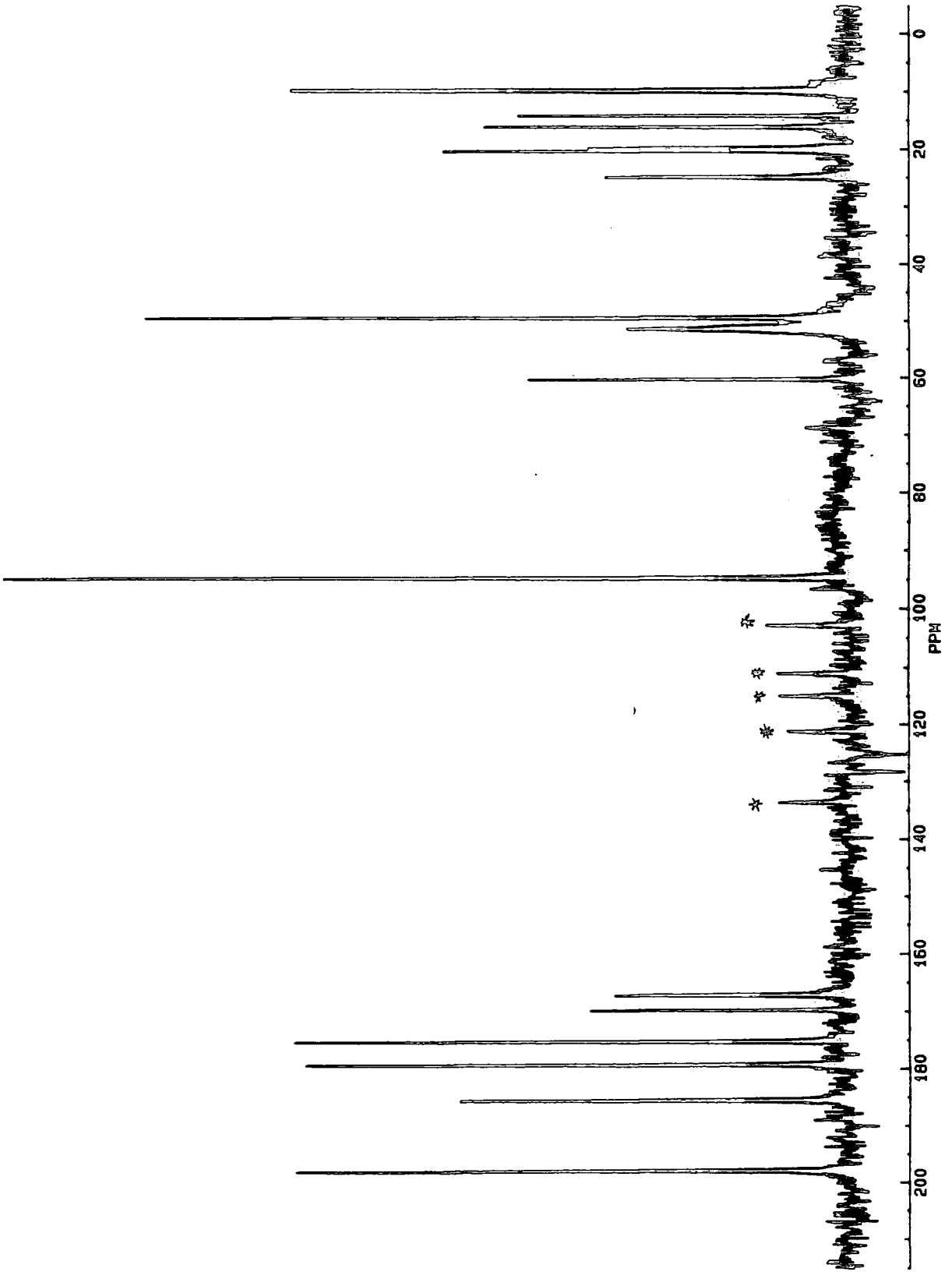

Figure 9.16 - The solid-state ^{1}H NMR spectrum of BDP ethyl acetate solvate.

operating conditions	^{1}H 90° pulse	acquisition time	recycle delay	number of transients	spin rate
50 MHz	4 μs	0.04 s	20 s	4	3.2 kHz

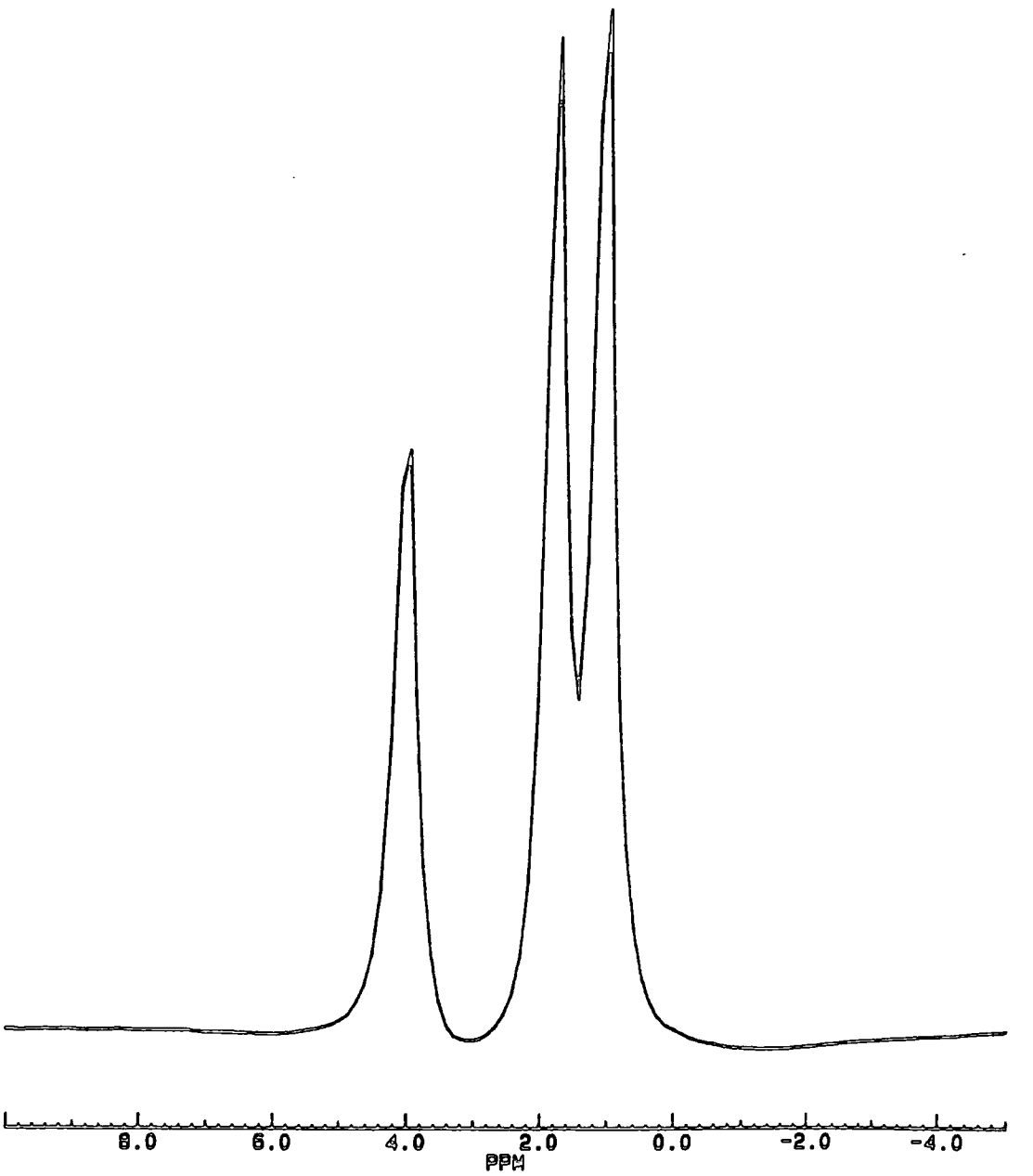

The spectrum is clearly that of the ethyl acetate molecule (although with the coupling obscured by the linewidths) and again one is lead to believe that the ethyl acetate is solution-like within the solvate structure. This is consistent with the ethyl acetate molecules occupying the channels within the solid-state, that are known to exist from the crystal structure determination.

9.6. Solvent Content By Solution-State NMR

A sample of freshly prepared ethyl acetate solvate was dissolved in deutero-chloroform and studied by solution-state proton NMR. The peak integrals of $CHCl_3$ present in the solvent may be compared with those of the steroid molecule and the ethyl acetate. Chloroform absorbs water to some extent and so the amount of water present in each solution was also monitored.

A 'blank' sample of only the solvent was studied for comparison purposes. The chloroform used to make the solution was taken from an open bottle and so already contained some water. The spectra were acquired about 10 minutes after making the solution and again approximately 24 hours later. The solution was left in the NMR tube sealed with a plastic cap when not in use. The results are presented in table 9.17.

Table 9.17 - The peak integrals of the 'blank' solvent

		δ_H / ppm	integral
after 10 minutes	$CHCl_3$	7.27	17.7
	H_2O	1.50	2.1
after 24 hours	$CHCl_3$	7.27	18.2
	H_2O	1.50	11.7

As each water molecule contains two protons, the integral must be halved in order to give a value per molecule, the chloroform contains only one proton. The ratio of $CHCl_3$:H_2O molecules is about 17:1 after only 10 minutes, but after 24 hours the ratio has changed to nearer 3:1 (remember that the solvent is ~99% $CDCl_3$, and so the amount of water present is still less than 2% of the total). All spectra of solutions of the BDP were acquired straight away and so should be compared to the first of the blank ratios.

Two samples of the ethyl acetate solvate of BDP were studied, each having been prepared only a few days before, and stored in a tight-fitting, screw top container. Sample 1 had been studied by solid-state NMR and so had been spinning at 3 kHz for several hours in the magnet. Sample 2 had no such treatment, and one aim of this experiment was to find out if there had been significant loss of ethyl acetate due to magic angle spinning. The results are given in table 9.18. A recycle delay of 5 s was used throughout to allow complete relaxation to occur.

Table 9.18 - Peak integrals for two samples of the ethyl acetate solvate of BDP

			Sample 1 (spun)		Sample 2 (fresh)	
molecule	δ_H / ppm	no. of protons	integral	integral / no. of protons	integral	integral / no. of protons
$CHCl_3$	7.27	1	6	6	6	6
BDP‡	1.00	3	24	8	24	8
ethyl acetate	1.25	3	24	8	24	8
ethyl acetate	2.04	3	17	5.7	18	6
ethyl acetate	4.12	2	12	6	12	6
H_2O	1.66	2	23	11.5	23	11.5

‡ This resonance is that of the methyl protons of C19.

This experiment shows that, within experimental error, there is the same amount of ethyl acetate in the fresh and spun samples. Thus little ethyl acetate is lost from samples of this polymorph by spinning the sample during the course of a solid-state NMR experiment. The ratio of BDP to ethyl acetate is approximately 1:1.

It is interesting to note that in both samples there is more water present than in the solvent alone. The ratio of $CHCl_3$:H_2O is 1:2. It seems unlikely that this could have been absorbed so quickly form the atmosphere. One likely cause is that there could be some of the hydrate present in the samples. After this solution-state experiment had been performed the solid-state NMR spectra of these samples were each recorded to reveal about 10% of the hydrate present.

9.7. The Effect Of Hydrogen Bonding On Chemical Shifts

The crystal structures of the three polymorphs have been found, so the mode and length of hydrogen bonds are known.

If one compares the chemical shifts of particular atoms in the three forms with that in solution, it is clear that there are large high-frequency shifts in certain cases. The chemical shifts of atoms potentially involved in hydrogen bonds are presented in table 9.19 along with other significant chemical shifts.

Table 9.19 - The chemical shifts of atoms potentially involved in hydrogen bonding

	chemical shift / ppm			
carbon no.	solution	anhydrate	monohydrate	ethyl acetate solvate
C3	186.4	188.4	185.9	185.5
C25	174.6	177.0	179.4	179.2
C22	174.1	172.4	176.5	175.2
C1	152.0	154.0	152.1	153.4
C5	165.6	169.5	166.3	167.2
C11	75.2	77.3	76.6	76.6

Now C11 is involved in hydrogen bonding in all three forms. As with other steroids, there does not appear to be a trend relating the chemical shift of C11 with the length of the hydrogen bonds formed.

The C3 carbonyl group is involved in hydrogen bonding in only the anhydrate. In this form the chemical shift is significantly higher than for the solution and other non-bonded solid polymorphs. It can also be seen that the chemical shifts of C1 and C5 have also moved to higher frequencies, compared with the other forms. As with cortisone acetate (see chapter 8), the formation of the hydrogen bond at C3 has a significant effect on the atoms at the termini of the conjugated system, i.e. the electron density is withdrawn from C1 and C5 via the conjugated system, in order that C3 does not have a greatly reduced electron density due to the formation of the hydrogen bond.

The ester carbons C22 and C25 are not easily distinguished even in the solution state. Therefore one may only make solid assignments by assuming that these high frequency shifts occur for the known hydrogen bonds.

If one considers first the case of the ethyl acetate solvate. From the crystal structure it is known that only C25 is involved in hydrogen bonding. Therefore one may assume that this resonance has been shifted to high frequency, and occurs at 179.2 ppm. So by elimination, the C22 resonance is at 175.2 ppm. This conclusion is supported by the fact that the asymmetry is higher for the higher frequency peak (hydrogen bonding causes deformation of the axial symmetry, thereby increasing η). Now the monohydrate is known to be hydrogen bonded via both C22 and C25. If one compares the chemical shifts with those of the ethyl acetate solvate, it seems reasonable that C25 should again resonate at a higher frequency than C22. Note that C22 resonates to higher frequency than in the ethyl acetate solvate, and that both peaks have large asymmetries. Moving on to the anhydrate, where neither are involved in hydrogen bonding, one finds that the resonances are to lower frequency than in the monohydrate. As C25 resonates at the higher frequency of the pair in other solid forms, I will assume that this is the case again here. Both peaks have small asymmetries that are consistent with not being involved in hydrogen bonding.

It seems then that the solution-state spectrum is unusual in that C22 and C25 resonate at about the same frequency. In the solid-state spectra, C25 resonates to high frequency of C22 in all three forms.

9.8. Conclusions

The solution assignment, the results of the NQS experiment and the determination of the shielding tensors for the high-frequency peaks have advanced the assignment of the solid-state NMR spectra of the polymorphs of BDP.

The effect of the quadrupolar ^{35}Cl nucleus upon the ^{13}C spectrum has been studied. In the anhydrate and ethyl acetate solvate, it has been seen that the strong quadrupolar interaction of the chlorine with C9 has caused a considerable degree of line broadening, almost to the extent that the signals are indistinguishable from the noise. Also the interaction of chlorine with carbon atoms further away has been seen, again by broadening of the resonances. This shows that quadrupolar interactions can extend over two bonds from the chlorine nucleus.

The effects of strong quadrupolar interactions have also been seen in the monohydrate. The splitting of the C9 resonance has allowed an estimate of the anisotropy of the spin-spin coupling constant to be made at about 250±100 Hz. Also there is reasonably close agreement between calculated and observed splittings for more distant carbons. Additional splitting caused by coupling to ^{37}Cl nucleus has not been observed. It is interesting that in the anhydrate and ethyl acetate solvate, the broad C9 resonance shows that there is moderately rapid relaxation of the quadrupolar nucleus. However, in the monohydrate, the occurrence of splitting of the C9 resonance shows that the rate of relaxation must be somewhat slower. The reason for the difference in rates of relaxation is unknown, but most be related to small differences in packing or conformation that occur between the polymorphs.

The crystal structure of the ethyl acetate solvate shows that the crystal contains channels where the ethyl acetate is present. The solid-state carbon and proton NMR spectra are so like the corresponding solution state spectra that one draws the conclusion that the ethyl acetate must be in a very mobile environment when in the solid. This means that there are no strong interactions or hydrogen bonds formed between the ethyl acetate and BDP molecules.

The relationship between chemical shift and hydrogen bonding has been explored. As with other steroids, there is some evidence that hydrogen bonds cause a high frequency shift, but firm conclusions are difficult to draw.

9.9. References

(1) Smith, M.M. *Glaxo Internal Report* (1990).

(2) Duax, W.L., Cody V., Strong P.D. *Acta Cryst.* B37, 383 (1981).

(3) Lancaster, R.W. *Glaxo Internal Report* (1991).

(4) Bellamy, L.J. *The infrared spectra of complex molecules;* 2nd ed.; Chapman and Hall: London, (1980); Vol. 2.

(5) Fletton, R. *Glaxo Internal Report* (1989).

(6) Veeman, W.S. *Prog. NMR Spectr.* 16, 193 (1984).

(7) Gobetto, R., Harris R.K., Apperley D.C. *J. Magn. Reson.* 96, 119 (1992).

(8) Harris, R.K., Personal communication.

(9) Olivieri, A., Frydman L., Grasselli M., Diaz L. *Magn. Reson. Chem.* 26, 615 (1988).

(10) Hexem, J.G., Frey M.H., Opella S.J. *J. Chem. Phys.* 77, 3847 (1982).

(11) Olivieri, A.C., Frydman L., Diaz L.E. *J. Magn. Reson.* 75, 50 (1987).

(12) Olivieri, A.C. *J. Magn. Reson.* 81, 201 (1989).

(13) Naito, A., Ganapathy S., McDowell C.A. *J. Magn. Reson.* 48, 367 (1982).

(14) Naito, A., Ganapathy S., McDowell C.A. *J. Chem. Phys.* 74, 5393 (1981).

(15) Zumbulyadis, N., Henrichs P.M., Young R.H. *J. Chem. Phys.* 75, 1603 (1981).

(16) Santuary, B.C., Campolieti G. *Can. J. Chem.* 65, 1746 (1987).

(17) Lide, D.R., Jen M. *J. Chem. Phys.* 38, 1504 (1963).

(18) Lindman, B., S.Forsen In *NMR Basic Principles and Progress*; Eds. Diehl, P., Fluck, E. and Kosfeld, R.; Springer-Verlag: Berlin, (1976); Vol. 12.

(19) Bohm, J., Fenzke D., Pfeifer H. *J. Magn. Reson.* 55, 197 (1983).

(20) Fleming, W.W., Fyfe C.A., Lyerla J.R., Vanni H., Yannoni C.S. *Macromol.* 13, 460 (1980).

(21) Lounila, J., Jokisaari J. In *Progress in NMR spectroscopy*; Eds. Emsley, J.W., Feeney, J. and Sutcliffe, L.H.; Pergamon: Oxford, (1983); Vol. 15; pp 249.

(22) Harris, R.K. *Nuclear magnetic resonance spectroscopy*; Pitman: London, (1983).

(23) Harris, R.K. *J. Magn. Reson.* 78, 389 (1988).

(24) Silverstein, R.M., Bassler G.C., Morrill T.C. *Spectrometric identification of organic compounds;* 4th ed.; J. Wiley & Sons: New York, (1981).

* Becotide, Becloforte and Ventide are trademarks of the Glaxo Group of Companies.

Chapter 10

Cefuroxime Axetil

Chapter 10 Cefuroxime Axetil

10.1. Introduction

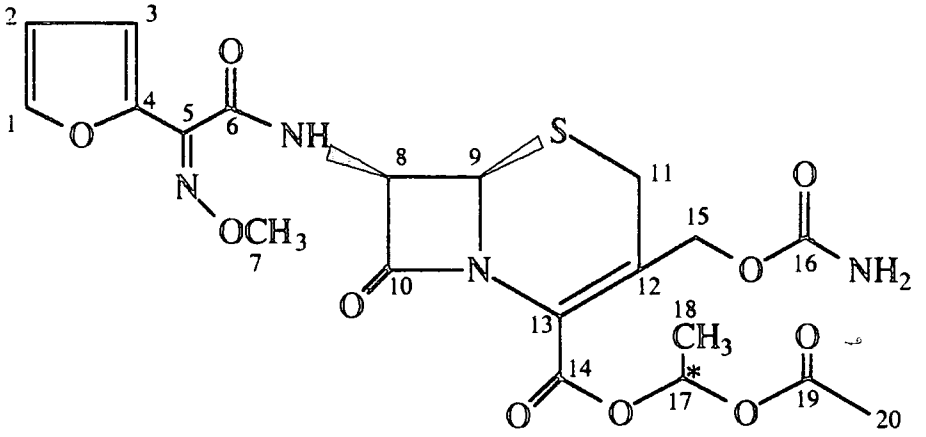

Cefuroxime Axetil

Cefuroxime axetil is a widely-prescribed orally administered antibiotic sold under the trademark ZINNAT*. The dosage form is amorphous, but there are four crystalline forms. The chemical structure is shown above and also the adopted numbering scheme. The carbon atom numbered 17 (and marked with an asterisk) is asymmetric so there are two diastereoisomers that are known as forms A and B. Each diastereoisomer exists as two polymorphs known as I and II. Thus there are four forms in total that are labelled AI, AII, BI and BII. Only the two forms of each diastereoisomer should strictly be regarded as polymorphs, but the existence of diastereoisomers brings an interesting aspect to this work.

For each diastereoisomer, the first forms (i.e. AI and BI) are prepared by recrystallising from organic solvents (a mixture of ethyl acetate and ether is usually used), whilst the second forms of each isomer (i.e. AII and BII) are prepared by recrystallising from aqueous solvents (usually a mixture of acetone and water).

Crystal structures of both forms of the B isomer are known. The structures of the A isomers are not known.

The crystal structure determinations of both forms of the B diastereoisomers have revealed that these have the R configuration at the asymmetric centre (i.e. C17, see figure 10.1). Crystallographic information is

given in table 10.1. The number of molecules in the crystallographic asymmetric unit is given in the table and denoted by Z, whilst the number of molecules in the unit cell is given by N.

Figure 10.1 - Showing the R conformation at the asymmetric carbon atom

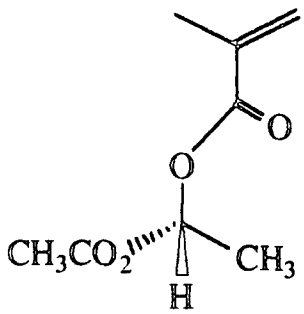

Table 10.1 - Crystallographic information on cefuroxime axetil

form	BI		BII	
space group	$P2_12_12_1$		$P2_1$	
unit cell dimensions§	a=5.047; b=22.176; c=22.738 /Å		a=8.520; b=11.885; c=24.587 /Å	
	α=β=γ=90°		α=γ=90°;β=97.67°	
N	4		4	
Z	1		2	
solvates / unit cell‡	0.1 ethyl acetate (disordered) 0.15 ether		2 water	
Hydrogen bonding *	C(6)NH···O=C(6)	2.938 Å	C_a(6)NH···O=C_a(16)	2.839 Å
	C(16)NH···O=C(10)	2.963 Å	C_a(16)NH···O=C_a(19)	2.998 Å
	C(16)NH···O=C(16)	2.862 Å	C_b(6)NH···O=C_b(16)	2.870 Å

§ unit cell dimensions are known to an accuracy of ±0.001Å

‡ the solvates present in form BI do not occur in stoichiometric amounts, and as the positions of the molecules within the crystal are not well defined, it is possible that the solvate molecules presence is simply the consequence of insufficient drying of the sample. The water present in form BII occupies specific sites within the crystal. There is one water molecule and two cefuroxime axetil molecules per asymmetric unit (twice this number in the unit cell).

* The hydrogen bond lengths given are N-O distances. The a and b subscripts for the BII polymorph indicate how each of the two molecules in the asymmetric unit are bonded.

Identification of the major components of a sample may be accomplished by infra-red spectroscopy, as each form shows some distinctive absorptions. These are summarised in table 10.2. Samples of the polymorphs appear to be stable for several years (at least 3 years).

Table 10.2 - The distinctive infra red absorptions of cefuroxime axetil polymorphs

	AI	AII	BI	BII
-OH and -NH region	3500 3351 3277 3196 (w)	3431 3339 3258	3417 3360 (w) 3303 3216	3615 3553 3497 (sh) 3479 3383 (sh) 3361 3191
C=O region	1779 1749 1711 1661 1612	1786 1771 1717 1699 1653	1782 }(d) 1772 } 1743 (w) 1716 }(d) 1708 } 1653 1626 (w)	1799 1785 1762 1730 1704 1676

Notes: 'w' represents a weak absorption, 'sh' represents a shoulder on a peak, and 'd' represents a doublet.

10.2. Assignment of Solid-State NMR Spectra

The solution-state proton and carbon NMR spectra have been recorded and assigned (see chapter 5). The solid-state carbon NMR spectra of all four forms have been acquired and are assigned in the following section. The chemical shifts are given in tables 10.3 - 10.6, along with information regarding the width of peaks, the peak integral, and whether the peaks remain in the NQS experiment. The assignments are also discussed. The spectra are presented in figures 10.2 -10.5.

Figure 10.2 - The solid-state ^{13}C NMR spectrum of cefuroxime axetil form AI
Spinning sidebands are marked with an asterisk.

operating conditions	^{1}H 90° pulse	contact time	acquisition time	recycle delay	number of transients	spin rate
50 MHz	4 μs	2 ms	0.16 s	10 s	5650	3.3 kHz

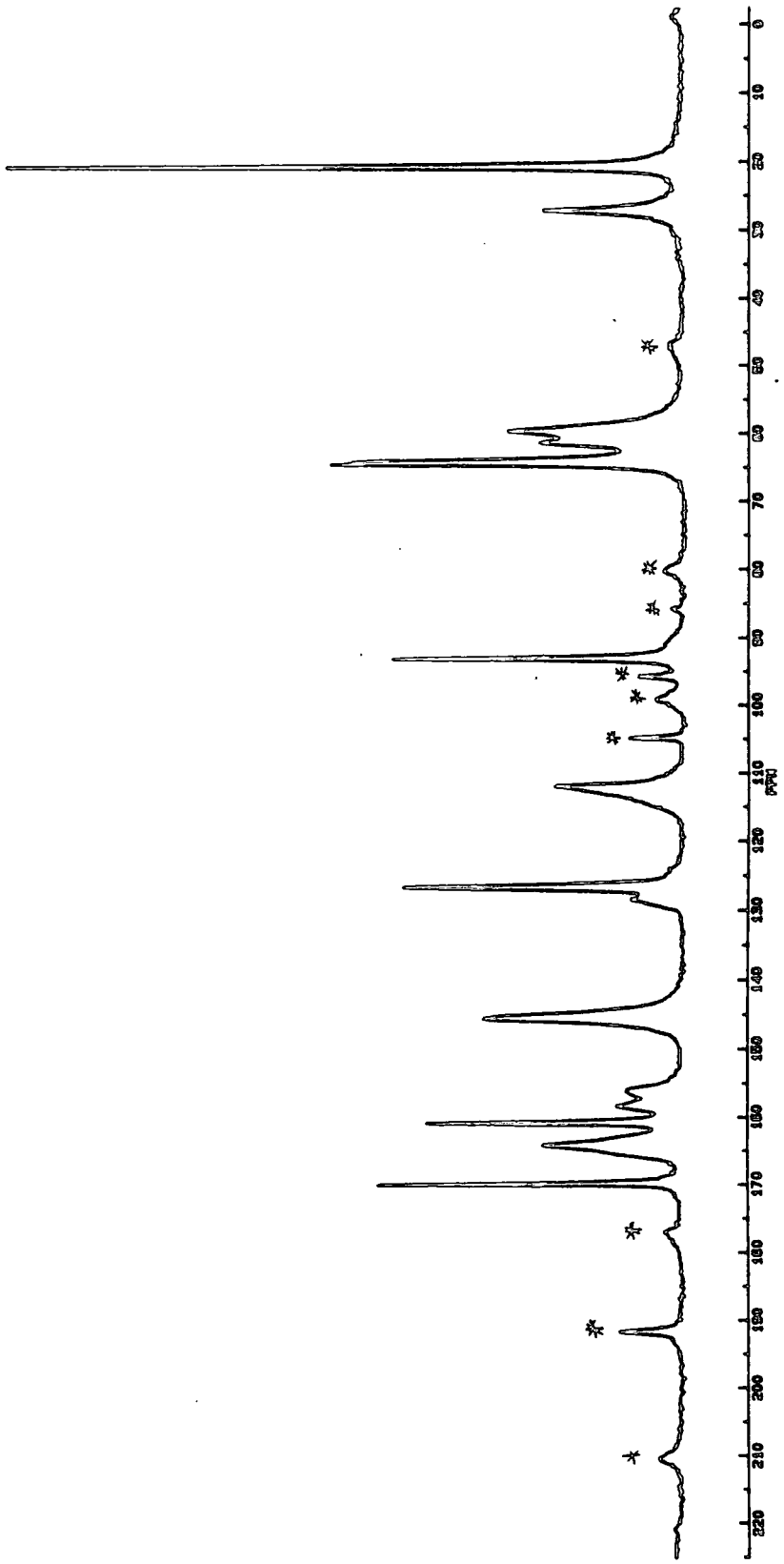

Figure 10.3 - The solid-state ^{13}C NMR spectrum of cefuroxime axetil form AII Spinning sidebands are marked with an asterisk.

operating conditions	^{1}H 90° pulse	contact time	acquisition time	recycle delay	number of transients	spin rate
50 MHz	4 µs	2 ms	0.16 s	10 s	1050	3.3 kHz

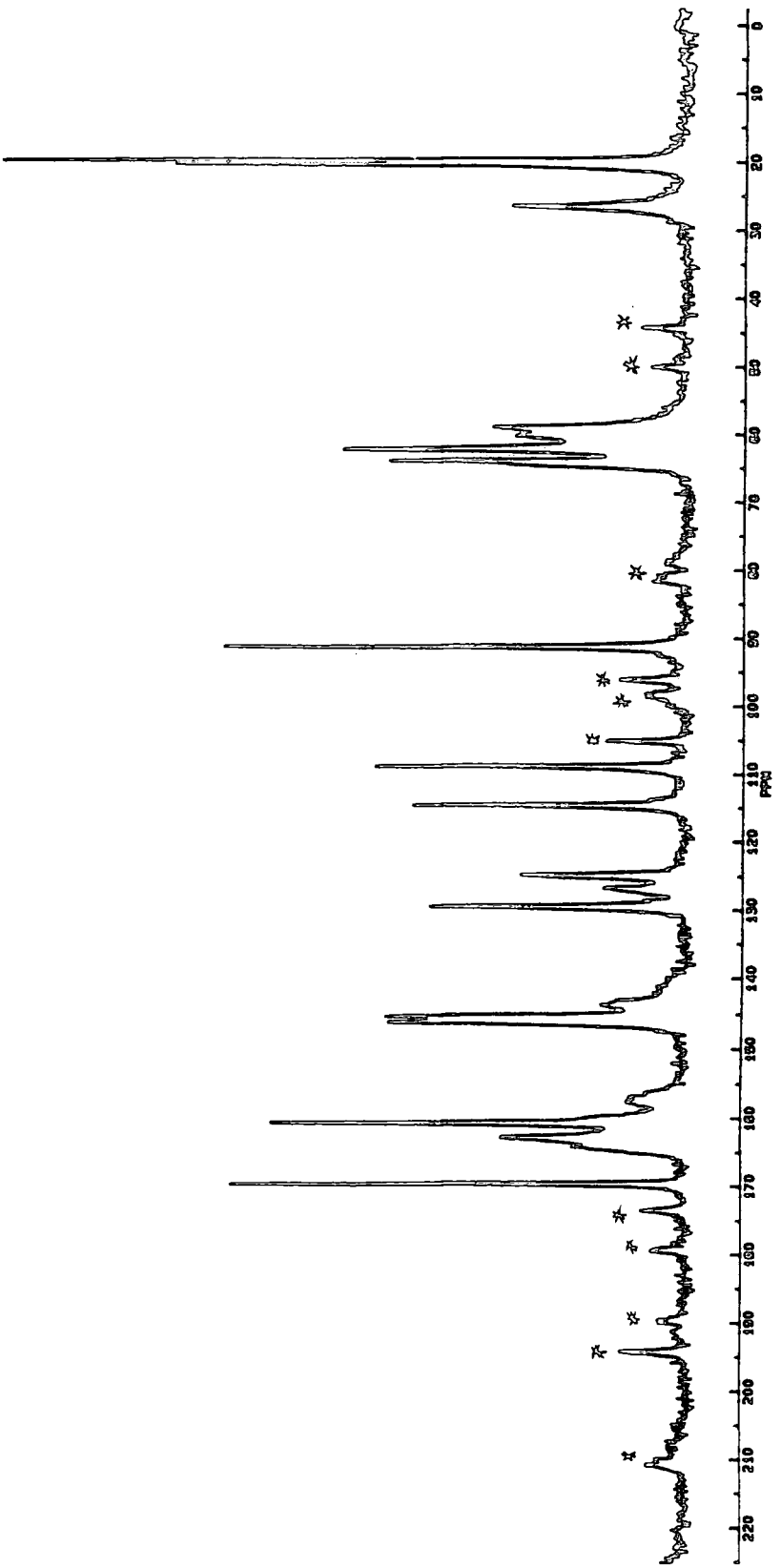

Figure 10.4 - The solid-state ^{13}C NMR spectrum of cefuroxime axetil form BI
Spinning sidebands are marked with an asterisk.

operating conditions	^{1}H 90° pulse	contact time	acquisition time	recycle delay	number of transients	spin rate
50 MHz	4 µs	2 ms	0.16 s	10 s	6400	3.4 kHz

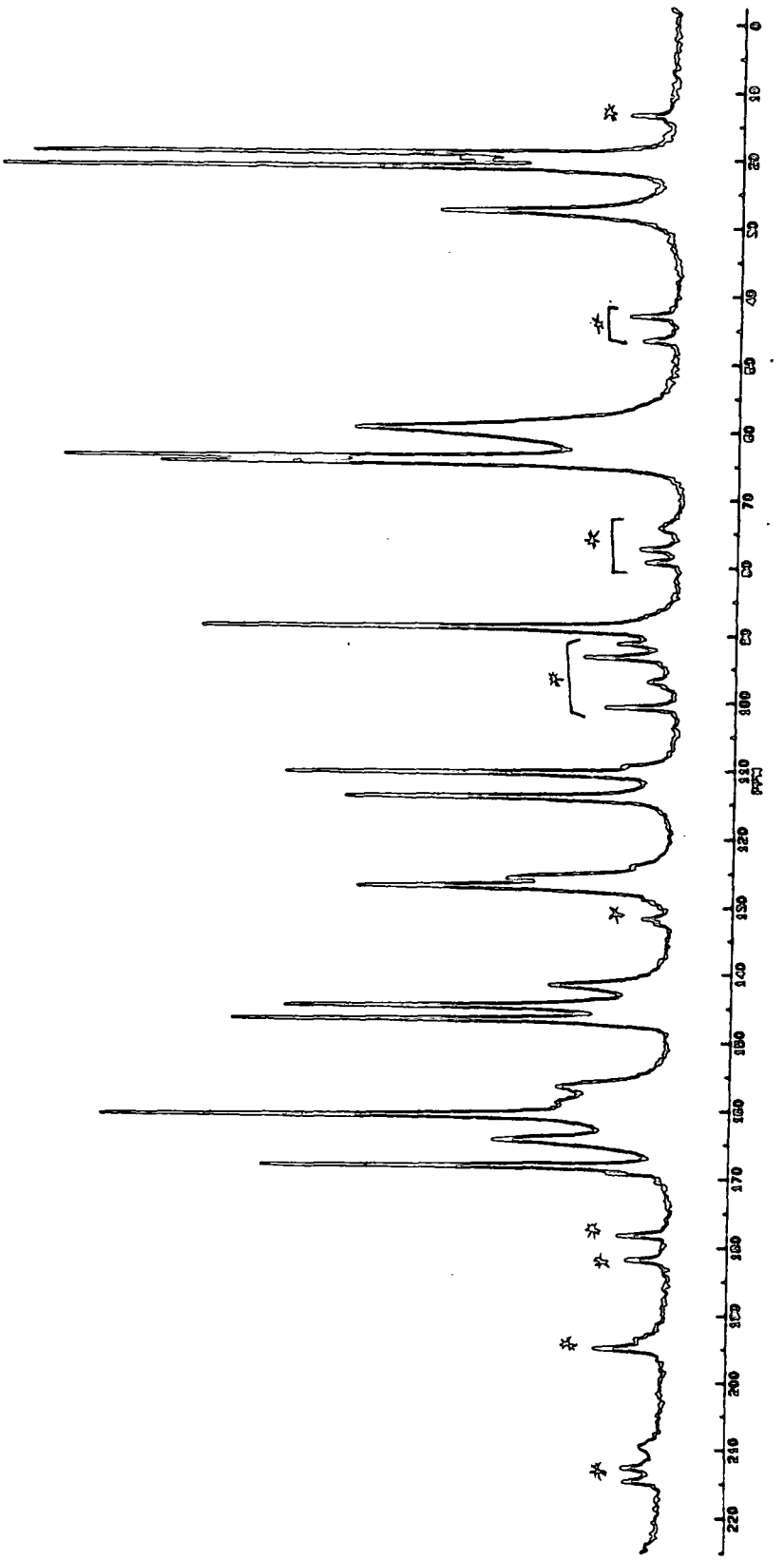

Figure 10.5 - The solid-state ^{13}C NMR spectrum of cefuroxime axetil form BII
Spinning sidebands are marked with an asterisk.

operating conditions	^{1}H 90° pulse	contact time	acquisition time	recycle delay	number of transients	spin rate
50 MHz	4 µs	2 ms	0.16 s	10 s	6360	3.4 kHz

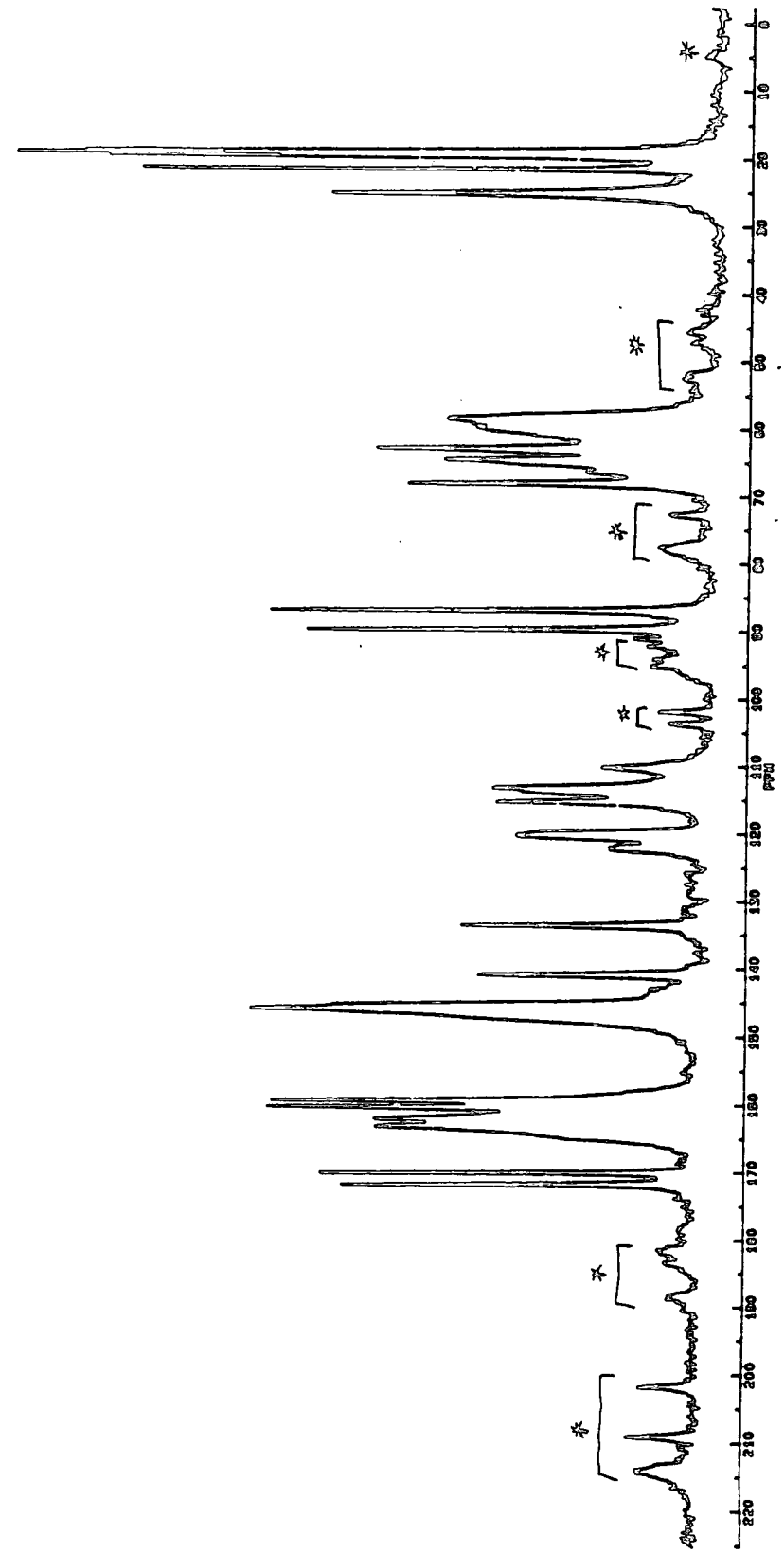

Large linewidths or splittings (into two peaks of relative intensities 2:1) of certain peaks in the spectrum may be expected when the carbon atom is bonded to nitrogen, and this information can aid the assignment. A fuller discussion of the effect of nitrogen on the carbon spectrum is given in section 10.3, and a more general approach is discussed in chapter 9.

10.2.1. Form AI

The solid-state NMR chemical shifts for this form are given in the table 10.3, along with the assigned solution-state shifts for comparison. The results of the NQS experiment are also shown, and broad peaks are also marked. Integration of peaks has also proved useful where peaks overlap.

The high-frequency region of the spectrum (170-150 ppm) is known to contain the resonances from five carbon atoms. As only two of these are from carbons that are not bonded to nitrogen, one assumes that these will be the sharp resonances at 169.8 and 160.7 ppm, so they are assigned C19 and C14 respectively. The peak integrals show that of the remaining three resonances, two are located at 164.1 ppm. This could explain the shoulders that appear on each side of the main peak if at least one resonance has been split into two. This broad peak is therefore assigned as C10 and C6. The two remaining peaks in this region (at 158.3 and 156.2 ppm) together have the intensity of only a single carbon, and as these two peaks have an intensity ratio of 2:1, the effect of the quadrupolar nucleus is clearly seen on this resonance, and is assigned to C16. The chemical shift of C16 should be reported as the weighted average of the two component peaks. Thus for C16 the shift is 157.6 ppm.

The three peaks expected at about 145 ppm (from C1, C4 and C5) are all coincident in form AI at 145.4 ppm. The next region of the spectrum should contain two peaks from C12 and C13. As C13 is bonded to nitrogen, some broadening of this peak may be expected. The peak at 128.3 ppm is broad, but has intensity of only about one half, whilst the sharp peak at 126.5 ppm has an intensity of about three halves. It seems then that the C12 resonance is at 126.5 ppm, but is also overlapping with part of the C13 resonance. As it is

impossible to see which of the two components of the C13 peak has the greater intensity, the chemical shift can only be estimated at around the mid-point of the two, at 127.4 ppm.

The unusual shape of the peak at 111.8 ppm can be ascribed to the overlap of two peaks arising from C2 and C3. The peak at 92.9 ppm can be assigned straightforwardly to C17.

The region of the spectrum around 60 ppm is not straightforward. The two sharp peaks arise from C7 and C15. The NQS experiment shows the methyl carbon (C7) to be at 64.0 ppm, so C15 is assigned as 64.4 ppm. The remaining two peaks at 61.3 and 59.5 ppm are the C8 and C9 resonances, although it is not possible to say exactly how these peaks are made up. Note however that the peak at 61.3 ppm has been boosted in intensity by a sideband of the 126.5 ppm peak.

The remaining region of the spectrum can be simply assigned by comparison with the solution-state shifts. The C11 resonance at 27.2 ppm is broad although it is not bonded to nitrogen. The cause might be insufficient decoupler power, as has been seen in the study of steroids (see chapter 4). The C18 and C20 resonances overlap at 20.8 ppm.

Table 10.3 -Summary of NMR chemical shifts for cefuroxime axetil form AI

Carbon no.	solution shift / ppm	AI solid-state chemical shifts / ppm			Intensity	Notes
19	170.0	169.8	N		1	
10	164.7	164.1	N	b	2	
6	162.6					
14	160.6	160.7	N		1	
16	157.4	157.6	N	b	1	{1}
4	146.6					
1	146.2	145.4	N	b	3	
5	145.4					
13	129.5	~ 127.4	N	b	1/2	{2}
12	125.5	126.5	N		3/2	
3	114.3	111.8		b	2	
2	112.9					
17	89.6	92.9			1	
15	63.7	64.4			1	
7	63.4	64.0	N		1	
8	60.1	61.3		b	2	
9	58.3	59.6		b		
11	27.1	27.2		b	1	
20	21.0	20.8	N		2	
18	19.7					

Notes: 'N' represents a peak that is present in the NQS experiment (i.e. it is a quaternary or methyl carbon atom), and 'b' represents a peak that is broad.

{1} a 2:1 doublet composed of peaks at 158.3 and 156.2 ppm caused by coupling to ^{14}N.

{2} a doublet of peaks at 128.3 and 126.5 ppm caused by coupling to ^{14}N. The relative intensities are obscured by overlap with the C12 resonance

10.2.2. Form AII

Starting again at the high-frequency end of the spectrum, the first region represents five carbon atoms. As with AI, the sharp peaks are easily assigned, and the peak integrals also aid the assignment. The next region around 145 ppm is resolved for form AII. The sharp peaks are C1 and C4, and the NQS experiment shows C4 is the 145.4 ppm peak. The broad peak at 143.8 ppm is from C5. At 125-130 ppm there are three peaks arising from two carbon atoms. The highest-frequency peak is sharp and assigned as C12, whilst the other two broader peaks (having integral ratios of 1:2) are assigned as C13. Thus the chemical shift is 125.5 ppm.

The C2 and C3 resonances at 108.9 and 114.8 ppm cannot be distinguished. The sharp C7 resonance (at 64.1 ppm) is identified by NQS, and C15 is the other sharp peak at 62.4 ppm. The 60.2 and 59.1 ppm peaks arise from C8 and C9, and as with form AI, the exact attribution is not clear. The C11 resonance is found at 26.7 ppm and the methyl resonances (C18 and C20) are resolved but not unambiguously assigned. The chemical shifts and assignments are summarised in table 10.4.

Table 10.4 - Summary of NMR chemical shifts for cefuroxime axetil form AII

Carbon no.	solution shift / ppm	AII solid-state chemical shift / ppm			intensity	Notes
19	170.0	169.8	N		1	
10	164.7	163.1	N	b	2	
6	162.6					
14	160.6	160.8	N		1	
16	157.4	157.5	N	b	1	
4	146.6	145.4	N		1	
1	146.2	146.2			1	
5	145.4	143.8	N	b	1	
13	129.5	125.5	N		1	{3}
12	125.5	129.6	N		1	
3	114.3	114.8			1	
2	112.9	108.9			1	
17	89.6	91.5			1	
15	63.7	62.4			1	
7	63.4	64.1	N		1	
8	60.1	60.2		b	2	
9	58.3	59.1		b		
11	27.1	26.7		b	1	
20	21.0	20.6	N		1	
18	19.7	19.9	N		1	

Notes: 'N' represents a peak that is present in the NQS experiment, and 'b' represents a peak that is broad.

{3} a 1:2 doublet of peaks at 126.8 and 124.9 ppm caused by quadrupolar coupling to ^{14}N.

10.2.3. Form BI

As with the other forms C19 is assigned as the high frequency sharp peak and C14 is the other sharp peak. The broad peak at 164.6 ppm represents one carbon atom only, probably C10. The other two peaks in this region, 158.9 and 156.8 ppm, along with the broad background under the peak at 161.1 ppm originates C6 and C16.

The sharp C4 resonance is identified from the NQS spectrum, and C1 is the other sharp peak. Therefore C5 is assigned as the broad peak at 141.9 ppm. C12 and C13 can be distinguished on the basis that C13 is the broader peak of the pair at 126.0 ppm. C2 and C3 still cannot be distinguished. C7 is identified by NQS and C15 is the sharp peak at 64.9 ppm. Therefore C8 and C9 are responsible for the broad resonance at 59.8 ppm. C18 and C20 cannot be distinguished. the chemical shifts are summarised in table 10.5.

Table 10.5 - Summary of NMR chemical shifts for cefuroxime axetil form BI

Carbon no.	solution shift / ppm	BI solid-state chemical shift / ppm			intensity
19	170.0	168.5	N		1
10	164.7	164.6	N	b	1
14	160.6	161.1	N		1
6	162.6	158.9	N	b	2
16	157.4	156.8	N	b	
4	146.6	147.0	N		1
1	146.2	145.0			1
5	145.4	141.9	N	b	1
13	129.5	126.0	N	b	1
12	125.5	127.3	N		1
3	114.3	114.2			1
2	112.9	110.7			1
17	89.6	89.1			1
15	63.7	64.9			1
7	63.4	64.1	N		1
8	60.1	59.8		b	2
9	58.3				
11	27.1	27.8		b	1
20	21.0	21.4	N		1
18	19.7	19.4	N		1

Notes: 'N' represents a peak that is present in the NQS experiment, and 'b' represents a peak that is broad.

10.2.4. Form BII

The most striking feature of the spectrum of form BII is the large number of peaks. From the crystal structure this form is known to have two molecules in the asymmetric unit with slightly different conformations. Therefore a doubling of the number of peaks in the spectrum may be expected.

C19 is assigned to the two sharp highest frequency peaks at 171.7 and 170.0 ppm, whilst C14 is assigned to the other two sharp peaks at 160.2 and 159.3 ppm. The other three carbons can account for the broad peaks at 163.2 and 162.0 ppm, along with the broad signal that extends under the sharp C14 resonances.

The broad and unusually shaped peak at 145.9 ppm may be assigned on the basis of peak integrals as C1, C4 and C5. At first, one may be tempted to assign the peak at 140.9 ppm to this group, and then the assignment of the 133.6 ppm peak is unclear. But I believe that this is not the case, and can be justified as follows. The C12 and C13 resonances are expected at 125-130 ppm, but for BII, there are no peaks in this region. One is forced therefore to look further away. The C13 resonances may be found at 122.4 and 120.3 ppm as a broad 1:2 doublet, and the peak integral allows only two atoms (both C13) to be assigned to this group. (The chemical shift should therefore be given as 121.0 ppm if both molecules have identical shifts for C13). To look to even lower frequency for the C12 resonance then becomes unreasonable, so the C12 resonances must be shifted to higher frequency. An obvious choice is the 133.6 ppm peak, but the peak integral shows this to arise from only one carbon. Therefore the other C12 resonance must be located at 140.9 ppm. This large frequency shift or the C12 nucleus will be discussed later.

To proceed with the assignment: the region 115-110 ppm must be assigned to C2 and C3. The integral for this region is consistent with four carbon atoms, although exact assignments are not possible. The 113.2 ppm peak has double intensity and this explains the apparent broadness of the peak as two resonances are not resolved here. Two peaks are clearly seen for C17 as expected.

The region around 60 ppm is not simple to assign. There are three reasonably sharp peaks at 68.1, 64.6 and 63.0 ppm, which have approximate intensities of 1:1:2, and only the 63.0 ppm peak remains in the NQS experiment. Therefore 68.1 and 64.6 ppm are assigned as C15, whilst 63.0 ppm is assigned as C7. The broad and ill-defined peak at 58.6 ppm corresponds in intensity to four carbons, so is assigned as C8 and C9.

The C11 carbons are not resolved at 25.2 ppm, but four methyl peaks are seen, although unambiguous assignment is not possible. The assignments are summarised in table 10.6.

Notes for table 10.6 : 'N' represents a peak that is present in the NQS experiment, and 'b' represents a peak that is broad. Each carbon atom should, for this form, have a total intensity of 2, as there are two crystallographically independent molecules in the asymmetric unit. The asterisk is to denote that even in the solution-state, the assignment of these two peaks is not certain.

{4} a 1:2 doublet of peaks at 122.4 and 120.3 ppm caused by quadrupolar coupling to ^{14}N.

Table 10.6 - Summary of NMR chemical shifts for cefuroxime axetil form BII

Carbon no.	solution shift /ppm	BII solid-state chemical shift / ppm			intensity	Notes
19	170.0	171.7	N		1	
		170.0	N		1	
10	164.7	163.2	N	b	6	
6	162.6	162.0	N	b		
16	157.4					
14	160.6	160.2	N		1	
		159.3	N		1	
4	146.6					
1	146.2	145.9	N	b	6	
5	145.4					
13	129.5*	121.0	N	b	2	{4}
12	125.5*	140.9	N		1	
		133.6	N		1	
3	114.3	115.3			1	
2	112.9	113.2		b	2	
		110.2			1	
17	89.6	89.8			1	
		87.0			1	
15	63.7	68.1			1	
		64.6		b	1	
7	63.4	63.0	N		2	
8	60.1	58.6		b	4	
9	58.3					
11	27.1	25.2		b	2	
20	21.0	21.6	N		1	
18	19.7	19.8	N		1	
		19.3	N		1	
		18.9	N		1	

10.3. The Effect Of A Quadrupolar Nucleus On The Spectrum Of A Spin-$\frac{1}{2}$ Nucleus.

The effect of a quadrupolar nucleus on the spectrum of a spin-1/2 nucleus was discussed in chapter 9. The shape of the line depends upon several factors, one of which is the rate of relaxation of the quadrupole. The spectrum of carbons bonded to nitrogen may appear as:

1) a single sharp line (if relaxation is rapid)
2) a single broad line (if relaxation is somewhat slower)
3) a pair of lines of 2:1 intensities that arise as a consequence of spin-spin and quadrupolar coupling (if relaxation is slow).

However, a single sharp (or broad) line can also occur if the quadrupolar coupling constant is small or for particular orientations of the internuclear distance in the electric field gradient.

A schematic diagram illustrates case (3) above. The sign of the splitting is positive.

Figure 10.6 - Schematic diagram showing the effect of a quadrupolar nucleus, of spin 1, on the spectrum of a spin $\frac{1}{2}$ nucleus.

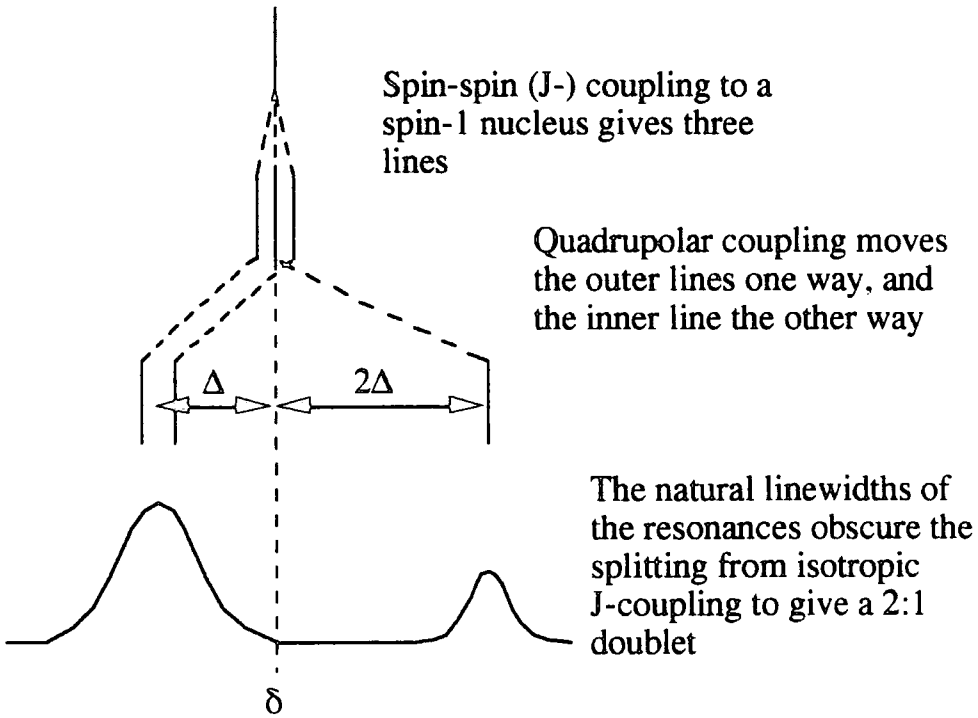

Broadness or splitting of these carbon resonances may be expected in certain cases and this can aid the assignment of the spectrum. The second-order splitting (Δ) is given by[1]:

$$\Delta = \frac{3\chi D'}{20\nu_S}\left(\frac{S(S+1)-3m_S^2}{S(2S-1)}\right)(3\cos^2\beta^D - 1 + \eta\sin^2\beta^D\cos 2\alpha^D) \quad \ldots\ldots 1$$

where χ is the quadrupolar coupling constant, D' is the effective dipolar coupling constant (which takes account of the anisotropy of the spin-spin coupling constant ΔJ ($D' = D - \frac{1}{3}\Delta J$)), ν_S is the Larmor frequency of the quadrupolar nucleus, S is the nuclear spin quantum number of the quadrupolar nucleus, m_S is the component of the nuclear spin quantum number, and the angles α^D and β^D describe the orientation of the internuclear distance with respect to the electric field gradient (see figure 9.11).

So, the effect of ^{14}N on the outer most lines (i.e. $S = 1$, $m_S = \pm 1$) will be to give a splitting of:

$$\Delta = \frac{-3\chi D'}{20\nu_S}(3\cos^2\beta^D - 1 + \eta\sin^2\beta^D\cos 2\alpha^D) \quad \ldots\ldots 2$$

Such effects were first reported several years ago[2-8] for the C-N case, and for other systems e.g. $^{35/37}Cl$—^{119}Sn [9-11] and ^{31}P—^{63}Cu [12]. There have since been may reports dealing with the effect from both experimental and theoretical view points[1,13-17]. There has also been a report of the effect of chlorine on the spectrum of the cephalosporin cefaclor dihydrate[18].

Now if the anisotropy in the spin-spin coupling (ΔJ) is small then:

$$D' = D = \frac{\mu_0\gamma_1\gamma_2\hbar\, r^{-3}}{8\pi^2} \quad \ldots\ldots 3$$

where μ_0 is the permeability of a vacuum, γ_1 and γ_2 are the magnetogyric ratios of ^{13}C and ^{14}N, and r is the internuclear distance ^{13}C-^{14}N. For C–N, ΔJ has been found for a few cases[19] and is about 10 Hz, which is very small compared with the value of D (which for a typical[20,21] organic compound r=1.46 Å, has the value D=702 Hz, or for a typical cephalosporin of r= 1.36 Å, so D=868 Hz), so the effect of ΔJ on D' may be ignored.

If Δ, $\mathbb{D}$' and ν_S are known, and some assumptions about the orientation of r in the electric field gradient can be made, then the quadrupolar coupling constant χ can be found.

The following constants have been used in the calculations.

$\mu_0 = 4\pi \times 10^{-7}$ kg m s^{-2} A^{-2}

γ_1 (^{13}C) = + 6.728 x 10^7 rad T^{-1} s^{-1}

γ_2 (^{14}N) = + 1.9338 x 10^7 rad T^{-1} s^{-1}

$\hbar = 1.055 \times 10^{-34}$ J s

$\nu_S = 7.2 \times 10^{-2} \times \nu_H$ (where ν_H is the proton Larmor frequency)

r is known from the crystal structure determination and the values are given in table 10.7.

Table 10.7 - The C-N bond lengths and the calculated values of D

bond	C13-N	C16-N	D (C13) / Hz	D (C16) / Hz
BI	1.389	1.325	+ 815	+ 939
BII (a)	1.408	1.306	+ 783	+ 981
BII (b)	1.415	1.330	+ 771	+ 929
average	1.404	1.320	+ 789	+ 950

The value of D calculated from the average bond lengths (i.e. 789 Hz) must be used for forms AI and AII as the actual bond lengths are not known for these forms. For form BII one must use the average of the two BII values (i.e. 777 Hz) as it is not known which molecule gives rise to each peak.

The splittings of peaks have been noted in the solid-state spectra and are summarised in table 10.8.

Table 10.8 - Splittings arising from coupling to ^{14}N

Form	Carbon no.	peak positions / ppm		intensity ratio	chemical shift /ppm	peak separation /Hz	Δ / Hz	χ / MHz
AI	C13	128.3	126.5	~1:1‡	127.4	90.6	± 30.2	± 5.54
AI	C16	158.2	156.2	2:1	157.6	100.6	+ 33.5	+ 3.25
AII	C13	126.8	124.9	1:2	125.5	95.6	- 31.9	- 5.86
BII	C13	122.4	120.3	1:2	121.0	105.7	- 35.2	- 6.46

Notes: ‡ the lower frequency peak is partially obscured and so the intensity ratio is not clear. For C13 values of β = 109.5°and η = 0 have been used. For

C16, $\beta = 90^\circ$, $\alpha = 50^\circ$ and $\eta = 0.263$ have been used. The choice of these orientations for C13 and C16 is discussed below.

Now to calculate the value of the quadrupolar coupling constant one must have some information about the orientation of the electric field gradient with respect to the molecule. For cefuroxime axetil, the orientation of the C–N bond in the electric field gradient is unknown, i.e. α and β are unknown. Also the asymmetry (η) is unknown. However, β and η are often zero for amino acids and nitriles[14]. For $N(CH_3)_3$ [22,23], triethylenediamine[13],and NR_3 [14], η is zero and β is given as, or assumed to be, the tetrahedral angle of 109.5°. In these cases χ is given as ±3.7 MHz. Whilst axial symmetry ($\eta = 0$) may not describe accurately the environment in cefuroxime axetil of the nitrogen atom bonded to C9, C10, and C13 (as these three atoms are not symmetrically disposed about the nitrogen) it may be a reasonable approximation. Therefore for the splittings at C13, β is assumed as 109.5° and η is assumed to be 0. The calculated quadrupolar coupling constants are given in table 10.8 and range from ± 5.54 to - 6.46 MHz (with an average value of - 5.95 MHz, assuming that in each case the sign is negative).

However, the situation with regards to C16 is not so clear as there is no reason to assume that there should be axial symmetry of the electric field gradient, or that the angle between the C-N bond and the electric field gradient will be the tetrahedral angle. The work of others[14,15] may give some clues as to a suitable approach. For aniline, the quadrupolar coupling constant is known to be - 3.977 MHz, the C-N bond length is 1.37 Å, and the asymmetry equals 0.263. The ^{13}C NMR spectrum could be simulated if $\beta^D = 90^\circ$ and $\alpha = 50^\circ$. The same parameters were used to simulate the CNH_2 resonance in the spectrum of 2,6-dimethyl-3-nitroaniline. So it does not seem unreasonable to use these parameters in order to calculate the quadrupolar coupling constant for cefuroxime axetil. Thus χ is calculated for C16-N using r = 1.32 Å (therefore D = 950 Hz), $\beta^D = 90^\circ$, $\alpha^D = 50^\circ$ and $\eta = 0.263$ to give a χ = + 3.25 MHz. This

is in reasonable agreement with the values obtained for aniline and its derivatives of about 4 MHz.

Now these calculations give reasonable values for the quadrupole coupling constants. But how inaccurate would such calculations be if the assumptions made were incorrect? The splitting is dependent upon α and β, and if β increases, the influence of α becomes stronger i.e. if $\beta = 0°$, then χ is independent of α, but when $\beta = 90°$, χ is heavily dependent upon α with a $(-1+\eta\cos 2\alpha)$ relationship. Also as β increases, the influence of the magnitude of η is more pronounced. Therefore in the above calculations, based upon $\beta = 109.5°$ (for C13) or $\beta = 90°$ (for C16), the actual values of α and η used will be important. This should be borne in mind when comparing the χ found here with a literature value for aniline of -3.977 MHz[14].

An example of the possible errors for C13 in form AI is as follows: D=789 Hz, Δ= 30.2 Hz and β=109.5°. Now if η=0.1 and α=5° (instead of both being zero), then χ = 6.38 MHz, i.e. an error of ~13% in the value of χ.

10.4. The Chemical Shifts Of C12 and C13 In Form BII

It was noted that the C13 resonances in form BII from both molecules in the asymmetric unit were coincident, or if they are not exactly coincident, the difference in chemical shifts is small. This ambiguity arises simply because each peak is split by the quadrupolar nitrogen into two, but the two patterns seem to overlap very closely. The chemical shifts have been moved to lower frequency compared with the other polymorphs and solution. However, the C12 resonances are well separated, and shifted to high frequency compared with other forms. The chemical shifts of the C12 and C13 resonances are given in table 10.9.

Figure 10.7 - Showing the conformation of the two molecules in the asymmetric unit for form BII. The four- and six-membered rings have been fitted together.

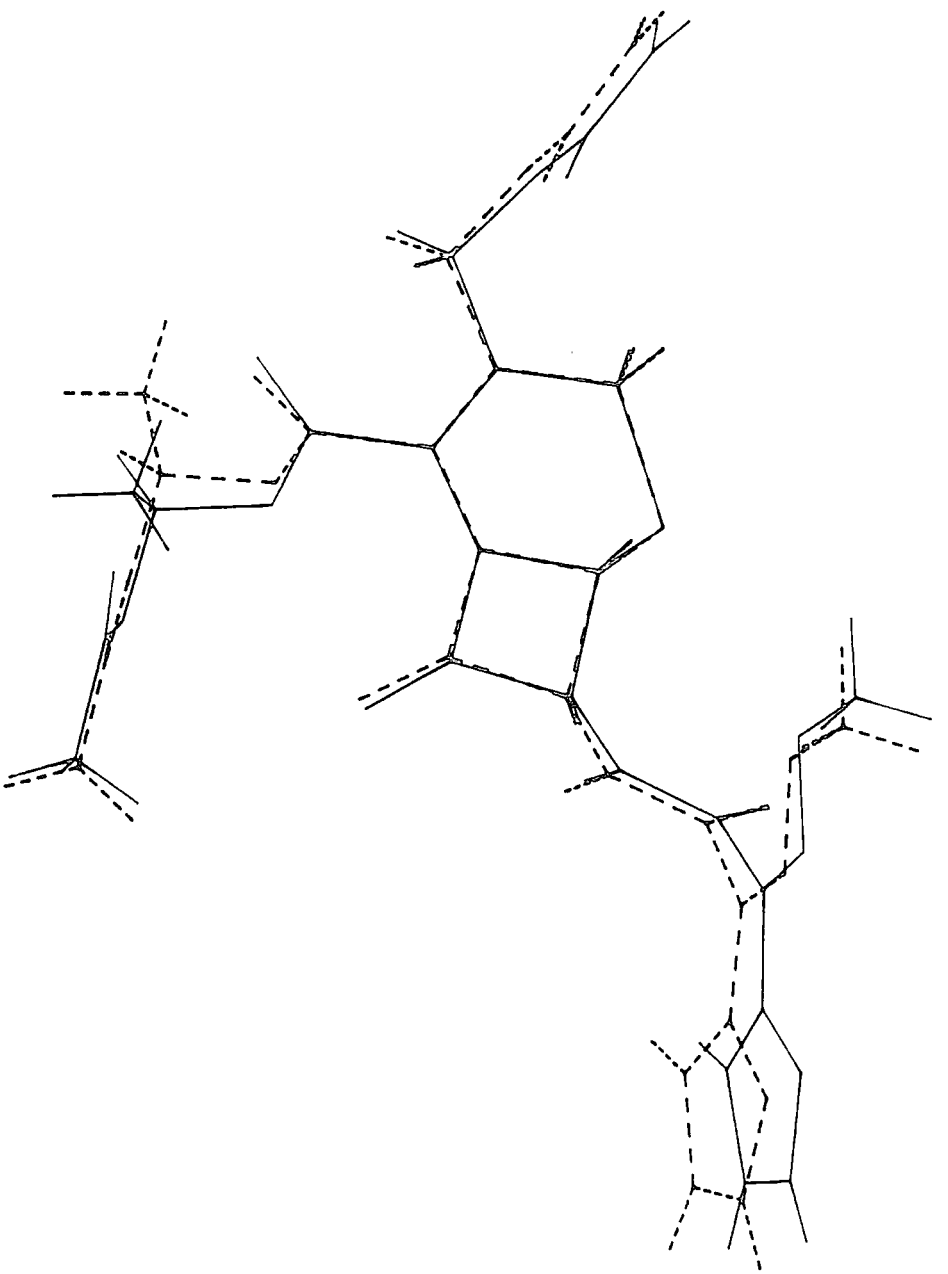

Table 10.9 - The chemical shifts of the C12 and C13 resonances

carbon number	average chemical shift *	BII chemical shifts / ppm	difference /ppm (BII - average)
C12	128.7	140.9 and 133.6	12.2 and 4.9
C13	125.9	121.0	-4.9

* the average chemical shift is that of the solution-state and three solid polymorphs, forms AI, AII and BI.

These figures clearly show that the chemical shift differences are large. A difference of nearly 5 ppm is significant (and larger than that caused by the formation of hydrogen bonds). However, the shift of one of the C12 resonances by more than 12 ppm is, on first appearances unlikely, and a reason for such a large shift must be sought.

The crystal structures of the BI and BII forms have been studied, and in particular, differences between the two molecules present in the asymmetric unit of form BII have been investigated. Figure 10.7 shows the two different molecules in the BII polymorph overlaid with the fitting about the four- and six-membered rings. The differences in conformation seem to be quite small, and so the large splitting of the C12 resonance is not easily explained. Also the bond distances of these two molecules and of form BI have been compared, see figure 10.8 and table 10.10.

Figure 10.8 - The numbering scheme around the four- and six-membered rings.

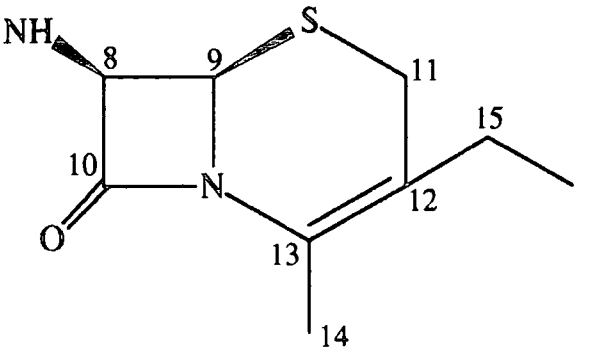

Table 10.10 - The bond lengths (in Å) around the four- and six-membered rings

bond length / Å	BI	BII (molecule a)	BII (molecule b)	
C8-C9	1.539	1.557	1.553	*
C9-S	1.801	1.799	1.799	
S-C11	1.818	1.807	1.817	*
C11-C12	1.518	1.509	1.520	*
C12-C13	1.334	1.358	1.342	*
C13-N	1.389	1.408	1.415	*
N-C10	1.382	1.392	1.368	*
N-C9	1.478	1.465	1.471	
C13-C14	1.505	1.507	1.516	
C12-C15	1.486	1.486	1.477	

Particularly noteworthy are the differences in the lengths of bonds marked with an asterisk. One is really looking for bonds that are rather different in all three forms - i.e. for BII bonds that are significantly different from BI, thus explaining a shift from the average chemical shift, and for BII bonds that are different from each other, thus causing significant splitting of the resonances. This is the case for bonds C12-C13, C13-N and N-C10. Therefore, the differences in bond lengths around C12 and C13 perhaps allow some scope for moderate chemical shift differences. However, I do not believe that the conformational differences alone could account for a shift of 12 ppm. Other differences could be in the packing. The 'a' molecules form two hydrogen bonds whilst the 'b' molecules form only one. Therefore the 'a' molecules are packed rather closer together.

The other possible assignment of the 140 ppm peak is that it is from C1 or C4. Bond lengths around the five-membered ring have also been investigated to see if there is a ready explanation for one peak being shifted to low frequency by about 5 ppm. See figure 10.9 and table 10.11.

Figure 10.9 - Numbering scheme around the five-membered ring

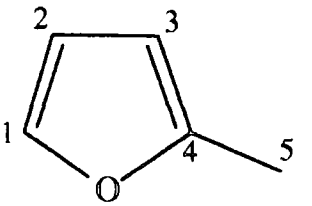

Table 10.11 - The bond lengths (in Å) around the five-membered ring

	BI	BII (a)	BII (b)
O-C1	1.383	1.372	1.389
C1-C2	1.295	1.312	1.320
C2-C3	1.477	1.445	1.397
C3-C4	1.360	1.330	1.367
C4-O	1.426	1.340	1.360
C4-C5	1.432	1.453	1.442

The table clearly shows that all bond lengths around the five-membered rings are different in these three molecules, so again firm conclusions are difficult to draw as to the reason for only one of the BII molecules exhibiting a low frequency shift at C1 or C4.

One must conclude then that there is no firm crystallographic evidence to confirm that the C12 resonance should shift by such a large amount. One must then regard the assignment with a degree of scepticism, remembering of course that the assignment is made solely on the basis of peak integrals (which are not normally regarded as quantitative in the solid-state). The possibility of the peak arising from either C1 or C4 can be neither confirmed nor rejected by crystallography. Therefore the assignment of the peak at 140 ppm remains uncertain. However, it is interesting to note that large chemical shift differences (between solid and solution) of more than 4 ppm have been noted for cefaclor dihydrate[18] at positions equivalent to C13 and C10. These differences were attributed to the presence of a hydrogen bond involving C10. It should be pointed out here that the quality of the solid-state spectra were rather poor due, it is said, to the presence of chlorine in the molecule. The broadness of the peaks in the spectrum of cefaclor prevents further comparisons being made with the spectra of cefuroxime axetil. The structure of cefaclor is presented in figure 10.10 with

the positions equivalent to C10 and C13 in cefuroxime axetil marked with an asterisk.

Figure 10.10 - The structure of cefaclor

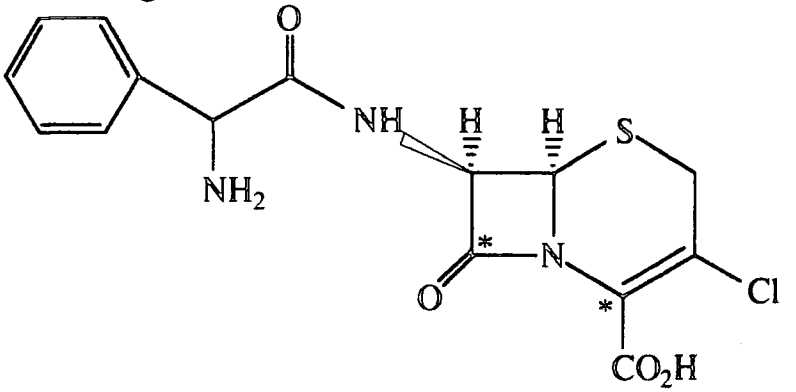

10.5. The Effect Of Hydrogen Bonding

As the mode of hydrogen bonding is known for two of the four forms, it is interesting to see if there are the high frequency shifts that one associates with the formation of hydrogen bonds. A summary of the bonding present is given in table 10.12.

Table 10.12 - The hydrogen bonds present in forms BI and BII

	BI	length / Å	BII	length / Å
Hydrogen bonding *	C(6)NH···O=C(6)‡	2.938	C_a(6)NH···O=C_a(16)	2.839
	C(16)NH···O=C(10)	2.963	C_a(16)NH···O=C_a(19)	2.998
	C(16)NH···O=C(16)‡	2.862	C_b(6)NH···O=C_b(16)	2.870

‡ these hydrogen bonds are between adjacent molecules.

* the bond lengths are N-O distances

Table 10.13 - The chemical shifts (in ppm) of atoms potentially involved in hydrogen bonding

	solution	AI	AII	BI	BII
C19	170.0	169.8	169.8	168.5	171.7 and 170.0
C10	164.7	164.1	163.1	164.6	
C6	162.6	164.1	163.1	158.9	163.2 and 162.0
C16	157.4	157.6(d)	157.5	156.8	

(d) denotes that the peak is seen as a 2:1 doublet

Starting with form BII, one might expect to see a high frequency shift for C19 in the 'a' molecule as this is involved in a hydrogen bond. The figures in

table 10.13 confirm this. The other C19 resonance and that in form BI have not been shifted to high frequency. Therefore as the other polymorphs do not show high frequency shifts at C19 one must assume that they too are not involved in hydrogen bonding.

Both C16 resonances in form BII are expected to show high frequency shifts as both are involved in hydrogen bonds. Although the C16 resonances cannot be differentiated from the other peaks (from C6 and C10) in this region, the general position has been shifted to high frequency compared to the solution-state. Therefore the chemical shifts are in accordance with what would be expected from the crystal structure.

For form BI, C6, C10 and C16 are all involved in hydrogen bonds and so might be expected to occur to high frequency of the solution-state positions. However, C10 has not shifted, and C6 and C16 seem to have moved to low frequency. There is no obvious reason for this result, and so it can only be suggested that small conformational differences have caused low frequency shifts at many positions in the molecule.

This makes prediction of the mode of hydrogen bonding in forms AI and AII very difficult. If one continues to assume that hydrogen bonds will cause high frequency shifts then one draws the conclusion that neither C19 nor C16 are involved in such bonds in forms AI and AII. The C6 resonance has moved a little to high frequency in form AI and so might be involved in a hydrogen bond, but as the difference is so small, a firm conclusion is difficult to draw. If however, there are conformational differences from the solution-state, the comparisons are invalid, and so no conclusions can be drawn in this case. Therefore the modes of hydrogen bonding in forms AI and AII remain unknown.

10.6. Conclusions

The study of the polymorphs of Cefuroxime axetil has allowed the effect of ^{14}N on the ^{13}C spectrum to be investigated. The occurrence of broadening of peaks has mostly aided the assignment of the spectra. It has also been possible to

calculate the quadrupolar coupling constant in certain favourable cases where splitting of peaks has occurred. For the ^{14}N-C16 case, χ has been calculated to be + 3.25 MHz, whilst for ^{14}N-C13 the average figure is - 5.95 MHz. It has been possible to find the sign of χ, assuming that the assumptions of orientation are correct.

10.7. References

(1) Olivieri, A.C. *J. Magn. Reson.* 81, 201 (1989).

(2) Frey, M.H., Opella S.J. *J. Chem. Soc. Chem. Commun.* 474 (1980).

(3) Groombridge, C.J., Harris R.K., Packer K.J., Say B.J., Tanner S.F. *J. Chem. Soc. Chem. Commun.* 174 (1980).

(4) Opella, S.J., Frey M.H., Cross T.A. *J. Am. Chem. Soc.* 101, 5856 (1979).

(5) Jonsen, P. Ph.D. Thesis, Univ. East Anglia, (1984).

(6) Harris, R.K., Jonsen P., Packer K.J. *Org. Magn. Reson.* 22, 784 (1984).

(7) Harris, R.K., Jonsen P., Packer K.J. *Magn. Reson. Chem.* 23, 565 (1985).

(8) Harris, R.K., Jonsen P., Packer K.J., Campbell C.D. *Magn. Reson. Chem.* 24, 977 (1986).

(9) Apperley, D.C., Bai H., Harris R.K. *Molec. Phys.* 68, 1277 (1989).

(10) Harris, R.K. *J. Magn. Reson.* 78, 389 (1988).

(11) Komoroski, R.A., Parker R.G., Mazany A.M. *J. Magn. Reson.* 73, 389 (1987).

(12) Menger, E.M., Veeman W.S. *J. Magn. Reson.* 46, 257 (1982).

(13) Hexem, J.G., Frey M.H., Opella S.J. *J. Chem. Phys.* 77, 3847 (1982).

(14) Olivieri, A.C., Frydman L., Diaz L.E. *J. Magn. Reson.* 75, 50 (1987).

(15) Naito, A., Ganapathy S., McDowell C.A. *J. Magn. Reson.* 48, 367 (1982).

(16) Naito, A., Ganapathy S., McDowell C.A. *J. Chem. Phys.* 74, 5393 (1981).

(17) Olivieri, A., Frydman L., Grasselli M., Diaz L. *Magn. Reson. Chem.* 26, 615 (1988).

(18) Martinez, H., Byrn S.R., Pfieffer R.R. *Pharmaceutical Research* 7, 147 (1990).

(19) Lounila, J., Jokisaari J. In *Progress in NMR spectroscopy*; Eds. Emsley, J.W., Feeney, J. and Sutcliffe, L.H.; Pergamon: Oxford, (1983); Vol. 15; pp 249.

(20) Pine, S.H., Hendrickson J.B., Cram D.J., Hammond G.S. *Organic Chemistry;* 4th ed.; McGraw-Hill: Singapore, (1981).

(21) Gilchrist, T.L. *Heterocyclic chemistry*; Pitman: London, (1985), pp 12.

(22) *Nitrogen NMR*; Witanowski, M., Webb G.A., Ed.; Plenum Press: (1973).

(23) Harris, R.K. *Nuclear magnetic resonance spectroscopy*; Pitman: London, (1983).

* ZINNAT is a trademark of the Glaxo Group of Companies.

Chapter 11

Concluding Remarks

Chapter 11 Concluding Remarks

A great deal of the work done during the course of study has been aimed at assigning solid-state NMR spectra. Several techniques have been employed: solution-state assignment, non-quaternary suppression, non-quaternary suppression with a variable decoupling window, variable contact time experiments and the determination of the time constant of the rate of cross-polarisation and single pulse experiments to identify solvate molecules. But perhaps the most important method that has been used in this work, is the determination of the shielding tensor components. This has allowed the high frequency region of the spectra of several steroids to be assigned. With the high frequency region assigned, the chemical shifts of atoms resonating at high frequency have been linked to the hydrogen bonds that are formed. This has allowed the mode of hydrogen bonding to be predicted in forms of cortisone acetate for which the crystal structure is not available. Thus important crystallographic information has been gleaned from the solid-state NMR spectrum. The effect of the formation of hydrogen bonds upon the shielding tensor components of carbonyl and ester carbons has been studied, and found to cause a high frequency shift in δ_{22}, which is probably oriented along the C=O bonds. This leads to a high frequency shift in the isotropic chemical shift, an effect that is often observed.

The effect of the conformation of the D ring in cortisone acetate on the chemical shifts of the atoms in that ring has been studied. On the basis of the results presented here, there appears to be distinctive chemical shifts of the C13 and C15 atoms that may allow the conformation of this ring to be identified in other forms.

The effect of the spinning speed upon the centreband intensity of a peak as the anisotropy and asymmetry are varied has been investigated. It has been found that at low spinning speeds, the centreband intensity does not vary in a simple

fashion. Thus it is recommended that a full shielding tensor analysis is performed when anisotropies of peaks are being compared.

The effect of the spinning speed on the sample temperature has also been studied, with a sample of samarium acetate. The results show that at low spinning speeds (up to about 2 kHz) there is sample cooling as the spinning speed increases (attributed to the Joule -Thompson effect). But at higher spinning speeds (above 2 kHz) then there is sample heating as the spinning speed increases. This is an important result as the use of very fast spinning probes is increasing, and care should be taken when calibrating variable temperature systems. Also commonly used 'ambient' temperatures may be well above room temperature.

The effect of quadrupolar nuclei (^{35}Cl and ^{14}N) upon the spectrum of a spin-$\frac{1}{2}$ nucleus (^{13}C) has been studied. In favourable cases, the anisotropy in the spin-spin coupling constant has been found, whilst in other cases, the sign and magnitude of the quadrupolar coupling constant has been found. The broadening of resonances of carbon atoms bonded to quadrupolar nuclei has been valuable in assigning the solid-state NMR spectra. In certain cases, broadening of carbon resonances adjacent to atoms attached to the quadrupolar nucleus has been seen (i.e atoms that are two bonds removed from the quadrupole). It has not been possible to distinguish the effect of the ^{37}Cl nucleus upon the carbon spectrum from the effect of the ^{35}Cl isotope in chlorine containing steroids.

Appendices:

1. Full Shielding Tensor Component Data

2. Computer Program SIMUL

3. List of Lectures and Seminars

Appendix 1 Full Shielding Tensor Component Data

Table A1.1 - The tensor components for cortisone acetate form I

Form I	RO/Hz	C22	C5	C3	C20	C11
	980	-85.5	123.5	117.2	101.1	106.1
$\Im$	1112	-71.4	109.4	106.4	93.2	97.6
	1308	-72.8	75.5	100.0	83.7	89.2
	980	0.12	0.68	0.00	0.35	0.14
η	1112	0.00	0.77	0.15	0.39	0.24
	1308	0.00	0.82	0.00	0.21	0.00
	980	-122.0	-279.6	-261.4	-273.0	-271.1
σ_{11}	1112	-134.1	-272.3	-264.0	-269.6	-271.2
	1308	-133.4	-244.4	-252.9	-255.7	-255.4
	980	-132.4	-195.3	-261.4	-237.9	-256.6
σ_{22}	1112	-134.1	-188.5	-248.1	-233.3	-248.0
	1308	-133.4	-182.6	-252.9	-237.8	-255.4
	980	-255.4	-52.2	-85.6	-103.8	-104.7
σ_{33}	1112	-241.2	-66.3	-96.5	-111.7	-113.2
	1308	-242.6	-100.2	-102.9	-121.2	-121.6
δ		169.8	175.7	202.9	204.9	210.8
	980	17	12	10	24	17
ssd	1112	20	100	57	85	81
	1308	29	210	83	26	66
	980	-4/3	-5/5	-4/5	-3/4	-3/5
range	1112	-4/2	-5/4	-3/4	-3/5	-3/4
	1308	-3/2	-3/3	-2/3	-2/3	-2/3

$\Im$, σ and δ are all in ppm. η, ssd and range are dimensionless.

Table A1.2 - The tensor components for cortisone acetate form II

Form II	RO/Hz	C5	C22	C3	C20	C11
	1042	117.5	-77.6	105.7	100.4	108.3
$\mathfrak{F}$	1112	114.3	-73.0	103.1	98.6	106.8
	1308	120.2	-78.0	105.9	101.0	109.2
	1042	0.68	0.39	0.22	0.25	0.17
η	1112	0.74	0.36	0.28	0.33	0.20
	1308	0.65	0.49	0.12	0.28	0.00
	1042	-269.9	-121.3	-263.4	-269.0	-273.1
σ_{11}	1112	-270.3	-125.7	-264.8	-272.0	-273.9
	1308	-269.9	-117.2	-258.0	-271.1	-264.3
	1042	-189.6	-151.7	-240.1	-243.9	-254.5
σ_{22}	1112	-186.0	-151.7	-236.1	-239.1	-252.2
	1308	-192.3	-155.1	-245.7	-242.5	-264.2
	1042	-53.4	-252.8	-93.2	-105.9	-101.5
σ_{33}	1112	-56.6	-248.1	-95.8	-107.6	-102.9
	1308	-50.7	-253.1	-93.0	-105.2	-100.5
δ		171.0	175.2	198.9	206.2	209.7
	1042	71	18	17	16	22
ssd	1112	40	14	26	29	27
	1308	40	7	14	8.4	11
	1042	-4/4	-3/3	-3/4	-3/4	-3/4
range	1112	-4/5	-3/2	-3/4	-3/4	-3/4
	1308	-3/3	-3/2	-2/3	-3/3	-2/3

$\mathfrak{F}$, σ and δ are all in ppm. η, ssd and range are dimensionless.

Table A1.3 - The tensor components for cortisone acetate form III

Form III	RO/Hz	C5	C22	C22	C5	C22
	1046	89.1	-83.5	-82.4	109.0	-77.8
$\tilde{\sigma}$	2270	113.1	-61.8	-75.1	112.8	-68.8
	1710	114.0	-79.7	-83.7	114.9	-79.5
	2083	109.2	-74.1	-77.0	109.8	-72.3
	1046	0.77	0.26	0.23	0.68	0.45
η	2270	0.37	0.99	0.00	0.36	0.69
	1710	0.28	0.45	0.36	0.49	0.58
	2083	0.46	0.14	0.00	0.47	0.12
σ_{11}	1046	-245.9	-118.0	-121.0	-265.5	-117.8
	2270	-244.4	-109.1	-133.9	-250.2	-116.1
	1710	-240.0	-112.5	-114.5	-259.1	-111.6
	2083	-246.3	-128.2	-132.9	-254.5	-133.9
σ_{22}	1046	-177.2	-139.5	-139.6	-190.9	-153.1
	2270	-202.7	-170.1	-134.0	-210.1	-163.8
	1710	-207.8	-148.6	-144.5	-203.0	-157.4
	2083	-196.6	-138.6	-132.9	-202.5	-142.3
σ_{33}	1046	-78.0	-254.0	-253.8	-64.7	-252.2
	2270	-53.9	-232.3	-246.6	-60.9	-243.1
	1710	-52.8	-250.1	-255.1	-58.7	-253.7
	2083	-57.7	-244.5	-248.3	-63.9	-246.6
δ		167.0	170.5	171.5	173.7	174.3
ssd	1046	32	4.3	9.7	39	5.7
	2270	98	0.32	4.4	80	2.8
	1710	2	7.3	19	8	44
	2083	96	1.2	35	110	5.8
range	1046	-4/2	-3/2	-3/2	-5/3	-4/2
	2270	-2/1	-2/1	-2/1	-2/1	-2/1
	1710	-3/2	-2/2	-2/2	-3/2	-3/2
	2083	-2/1	-2/1	-2/1	-2/1	-2/1
intensity ratio		1	1	1	2	1

$\tilde{\sigma}$, σ and δ are all in ppm. η, ssd and range are dimensionless.

Table A1.3 continued - The tensor components for cortisone acetate form III

Form III	RO/Hz	C3	C3	C20	C20	C11	C11
	1046	106.7	123.2	104.4	101.9	111.4	109.6
$\Im$	2270	100.3	119.6	106.4	101.3	100.7	109.9
	1710	103.7	118.8	105.1	104.7	104.5	105.8
	2083	97.4	113.3	102.9	94.7	100.4	102.6
	1046	0.25	0.13	0.36	0.21	0.17	0.22
η	2270	0.00	0.00	0.10	0.00	0.00	0.00
	1710	0.00	0.00	0.26	0.00	0.00	0.00
	2083	0.00	0.00	0.26	0.00	0.00	0.00
	1046	-264.8	-272.9	-275.0	-267.5	-274.8	-277.3
σ_{11}	2270	-248.4	-262.8	-262.1	-256.6	-260.1	-265.2
	1710	-249.9	-262.3	-270.0	-258.2	-261.9	-263.0
	2083	-246.8	-259.6	-268.7	-253.1	-259.9	-261.4
	1046	-238.3	-256.4	-236.9	-246.2	-256.1	-252.7
σ_{22}	2270	-248.4	-262.8	-251.7	-256.6	-260.1	-265.2
	1710	-249.9	-262.3	-242.4	-258.2	-261.8	-263.0
	2083	-246.8	-259.6	-241.6	-253.1	-259.8	-261.4
	1046	-91.5	-79.8	-99.3	-104.0	-98.3	-100.6
σ_{33}	2270	-97.9	-83.3	-97.4	-104.6	-109.1	-100.3
	1710	-94.5	-84.1	-98.5	-101.1	-105.2	-104.2
	2083	-100.7	-89.6	-100.7	-111.1	-109.2	-107.4
δ		198.2	203.0	203.7	205.8	209.7	210.2
	1046	21	7.8	18	14	8.1	33
ssd	2270	11	54	13	6.6	15	18
	1710	83	7.7	10	20	9.6	35
	2083	64	36	62	68	32	15
	1046	-3/3	-3/4	-3/4	-3/3	-3/4	-2/3
range	2270	-2/2	-2/2	-2/2	-2/2	-2/2	-2/2
	1710	-2/2	-2/3	-2/3	-2/2	-2/3	-1/3
	2083	-1/2	-1/2	-1/2	-1/2	-1/2	-1/2
intensity ratio		1	2	2	1	2	1

$\Im$, σ and δ are all in ppm. η, ssd and range are dimensionless.

Table A1.4 - The tensor components for cortisone acetate form IV_{aq}

Form IV_{aq}	RO/Hz	C22	C5	C3/20	C11
	1046	-80.4	108.7	109.1	98.8
$\Im$	1120	-76.1	112.8	112.0	104.4
	1300	-78.4	112.1	106.2	97.4
	1046	0.00	0.73	0.25	0.31
η	1120	0.00	0.61	0.00	0.00
	1300	0.00	0.61	0.16	0.00
	1046	-131.4	-268.4	-272.2	-275.2
σ_{11}	1120	-133.5	-265.0	-260.2	-262.5
	1300	-132.4	-264.6	-266.0	-259.0
	1046	-131.4	-189.1	-245.3	-244.2
σ_{22}	1120	-133.6	-196.4	-260.2	-262.5
	1300	-132.4	-196.1	-248.6	-259.0
	1046	-252.1	-65.7	-95.1	-111.5
σ_{33}	1120	-247.7	-61.5	-92.2	-105.9
	1300	-250.0	-62.2	-98.0	-112.9
δ		171.6	174.3	204.2	210.3
	1046	20	45	16	55
ssd	1120	28	39	18	50
	1300	25	110	20	100
	1046	-4/3	-4/5	-4/4	-3/4
range	1120	-3/2	-4/4	-3/4	-3/4
	1300	3/2	-4/3	-3/4	-3/3

$\Im$, σ and δ are all in ppm. η, ssd and range are dimensionless.

Table A1.5 - The tensor components for cortisone acetate form IV_{et}

Form IV_{et}	RO/Hz	C22	C5	C3	C20	C11
	1112	-80.1	112.7	114.3	102.0	105.6
$\mathfrak{F}$	1177	-69.4	99.7	107.4	95.7	93.9
	1308	-73.1	111.6	109.4	94.6	97.9
	1112	0.00	0.67	0.15	0.34	0.24
η	1177	0.00	0.76	0.12	0.30	0.30
	1308	0.00	0.67	0.19	0.35	0.26
	1112	-131.2	-265.9	-269.0	-272.9	-275.5
σ_{11}	1177	-136.6	-259.9	-263.3	-267.0	-271.2
	1308	-134.7	-265.4	-268.4	-268.6	-272.0
	1112	-131.3	-191.0	-251.9	-238.4	-250.7
σ_{22}	1177	-136.6	-184.0	-250.7	-237.9	-243.4
	1308	-134.8	-190.4	-247.6	-235.2	-246.6
	1112	-251.4	-59.4	-89.0	-102.6	-104.7
σ_{33}	1177	-240.7	-72.5	-95.9	-108.9	-116.4
	1308	-244.5	-60.6	-93.9	-110.1	-112.4
δ		171.3	172.2	203.3	204.6	210.3
	1112	19	19	18	21	25
ssd	1177	40	78	67	65	150
	1308	20	66	24	11	82
	1112	-4/3	-4/4	-3/4	-3/4	-3/4
range	1177	-3/2	-4/3	-3/3	-3/3	-3/3
	1308	-4/3	-4/3	-3/4	-3/4	-3/4

$\mathfrak{F}$, σ and δ are all in ppm. η, ssd and range are dimensionless.

Table A1.6 - The tensor components for cortisone acetate form IV_{ac}

Form IV_{ac}	RO/Hz	C5	C22	C3	C20	C11	acetone
	1177	98.9	-67.6	91.1	87.5	88.7	87.1
$\mathfrak{F}$	1079	103.8	-84.9	108.5	105.4	102.4	-
	1276	64.1	-63.7	79.8	79.8	74.1	87.2
	1177	0.72	0.00	0.00	0.18	0.04	0.21
η	1079	0.67	0.25	0.12	0.28	0.25	-
	1276	0.62	0.00	0.00	0.22	0.00	0.00
	1177	-253.5	-137.3	-244.1	-257.2	-256.3	-266.9
σ_{11}	1079	-255.3	-117.9	-259.4	-272.9	-274.1	-
	1276	-220.3	-139.3	-238.5	-254.2	-247.2	-257.7
	1177	-182.3	-137.3	-244.1	-241.5	-252.6	-248.2
σ_{22}	1079	-185.4	-139.5	-246.2	-243.8	-248.4	-
	1276	-180.7	-139.3	-238.4	-236.9	-247.2	-257.7
	1177	-69.5	-238.7	-107.4	-118.1	-121.4	-126.9
σ_{33}	1079	-64.7	-256.0	-90.1	-100.2	-107.6	-
	1276	-104.4	-234.8	-118.7	-125.8	-136.0	-126.9
δ		168.4	171.1	198.5	205.6	210.1	-
	1177	230	32	87	95	170	3.7
ssd	1079	29	16	20	16	26	-
	1276	16	21	96	56	140	80
	1177	-4/3	-3/2	-3/3	-3/3	-3/3	-2/3
range	1079	-4/3	-4/2	-3/4	-3/4	-3/3	-
	1276	-3/3	-3/2	-3/3	-3/3	-3/3	-2/2

$\mathfrak{F}$, σ and δ are all in ppm. η, ssd and range are dimensionless.

Table A1.7 - The tensor components for cortisone acetate form V_{aq}

Form V_{aq}	RO/Hz	C5	C22	C3	C11	C20
	1079	122.7	-86.5	114.8	109.0	105.3
$\mathfrak{F}$	1145	97.6	-77.3	110.1	109.4	103.5
	1308	81.4	-70.8	102.3	101.3	85.8
	1079	0.67	0.28	0.23	0.24	0.36
η	1145	0.86	0.10	0.00	0.16	0.21
	1308	0.85	0.00	0.00	0.00	0.00
	1079	-273.0	-116.3	-271.6	-276.7	-281.6
σ_{11}	1145	-261.8	-129.5	-256.9	-272.7	-273.0
	1308	-246.5	-136.5	-253.0	-260.3	-253.3
	1079	-191.1	-140.8	-245.6	-250.7	-244.2
σ_{22}	1145	-178.3	-137.0	-256.9	-255.8	-251.4
	1308	-177.4	-136.5	-253.0	-260.3	-253.3
	1079	-48.0	-258.2	-86.4	-100.3	-105.0
σ_{33}	1145	-73.6	-249.2	-91.8	-100.2	-106.9
	1308	-89.8	-242.6	-99.6	-108.4	-124.7
δ		171.2	171.9	201.9	209.6	210.4
	1079	18	4.5	1.0	3.5	10
ssd	1145	44	15	50	10	48
	1308	79	14	55	24	120
	1079	-4/5	-4/3	-3/5	-3/4	-3/4
range	1145	-4/4	-3/2	-3/4	-3/4	-3/4
	1308	-4/4	-2/2	-3/3	-3/4	-3/4

$\mathfrak{F}$, σ and δ are all in ppm. η, ssd and range are dimensionless.

Table A1.8 - The tensor components of α-testosterone

α-form	RO/Hz	C3	C3	C5	C5	C4	C4
	1340	109.2	102.6	115.9	113.1	-67.4	-67.5
$\mathfrak{F}$	1400	109.2	103.1	116.6	113.0	-64.9	-68.4
	1700	107.9	103.4	119.5	106.6	-69.5	-72.0
	1340	0.00	0.00	0.68	0.73	0.60	0.66
η	1400	0.00	0.00	0.68	0.71	0.67	0.68
	1700	0.00	0.00	0.60	0.54	0.82	0.90
	1340	-257.3	-252.6	-269.3	-268.5	-71.6	-69.3
σ_{11}	1400	-257.4	-253.0	-269.9	-267.4	-71.7	-67.7
	1700	-256.7	-253.1	-268.0	-252.9	-62.6	-57.0
	1340	-257.3	-252.6	-190.8	-186.0	-112.4	-113.6
σ_{22}	1400	-257.4	-253.0	-191.1	-187.0	-115.0	-114.5
	1700	-256.7	-253.1	-195.8	-195.1	-119.5	-121.6
	1340	-93.5	-98.7	-56.2	-57.6	-193.1	-192.7
σ_{33}	1400	-93.6	-98.3	-55.6	-57.7	-190.7	-193.7
	1700	-94.9	-98.0	-52.7	-64.1	-195.3	-197.3
δ		202.8	201.4	172.2	170.7	125.8	125.3
	1340	35	44	87	83	1.3	0.9
ssd	1400	23	33	76	84	3.2	4.5
	1700	17	23	28	2.9	19	19
	1340	-3/3	-3/3	-4/3	-4/3	-3/2	-3/2
range	1400	-2/4	-2/3	-3/3	-3/3	-2/2	-2/2
	1700	-2/2	-2/2	-2/3	-2/2	-2/2	-2/2

$\mathfrak{F}$, σ and δ are all in ppm. η, ssd and range are dimensionless.

Table A1.9 - The tensor components of cortisone

	RO/Hz	C11/20	C3	C5	C4
$\Im$	1280	107.3	111.8	111.0	-65.3
	1390	107.0	112.3	127.9	-65.7
	1600	109.8	109.4	123.5	-67.1
η	1280	0.00	0.00	0.54	0.67
	1390	0.00	0.00	0.66	0.79
	1600	0.00	0.00	0.58	0.78
σ_{11}	1280	-264.7	-260.4	-253.6	-70.4
	1390	-264.5	-260.7	-274.1	-66.0
	1600	-265.9	-259.2	-265.7	-65.3
σ_{22}	1280	-264.7	-260.4	-193.6	-114.2
	1390	-264.5	-260.6	-189.9	-118.1
	1600	-265.9	-259.2	-194.0	-117.4
σ_{33}	1280	-103.7	-92.7	-57.1	-190.2
	1390	-104.0	-92.2	-40.2	-190.6
	1600	-101.2	-95.1	-44.6	-192.0
δ		211.0	204.5	168.1	124.9
ssd	1280	34	140	135	34
	1390	8.6	25	21	4.6
	1600	5.5	25	15	4.6
range	1280	-3/4	-3/5	-3/2	-2/2
	1390	-3/5	-3/4	-3/4	-3/2
	1600	-3/4	-2/3	-3/3	-2/2

$\Im$, σ and δ are all in ppm. η, ssd and range are dimensionless.

Table A1.10 - The tensor components of androstanolone

		hydrate		anhydrate	
	RO/Hz	C3	C17	RO/Hz	C3
$\Im$	800	128.3	30.8		
	1000	128.2	33.4	1140	118.9
	1140	118.0	-30.5	1210	127.7
	1250	118.6		1360	117.4
	1300	118.3	-64.9		
η	800	0.00	0.79		
	1000	0.00	0.63	1140	0.09
	1140	0.26	0.87	1210	0.00
	1250	0.18		1360	0.00
	1300	0.16	0.45		
σ_{11}	800	-279.7	-109.1		
	1000	-279.6	-108.8	1140	-280.7
	1140	-289.7	-53.1	1210	-279.6
	1250	-285.3		1360	-274.5
	1300	-284.1	-34.4		
σ_{22}	800	-279.6	-84.8		
	1000	-279.6	-87.6	1140	-269.8
	1140	-259.4	-79.5	1210	-279.6
	1250	-264.3		1360	-274.5
	1300	-265.2	-63.9		
σ_{33}	800	-87.2	-50.7		
	1000	-87.3	-48.1	1140	-96.9
	1140	-97.6	-112.0	1210	-88.0
	1250	-96.9		1360	-98.4
	1300	-97.3	-146.5		
δ		215.5	81.5		215.8
ssd	800	11	32		
	1000	16	1.2	1140	21
	1140	54	1.4	1210	113
	1250	23		1360	66
	1300	33	316		
range	800	-5/7	-2/1		
	1000	-4/5	-2/2	1140	-3/4
	1140	-4/4	-2/1	1210	-3/3
	1250	-3/5		1360	-3/3
	1300	-3/4	-2/1		

$\Im$, σ and δ are all in ppm. η, ssd and range are dimensionless.

Table A1.11 - The tensor components of ^{13}C labelled cortisone acetate samples

		form II		form IV_{aq}
	RO/Hz	C22	RO/Hz	C22
$\mathfrak{R}$	1024	-76.5	1046	-89.9
	1112	-72.9	1120	-86.1
	1308	-68.2	1300	-86.4
η	1024	0.51	1046	0.32
	1112	0.49	1120	0.20
	1308	0.39	1300	0.00
σ_{11}	1024	-117.4	1046	-112.0
	1112	-121.0	1120	-120.1
	1308	-127.8	1300	-128.4
σ_{22}	1024	-156.5	1046	-141.2
	1112	-156.5	1120	-137.0
	1308	-154.5	1300	-128.4
σ_{33}	1024	-251.7	1046	-261.5
	1112	-248.1	1120	-257.7
	1308	-243.4	1300	-258.0
δ		175.2		171.6
range	1024	-4/4	1046	-5/4
	1112	-4/3	1120	-4/3
	1308	-3/3	1300	-3/3
ssd	1024	11	1046	8
	1112	11	1120	5
	1308	8	1300	2

$\mathfrak{R}$, σ and δ are all in ppm. η, ssd and range are dimensionless.

Table A1.12 - The tensor components of BDP Anhydrate

	RO/Hz	C20	C3	C25	C22	C5
δ		198.5	188.5	177.1	172.5	169.5
$\mathfrak{A}$	1570	94.4	107.0	-91.7	-77.2	132.1
	1370	93.6	106.5	-93.6	-77.6	131.7
	1177	87.2	104.8	-87.5	-77.4	115.4
η	1570	0.59	0.35	0.20	0.24	0.64
	1370	0.57	0.21	0.34	0.00	0.60
	1177	0.49	0.34	0.25	0.00	0.73
σ_{11}	1570	-273.4	-260.7	-121.9	-124.7	-277.7
	1370	-272.1	-252.7	-114.2	-133.7	-275.1
	1177	-263.3	-258.9	-122.5	-133.7	-269.4
σ_{22}	1570	-218.0	-223.3	-140.7	-143.1	-193.4
	1370	-218.5	-230.8	-146.4	-133.7	-195.6
	1177	-220.9	-222.9	-144.1	-133.7	-184.9
σ_{33}	1570	-104.1	-81.5	-268.8	-249.7	-37.4
	1370	-104.9	-82.0	-270.7	-250.1	-37.8
	1177	-111.3	-83.7	-264.6	-249.8	-54.2
range	1570	-3/3	-3/3	-3/2	-3/3	-3/3
	1370	-3/4	-3/3	-4/3	-3/2	-4/3
	1177	-3/4	-3/4	-4/2	-3/2	-4/3
ssd	1570	15	7	11	13	28
	1370	4	13	18	5	32
	1177	17	17	9	30	50

Table A1.12 - continued (the tensor components of BDP Anhydrate)

	RO/Hz	C1	C2	C4
δ		154.1	130.3	125.0
$\mathfrak{A}$	1370	97.3	-78.3	-77.0
η	1370	0.95	0.75	0.37
σ_{11}	1370	-249.1	-61.9	-72.4
σ_{22}	1370	-156.4	-120.4	-100.6
σ_{33}	1370	-56.8	-208.6	-202.0
range	1370	-4/2	-3/1	-3/1
ssd	1370	58	80	95

δ, $\mathfrak{A}$, and all σ values are in ppm.

Table A1.13 - The tensor components of BDP Micronised Monohydrate

	RO/Hz	C20	C3	C25	C22
δ		198.4	185.9	179.3	176.5
$\Im$	1550	95.9	114.4	-87.1	-85.5
	1880	96.4	106.7	-90.5	-85.1
	2230	96.0	104.1	-93.5	-85.1
	1225	92.7	101.5	-86.5	-85.1
	1550	93.8	103.4	-84.5	-86.9
η	1550	0.48	0.50	0.37	0.35
	1880	0.45	0.17	0.46	0.37
	2230	0.43	0.22	0.75	0.38
	1225	0.49	0.34	0.29	0.30
	1550	0.45	0.35	0.38	0.00
σ_{11}	1550	-269.4	-271.7	-119.5	-118.9
	1880	-268.1	-248.4	-113.3	-118.2
	2230	-267.0	-249.5	-97.4	-117.8
	1225	-267.3	-253.8	-123.5	-121.1
	1550	-266.5	-255.9	-121.2	-133.0
σ_{22}	1550	-223.3	-214.5	-152.0	-148.6
	1880	-225.0	-230.1	-154.8	-149.7
	2230	-225.7	-226.4	-167.7	-150.0
	1225	-222.3	-219.4	-148.6	-146.8
	1550	-224.1	-219.2	-153.0	-133.0
σ_{33}	1550	-103.5	-71.5	-266.4	-262.0
	1880	-102.0	-79.2	-269.8	-261.6
	2230	-102.4	-81.8	-272.8	-261.6
	1225	-105.7	-84.4	-265.8	-261.6
	1550	-104.6	-82.5	-263.8	-263.4
range	1550	-3/3	-3/3	-3/2	-3/2
	1880	-2/2	-2/2	-2/2	-2/2
	2230	-2/2	-2/1	-2/2	-2/1
	1225	-3/3	-3/3	-3/2	-3/2
	1550	-2/2	-2/2	-2/2	-2/2
ssd	1550	5.4	65	3.2	2.0
	1880	13	7.6	0.8	4.0
	2230	10	35	136	4.2
	1225	6.6	9.3	5.0	5.8
	1550	13	58	32	20

δ, $\Im$, and all σ values are in ppm.

Table A1.13 - continued (the tensor components of BDP Micronised Monohydrate)

	RO/Hz	C5	C1	C2	C4
δ		166.3	152.1	130.1	126.3
	1550	135.4	-134.7	-89.7	-74.0
	1880	127.0	-126.0	-91.8	-78.2
ℜ	2230			-85.4	-84.9
	1225	122.8			
	1550	116.9			
	1550	0.68	0.77	0.49	0.61
	1880	0.66	0.94	0.66	0.57
η	2230			0.84	0.38
	1225	0.75			
	1550	0.74			
	1550	-279.8	-33.0	-63.2	-66.6
	1880	-271.4	-29.9	-53.8	-64.9
σ_{11}	2230			-51.3	-67.6
	1225	-273.4			
	1550	-267.9			
	1550	-188.2	-136.4	-107.2	-112.0
	1880	-188.1	-148.3	-114.6	-109.5
σ_{22}	2230			-123.5	-100.1
	1225	-181.9			
	1550	-181.6			
	1550	-30.9	-286.8	-219.8	-200.3
	1880	-39.4	-278.1	-221.9	-204.5
	2230			-215.5	-211.2
σ_{33}	1225	-43.6			
	1550	-49.4			
	1550	-4/3	-4/3	-2/1	-2/1
	1880	-3/2	-3/3	-1/1	-1/1
range	2230			-2/1	-2/1
	1225	-4/3			
	1550	-3/3			
	1550	40	93	143	28
	1880	48	33	0.00	0.00
ssd	2230			8.7	3.9
	1225	115			
	1550	49			

δ, ℜ, and all σ values are in ppm.

Table A1.14 - The tensor components of BDP ethyl acetate solvate

	RO/Hz	C20	C3	C25	C22	C5
δ		197.8	185.4	179.2	175.1	167.1
$\mathfrak{A}$	1340	90.9	95.7	-82.8	-86.4	113.7
	1243	85.8	105.0	-83.2	-82.5	123.4
	1014	93.2	98.0	-86.3	-86.9	110.1
η	1340	0.46	0.42	0.28	0.00	0.70
	1243	0.40	0.26	0.34	0.00	0.65
	1014	0.44	0.40	0.37	0.26	0.62
σ_{11}	1340	-264.0	-253.4	-126.2	-131.9	-263.6
	1243	-257.9	-251.8	-123.3	-133.8	-269.1
	1014	-265.0	-253.8	-120.0	-120.4	-256.5
σ_{22}	1340	-222.5	-213.1	-149.4	-131.9	-184.3
	1243	-223.5	-224.0	-151.9	-133.8	-188.5
	1014	-223.8	-215.0	-152.0	-142.9	-187.8
σ_{33}	1340	-106.8	-89.7	-262.0	-261.5	-53.4
	1243	-112.0	-80.4	-262.4	-257.6	-43.7
	1014	-104.6	-87.4	-265.5	-262.0	-57.0
range	1340	-3/3	-3/3	-3/2	-3/2	-3/2
	1243	-3/3	-3/3	-3/3	-3/2	-3/3
	1014	-3/4	-3/4	-4/3	-3/3	-4/4
ssd	1340	10	6	25	9	56
	1243	6	2	6	2	71
	1014	74	82	6	16	11

δ, $\mathfrak{A}$, and all σ values are in ppm.

Computer Program SIMUL

```
      PROGRAM SIMUL

C      THIS PROGRAM SIMULATES THE SPINNING SIDEBAND INTENSITIES GIVEN
C      VALUES OF SHIELDING ANISOTROPY AND ASYMMETRY AND WRITES THE
C      CENTRE BAND INTENSITY TO A FILE FOR PLOTTING WITH UNIPAS.
C      E.A. Christopher Last modified 16-12-91

      IMPLICIT DOUBLE PRECISION (A-H,O-Z)
      DIMENSION SURFAS(500,500)
      DIMENSION X(50),Y(50),WORK(50),SUMR(50),SUMI(50),TEMP(50)
      DIMENSION ST(0:90),CT(0:90),CE2(50),X2(1024)
      DIMENSION SPC(-25:25),Z2(50)
      CHARACTER*80 TITL
      INTEGER NN,NS
      REAL PDELP,PEETA,PSF,PVR,LEFT,RIGHT,DEPTH,HEIGHT,CHARHT,PSHIF
      REAL ASL,ASH,ASS,ANL,ANH,ANS
      DATA INT,NOR,TWOPI,PI /16,20,6.283185307,3.141592653/
      DATA THD /0.33333333333333/
C
C      Data Input Section ==========================================
C
      READ(5,100) TITL
  100 FORMAT(A80)
      READ(5,*) VR,SF
      READ(5,*) NSB,IH,IL
      READ(5,*) SHIF
      READ(5,*) ANL,ANH,ANS
      READ(5,*) ASL,ASH,ASS

C      ========= Calculate angular spinning speed ,  Calculate sin and cos
C      look-up tables=============================================================

      WR=VR*TWOPI
      DO 90 I=0,NOR
          ARG=I*PI/NOR
          ST(I)=DSIN(ARG)
          CT(I)=DCOS(ARG)
   90 CONTINUE

      WRITE(6,95)
   95 FORMAT(' IX    JY   DELP      EETA     SPC(0)')

      SIGBAR=-SHIF
      RP=1.0/(NSB*VR)
      AA=1.0*(ANH-ANL)/ANS+0.5
      NN=AA
      BB=1.0*(ASH-ASL)/ASS+0.5
      NS=BB
C=============================================================================
C                      OUTER  LOOP
C=============================================================================
      DO 500 JY=0,NN
      DELP=ANL+JY*ANS
C=============================================================================
C                      INNER  LOOP
C=============================================================================
      DO 450 IX=0,NS
      EETA=ASL-IX*ASS

      S33=DELP-SIGBAR
```

```
      S11=(3.0*SIGBAR-EETA*DELP-S33)/2.0
      S22=S11-EETA*DELP

C     ======== SET SIGMAS IN PROPER SIZE ORDER ========

      IF (ABS(S33-SIGBAR).GT.ABS(S11-SIGBAR)) GO TO 60
      TEM=S11
      S11=S33
      S33=TEM
   60 IF (ABS(S11-SIGBAR).GT.ABS(S22-SIGBAR)) GO TO 70
      TEM=S22
      S22=S11
      S11=TEM
   70 IF (ABS(S33-SIGBAR).GT.ABS(S11-SIGBAR)) GO TO 80
      TEM=S11
      S11=S33
      S33=TEM

   80 SIGMA1=-S11
      SIGMA2=-S22
      SIGMA3=-S33


C     =======  Zero arrays - Calculate spectrum over Euler angles and rotor
C              period ======

      DO 105 I=1,NSB
          X(I)=0.0
          Y(I)=0.0
  105 CONTINUE
      DO 140 I=1, NOR
        SINA=ST(I)
        COSA=CT(I)
        SIN2A=2.0*ST(I)*CT(I)
        COS2A=CT(I)*CT(I)-ST(I)*ST(I)
        DO 130 J=1, NOR
          SINB=ST(J)
          COSB=CT(J)
          SSQB=SINB*SINB
          CO1=0.4714045*SINB
          CSQB=COSB*COSB
          DO 120 K=1, NOR
            SIN2C=2.0*ST(K)*CT(K)
            COS2C=CT(K)*CT(K)-ST(K)*ST(K)
            CO2=EETA*COS2C
            CO3=(1.5*SSQB+(EETA/2)*COS2C*(1+CSQB))
            C1=CO1*(COSB*(CO2-3)*COSA-EETA*SIN2C*SINA)
            S1=CO1*(COSB*(3-CO2)*SINA-EETA*SIN2C*COSA)
            C2=THD*(CO3*COS2A-EETA*COSB*SIN2C*SIN2A)
            S2=-THD*(CO3*SIN2A+EETA*COSB*SIN2C*COS2A)
            DO 110 L=1,NSB
              T=(L-1)*RP
              AN=WR*T
              AN2=2.0*AN
              XI=(1.0/WR)*(S1+0.5*S2+C1*DSIN(AN)-S1*DCOS(AN)
     1           +0.5*(C2*DSIN(AN2)-S2*DCOS(AN2)))
              PT=XI*DELP*SF*TWOPI
              SUMR(L)=DCOS(PT)
              SUMI(L)=DSIN(PT)
              X(L)=X(L)+SUMR(L)*SINB
```

```
            Y(L)=Y(L)+SUMI(L)*SINB
  110       CONTINUE
  120     CONTINUE
  130   CONTINUE
  140 CONTINUE

      ORC=0.0
      DO 142 I=1,NSB
         ORC=ORC+X(I)*X(I)+Y(I)*Y(I)
  142 CONTINUE
      ORC=DSQRT(ORC)
      DO 143 I=1,NSB
         X(I)=X(I)/ORC
         Y(I)=Y(I)/ORC
  143 CONTINUE


C     ====== DO FT  ========

      IFAIL2=0
      CALL C06FCF(X,Y,NSB,WORK,IFAIL2)

      SNRM=0.0
      DO 200 I=1,NSB
         SNRM=SNRM+X(I)
  200 CONTINUE
      DO 210 I=1,NSB
         X(I)=(X(I)*100.0)/SNRM
  210 CONTINUE

C     =======  PUT SSB IN PROPER ORDER ======

      NCUT=IL+1
      NSTART=NSB+IH+1
      J=1
      DO 220 I=NSTART,NSB
         TEMP(J)=X(I)
         J=J+1
  220 CONTINUE
      DO 230 I=1,NCUT
         TEMP(J)=X(I)
         J=J+1
  230 CONTINUE
      J=1
      DO 240 I=IH,IL
         SPC(I)=TEMP(J)
         J=J+1
  240 CONTINUE

      WRITE(6,400) IX,JY,DELP,EETA,SPC(0)
  400 FORMAT(I3,3X,I3,3X,F6.2,3X,F6.4,3X,F6.2)
      SURFAS(IX,JY)=SPC(0)
  450 CONTINUE
  500 CONTINUE

      END
```

UNIVERSITY OF DURHAM

Board of Studies in Chemistry

COLLOQUIA, LECTURES AND SEMINARS GIVEN BY INVITED SPEAKERS 1ST AUGUST 1989 TO 31ST JULY 1990

BADYAL, Dr. J.P.S. (Durham University) Breakthoughs in Heterogeneous Catalysis	1st November, 1989
BECHER, Dr. J. (Odense University) Synthesis of New Macrocylic Systems using Heterocyclic Building Blocks	13th November, 1989
BERCAW, Prof. J.E. (California Institute of Technology) Synthetic and Mechanistic Approaches to Ziegler–Natta Polymerization of Olefins	10th November, 1989
BLEASDALE, Dr. C. (Newcastle University) The Mode of Action of some Anti–tumour Agents	21st February, 1990
BOWMAN, Prof. J.M. (Emory University) Fitting Experiment with Theory in Ar–OH	23rd March, 1990
BUTLER, Dr. A. (St. Andrews University) The Discovery of Penicillin: Facts and Fancies	7th December, 1989
CHEETHAM, Dr. A.K. (Oxford University) Chemistry of Zeolite Cages	8th March, 1990
CLARK, Prof. D.T. (ICI Wilton) Spatially Resolved Chemistry (using Natures's Paradigm in the Advanced Materials Arena)	22nd February, 1990
COLE–HAMILTON, Prof. D.J. (St. Andrews University) New Polymers from Homogeneous Catalysis	29th November, 1989
CROMBIE, Prof. L. (Nottingham University) The Chemistry of Cannabis and Khat	15th February, 1990
DYER, Dr. U. (Glaxo) Synthesis and Conformation of C–Glycosides	31st January, 1990
FLORIANI, Prof. C. (University of Lausanne, Switzerland) Molecular Aggregates – A Bridge between homogeneous and Heterogeneous Systems	25th October, 1989
GERMAN, Prof. L.S. (USSR Academy of Sciences – Moscow) New Syntheses in Fluoroaliphatic Chemistry: Recent Advances in the Chemistry of Fluorinated Oxiranes	9th July, 1990
GRAHAM, Dr. D. (B.P. Reserch Centre) How Proteins Absorb to Interfaces	4th December, 1989
GREENWOOD, Prof. N.N. (University of Leeds) Novel Cluster Geometries in Metalloborane Chemistry	9th November, 1989

HOLLOWAY, Prof. J.H. (University of Leicester) Noble Gas Chemistry	1st February, 1990
HUGHES, Dr. M.N. (King's College, London) A Bug's Eye View of the Periodic Table	30th November, 1989
HUISGEN, Prof. R. (Universität München) Recent Mechanistic Studies of [2+2] Additions	15th December, 1989
○ KLINOWSKI, Dr. J. (Cambridge University) Solid State NMR Studies of Zeolite Catalysts	13th December 1989
○ LANCASTER, Rev. R. (Kimbolton Fireworks) Fireworks – Principles and Practice	8th February, 1990
○ LUNAZZI, Prof. L. (University of Bologna) Application of Dynamic NMR to the Study of Conformational Enantiomerism	12th February, 1990
○ PALMER, Dr. F. (Nottingham University) Thunder and Lightning	17th October, 1989
○ PARKER, Dr. D. (Durham University) Macrocycles, Drugs and Rock 'n' roll	16th November, 1989
PERUTZ, Dr. R.N. (York University) Plotting the Course of C–H Activations with Organometallics	24th January, 1990
PLATONOV, Prof. V.E. (USSR Academy of Sciences – Novosibirsk) Polyfluoroindanes: Synthesis and Transformation	9th July, 1990
POWELL, Dr. R.L. (ICI) The Development of CFC Replacements	6th December, 1989
○ POWIS, Dr. I. (Nottingham University) Spinning off in a huff: Photodissociation of Methyl Iodide	21st March, 1990
ROZHKOV, Prof. I.N. (USSR Academy of Sciences – Moscow) Reactivity of Perfluoroalkyl Bromides	9th July, 1990
○ STODDART, Dr. J.F. (Sheffield University) Molecular Lego	1st March, 1990
SUTTON, Prof. D. (Simon Fraser University, Vancouver B.C.) Synthesis and Applications of Dinitrogen and Diazo Compounds of Rhenium and Iridium	14th February, 1990
○ THOMAS, Dr. R.K. (Oxford University) Neutron Reflectometry from Surfaces	28th February, 1990
THOMPSON, Dr. D.P. (Newcastle University) The role of Nitrogen in Extending Silicate Crystal Chemistry	7th February, 1990

UNIVERSITY OF DURHAM

Board of Studies in Chemistry

COLLOQUIA, LECTURES AND SEMINARS GIVEN BY INVITED SPEAKERS
1ST AUGUST 1990 TO 31ST JULY 1991

o ALDER, Dr. B.J. (Lawrence Livermore Labs., California) 15th January, 1991
Hydrogen in all its Glory

o BELL†, Prof. T. (SUNY, Stoney Brook, U.S.A.) 14th November, 1990
Functional Molecular Architecture and Molecular Recognition

BOCHMANN†, Dr. M. (University of East Anglia) 24th October, 1990
Synthesis, Reactions and Catalytic Activity of Cationic Titanium Alkyls

BRIMBLE, Dr. M.A. (Massey University, New Zealand) 29th July, 1991
Synthetic Studies Towards the Antibiotic Griseusin-A

BROOKHART, Prof. M.S. (University of N. Carolina) 20th June, 1991
Olefin Polymerizations, Oligomerizations and Dimerizations Using Electrophilic Late Transition Metal Catalysts

BROWN, Dr. J. (Oxford University) 28th February, 1991
Can Chemistry Provide Catalysts Superior to Enzymes?

BUSHBY†, Dr. R. (Leeds University) 6th February, 1991
Biradicals and Organic Magnets

COWLEY, Prof. A.H. (University of Texas) 13th December, 1990
New Organometallic Routes to Electronic Materials

CROUT, Prof. D. (Warwick University) 29th November, 1990
Enzymes in Organic Synthesis

• DOBSON†, Dr. C.M. (Oxford University) 6th March, 1991
NMR Studies of Dynamics in Molecular Crystals

• GERRARD†, Dr. D. (British Petroleum) 7th November, 1990
Raman Spectroscopy for Industrial Analysis

HUDLICKY, Prof. T. (Virginia Polytechnic Institute) 25th April, 1991
Biocatalysis and Symmetry Based Approaches to the Efficient Synthesis of Complex Natural Products

JACKSON†, Dr. R. (Newcastle University) 31st October, 1990
New Synthetic Methods: α-Amino Acids and Small Rings

KOCOVSKY†, Dr. P. (Uppsala University) 6th November, 1990
Stereo-Controlled Reactions Mediated by Transition and Non-Transition Metals

LACEY, Dr. D. (Hull University) Liquid Crystals	31st January, 1991
LOGAN, Dr. N. (Nottingham University) Rocket Propellants	1st November, 1990
MACDONALD, Dr. W.A. (ICI Wilton) Materials for the Space Age	11th October, 1990
MARKAM, Dr. J. (ICI Pharmaceuticals) DNA Fingerprinting	7th March, 1991
PETTY, Dr. M.C. (Durham University) Molecular Electronics	14th February, 1991
PRINGLE+, Dr. P.G. (Bristol University) Metal Complexes with Functionalised Phosphines	5th December, 1990
PRITCHARD, Prof. J. (Queen Mary & Westfield College, London University) Copper Surfaces and Catalysts	21st November, 1990
SADLER, Dr. P.J. (Birkbeck College London) Design of Inorganic Drugs: Precious Metals, Hypertension + HIV	24th January, 1991
SARRE, Dr. P. (Nottingham University) Comet Chemistry	17th January, 1991
SCHROCK, Prof. R.R. (Massachusetts Institute of Technology) Metal-ligand Multiple Bonds and Metathesis Initiators	24th April, 1991
SCOTT, Dr. S.K. (Leeds University) Clocks, Oscillations and Chaos	8th November, 1990
SHAW+, Prof. B.L. (Leeds University) Syntheses with Coordinated, Unsaturated Phosphine Ligands	20th February, 1991
SINN+, Prof. E. (Hull University) Coupling of Little Electrons in Big Molecules. Implications for the Active Sites of (Metalloproteins and other) Macromolecules	30th January, 1991
SOULEN+, Prof. R. (South Western University, Texas) Preparation and Reactions of Bicycloalkenes	26th October, 1990
WHITAKER+, Dr. B.J. (Leeds University) Two-Dimensional Velocity Imaging of State-Selected Reaction Products	28th November, 1990

+ Invited specifically for the postgraduate training programme.

UNIVERSITY OF DURHAM

Board of Studies in Chemistry

COLLOQUIA, LECTURES AND SEMINARS FROM INVITED SPEAKERS

1991 – 1992 (August 1 – July 31)

1991

October	17	Dr. J.A. Salthouse, University of Manchester Son et Lumiere – a demonstration lecture
October	31	Dr. R. Keeley, Metropolitan Police Forensic Science Modern forensic science
◦November	6	Prof. B.F.G. Johnson†, Edinburgh University Cluster–surface analogies
November	7	Dr. A.R. Butler, St. Andrews University Traditional Chinese herbal drugs: a different way of treating disease
November	13	Prof. D. Gani†, St. Andrews University The chemistry of PLP–dependent enzymes
November	20	Dr. R. More O'Ferrall†, University College, Dublin Some acid–catalysed rearrangements in organic chemistry
◦ November	28	Prof. I.M. Ward, IRC in Polymer Science, University of Leeds The SCI lecture: the science and technology of orientated polymers
December	4	Prof. R. Grigg†, Leeds University Palladium–catalysed cyclisation and ion–capture processes
◦ December	5	Prof. A.L. Smith, ex Unilever Soap, detergents and black puddings
◦ December	11	Dr. W.D. Cooper†, Shell Research Colloid science: theory and practice

1992

January	22	Dr. K.D.M. Harris†, St. Andrews University Understanding the properties of solid inclusion compounds
January	29	Dr. A. Holmes†, Cambridge University Cycloaddition reactions in the service of the synthesis of piperidine and indolizidine natural products

January	30	Dr. M. Anderson, Sittingbourne Research Centre, Shell Research Recent Advances in the Safe and Selective Chemical Control of Insect Pests
February	12	Prof. D.E. Fenton†, Sheffield University Polynuclear complexes of molecular clefts as models for copper biosites
February	13	Dr. J. Saunders, Glaxo Group Research Limited Molecular Modelling in Drug Discovery
February	19	Prof. E.J. Thomas†, Manchester University Applications of organostannanes to organic synthesis
February	20	Prof. E.Vogel, University of Cologne *The Musgrave Lecture* Porphyrins: Molecules of Interdisciplinary Interest
February	25	Prof. J.F. Nixon, University of Sussex *The Tilden Lecture* Phosphaalkynes: new building blocks in inorganic and organometallic chemistry
February	26	Prof. M.L. Hitchman†, Strathclyde University Chemical vapour deposition
March	5	Dr. N.C. Billingham, University of Sussex Degradable Plastics – Myth or Magic?
March	11	Dr. S.E. Thomas†, Imperial College Recent advances in organoiron chemistry
March	12	Dr. R.A. Hann. ICI Imagedata Electronic Photography – An Image of the Future
March	18	Dr. H. Maskill†, Newcastle University Concerted or stepwise fragmentation in a deamination–type reaction
April	7	Prof. D.M. Knight, Philosophy Department, University of Durham Interpreting experiments: the beginning of electrochemistry
May	13	Dr. J–C Gehret, Ciba Geigy, Basel Some aspects of industrial agrochemical research

† Invited specially for the postgraduate training programme.